University of Cyprus

DEPARTMENT OF PHYSICS

PERTURBATIVE RENORMALIZATION OF HADRON OPERATORS AND OTHER FUNDAMENTAL QUANTITIES IN LATTICE QUANTUM CHROMODYNAMICS

DOCTOR OF PHILOSOPHY DISSERTATION

GREGORIS SPANOUDES

2019

University of Cyprus

Department of Physics

Perturbative renormalization of hadron operators and other fundamental quantities in Lattice Quantum Chromodynamics

Gregoris Spanoudes

A dissertation submitted to the University of Cyprus in partial fulfillment of the requirements for the degree of Doctor of Philosophy.

May 2019

Validation page

Doctoral Candidate: Gregoris Spanoudes

Doctoral Thesis Title: Perturbative renormalization of hadron operators and other fundamental quantities in Lattice Quantum Chromodynamics

The present Doctoral Dissertation was submitted in partial fulfillment of the requirements for the Degree of Doctor of Philosophy at the ***Department of Physics*** *and was approved on May 9, 2019 by the members of the* ***Examination Committee****.*

Examination Committee:

Research Supervisor: Prof. Haralambos Panagopoulos _____

Committee Chairman: Prof. Fotios Ptochos _____

Committee Member: Prof. Constantia Alexandrou _____

Committee Member: Prof. Giannis Koutsou _____

Committee Member: Prof. Stefan Sint _____

Declaration of doctoral candidate

The present doctoral dissertation was submitted in partial fulfillment of the requirements for the degree of Doctor of Philosophy of the University of Cyprus. It is a product of original work of my own, unless otherwise mentioned through references, notes, or any other statements.

Gregoris Spanoudes

_____

Acknowledgements

First of all, I would like to sincerely thank my advisor Prof. Haralambos Panagopoulos for the valuable guidance, the broad knowledge, and the continuous encouragement and support that he has provided to me throughout my PhD studies. He is an inspiration to me and a role model. I am certainly honoured to be his student.

Secondly, I would like to thank Prof. Martha Constantinou and Dr. Marios Costa for our collaboration in many of the present calculations.

I do not have enough words to thank my parents and my sisters for their endless love, continuous support, personal attention and care.

Last but not least, I thank the University of Cyprus for financial support over the last three years, within the framework of Ph.D. student scholarships.

Περίληψη

Στην παρούσα διατριβή, παρουσιάζεται ένας αριθμός από διαταρακτικούς υπολογισμούς που αφορούν την επανακανονικοποίηση διάφορων τοπικών και μη τοπικών αδρονικών τελεστών, όπως επίσης την επανακανονικοποίηση άλλων θεμελιωδών ποσοτήτων της Κβαντικής Χρωμοδυναμικής, για παράδειγμα της ισχυρούς σταθεράς σύζευξης. Οι περισσότεροι από αυτούς τους υπολογισμούς έχουν πραγματοποιηθεί στο φορμαλισμό της Θεωρίας Πεδίων στο Πλέγμα, χρησιμοποιώντας μια μεγάλη οικογένεια βελτιωμένων διακριτοποιημένων δράσεων, οι οποίες εφαρμόζονται ευρέως σε αριθμητικές προσομοιώσεις από μεγάλες διεθνείς ομάδες (π.χ. ETMC, QCDSF, Wuppertal-Budapest Collaboration). Οι υπολογισμοί είναι οι ακόλουθοι:

- Η μελέτη ενός βρόχου στην θεωρία διαταραχών της επανακανονικοποίησης και μίξης μη τοπικών φερμιονικών τελεστών, που περιλαμβάνουν μία ευθεία γραμμή Wilson (straight Wilson line), χρησιμοποιώντας διαστατική ομαλοποίηση της θεωρίας και στην παρουσία μη μηδενικών μαζών των κουάρκ. Τέτοιοι τελεστές εμφανίζονται σε μία καινούργια, πολλά υποσχόμενη προσέγγιση για τον υπολογισμό παρτονικών κατανομών στο πλέγμα.

- Ο υπολογισμός ενός βρόχου στην θεωρία διαταραχών των συναρτήσεων επανακανονικοποίησης και συντελεστών μίξης μη τοπικών φερμιονικών τελεστών, που περιλαμβάνουν μία γραμμή Wilson σχήματος staple (staple-shaped Wilson line), χρησιμοποιώντας διαστατική ομαλοποίηση και ομαλοποίηση στο πλέγμα (φερμιόνια τύπου Wilson/clover και γκλουόνια τύπου Symanzik-improved). Η εργασία αυτή σχετίζεται με τις μη διαταρακτικές μελέτες παρτονικών κατανομών που εξαρτώνται από την εγκάρσια ορμή των παρτονίων.

- Η γενίκευση της διαταρακτικής μας μελέτης στο πλέγμα για μη τοπικούς φερμιονικούς τελεστές, που περιλαμβάνουν μια γραμμή Wilson (Wilson line) με ένα αυθαίρετο αριθμό από γωνιώδη σημεία.

- Η υπό εξέλιξη μελέτη διορθώσεων ανώτερης τάξης στους συντελεστές μετατροπής από το RI′ σχήμα επανακανονικοποίησης στο $\overline{\text{MS}}$. Ο υπολογισμός αφορά μη τοπικούς τελεστές με μία ευθεία γραμμη Wilson (straight Wilson line).

- Ο υπολογισμός δύο βρόχων στην θεωρία διαταραχών της διαφοράς μεταξύ των συντελεστών επανακανονικοποίησης των μονήρων και μη μονήρων ως προς τη γεύση

διγραμμικών φερμιονικών τελεστών, χρησιμοποιώντας την εξής βελτιωμένη δράση: γκλουόνια τύπου Symanzik και φερμιόνια τύπου staggered με διπλά "εύσωμους" (stout-smeared) γκλουονικούς συνδέσμους (links). Τα αποτελέσματά μας μπορούν να συνδυαστούν με δεδομένα από προσομοιώσεις προκειμένου να ληφθεί μια μη διαταρακτική εκτίμηση των συντελεστών επανακανονικοποίησης για τους μονήρεις τελεστές.

- Ο υπό εξέλιξη υπολογισμός του συντελεστή τριών βρόχων της συνάρτησης β στο πλέγμα, χρησιμοποιώντας την εξής βελτιωμένη δράση: γκλουόνια τύπου Symanzik και φερμιόνια με εύσωμους (stout-smeared) γκλουονικούς συνδέσμους (links). Τα αποτελέσματά μας μπορούν να συνδυαστούν με εκτεταμένες προσομοιώσεις προκειμένου να προσεγγίσουμε την επανακανονικοποιημένη σταθερά σύζευξης στο σχήμα "Wilson flow", η οποία επί του παρόντος τυγχάνει ενεργούς διερεύνησης από έναν αριθμό ερευνητικών ομάδων.

Abstract

In this Thesis, we present a number of perturbative calculations regarding the renormalization of several local and nonlocal hadron operators, as well as the renormalization of other fundamental quantities of Quantum Chromodynamics, such as the strong running coupling. Most of our computations have been performed in the context of Lattice Field Theory using a large family of improved lattice actions, which are currently employed in numerical simulations by major international groups (e.g. ETMC, QCDSF, Wuppertal-Budapest Collaboration). The calculations are the following:

- The one-loop study of renormalization and mixing of nonlocal straight Wilson-line operators in dimensional regularization and in the presence of nonzero quark masses. These operators are relevant to a novel and very promising approach for calculating parton distribution functions on the lattice.

- The one-loop calculation of the renormalization factors and mixing coefficients of nonlocal staple-shaped Wilson-line operators, in both continuum (dimensional regularization) and lattice regularizations (Wilson/clover fermions and Symanzik-improved gluons). Our work is relevant to the nonperturbative investigations of transverse momentum-dependent distribution functions on the lattice.

- The extension of our perturbative study to general Wilson-line lattice operators with an arbitrary number of cusps.

- The ongoing study of higher-loop contributions to the conversion factors between the RI′ and the $\overline{\text{MS}}$ schemes for the straight Wilson-line operators.

- The two-loop computation of the difference between the renormalization factors of flavor singlet and nonsinglet bilinear quark operators, using Symanzik improved gluons and staggered fermions with twice stout-smeared links. Our results can be combined with nonperturbative data in order to estimate the nonperturbative renormalization factors for the singlet operators.

- The ongoing calculation of the three-loop coefficient of the lattice β-function, using Symanzik improved gluons and stout-smeared fermions. Our results can be combined with extensive simulations in order to make contact with the renormalized coupling in the "Wilson flow" renormalization scheme, which is being very actively investigated by a number of groups at present.

Contents

List of Figures

List of Tables

Chapter 1

Introduction

One of the four known fundamental interactions of nature, which act between elementary particles, is the strong interaction. It is responsible for giving most of the mass that we see in the Universe, as its action causes the binding of nucleons to form atomic nuclei. Quantum Chromodynamics (QCD) is believed to be the fundamental theory which describes strong interactions. In this theory, hadrons, the structural elements of visible matter, are not elementary particles; they consist of quarks (fermions) and gluons (gauge bosons), which are governed by the strong force. These particles have an additional quantum number, called color charge, which allows gluons (in contrast to photons) to be self-interacting. Today we know that quarks come in six flavors (up, down, charm, strange, top, bottom) and three color charges. Given that QCD is based on the nonabelian group SU(3), there are eight species of gluons carrying a color charge, corresponding to the eight generators of SU(3).

QCD is different from other fundamental theories in that it has two specific features: it is an asymptotically free theory in high-energy regions, i.e., quarks and gluons interact very weakly at short distances, and it is a confining theory, i.e., it forbids break-up of hadrons into their constituent quarks; this is why quarks have never been seen as isolated entities. The latter property poses fundamental difficulties in applying to QCD the classical analytical methods of Quantum Field Theory, which were very successful in the study of Quantum Electrodynamics. Since confinement is a consequence of the dynamics at low-energy regions where perturbation theory breaks down, a nonperturbative treatment of the theory is needed. The best method, at present, to evaluate hadronic observables is using the space-time discrete version of

QCD known as Lattice QCD; it can only be carried out by numerical simulations, usually on the fastest possible supercomputers.

1.1 QCD on the lattice

The lattice formulation of QCD was first proposed in 1974 by K. Wilson [1]; it opened the way to the study of nonperturbative phenomena using numerical methods. It is the only known nonperturbative regularization of QCD that provides a powerful tool for studying the low-energy properties of strong interactions from first principles. In particular, lattice QCD calculations can give information for the dynamics of QCD from low to high momentum regions (e.g. studies of scaling phenomena, or quark confinement) and for the hadron structure and properties (e.g. hadron masses, decay constants, electromagnetic and weak form factors, quark and gluon structure functions (parton distribution functions), spin and topological features) [2, 3]. They also provide input to phenomenology and to searches for Physics beyond the Standard Model (e.g. nucleon σ-terms related to the scattering cross section of dark matter candidates on nucleons [4]). Furthermore, they provide input to ongoing experiments, give predictions on observables that are not easily accessible experimentally and give guidance to new experiments within a robust theoretical framework [5].

In the lattice regularization of QCD, Euclidean space-time is discretized on a hypercubic lattice with lattice spacing a. The fermionic degrees of freedom are distributed on lattice sites, while the bosonic ones are placed on the links connecting neighbouring sites. The (finite) lattice spacing acts as the ultraviolet regulator, which renders the quantum field theory finite at high-energy regions; in particular, a induces a momentum cutoff, which restricts the domain of integration to the finite interval $-\pi/a < p_\mu < \pi/a$ (first Brillouin zone), when lattice calculations are made in momentum space. At low-energy regions, the (finite) lattice size L plays the role of the infrared regulator. The continuum theory is recovered by extrapolating lattice results to an infinite lattice size ($L \longrightarrow \infty$) and by taking the limit of vanishing lattice spacing ($a \longrightarrow 0$), which can be reached by tuning the bare coupling constant to zero according to the renormalization group.

Unlike continuum regularization schemes, lattice QCD allows numerical computations of the path integral that defines the theory. These computations are performed by

means of Monte Carlo simulations, with inputs the hadronic scale and bare quark masses. The Wick rotation leading from Minkowski to Euclidean spacetime is a necessary step in order to enable simulations via Monte Carlo methods. However, not all physical quantities are amenable to a Wick rotation; a notable case is the scattering amplitudes. A number of methods have been devised to circumvent this limitation for some of these quantities. A particular case regards distribution functions on the lattice; it will be discussed further in Chapter 2. The accuracy of such numerical calculations, however, is limited by the presence of statistical and systematic errors. The statistical error arises by the use of Monte Carlo importance sampling to evaluate the path integral and it is the most straightforward error to estimate. There are various sources of systematic uncertainties and their significance depends on the particular quantity under consideration and on the parameters of the lattice being used. Some of the main systematic errors are: discretization effects (lattice artifacts), finite volume effects, extrapolation from unphysically heavy pion masses, and truncation effects in renormalization of composite operators. Simulations are performed at finite (nonzero) values of the lattice spacing and at finite values of lattice size, giving unwanted contributions to the nonperturbative estimates, even in the continuum limit. Due to large computational cost, lattice calculations are often performed at a sequence of unphysically heavy pion masses and then extrapolated to the physical pion mass, leading to systematic uncertainties. Also, before taking the continuum limit, one must renormalize the corresponding operators and fields that are involved in the calculations, and match them to some common continuum scheme [typically the perturbatively-defined modified minimal subtraction ($\overline{\text{MS}}$) scheme] used by phenomenologists; a conversion factor from the nonperturbative lattice scheme to the $\overline{\text{MS}}$ scheme must be used, which is calculated necessarily in perturbation theory giving truncation effects. All these sources of errors need to be under control by the current lattice calculations in order to make meaningful contact with experimental data.

A significant progress in numerical simulations has taken place in the last years. This has been due to improvements in the algorithms and the development of new techniques, as well as, the increase in computational power, that have enabled simulations to be carried out at parameters very close to their physical values. In this respect, lattice-QCD calculations have reached a level where they not only complement, but also guide current and forthcoming experimental programs [6, 7]. Some examples of the advances of numerical simulations within lattice QCD are the calculations of the low-lying hadron

spectrum, hadron structure calculations [2, 3] addressing open questions, such as the spin decomposition [8] of the proton, and the calculation of the hadronic contributions to the anomalous magnetic moment of the muon $g-2$ [9, 10].

1.2 Improved lattice actions

The formulation of a continuum action on the lattice is not unique. In principle, the only restriction in discretizing the Lagrangian of a continuum theory is its recovery in the continuum limit[1]. In general, lattice actions cannot preserve all of the symmetries of the continuum actions; for instance, it is obvious that Lorentz invariance is violated by the discrete grid. However, it is important to construct gauge invariant lattice actions as the renormalizability of a quantum field theory of vector fields is based on gauge symmetry. There is not an optimal lattice action to use in all cases; each version has advantages and disadvantages depending on what features are of interest in the physical system under study, e.g., chiral symmetry, flavor symmetry, locality, or unitarity. Furthermore, any lattice action gives rise to discretization effects, which are irrelevant to the continuum theory. These effects disappear only in the continuum limit when the lattice spacing is sent to zero. In a numerical simulation one always works with finite a, and the discretization errors have to be under control before taking the continuum limit, i.e. before extrapolating to vanishing a; having small errors the extrapolation will be safer and more reliable, and quite accurate results will be produced even from calculations with larger values of a, which are less expensive in terms of computer time. Improved actions with smaller discretization errors have been constructed for a better behavior at all lattice spacings.

Presently, many improved versions of lattice actions are used in numerical simulations by major international groups (e.g., ETMC, MILC, QCDSF, etc.). The most frequent fermion actions are the Wilson/clover [12], the staggered [13], and the Ginsparg-Wilson (overlap [14–16] and domain wall [17, 18]). All of these actions have discretization errors of order $\mathcal{O}(a^2)$. The main problem in a naïve lattice formulation of fermion action is that it describes 2^4 equivalent fermion fields in the continuum limit; this is known as "doubling problem". All the above improved actions have dealt with this problem sacrificing, however, some features/symmetries of the

[1] Actually, even this natural requirement can be by-passed [11].

continuum theory. According to the Nielsen-Ninomiya theorem [19], a lattice fermion formulation with locality, without species doubling and with an explicit continuous chiral symmetry is impossible. The Wilson/clover action has no doublers and is local; thus, it breaks chiral symmetry explicitly. A variant of the Wilson/clover action is the twisted-mass action [20], in which all errors linear in a are automatically removed (without tuning of parameters) under "maximal twist" [21–23]. Also, a simple modification which can reduce chiral-symmetry breaking errors and can lead to more convergent results in simulations is the use of smeared gauge fields in the covariant derivatives of the fermion action, such as stout [24] (e.g., SLiNC fermions [25]), HYP [26] and HEX [27] links. The staggered action is also local, however, it introduces four (instead of sixteen) doublers. It has the advantage of preserving one nonsinglet axial symmetry and, consequently of having automatic $\mathcal{O}(a)$ improvement and no additive mass renormalization; however, it has the disadvantage of generating four unphysical species of fermions, which are characterized by a new degree of freedom, called "taste". Contributions from the unwanted tastes are removed by taking the fourth-root of the fermion determinant appearing in the path integral. However, for nonzero values of lattice spacing taste-mixing effects occur. Smearing techniques can also reduce taste-symmetry violating errors of staggered actions (e.g., Asqtad fermions [28], HISQ [29]). Ginsparg-Wilson actions pose a continuum-like chiral symmetry [30] without introducing unwanted doublers at the expense of being nonultralocal. However, they have the drawback of being computationally expensive with their cost being at least an order of magnitude greater than for other actions.

In the gauge part of the improved actions, the Symanzik-improvement program [31] has been applied using the concept of "on-shell improvement" [32] for reducing disretization errors of order $\mathcal{O}(a^2)$. The Symanzik-improved action includes four parts corresponding to all possible independent closed loops made of four and six links. It depends on four parameters (one for each loop); each particular choice for the values of these coefficients leads to a different improved action. The most popular actions (choices) are the tree-level Symanzik, tadpole improved Lüscher-Weisz [32, 33], DBW2 [34], and Iwasaki [35]. There is also a "nonperturbative" Symanzik improvement program, where the coefficients are determined by evaluating an improvement condition nonperturbatively (see [36]). In the following chapters we will concentrate on the actions used for our calculations: Wilson/clover, stout-smeared staggered, and SLiNC fermions and Wilson, tree-level Symanzik, and Iwasaki gluons.

1.3 Perturbative calculations in lattice QCD

Although lattice regularization is adopted for nonperturbative calculations via numerical simulations, perturbative computations on the lattice are still essential. Comparison of lattice results to experimental data requires appropriate renormalization of the lattice fields, bare parameters and composite operators, as dictated by Quantum Field Theory. This often relies on perturbation theory. In many cases nonperturbative estimates of renormalization factors are very difficult to obtain via numerical simulations due to complications such as possible mixing with other operators, whose signals are hard to disentangle. In this case, mixing patterns become more transparent when looked at using perturbative renormalization rather than nonperturbatively. Also, perturbative results for short-distance quantities can be compared with the corresponding results taken by nonperturbative techniques, in order to check the validity of perturbative and nonperturbative methods.

Furthermore, progress in modern simulation algorithms, along with a continuous increase in computational power in Supercomputing Centers, has made it possible for present-day numerical simulations to be performed at ever decreasing values of the lattice spacing; nevertheless, the values of a which are attainable at present, still lead to substantial deviations of lattice results from the continuum limit ($a \longrightarrow 0$), and sophisticated extrapolations to that limit are essential before accurate predictions can be made from lattice simulations. To this end, it is very important to devise means of reducing lattice artifacts from measured quantities. This can be done in lattice perturbation theory.

In addition, perturbation theory provides a method for systematically matching between different renormalization schemes. In particular, in order to establish the right connection of the lattice scheme to the physical continuum theory, the evaluation of the conversion factor which turns renormalized quantities defined in a nonperturbative scheme on the lattice, e.g., the modified regularization-independent (RI′) scheme [37, 38], to a continuum scheme, e.g., $\overline{\text{MS}}$, is required; this calculation can be done only in perturbation theory, since continuum schemes are typically defined perturbatively.

Perturbative calculations are extremely complex on the lattice. Algebraic expressions for typical two-loop Feynman diagrams contain millions of terms. Consequently, most

of the observables under study, despite their great physical importance, have only been studied partially (e.g. to one loop, to the lowest order in lattice spacing, using unimproved lattice actions). This constitutes a major source of systematic error, at a time when simulations are striving at becoming ever more precise. There are a small number of higher-loop calculations performed on the lattice in the last decades. Some of them are: the two-loop relation between the bare lattice coupling and the $\overline{\text{MS}}$ coupling in SU(N) gauge theories [39]; the two-loop calculation of running coupling, using the Schrödinger functional, in pure SU(2) gauge theory [40], in pure SU(3) gauge theory [41], and in QCD [42, 43]; the three-loop β function with Wilson fermions [44], clover fermions [45, 46], and overlap fermions [47]; the two-loop matching of the lattice bare quark masses to the $\overline{\text{MS}}$ masses with staggered quarks [48]; the two-loop renormalization functions of local fermion bilinear operators [49, 50], and the $\mathcal{O}(a^2)$ corrections to various fermionic matrix elements [51–53]. There has been also progress in the context of numerical stochastic perturbation theory, e.g. the three-loop renormalization of fermion bilinear operators [54], and the two-loop calculation of gradient-flow coupling in finite volume with Schrödinger functional boundary conditions in pure SU(3) gauge theory [55].

1.4 Thesis overview

The present dissertation focuses on two main directions: the perturbative renormalization of several quantum local and nonlocal operators, which are related to hadron structure, and the perturbative study of other fundamental quantities of QCD, in particular the β-function and Λ-scale. Our calculations have been performed using improved versions of lattice actions used in state-of-the-art numerical simulations. The outline of this thesis is as follows.

In Chapter 2 we provide a brief introduction to the main directions of hadron structure calculations on the lattice, giving emphasis on the topics of nucleon spin content and parton distributions, which are related to a part of our calculations presented in Chapters 3 – 6.

In Chapter 3 we examine the effect of nonzero quark masses on the renormalization of gauge-invariant nonlocal quark bilinear operators, including a finite-length Wilson

line (called Wilson-line operators). These operators are involved in a novel and very promising approach for computing parton distribution functions on the lattice. We present our perturbative calculations of the bare Green's functions, the renormalization factors in RI′ and $\overline{\text{MS}}$ schemes, as well as the conversion factors of these operators between the two renormalization schemes. Our computations have been performed in dimensional regularization at one-loop level, using massive quarks. The conversion factors can be used to convert the corresponding lattice nonperturbative results to the $\overline{\text{MS}}$ scheme. Also, our study is relevant for disentangling the additional operator mixing which occurs in the presence of nonzero quark masses, both on the lattice and in dimensional regularization.

In Chapter 4 we present one-loop results for the renormalization of nonlocal quark bilinear operators, containing a staple-shaped Wilson line, in both continuum and lattice regularizations. The continuum calculations were performed in dimensional regularization, and the lattice calculations for the Wilson/clover fermion action and for a variety of Symanzik-improved gauge actions. We extract the strength of the one-loop linear and logarithmic divergences (including cusp divergences), which appear in such nonlocal operators; we identify the mixing pairs which occur among some of these operators on the lattice, and we calculate the corresponding mixing coefficients. We also provide the appropriate RI′-like scheme, which disentangles this mixing nonperturbatively from lattice simulation data, as well as the one-loop expressions of the conversion factors, which convert the lattice data to the $\overline{\text{MS}}$ scheme. Our results can be immediately used for improving recent nonperturbative investigations of transverse momentum-dependent distribution functions on the lattice. Furthermore, extending our perturbative study to general Wilson-line lattice operators with an arbitrary number of cusps, we present results for their renormalization factors, including identification of mixing and determination of the corresponding mixing coefficients, based on our results for the staple operators.

In Chapter 5 we extend the work in Chapter 3 including a two-loop calculation of straight Wilson-line operators for massless fermions in dimensional regularization, from which one can extract the conversion factor between different renormalization schemes, as well as the anomalous dimension of the operators. The conversion factor up to two loops may be applied to nonperturbative data on the renormalization functions, to bring them to the $\overline{\text{MS}}$-scheme at a better accuracy. Furthermore, knowledge of the two-loop expression for the anomalous dimension of Wilson-line operators will improve the

method for extracting linear divergences, and will eliminate systematic uncertainties related to the truncation of the conversion factor. As the computation is still ongoing we present our preliminary results.

In Chapter 6 we present the perturbative computation of the difference between the renormalization factors of flavor singlet ($\sum_f \bar{\psi}_f \Gamma \psi_f$, f: flavor index) and nonsinglet ($\bar{\psi}_{f_1} \Gamma \psi_{f_2}, f_1 \neq f_2$) bilinear quark operators (where $\Gamma = \mathbb{1}$, γ_5, γ_μ, $\gamma_5 \gamma_\mu$, $\gamma_5 \sigma_{\mu\nu}$) on the lattice. The computation is performed to two loops and to lowest order in the lattice spacing, using Symanzik improved gluons and staggered fermions with twice stout-smeared links. The stout smearing procedure is also applied to the definition of bilinear operators. A significant part of this work is the development of a method for treating some new peculiar divergent integrals stemming from the staggered formulation. Our results can be combined with precise simulation results for the renormalization factors of the nonsinglet operators, in order to obtain an estimate of the renormalization factors for the singlet operators.

Chapter 7 includes some background information for the strong running coupling, the β-function and Λ-parameter of QCD, as well as a brief description of the background field method which is applied in our calculations of Chapter 8.

The computation of the three-loop coefficient of the lattice β-function, using Symanzik improved gluons and SLiNC fermions in an arbitrary representation of the gauge group $SU(N_c)$, is the main goal of the ongoing project described in Chapter 8. This computation allows us to evaluate the ratio of energy scales $\Lambda_L/\Lambda_{\overline{\rm MS}}$ and the two-loop relation between the bare coupling constant g_0 and the renormalized one in the $\overline{\rm MS}$ scheme, $g_{\overline{\rm MS}}$. Our results can be combined with extensive simulations and the scaling properties of $g_{\overline{\rm MS}}$, in order to reach a low momentum-regime. A similar procedure can be applied to make contact with the renormalized coupling in the "Wilson gradient flow" renormalization scheme, which is being very actively investigated by a number of groups at present (e.g. QCDSF Collaboration).

Finally, in Chapter 9 we summarize and present our conclusions.

For completeness, we have included an appendix containing notation and conventions adopted in the main body of the Thesis.

Most of the results presented here have already been published in the following papers and conference proceedings:

1. M. Constantinou, M. Hadjiantonis, H. Panagopoulos, G. Spanoudes, *"Singlet versus Nonsinglet Perturbative Renormalization of Fermion Bilinears"*, Phys. Rev. D94 (2016) 114513, arXiv: 1610.06744.

2. H. Panagopoulos, G. Spanoudes, *"Singlet vs Nonsinglet Perturbative Renormalization factors of Staggered Fermion Bilinears"*, EPJ Web of Conferences 175 (Proceedings of Lattice 2017 Conference) (2017) 14004, arXiv: 1709.10447.

3. G. Spanoudes, H. Panagopoulos, *"Renormalization of Wilson-line operators in the presence of nonzero quark masses"*, Phys. Rev. D98 (2018) 014509, arXiv: 1805.01164.

4. G. Spanoudes, H. Panagopoulos, *"Perturbative investigation of Wilson-line operators in Parton Physics"*, PoS Confinement2018 094 (Conference proceedings of XIIIth Quark Confinement and the Hadron Spectrum), 2018, arXiv: 1811.03524.

5. M. Constantinou, H. Panagopoulos, G. Spanoudes, *"One-loop renormalization of staple-shaped operators in continuum and lattice regularizations"*, Phys. Rev. D99 (2019) 074508, arXiv: 1901.03862.

Chapter 2

Hadron structure on the lattice

2.1 Introduction

Among the frontiers of hadronic Physics is the investigation of the structure of hadrons from first principles. Lattice QCD is an ideal *ab initio* formulation to study hadron structure since benchmark quantities of QCD, such as hadron form factors, can be determined directly from the evaluation of hadron matrix elements without ambiguities associated to fits. The computation of these key observables within the lattice QCD formulation is a fundamental element for obtaining reliable predictions on quantities which are not easily accessible in experiments, and also on observables which explore Physics beyond the Standard Model.

Hadron structure calculations are typically based on studying two-point and three-point correlation functions defined as:

$$G^{2-\mathrm{pt}}(\overrightarrow{p}', t_f) = \sum_{\overrightarrow{x_f}} e^{-i\overrightarrow{x_f}\cdot\overrightarrow{p}'} \Gamma^0_{\beta\alpha} \langle J_\alpha(\overrightarrow{x_f}, t_f) \overline{J}_\beta(\overrightarrow{0}, 0)\rangle, \tag{2.1}$$

$$G^{3-\mathrm{pt}}_{\mathcal{O}}(\Gamma^\mu; \overrightarrow{p}', t_f; \overrightarrow{q}, t) = \sum_{\overrightarrow{x_f}, \overrightarrow{x}} e^{-i\overrightarrow{x_f}\cdot\overrightarrow{p}'} e^{i\overrightarrow{x}\cdot\overrightarrow{q}} \Gamma^\mu_{\beta\alpha} \langle J_\alpha(\overrightarrow{x_f}, t_f) \mathcal{O}(\overrightarrow{x}, t) \overline{J}_\beta(\overrightarrow{0}, 0)\rangle, \tag{2.2}$$

where $\Gamma^k \equiv \Gamma^0\gamma_5\gamma_k$ $(k = 1, 2, 3)$, $\Gamma^0 \equiv (\mathbb{1} + \gamma_0)/4$, $\mathcal{O}(\overrightarrow{x}, t)$ is a local fermion bilinear operator, $J_\alpha(\overrightarrow{x}, t)$ is a hadron interpolating operator, $(\overrightarrow{0}, 0)$, $(\overrightarrow{x}, t)$, $(\overrightarrow{x_f}, t_f)$ are the source, insertion and sink space-time coordinates, respectively, and $\overrightarrow{p}$, $\overrightarrow{q} = \overrightarrow{p}' - \overrightarrow{p}$, $\overrightarrow{p}'$ are the momentum of the initial hadron state, transfer momentum, and momentum

of the final hadron state, respectively. Physical signals are extracted from appropriate dimensionless ratios of $G^{2-\mathrm{pt}}$ and $G_{\mathcal{O}}^{3-\mathrm{pt}}$, such as:

$$R_{\mathcal{O}}(\Gamma^{\mu};\overrightarrow{p}',t_f;\overrightarrow{p},t) = \frac{G_{\mathcal{O}}^{3-\mathrm{pt}}(\Gamma^{\mu};\overrightarrow{p}',t_f;\overrightarrow{q},t)}{G^{2-\mathrm{pt}}(\overrightarrow{p}',t_f)} \times \sqrt{\frac{G^{2-\mathrm{pt}}(\overrightarrow{p}',t_f)\ G^{2-\mathrm{pt}}(\overrightarrow{p}',t)\ G^{2-\mathrm{pt}}(\overrightarrow{p},t_f-t)}{G^{2-\mathrm{pt}}(\overrightarrow{p},t_f)\ G^{2-\mathrm{pt}}(\overrightarrow{p},t)\ G^{2-\mathrm{pt}}(\overrightarrow{p}',t_f-t)}}, \quad (2.3)$$

by searching for a plateau region in the t-dependence. The above ratio is considered optimized since it does not contain potentially noisy two-point functions at large separations and because correlations between its different factors reduce the statistical noise. From three-point correlation functions one extracts matrix elements of fermion bilinear operators, which can be parametrized in terms of generalized form factors, e.g.,

$$\langle N(p',s')|\overline{\psi}(x)\gamma_\mu\gamma_5\psi(x)|N(p,s)\rangle \sim \overline{u}_N(p',s')[G_A(q^2)\gamma_\mu\gamma_5 + G_P(q^2)\frac{q_\mu\gamma_5}{2m_N}]u_N(p,s). \quad (2.4)$$

A number of observables probing hadron structure can be derived by the calculation of hadron form factors, such as axial charge, quark momentum fraction, Dirac and Pauli radii, nucleon spin and parton distributions. In this work, our calculations focus on nucleon spin content and parton distributions.

2.2 Nucleon spin

An important open issue in hadronic Physics is the nucleon spin structure; the question of how the nucleon spin is distributed amongst its constituent particles is still unsolved. The original interpretation of this puzzle was that valence quarks carry all of the nucleon spin; since the proton is a stable particle, it exists in the lowest possible energy level. This means that its quark wave function is in the s-orbital ground state, which is spherically symmetric with no spatial contribution to its angular momentum. Thus, the proton spin is expected to be equal to the sum of the constituent quark spin. As the magnitude of proton spin is 1/2, it was assumed that two of the valence quarks have their spins parallel to the proton spin, while the third one is polarized in the opposite direction. However, in 1987 DIS experiments of European Muon Collaboration at

CERN showed that only a small amount of the proton spin was actually carried by the valence quarks [56]. The problem of where the missing spin lies was called "the proton spin crisis". More recent experiments have tried to resolve this problem; we now know that a part of the nucleon spin is carried by polarized gluons and sea quarks. Also, the orbital angular momentum of both quarks and gluons contributes to the total nucleon spin. These facts are expressed by the sum rule [57, 58]:

$$\frac{1}{2} = \sum_q (L^q + \frac{1}{2}\Delta\Sigma^q) + J^g, \tag{2.5}$$

where L^q is the total quark orbital angular momentum, $\Delta\Sigma^q/2$ is the total quark spin and J^g is the total gluon angular momentum (spin + orbital angular momentum). Therefore, it is understood that the complete picture of the spin content of a nucleon requires to take into account its nonperturbative structure. Lattice calculations can strongly contribute to this direction of research.

The individual quark contributions (valence and see quarks) to the nucleon spin can be determined by the evaluation of nucleon matrix elements of local fermion bilinear operators; in particular, the total sum of the quark spin equals to the axial charge g_A^q: $\Sigma^q = g_A^q$. This quantity is defined by the forward matrix element of the axial current. There are two types of diagrams entering the evaluation of nucleon matrix elements, shown in Fig. 2.1: connected and disconnected[1] diagrams of three-point correlation functions of local fermion bilinear operators. The axial charge is defined

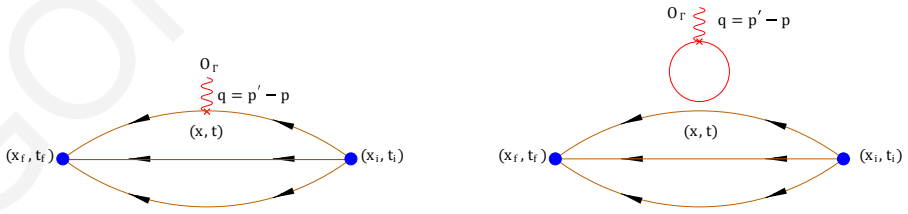

FIGURE 2.1: Connected (left) and disconnected (right) contributions to the nucleon three-point function.

as $g_A^q = G_A^q(0)$, where $G_A^q(q^2)$ is the axial form factor given in Eq. (2.4). While matrix elements of connected diagrams can be evaluated nonperturbatively with quite good precision, the disconnected ones are notoriously difficult to study via numerical

[1]It is called disconnected diagram because there is a fermion loop, which is not directly connected to the external points; however, as the diagram involves full propagators, it includes also virtual gluons emmited and absorbed from the fermion lines. In this sense, all elements of this diagram are connected with each other.

simulations; in principle, disconnected diagrams require the nonperturbative evaluation of the full fermion propagator, which is a very noisy and expensive to compute task. During the last few years various stochastic noise reduction techniques (see e.g., [59] and references therein) have been employed for the computation of the disconnected loop and first results already appear in the literature [60–64]. Also, an alternative method for the calculation of the matrix elements of local fermion bilinear operators, which avoids the direct evaluation of the noisy disconnected diagram, is the Feynman-Hellmann approach [65, 66].

In order to establish connection to experiments, proper renormalization of the matrix elements is essential. For the renormalization of disconnected contributions one should take into account the flavor singlet operators. For example, the knowledge of the axial singlet renormalization factor is required to compute the light quarks' contribution to the nucleon spin [67]. Given that the renormalization factors of the nonsinglet operators can be calculated nonperturbatively with quite good precision, we can combine the perturbative result of the difference between the renormalization factors of singlet and nonsinglet operators with the nonperturbative nonsinglet estimates of Z-factors, in order to renormalize the disconnected contributions. The computation of this difference at two-loop level using improved staggered actions is presented in Chapter 6.

2.2.1 Renormalization of local operators

Matrix elements of local operators appear often in quantum field theory calculations. A plethora of hadronic properties, such as hadron masses and decay constants, can be extracted by matrix elements and correlation functions of composite quantum field operators. A whole variety of such operators, made out of quark fields, has been considered and studied in numerical simulations on the lattice, including local bilinears $\bar{\psi}(x)\Gamma\psi(x)$, extended bilinears $\bar{\psi}(x)\Gamma D_\mu D_\nu \ldots \psi(x)$, and four-fermi operators $(\bar{\psi}\Gamma_1\psi)(\bar{\psi}\Gamma_2\psi)$, where Γ (and Γ_1, Γ_2) $= \mathbb{1}$, γ_5, γ_μ, $\gamma_5\gamma_\mu$, $\sigma_{\mu\nu}$ ($\sigma_{\mu\nu} = [\gamma_\mu, \gamma_\nu]/2i$). In particular, fermion bilinear operators are related to conserved fermion currents appearing in calculations of mass spectrum, form factors and structure functions of hadrons. Extended bilinear operators, including covariant derivatives, are related to the moments of unpolarized, helicity and transversity parton distributions. An example of such extended operators is the energy-momentum tensor, e.g., $\bar{\psi}\gamma_{\{\mu}D_{\nu\}}(\tau^a/2)\ \psi$ (curly brackets denote symmetrization and subtraction of the trace;

τ^a are flavor matrices), whose matrix elements are connected with the anomalous magnetic moment of the muon. Four-fermi operators are related to the transition amplitudes between hadronic states. A proper renormalization of these operators is essential for the extraction of physical results from the dimensionless quantities measured in numerical simulations.

An issue that arises in studying renormalization of local operators is whether the latter is multiplicative or if mixing occurs. Operators with the same quantum numbers and the same or lower mass dimension, can mix due to quantum corrections. In general, action symmetries (e.g. C, P, T symmetries) can restrict the operator mixing: operators which have a different behavior under symmetry transformations cannot mix. Admissible candidates for mixing are operators which either are gauge invariant, or BRS-variations, or vanishing by the equation of motion. On the lattice, where some symmetries (e.g. rotational invariance) possessed by continuum theories are restored only asymptotically, mixing is far more pronounced than in continuum regularization schemes. For instance, operator mixing is exacerbated when using lattice actions with inexact chiral symmetry; in this case operators with different chiralities can mix. In the case of fermion bilinear operators of dimension 3, there is no mixing (except flavor singlet scalar operator $\sum_f \bar{\psi}_f \mathbb{1} \psi_f$, f: flavor content), and, thus, they can be multiplicatively renormalized. The flavor singlet scalar operator mixes with the identity at the quantum level since it has a nonzero perturbative vacuum expectation value; thus it receives also an additive renormalization which subtracts its vacuum expectation value. In the case of higher dimensional fermion operators, such as bilinear operators with covariant derivatives and four-fermi operators, a complicated mixing pattern is induced. Therefore, the perturbative computation of the mixing matrices for the renormalization of such operators is essential, in order to disentangle as much as possible the corresponding physical signals from Monte Carlo measurements.

2.3 Parton distributions on the lattice

Parton distributions are an essential tool for studying the rich internal structure of hadrons. They encode the distribution of a hadron's momentum and spin among its constituent parts (called partons), in a reference frame where the hadron has infinite

momentum. In such a frame the momentum of the parton is almost collinear with the hadron momentum, so that the hadron can be seen as a stream of free partons, each carrying a fraction of the longitudinal momentum. The parton model was originally introduced by Richard Feynman in 1969 as a way to analyze high-energy hadron collisions [68, 69]. After the validation of quark model and the consolidation of the confining theory of Quantum Chromodynamics (QCD), partons were matched to the fundamental particles: quarks, antiquarks and gluons. Since then parton distributions are widely employed in collider experiments for interpreting the showers of radiation produced from QCD processes.

There are three categories of parton distributions based on their dependence on variables defined in the longitudinal and transverse directions with respect to the hadron momentum:

1. Parton distribution functions (PDFs) are single-variable functions which represent the number density of partons carrying a given fraction x of the longitudinal hadron momentum, while the hadron is moving with a large (infinite-limit) momentum. For example, the quark PDFs are defined as:

$$q_{\Gamma}(x) \ = \int_{-\infty}^{\infty} \frac{dz^-}{4\pi} \exp(-ixP^+z^-) \Big\langle N \Big| \overline{\psi}(z^-) \ \Gamma \ W(z^-,0)\psi(0) \Big| N \Big\rangle, \tag{2.6}$$

   where $W(z^-,0)$ is the Wilson line, which joins the light-like separated quark and antiquark fields together, given by:

$$W(z^-,0) \ = \mathcal{P}\Big\{ \exp\Big[-ig \int_0^{z^-} d\eta^- A^+(\eta^-) \Big] \Big\}, \tag{2.7}$$

   $z^{\pm} \equiv (z^0 \pm z^i)/\sqrt{2}$ and $P^{\pm} \equiv (P^0 \pm P^i)/\sqrt{2}$ are the light-cone space and momentum coordinates of a hadron moving to the i$^{\text{th}}$ direction, respectively, x is the fraction of the hadron momentum carried by each constituent parton, $\Big| N \Big\rangle$ is a hadron state, and $\Gamma = \gamma^+, \gamma_5\gamma^+, \gamma^+\gamma^\perp$ (where $\gamma^+ \equiv (\gamma^0 + \gamma^i)/\sqrt{2}$ and $\gamma^\perp \cdot \gamma^+ = 0$) corresponds to the unpolarized, helicity and transversity types of PDFs respectively.

2. Generalized parton distributions (GPDs) [58, 70–73] are a generalization of PDFs, which involve off-diagonal matrix elements of parton fields at a light-like separation. They depend on two additional kinematic variables, besides the

fraction x: $t \equiv \Delta^2$ and $\xi \equiv -2\Delta^+/\overline{P}$, where $\overline{P} \equiv (P + P')/2$, $\Delta \equiv P' - P$, and $P(P')$ is the incoming (outgoing) hadron momentum. While PDFs provide information on the one-dimensional structure of a hadron (in the longitudinal direction with respect to the hadron momentum), GPDs contribute to the whole three-dimensional hadron picture. For example, the definition of the quark GPDs is given below:

$$F^q_\Gamma(x,\xi,t) = \int_{-\infty}^{\infty} \frac{dz^-}{4\pi} \exp(ix\overline{P}^+ z^-) \Big\langle N' \Big| \overline{\psi}\Big(-\frac{z^-}{2}\Big)\, \Gamma\, W\Big(-\frac{z^-}{2}, \frac{z^-}{2}\Big) \psi\Big(\frac{z^-}{2}\Big) \Big| N \Big\rangle \Big|_{\substack{z^+=0,\\ z^T=0}}. \tag{2.8}$$

3. Transverse-momentum dependent parton distribution functions (TMDs) [74–77] are also a generalization of PDFs, which involve the transverse momentum k_T of the parton to the hadron's direction of movement. They complement the GPDs picture of the three-dimensional hadron structure. For example, the quark TMDs are defined as:

$$\Phi^q_\Gamma(x,k_T) = \int_{-\infty}^{\infty} \frac{d^2 z^T}{(2\pi)^2} \int_{-\infty}^{\infty} \frac{dz^-}{4\pi} \exp(ixP^+ z^- - ik^T \cdot z^T) \cdot \Big\langle N \Big| \overline{\psi}(0)\, \Gamma\, W[0, \pm\infty, (z^-, z^T)] \psi(z^-, z^T) \Big| N \Big\rangle \Big|_{z^+=0}, \tag{2.9}$$

where z^T is the transverse space coordinates to the $z^\pm$. The path of the Wilson line $W[0, \pm\infty, (z^-, z^T)]$, which connects the quark and antiquark fields, can be a product of two subsequent Wilson lines from 0 to infinity and back from infinity to (z^-, z^T). Another way of parametrizing this Wilson line is to take a staple-shaped link with its vertical segments having infinite length.

Important information is still missing for all three types of distributions: The most well-studied are PDFs, while GPDs and TMDs are only very limitedly studied due to the difficulty in extracting them experimentally and theoretically. All these functions are crucial for the complete understanding of the three-dimensional structure of hadrons.

Parton distributions have the advantage of being process-independent; this means that measurements from different processes can give information on these quantities. They have also the advantage of being accessible both experimentally and theoretically. Ever since the discovery of quarks in the nucleon, tremendous experimental effort and resources have been devoted to the measurement of the detailed distribution of quarks and gluons in the hadrons. According to QCD

factorization theorems [78], the cross section for a hard scattering process can be factorized as convolution of a partonic cross section, which is analytically calculable in perturbative QCD, and a parton distribution: PDFs are accessed in inclusive or semi-inclusive processes, such as deep inelastic scattering (DIS) and semi-inclusive DIS (SIDIS)[79]; GPDs are reached in exclusive scattering processes, such as deeply virtual Compton scattering (DVCS) [80], and TMDs in hard processes in SIDIS [75, 76]. Global analyses of cross section data [81–90] from high-energy experiments have provided precise results for parton distributions for certain cases of parton flavors, spin structures and kinematic regions. However, a complete picture of parton distributions is yet to be achieved due to several limitations in the experimental programs or in the phenomenological models, e.g., the very small x-region is difficult to access from experiments [91–93] and models cannot capture the full QCD dynamics. Theoretical investigations of parton distributions from first principles are possible candidates to overcome these limitations and, thus, they are expected to provide complementary information in this area of research. The development of a theoretical systematic approach for calculating parton distributions leads to a faster and less expensive way of improving the precision of such computations than the construction of more advanced and powerful colliders. Lattice QCD simulations are the only current tool for such *ab-initio* investigations.

Because of the highly nonlinear nature of the parton dynamics, parton distributions can be fully evaluated only with nonperturbative methods, such as lattice simulations. However, they are light-cone correlation functions, and thus their time dependence does not allow the direct computation of parton distributions on a Euclidean lattice. This led to a long history of investigations of alternative quantities related to the distribution functions, which are accessible in a Euclidean spacetime. Such quantities are the Mellin moments of parton distributions; using the operator product expansion (OPE), the distribution functions can be parametrized in terms of local operators with covariant derivatives which give their moments. First moments of PDFs have been computed accurately in Refs. [94–97], via calculations of matrix elements of local operators in lattice simulations. These moments are directly related to measurable quantities, for example, the axial charge and quark momentum fraction. However, a precise calculation of higher moments is extremely difficult to obtain via lattice simulations: Signal-to-noise ratio decreases with the addition of covariant derivatives in the operators and an unavoidable power-law mixing under renormalization appears

for higher moments. Hence, the reconstruction of the full parton distributions from their moments is practically unfeasible.

2.3.1 Quasi-PDFs approach

Novel approaches for an *ab initio* evaluation of distribution functions on the lattice have been employed in recent years. Such an approach is "quasi-PDFs", proposed by X. Ji [98]. This method is summarized in three steps:

1. First, instead of computing light-cone correlation functions, one projects outside of the light cone and considers equal-time correlation functions, which are called quasi-distribution functions. For example, the definition of parton quasi-distribution functions (quasi-PDFs) is:

$$\widetilde{q}_\Gamma(x,\mu,P_\mu) \;= \int_{-\infty}^{\infty} \frac{dz}{4\pi} e^{-ixP_\mu z} \Big\langle N \Big| \overline{\psi}(z)\; \Gamma\; W(z,0)\psi(0) \Big| N \Big\rangle, \tag{2.10}$$

   where

$$W(z,0) \;= \mathcal{P}\Big\{ \exp\Big[-ig \int_0^z d\zeta A_\mu(\zeta) \Big] \Big\} \tag{2.11}$$

   and $\Gamma = \gamma_\mu, \gamma_5\gamma_\mu, \gamma_\mu\gamma_\perp$. These functions are purely spatial and thus they are accessible on the lattice. We note that the Wilson line involved in quasi-PDFs is a straight line in a spatial direction μ.

2. The second step is the renormalization of quasi-distribution functions. Since these functions are calculable on the lattice, one can renormalize them nonperturbatively in the lattice regularization, using a Regularization-Independed (RI′)-like scheme [99, 100]. The lattice version of the straight Wilson line is given by $W(z,0) = \Big(\prod_{\ell=0}^{n\mp 1} U_{\pm\mu}(\ell a\hat{\mu}) \Big)^\dagger$, $n \equiv z/a$, where upper (lower) signs correspond to $n > 0$ ($n < 0$).

3. The last step is the matching of the renormalized quasi distributions to the corresponding physical light-cone distributions, using the Large Momentum Effective Field Theory (LaMET) [101]. The generic matching formula for

quasi-PDFs is:

$$q\left(x,\mu\right) = \tilde{q}(x,\mu,P_\mu) - \frac{\alpha_s(\mu)}{2\pi}\,\tilde{q}(x,\mu,P_\mu)\,\delta Z^{(1)}\left(\frac{\mu}{P_\mu}\right) - \frac{\alpha_s(\mu)}{2\pi}\int_{-\infty}^{\infty} Z^{(1)}\left(\xi,\frac{\mu}{P_\mu}\right)\tilde{q}\left(\frac{x}{\xi},\mu,P_\mu\right)\frac{d\xi}{|\xi|} + \mathcal{O}(\alpha_s^2), \quad (2.12)$$

where $\alpha_s(\mu)$ is the strong coupling constant at the scale μ and $Z^{(1)}$ ($\delta Z^{(1)}$) is the one-loop difference between vertex (wave function) corrections for the finite and infinite momentum cases. The matching can also be performed using an intermediate step of converting the RI′-renormalized quasi distribution to the $\overline{\text{MS}}$ scheme (commonly used in phenomenology) and after that matching to the physical distribution.

The application of Ji's approach on the lattice is currently under investigation by many research groups and so far the outcomes are very promising for the correct estimate of a physical distribution function. Exploratory lattice simulations [102–111], as well as perturbative one-loop calculations [112–114] of quasi-PDFs for the unpolarized, helicity, and transversity cases, have been performed. Furthermore, perturbative calculations of the matching between quasi-PDFs and physical PDFs have been implemented in Refs.[101, 115–120]; a discussion about subtleties on the continuation of PDFs to the Euclidean region can be found in Refs.[112, 121–123]. The quasi-PDF framework is also applied to TMDs [124–130], GPDs [131, 132], hadronic light-cone distribution amplitudes (DA) [133–137], and proton spin structure [138]. An overview of recent progress in the study of quasi-PDFs can be found in Ref. [139]. The increasing progress in studying these functions on the lattice has led to more and more reliable results. However, many theoretical and technical challenges are still needed to be overcomed.

2.3.2 Renormalization of nonlocal Wilson-line operators

An important issue, which needs to be addressed in order to obtain meaningful results from lattice investigations, is the renormalization of quasi-distribution functions in a fully nonperturbative manner. This can be obtained by the renormalization of the corresponding nonlocal operator $\mathcal{O}^z_\Gamma$, which is involved in the definition of Eq. (2.10):

$$\mathcal{O}^z_\Gamma = \bar{\psi}(z)\Gamma\mathcal{P}\left\{\exp\left(\mathrm{i}g\int_0^z d\zeta A_\mu(\zeta)\right)\right\}\psi(0), \quad (2.13)$$

where $\Gamma = \mathbb{1}, \gamma_5, \gamma_\mu, \gamma_\nu, \gamma_5\gamma_\mu, \gamma_5\gamma_\nu, \gamma_\mu\gamma_\nu, \gamma_\nu\gamma_\rho,\ \mu \neq \nu \neq \rho \neq \mu$, and z is the Wilson line's length; the presence of a Wilson line ensures the gauge invariance of the nonlocal operator. While local operators have been used extensively in perturbative and nonperturbative calculations, nonlocal operators were limitedly studied. In particular, calculations using nonlocal operators with Wilson lines in a variety of shapes appear in the literature within continuum perturbation theory.

Starting from the seminal work of Mandelstam [140], Polyakov [141], Makeenko-Migdal [142], there have been investigations of the renormalization of Wilson loops for both smooth [143] and nonsmooth [144] contours. Due to the presence of the Wilson line, power-law divergences arise for cutoff regularized theories, such as lattice QCD. These divergences can be eliminated to all orders in perturbation theory, by an exponential renormalization factor that depends on the length L of the contour and the ultraviolet cutoff scale a: $Z \sim \exp(-c\ L/a)$, where c is a dimensionless quantity. Also, contours containing singular points [144], such as cusps and self-intersections, introduce additional multiplicative renormalization factors. In the case of dimensional regularization and in the absence of cusps and self-intersections, it has been proven that all divergences in Wilson loops can be reabsorbed into a renormalization of the coupling constant [143]. Wilson-line operators have been further studied in continuum theory with a number of approaches, including an auxiliary-field formulation [145, 146], and the Mandelstam formulation [147]. Particular studies of Wilson-line operators with cusps in one and two loops, can be found in Refs. [144, 148, 149]. There is also related work, in the context of the heavy quark effective theory (HQET)[2] [151–154], including investigations in three loops [155].

In recent years, several aspects of the properties of nonlocal Wilson-line operators have been addressed, including the feasibility of a calculation from lattice QCD [102, 105, 107, 110], their renormalizability [113, 156–161] and appropriate renormalization prescriptions [99, 114, 162]. The renormalization has proven to be a challenging and delicate process in which a number of new features emerge, as compared to the case of local operators: power-law divergences (as in continuum), mixing between operators with different Dirac structures and the matrix elements contain an imaginary part. While information on physical quantities is obtained from hadron matrix elements, calculated nonperturbatively in numerical simulations of

[2]The interrelation between Wilson-line operators and HQET currents is demonstrated in Ref. [150].

lattice QCD, perturbation theory played a crucial role in the development of a complete renormalization prescription. Perturbative calculations can reveal possible mixing with operators of equal or lower dimension, which must be taken into account in the nonperturbative renormalization prescriptions. In this case, the nonlocality of Wilson-line operators combined with a chiral-symmetry breaking lattice action lead to the appearance of finite mixing. Also, nonperturbative evaluations of the renormalization factors cannot be obtained directly in the $\overline{\text{MS}}$ scheme, which is typically used in phenomenology, since the definition of $\overline{\text{MS}}$ is perturbative in nature. Most naturally, one calculates them in a RI′-like scheme, and then introduces the corresponding conversion factors between RI′ and $\overline{\text{MS}}$ schemes, which rely necessarily on perturbation theory.

The first perturbative lattice calculation of Wilson-line operators was made in Ref. [114], to one loop for massless quarks, using the Wilson/clover fermion action and a variety of Symanzik-improved gluon actions. It was shown that besides the presence of logarithmic and linear divergences, similar to those expected from the continuum, finite mixing is also present among operators of twist-2 and twist-3, i.e. there are 4 mixing pairs between operators with the following Dirac matrices: $(\mathbb{1}, \gamma_1)$, $(\gamma_5\gamma_2, \gamma_3\gamma_4)$, $(\gamma_5\gamma_3, \gamma_4\gamma_2)$, and $(\gamma_5\gamma_4, \gamma_2\gamma_3)$, where by convention 1 is the direction of the straight Wilson line and 2, 3, and 4 are directions perpendicular to it. The complete mixing pattern led to the proposal of a nonperturbative RI-type scheme [99, 163], also employed in Ref. [100]. In this scheme, the elimination of both linear and logarithmic divergences is ensured by the same renormalization condition. This development of the renormalization of nonlocal operators has been a crucial aspect in state-of-the-art numerical simulations, e.g. the work of Refs. [164, 165]. There are also other attempts for renormalizing the straight-line operators or directly the quasiPDFs nonperturbatively, using alternative techniques, such as the static quark potential [115, 166, 167], the gradient flow [168–170] and the auxiliary-field formalism [118, 146, 158, 159, 171]. This perturbative calculation was the starting point and the inspiration for further studies of Wilson-line operators leading to a number of extensions with the goal of improving current nonperturbative investigations. Such extensions are:

- The one-loop calculation of Green's functions at a nonzero fermion mass. The inclusion of nonzero quark masses can cause perceptible changes in the renormalization of heavy-quark quasi-PDFs, as simulations cannot be

performed exactly at zero renormalized mass; these changes includes the operator-mixing pattern. The calculation of the conversion factors between a massive RI′ and $\overline{\text{MS}}$ schemes, appropriate for such nonlocal operators, has been studied by our group and it is presented in Chapter 3.

- The one-loop study of the renormalization for staple-shaped operators both in continuum and lattice regularizations. After the work of Ref. [114] on straight Wilson-line operators, in which operator mixing was revealed, the question of whether nonlocal operators with staple-shaped Wilson lines renormalize multiplicatively was raised. These operators are involved in a Euclidean formulation of TMDs, which are currently under investigation for the nucleon and pion in lattice QCD [125, 126, 128]. Our work on staple operators is presented in Chapter 4.

- The higher-loop calculation of the conversion factors between RI′ and $\overline{\text{MS}}$ schemes. Such calculations can eliminate systematic uncertainties related to the truncation of the conversion factor applied to nonperturbative data. The two-loop calculation for straight Wilson-line operators has been performed by our group and it is described in Chapter 5.

- The calculation of the one-loop lattice artifacts to all orders in the lattice spacing. Such a procedure has been successfully employed to local operators [67-69]. The subtraction of the unwanted contributions of the finite lattice spacing from the nonperturbative estimates is essential in order to reduce large cut-off effects in the renormalized Green's functions of the operators and to guarantee a rapid convergence to the continuum limit. A preliminary work on the lattice artifacts of straight Wilson-line operators has been performed by M.Constantinou and H. Panagopoulos. This project is beyond the scope of the current thesis.

2.3.3 Other approaches

For completeness, we note that there are also alternative approaches for extracting physical PDFs on the lattice, which are currently under investigation, e.g., Ioffe-time distributions (called pseudo-PDFs) [172–175], in which the same Wilson-line operators are involved as in the case of quasi-PDFs, Compton amplitudes utilizing the operator product expansion [176], and "lattice cross sections" [115, 177].

Chapter 3

Perturbative renormalization of nonlocal operators related to heavy-quark quasi-PDFs

3.1 Introduction

Parton quasi-distribution functions (quasi-PDFs) are nowadays widely employed in the nonperturbative study of hadron structure in lattice QCD. So far, they have been studied from many points of view. Several aspects are being investigated both perturbatively and nonperturbatively, using various techniques (see a review in Ref. [178]). An important issue, which needs to be addressed in order to obtain meaningful results from lattice investigations, is the renormalization of quasi-PDFs in a fully nonperturbative manner. Given that quasi-PDFs are directly related to the matrix elements of nonlocal Wilson-line operators, the renormalization of quasi-PDFs can be obtained by the renormalization of the corresponding operator. To date, all lattice studies of the renormalization of Wilson-line operators have only considered massless fermions, expecting that the presence of quark masses can cause only imperceptible changes; this is indeed a reasonable assumption for light quarks. However, for heavy quarks this statement does not hold. In addition, simulations cannot be performed exactly at zero renormalized mass. One could, of course, adopt a zero-mass renormalization scheme even for heavy quarks, but such a scheme is less direct and entails additional complications. Thus, it would be useful to investigate

the significance of finite quark masses on the renormalization of Wilson-line operators. This is the goal of the present work.

In this work, we calculate the conversion factors from RI′ to the $\overline{\text{MS}}$ scheme, in dimensional regularization (DR) at one-loop level for massive quarks. The conversion factors can be combined with the regularization independent (RI′)-renormalization factors of the operators, computed in lattice simulations, in order to calculate the nonperturbative renormalization of these operators in $\overline{\text{MS}}$. Nonperturbative evaluations of the renormalization factors cannot be obtained directly in the $\overline{\text{MS}}$ scheme, since the definition of $\overline{\text{MS}}$ is perturbative in nature; most naturally, one calculates them in a RI′-like scheme, and then introduces the corresponding conversion factors between RI′ and the $\overline{\text{MS}}$ scheme, which rely necessarily on perturbation theory. Given that the conversion between the two renormalization schemes does not depend on regularization, it is more convenient to evaluate it in DR. Thus, the perturbative calculation of conversion factors is an essential ingredient for a complete study of quasi-PDFs. This work is a continuation of Ref. [114], in which, among other results, one-loop conversion factors of Wilson-line operators are presented for the case of massless quarks.

In studying composite operators, one issue which must be carefully addressed is that of possible mixing with other similar operators. Many possibilities are potentially present for the nonlocal operators which we study:

(A) Operators involving alternative paths for the Wilson line joining the quark pair will not mix among themselves, as demonstrated in Ref. [146] (and also in Refs. [143, 144] for the case of closed Wilson loops). This property is related to translational invariance and is similar to the lack of mixing between a local composite operator $\mathcal{O}(x)$ with $\mathcal{O}(y)$. Given that a discrete version of translational invariance is preserved on the lattice, nonlocal operators involving different paths should not mix also on the lattice.

(B) Operators involving only gluons will also not mix. This can be seen, e.g., via the auxiliary field approach (e.g., Ref. [146]); as a specific case, the operator of Eq. (3.1) cannot mix with an operator containing the gluon field strength tensor in lieu of the quark fields (joined by a Wilson line in the adjoint representation), since this operator is higher dimensional.

(C) There may also be mixing among operators with different flavor content in a RI′ scheme, depending on the scheme's precise definition. However, the mixing is expected to be at most finite and thus not present in the $\overline{\text{MS}}$ scheme; by comparing to the massless case, in which exact flavor symmetry allows no such mixing, the difference between the massive and massless case will bear no superficial divergences, since the latter are UV regulated by the masses. The auxiliary field approach, by involving only composite operators in the (anti-)fundamental representation of the flavor group, shows that no flavor mixing needs to be introduced.

Even in the absence of quark masses, bare Green's functions of Wilson-line operators may contain finite, regulator-dependent contributions which cannot be removed by a simple multiplicative renormalization; as a consequence, an appropriate (i.e., regularization-independent) choice of renormalization prescription for RI' necessitates the introduction of mixing matrices for certain pairs of operators [114], both in the continuum and on the lattice. The results of the present work demonstrate that the presence of quark masses affects the observed operator-mixing pairs, due to the chiral-symmetry breaking of mass terms in the fermion action. Compared to the massless case on the lattice [114], the mixing pairs remain the same for operators with equal masses of external quark fields, i.e., $(\mathbb{1}, \gamma_1)$, $(\gamma_5\gamma_2, \gamma_3\gamma_4)$, $(\gamma_5\gamma_3, \gamma_4\gamma_2)$, and $(\gamma_5\gamma_4, \gamma_2\gamma_3)$, where by convention 1 is the direction of the straight Wilson line and 2, 3, and 4 are directions perpendicular to it. However, for operators with different masses of external quark fields, flavor-symmetry breaking leads to additional mixing pairs: $(\gamma_5, \gamma_5\gamma_1)$, $(\gamma_2, \gamma_1\gamma_2)$, $(\gamma_3, \gamma_1\gamma_3)$, and $(\gamma_4, \gamma_1\gamma_4)$. As a consequence, the conversion factors are generally nondiagonal 2×2 matrices. This is relevant for disentangling the observed operator mixing on the lattice. Also, comparing the massive and the massless cases, the effect of finite mass on the renormalization of Wilson-line operators becomes significant for strange quarks, as well as for heavier quarks. These are features of massive quasi-PDFs, which must be taken into account in their future nonperturbative study.

The outline of this chapter is as follows. In Sec. 3.2 we provide the theoretical setup related to the definition of the operators which we study, along with the necessary prescription of the renormalization schemes. Sec. 3.3 contains our results for the bare Green's functions in DR, the renormalization factors, as well as the conversion factors

of these operators between the renormalization schemes. Also, a discussion on technical aspects, such as the methods that we used to calculate the momentum-loop integrals, as well as the limits of vanishing regulator and/or masses, is provided in this section. In Sec. 3.4, we present several graphs of the conversion factor matrix elements for certain values of free parameters. Finally, in Sec. 3.5, we summarize and conclude.

We have also included an appendix; a list of Feynman parameter integrals, which appear in the expressions of our results, is relegated to Appendix 3.A.

3.2 Theoretical Setup

3.2.1 Definition of Wilson-line operators

The Wilson-line operators are defined by a quark and an antiquark field in two different positions, a product of Dirac gamma matrices and a path-ordered exponential of the gauge field (called Wilson line), which joins the fermion fields together, in order to ensure gauge invariance. For simplicity, we choose the Wilson line to be a straight path of length z in the μ direction[1]; thus, the operators have the form:

$$\mathcal{O}_\Gamma = \bar{\psi}(x)\Gamma\mathcal{P}\left\{ \exp\left(\mathrm{i}g \int_0^z d\zeta A_\mu(x+\zeta\hat{\mu}) \right) \right\}\psi(x+z\hat{\mu}), \tag{3.1}$$

where $\Gamma = \mathbb{1}$, γ_5, γ_μ, γ_ν, $\gamma_5\gamma_\mu$, $\gamma_5\gamma_\nu$, $\gamma_\mu\gamma_\nu$, $\gamma_\nu\gamma_\rho$, $\mu \neq \nu \neq \rho \neq \mu$, and z is the length of the Wilson line; $\gamma_5 = \gamma_1\gamma_2\gamma_3\gamma_4$. The quark and antiquark fields may have different flavors: ψ_f and $\bar{\psi}_{f'}$; flavor indices will be implicit in what follows. Operators with $\Gamma = (\gamma_\mu \text{ or } \gamma_\nu)$, $(\gamma_5\gamma_\mu \text{ or } \gamma_5\gamma_\nu)$, $(\gamma_\mu\gamma_\nu \text{ or } \gamma_\nu\gamma_\rho)$ correspond to the three types of PDFs: unpolarized, helicity, and transversity, respectively.

3.2.2 Definition of renormalization schemes

Taking into account the presence of nonzero fermion masses in our calculations, we adopt mass-dependent prescriptions for the renormalization of Wilson-line operators.

[1]For the sake of definiteness, we will often choose $\mu = 1$ in the sequel.

We define the renormalization factors which relate the bare $\mathcal{O}_\Gamma$ with the renormalized operators $\mathcal{O}_\Gamma^R$ via[2]

$$\mathcal{O}_\Gamma^R = Z_\Gamma^{-1}\mathcal{O}_\Gamma. \tag{3.2}$$

[In the presence of operator mixing, this relationship is appropriately generalized; see Eq. (3.8)]. The corresponding renormalized one-particle irreducible (1-PI) amputated Green's functions of Wilson-line operators $\Lambda_\Gamma^R = \langle \psi^R \, \mathcal{O}_\Gamma^R \, \bar{\psi}^R \rangle_{amp}$ are given by

$$\Lambda_\Gamma^R = Z_{\psi_f}^{1/2} Z_{\psi_{f'}}^{1/2} \, Z_\Gamma^{-1} \Lambda_\Gamma, \tag{3.3}$$

where $\Lambda_\Gamma = \langle \psi \, \mathcal{O}_\Gamma \, \bar{\psi} \rangle_{amp}$ are the bare amputated Green's functions of the operators and Z_{ψ_f} is the renormalization factor of the fermion field with flavor f, defined by $\psi_f^R = Z_{\psi_f}^{-1/2} \psi_f$ [$\psi_f(\psi_f^R)$ is the bare (renormalized) fermion field]. In the massive case, renormalization factors of the fermion and antifermion fields appearing in bilinear operators of different flavor content may differ among themselves, as the fields have generally different masses.

3.2.2.1 Renormalization conditions for fermion fields and masses

At this point, we provide the conditions for the mass-dependent renormalization of fermion fields, as well as the multiplicative renormalization of fermion masses: $m^R = Z_m^{-1} m^B$ [m^B (m^R) are the bare (renormalized) masses for each flavor]; the latter is not involved in our calculations, but we include it for completeness.

In $\overline{\text{MS}}$, renormalization factors Z_ψ of the fermion field and Z_m of the fermion mass must contain, beyond tree level, only negative powers of ε (the regulator in DR in D dimensions, $D \equiv 4-2\varepsilon$); their values are fixed by the requirement that the renormalized fermion self-energy be a finite function of the renormalized parameters $m^{\overline{\text{MS}}}$ and $g^{\overline{\text{MS}}}$ ($g = \mu^\varepsilon Z_g g^{\overline{\text{MS}}}$; μ is a dimensionful scale):

$$\langle \psi^{\overline{\text{MS}}} \bar{\psi}^{\overline{\text{MS}}} \rangle = \lim_{\varepsilon \to 0} \left(Z_\psi^{-1} \langle \psi \bar{\psi} \rangle \Big|_{\substack{g = \mu^\varepsilon Z_g g^{\overline{\text{MS}}} \\ m^B = Z_m m^{\overline{\text{MS}}}}} \right). \tag{3.4}$$

[2] All renormalization factors, generically labeled Z, depend on the regularization X (X = DR, LR, etc.) and on the renormalization scheme Y ($Y = \overline{\text{MS}}$, RI′, etc.) and should thus properly be denoted as $Z^{X,Y}$, unless this is clear from the context.

In RI′, convenient conditions for the fermion field of a given flavor and the corresponding mass are

$$Z_\psi^{X,RI'}\ \mathrm{tr}\Big(-i\not{q}\langle\psi\bar{\psi}\rangle^{-1}\Big)\Big|_{q_\nu=\bar{q}_\nu} = 4N_c\ \bar{q}^2, \tag{3.5}$$

$$Z_\psi^{X,RI'}\ \mathrm{tr}\Big(\mathbb{1}\langle\psi\bar{\psi}\rangle^{-1}\Big)\Big|_{q_\nu=\bar{q}_\nu} = 4N_c\ m^{\mathrm{RI}'} = 4N_c\ (Z_m^{X,RI'})^{-1} m^B, \tag{3.6}$$

where $\bar{q}_\nu$ is the RI′ renormalization scale 4-vector, $m^{\mathrm{RI}'}$ is the RI′-renormalized fermion mass, N_c is the number of colors, and the symbol X can be any regularization, such as DR or lattice. These conditions are appropriate for lattice regularizations which do not break chiral symmetry, so the Lagrangian mass m_0 coincides with the bare mass m^B, e.g., staggered/overlap/domain wall fermions. For regularizations which break chiral symmetry, such as Wilson/clover fermions, a critical mass m_c is induced; one must first find the value of m_c by a calibration in which one requires that the renormalized mass for a "benchmark" meson attains a desired value, e.g., zero pion mass, and then set $m^B = m_0 - m_c$.

3.2.2.2 Renormalization conditions for Wilson-line operators

As is standard practice, we will derive the factors Z_Γ by imposing appropriate normalization conditions on the quark-antiquark Green's functions of $\mathcal{O}_\Gamma$.

In the spirit of $\overline{\mathrm{MS}}$, $Z_\Gamma^{DR,\overline{\mathrm{MS}}}$ contains, beyond tree level, only negative powers of ε. Here, we note that the leading poles in n-loop diagrams of bare Green's functions, $\mathcal{O}(1/\varepsilon^n)$ ($n \in \mathbb{Z}^+$), are multiples of the corresponding tree-level values and thus do not lead to any mixing. Subleading poles will not lead to divergent mixing coefficients, as is implicit in the renormalizability proofs of Refs. [143, 144, 146]. So, in the $\overline{\mathrm{MS}}$ scheme, we can use the standard definitions of renormalization factors, as in Eq. (3.2).

In RI′, things are more complicated. There is, *a priori*, wide flexibility in defining RI′-like normalization conditions for Green's functions. Given that no mixing is encountered in $\overline{\mathrm{MS}}$ renormalization and given that any other scheme can only differ from $\overline{\mathrm{MS}}$ by finite factors, one might *a priori* expect to be able to adopt a deceptively simple prescription, in which RI′-renormalized operators are simply multiples of their bare counterparts, satisfying a standard normalization condition:

$$\mathrm{Tr}\Big[\Lambda_\Gamma^{\mathrm{RI}'}(\Lambda_\Gamma^{tree})^\dagger\Big]_{q_\nu=\bar{q}_\nu} = \mathrm{Tr}\Big[\Lambda_\Gamma^{tree}(\Lambda_\Gamma^{tree})^\dagger\Big] = 4N_c, \tag{3.7}$$

where $\Lambda_\Gamma^{\rm tree} = \Gamma \exp(iq_\mu z)$ is the tree-level value of the Green's function of operator $\mathcal{O}_\Gamma$ and $\Lambda_\Gamma^{\rm RI'}$ is defined through Eqs. (3.2) and (3.3). There is, however, a fundamental problem with such a prescription: the renormalized Green's function resulting from Eq. (3.7) will depend on the regulator which was used in order to compute it (and, thus, it will not be regularization independent, as the name RI suggests). As was pointed out in Ref. [114], bare Green's functions of $\mathcal{O}_\Gamma$, computed on the lattice, contain additional contributions proportional to the tree-level Green's function of $\mathcal{O}_{\Gamma'}$, where $\Gamma' = \Gamma\gamma_\mu + \gamma_\mu\Gamma$ (whenever the latter differs from zero). Such contributions will not be eliminated by applying the renormalization prescription of Eq. (3.7), thus leading to renormalized Green's functions which differ from those obtained in DR. It should be pointed out that, in all cases, the renormalized functions will contain a number of tensorial structures, the elimination of which may be possible at best only at a given value of the renormalization scale. However, the main concern here is not the elimination of mixing contributions, desirable as this might be; what is more important is to establish a RI′ scheme which is indeed regularization independent, so that nonperturbative estimates of renormalization factors can be converted to the $\overline{\rm MS}$ scheme using conversion factors which are regulator independent.

Given the preferred direction μ of the Wilson-line operator, there is a residual rotational (or cubic, on the lattice) symmetry with respect to the three remaining transverse directions, including also reflections. As a consequence, given an appropriate choice of a renormalization scheme, no mixing needs to occur among operators which do not transform in the same way under this residual symmetry. In particular, mixing can occur only among pairs of operators $(\mathcal{O}_\Gamma, \mathcal{O}_{\Gamma\gamma_\mu})$.

Denoting generically the two operators in such a pair by $(\mathcal{O}_{\Gamma_1}, \mathcal{O}_{\Gamma_2})$, the corresponding renormalization factors will be 2×2 mixing matrices:

$$\mathcal{O}_{\Gamma_i}^{RI'} = \sum_{j=1}^{2} \left[\left(Z_{\Gamma_1,\Gamma_2}^{X,RI'} \right)^{-1} \right]_{ij} \mathcal{O}_{\Gamma_j}, \quad (i = 1, 2). \tag{3.8}$$

More precisely, the mixing pairs $(\mathcal{O}_{\Gamma_1}, \mathcal{O}_{\Gamma_2})$ are formed by $(\Gamma_1, \Gamma_2) = (\mathbb{1}, \gamma_1)$, $(\gamma_5, \gamma_5\gamma_1)$, $(\gamma_2, \gamma_1\gamma_2)$, $(\gamma_3, \gamma_1\gamma_3)$, $(\gamma_4, \gamma_1\gamma_4)$, $(\gamma_5\gamma_2, \gamma_3\gamma_4)$, $(\gamma_5\gamma_3, \gamma_4\gamma_2)$, and $(\gamma_5\gamma_4, \gamma_2\gamma_3)$. Therefore, the renormalized 1-PI amputated Green's functions of Wilson-line operators have the

following form:

$$\Lambda_{\Gamma_i}^{RI'} = \sum_{j=1}^{2} (Z_{\psi_f}^{X,RI'})^{1/2} \, (Z_{\psi_{f'}}^{X,RI'})^{1/2} \left[(Z_{\Gamma_1,\Gamma_2}^{X,RI'})^{-1} \right]_{ij} \Lambda_{\Gamma_j}. \tag{3.9}$$

Thus, an appropriate renormalization condition, especially for lattice simulations, is

$$\mathrm{T}r\Big[\Lambda_{\Gamma_i}^{\mathrm{R}I'}(\Lambda_{\Gamma_j}^{tree})^{\dagger}\Big]_{q_\nu = \bar{q}_\nu} = \mathrm{T}r\Big[\Lambda_{\Gamma_i}^{tree}(\Lambda_{\Gamma_j}^{tree})^{\dagger}\Big] = 4N_c \, \delta_{ij}. \tag{3.10}$$

Combining Eqs. (3.9) and (3.10), the RI′ condition takes the form:

$$(Z_{\Gamma_1,\Gamma_2}^{X,\mathrm{R}I'})_{ij} = \frac{1}{4N_c} (Z_{\psi_f}^{X,RI'})^{1/2} \, (Z_{\psi_{f'}}^{X,RI'})^{1/2} \, \mathrm{T}r\Big[\Lambda_{\Gamma_i} \, (\Lambda_{\Gamma_j}^{tree})^{\dagger}\Big]_{q_\nu = \bar{q}_\nu}. \tag{3.11}$$

Based on the above symmetry arguments, such a RI′ condition will indeed be regularization independent, for all regularizations which respect the above symmetries.

One could of course adopt more general definitions of RI′, e.g., a prescription in which each of the 16 operators $\mathcal{O}_\Gamma$ can contain admixtures of some of the remaining operators:

$$\mathcal{O}_{\Gamma_i}^{\mathrm{RI}'} = \sum_{j=1}^{16} \Big[(Z^{\mathrm{X,RI}'})^{-1} \Big]_{ij} \mathcal{O}_{\Gamma_j}, \quad (i = 1, \cdots, 16), \tag{3.12}$$

in such a way that the renormalized Green's functions will satisfy a condition similar to Eq. (3.10), but with the indices i, j ranging from 1 to 16. However, such a definition would introduce additional finite mixing, which would violate the rotational symmetry in the transverse directions, e.g., mixing among $\mathcal{O}_{\gamma_1}$ and $\mathcal{O}_{\gamma_2}$; such a violation would occur whenever the RI′ renormalization scale four-vector $\bar{q}$ is chosen to lie in an oblique direction. To avoid such unnecessary mixing, it is thus natural to adopt the "minimal" prescription of Eqs. (3.8) - (3.11). Since this prescription extends beyond one-loop order, it may be applied to nonperturbative evaluations of the renormalization matrices $Z^{\mathrm{L,RI}'}$.

Let us note that, as it stands, Eq. (3.10) leads to renormalization factors which depend on the individual components of $\bar{q}$, rather than just $\bar{q}^2$ and $\bar{q}_\mu$; consequently, the renormalization factors of, e.g., $\mathcal{O}_{\gamma_2}$ and $\mathcal{O}_{\gamma_3}$ will have different numerical values. One could, of course, define RI′ in such a way that the residual invariance is manifest;

this can be seen by analogy with local operators, e.g., $\mathcal{O}_{V_i} = \bar{\psi}(x)\gamma_i\psi(x)$, where Z_V is often defined as the average over Z_{V_i} (i = 1,2,3,4), and, in doing so, Z_V turns out to depend only on the length of the renormalization scale four-vector. Adopting such a definition, the values of the conversion factors can be read off our bare Green's functions [see Eqs. (3.23) - (3.34) below] in a rather straightforward way, and they will indeed depend only on $\bar{q}^2$ and $\bar{q}_\mu$. However, in defining the RI′ scheme for Wilson-line operators, we have aimed at being as general as possible and thus did not take any averages, as above, in order to accommodate possible definitions employed in nonperturbative investigations of the renormalization factors; after all, the conversion factors which we calculate must be applicable precisely to these investigations. It goes without saying that if one chooses all components of the renormalization scale four-vector, perpendicular to the Wilson line, to vanish, then residual rotational invariance is automatically restored.

Finally, one could define RI′ in such a way that renormalization factors would be strictly real, e.g., by taking the absolute value of the lhs in Eq. (3.10); indeed, the choice of the definition of RI′, leading to complex renormalization factors, is not mandatory, but it is a natural one, following the definition used in nonperturbative investigations. All these choices are related to the $\overline{\text{MS}}$ scheme via finite conversion factors; thus, no particular choice is dictated by the need to remove divergences, either in dimensional regularization or on the lattice.

3.2.3 Conversion factors

As a consequence of the 2×2 matrix form of the RI′ renormalization factors, the conversion factors between RI′ and $\overline{\text{MS}}$ schemes will also be 2×2 mixing matrices. Being regularization independent, they can be evaluated more easily in DR. They are defined as

$$\left[\mathcal{C}^{\overline{\text{MS}},\text{R}I'}_{\Gamma_1,\Gamma_2}\right]_{ij} = (Z^{DR,\overline{\text{MS}}}_{\Gamma_i})^{-1} \cdot \left[Z^{DR,\text{R}I'}_{\Gamma_1,\Gamma_2}\right]_{ij} = \sum_{k=1}^{2} \left[(Z^{LR,\overline{\text{MS}}}_{\Gamma_1,\Gamma_2})^{-1}\right]_{ik} \cdot \left[Z^{LR,\text{R}I'}_{\Gamma_1,\Gamma_2}\right]_{kj}. \quad (3.13)$$

We note in passing that the definition of the $\overline{\text{MS}}$ scheme depends on the prescription used for extending γ_5 to D dimensions[3]; this, in particular, will affect conversion factors

[3]See, e.g., Refs. [50, 179–183] for a discussion of four relevant prescriptions and some conversion factors among them.

for the pseudoscalar and axial-vector operators. However, such a dependence will only appear beyond one loop. Now, the Green's functions in the RI′ scheme can be directly converted to the $\overline{\text{MS}}$ scheme through

$$\begin{aligned}\begin{pmatrix}\Lambda_{\Gamma_1}^{\overline{\text{MS}}}\\ \Lambda_{\Gamma_2}^{\overline{\text{MS}}}\end{pmatrix} &= \left(\frac{Z_{\psi_f}^{LR,\overline{\text{MS}}}}{Z_{\psi_f}^{LR,\text{R}I'}}\right)^{1/2}\left(\frac{Z_{\psi_{f'}}^{LR,\overline{\text{MS}}}}{Z_{\psi_{f'}}^{LR,\text{R}I'}}\right)^{1/2}(Z_{\Gamma_1,\Gamma_2}^{LR,\overline{\text{MS}}})^{-1}\cdot(Z_{\Gamma_1,\Gamma_2}^{LR,\text{R}I'})\cdot\begin{pmatrix}\Lambda_{\Gamma_1}^{\text{R}I'}\\ \Lambda_{\Gamma_2}^{\text{R}I'}\end{pmatrix}\\ &= \frac{1}{(\mathcal{C}_{\psi_f}^{\overline{\text{MS}},\text{R}I'})^{1/2}\,(\mathcal{C}_{\psi_{f'}}^{\overline{\text{MS}},\text{R}I'})^{1/2}}(\mathcal{C}_{\Gamma_1,\Gamma_2}^{\overline{\text{MS}},\text{R}I'})\cdot\begin{pmatrix}\Lambda_{\Gamma_1}^{\text{R}I'}\\ \Lambda_{\Gamma_2}^{\text{R}I'}\end{pmatrix},\end{aligned}\tag{3.14}$$

where $\mathcal{C}_{\psi_f}^{\overline{\text{MS}},\text{R}I'} \equiv Z_{\psi_f}^{LR,\text{R}I'}/Z_{\psi_f}^{LR,\overline{\text{MS}}} = Z_{\psi_f}^{DR,\text{R}I'}/Z_{\psi_f}^{DR,\overline{\text{MS}}}$ is the conversion factor for a fermion field of a given flavor.

3.3 Computation and Results

In this section, we present our one-loop results for the bare Green's functions of Wilson-line operators, the renormalization factors, and the conversion factors between RI′ and $\overline{\text{MS}}$ schemes, using dimensional regularization. In this regularization, Green's functions are Laurent series in ε, where ε is the regulator, defined by $D \equiv 4 - 2\varepsilon$, and D is the number of Euclidean spacetime dimensions, in which momentum-loop integrals are well defined. We also describe the method that we used to calculate the momentum-loop integrals presented in the Green's functions. Furthermore we investigate the operator mixing.

3.3.1 The integration method

In this subsection, we describe the method that we used to evaluate the D-dimensional momentum-loop integrals, appearing in the calculation of the bare Green's functions. First, we introduce Feynman parameters. Second, we perform the standard integrations over the $(D-1)$ directions perpendicular to the Wilson line (see, e.g., Ref. [184]). Next, we perform the remaining nontrivial integration over the parallel direction, which has an exponential z dependence. This procedure gives the following formulae, in terms of

modified Bessel functions of the second kind, K_ν:

$$A(\alpha) \;= \int \frac{d^D p}{(2\pi)^D} \frac{e^{ip_\mu z}}{(p^2 + 2\; k\cdot p + m^2)^\alpha} \quad = \quad \frac{2^{1-\alpha-D/2}\; |z|^{\alpha-D/2}\; e^{-ik_\mu z}}{\pi^{D/2}\; \Gamma(\alpha)\; (m^2-k^2)^{\alpha/2-D/4}}\; \cdot \\ K_{-\alpha+D/2}(\sqrt{m^2-k^2}\;|z|), \tag{3.15}$$

$$\int \frac{d^D p}{(2\pi)^D} \frac{e^{ip_\mu z}\; p_{\nu_1}\cdots p_{\nu_n}}{(p^2 + 2\; k\cdot p + m^2)^\alpha} \;= \frac{(-1)^n\; \Gamma(\alpha-n)}{2^n\; \Gamma(\alpha)} \frac{\partial}{\partial k_{\nu_1}} \cdots \frac{\partial}{\partial k_{\nu_n}} A(\alpha-n). \tag{3.16}$$

After the momentum integrations, we perform Laurent expansion in ε, keeping terms up to $\mathcal{O}(\varepsilon^0)$. In this step, we have to be careful when interchanging the integration over Feynman parameters with the limit of a vanishing regulator ($\varepsilon \to 0$). In the massive case, studied in the present paper, the interchange is permissible; however this interchange is not generally valid, as is exemplified by the following term stemming from diagram 1 of Fig. 3.1, in the massless case[4]:

$$B(\varepsilon) \;= \int_0^1 dx\; \frac{\exp(\mathrm{i}q_\mu z x)\; q^2 x^2\; |z|^{\,1+\varepsilon}\; \varepsilon}{\Big(q^2\; x\; (1-x)\Big)^{(1+\varepsilon)/2}}\; K_{1+\varepsilon}(\sqrt{q^2 x(1-x)}\,|z|). \tag{3.17}$$

A naive limit $\varepsilon \to 0^-$ of this term would simply give 0, due to the multiplicative factor of ε. However, this is incorrect, given the existence of a pole at x = 1. Expanding the integrand of Eq. (3.17) into a power series of $(1-x)$:

$$K_{1+\varepsilon}(\sqrt{q^2 x(1-x)}\,|z|) \;= \frac{1}{2}\,\Gamma(1+\varepsilon) \frac{(\sqrt{q^2 x(1-x)}\,|z|)^{-1-\varepsilon}}{2^{-1-\varepsilon}} + \mathcal{O}\Big((1-x)^{(1+\varepsilon)/2}\Big), \tag{3.18}$$

$$\exp(\mathrm{i}q_\mu z x) \;= \exp(\mathrm{i}q_\mu z) + \mathcal{O}(1-x), \tag{3.19}$$

we isolate the pole:

$$\int_0^1 dx\; \left[2^\varepsilon\; \varepsilon\; \Gamma(1+\varepsilon)\; \frac{\exp(\mathrm{i}q_\mu z)}{(q^2)^\varepsilon (1-x)^{1+\varepsilon}} + \mathcal{O}\Big((1-x)^{(1+\varepsilon)/2}\Big)\right]. \tag{3.20}$$

The terms of order $\mathcal{O}\Big((1-x)^{(1+\varepsilon)/2}\Big)$ are integrable in the limit $\varepsilon \to 0^-$, and thus they give 0. In the leading term of Eq. (3.20), we must perform the Feynman parameter integral first, and after that, we take the limit $\varepsilon \to 0^-$. Then, a finite but nonzero result remains:

$$\lim_{\varepsilon\,\to 0^-} B(\varepsilon) \;= -\exp(\mathrm{i}q_\mu z). \tag{3.21}$$

[4]Diagram 1 is actually UV convergent; however, in order to avoid spurious IR divergences, it is convenient to evaluate it in $D > 4$ dimensions ($\varepsilon < 0$) and take the limit $\varepsilon \to 0^-$ in the end.

Therefore, the naive interchange of limit and integration sets a contribution erroneously to zero. To avoid such errors, we use a subtraction of the form:

$$\lim_{\varepsilon\to 0}\int dx\; I(\varepsilon,x) \;=\; \int dx \lim_{\varepsilon\to 0}\Big(I(\varepsilon,x)-I_1(\varepsilon,x)\Big)+\lim_{\varepsilon\to 0}\int dx\; I_1(\varepsilon,x), \tag{3.22}$$

where $I(\varepsilon,x)$ is a term of the original expression and $I_1(\varepsilon,x)$ denotes the leading terms of $I(\varepsilon,x)$ in a power series expansion with respect to $(x-x_i)$ about all singular points x_i; here, x denotes Feynman parameters and/or ζ variables stemming from the definition of $\mathcal{O}_\Gamma$. Such a subtraction must also be applied when we take the massless limit of our results, $m\to 0$, for the same reasons.

The final expression depends on the Feynman parameter integrals and/or the integrals stemming from the definition of $\mathcal{O}_\Gamma$; these can be integrated numerically for all values of q, z, and quark masses used in simulations.

3.3.2 Bare Green's functions

There are four one-loop Feynman diagrams corresponding to the two-point Green's functions of operators $\mathcal{O}_\Gamma$, shown in Fig. 3.1. The last diagram (d_4) does not depend

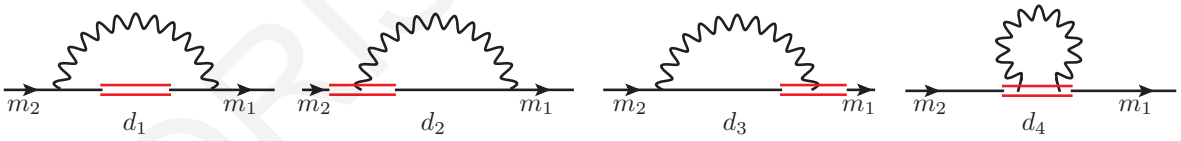

FIGURE 3.1: Feynman diagrams contributing to the one-loop calculation of the Green's functions of Wilson-line operator $\mathcal{O}_\Gamma$. The straight (wavy) lines represent fermions (gluons). The operator insertion is denoted by double straight line.

on the quark masses, and therefore its contribution is the same as that of the massless case. Below, we provide our results for the bare Green's function of operators for each Feynman diagram separately. Our expressions depend on integrals of modified Bessel functions of the second kind, K_n, over Feynman parameters. These integrals are presented in Eqs. (3.65) - (3.80) of Appendix 3.A. For the sake of brevity, we use the following notation: $f_{ij}\equiv f_i\,(q,z,m_j)$, $g_{ij}\equiv g_i\,(q,z,m_j)$, and $h_i\equiv h_i\,(q,z,m_1,m_2)$. Also, index μ is the direction parallel to the Wilson line; indices ν, ρ, and σ are the directions perpendicular to the Wilson line; and μ, ν, ρ, and σ are all different among themselves. Furthermore, $\bar{\mu}$ is the $\overline{\text{MS}}$ renormalization scale, $\bar{\mu}\equiv\mu\,(4\pi/e^{\gamma_E})^{1/2}$, where

μ (not to be confused with the spacetime index μ) appears in the renormalization of the D-dimensional coupling constant; $g = \mu^{\varepsilon}\ Z_g\ g^R$, and γ_E is the Euler constant. In addition, $C_f = (N_c^2 - 1)/(2N_c)$ is the Casimir operator, and β is the gauge fixing parameter, defined such that $\beta = 0$ (1) corresponds to the Feynman (Landau) gauge. Finally, symbols S (scalar), P (pseudoscalar), V_μ (vector in the μ direction), V_ν (vector in the ν direction), A_μ (axial-vector in the μ direction), A_ν (axial-vector in the ν direction), $T_{\mu\nu}$ (tensor in the μ, and ν directions), and $T_{\nu\rho}$ (tensor in the ν, and ρ directions) correspond to the operators $\mathcal{O}_\Gamma$ with $\Gamma = \mathbb{1},\ \gamma_5,\ \gamma_\mu,\ \gamma_\nu,\ \gamma_5\gamma_\mu,\ \gamma_5\gamma_\nu,\ \gamma_\mu\gamma_\nu$, $\gamma_\nu\gamma_\rho$, respectively. We note that only tree-level values for the quark masses appear in the following one-loop expressions:

$$\begin{aligned}\Lambda_S^{\mathrm{d_1}} = \frac{g^2 C_f}{16\pi^2}\Bigg\{ & \Lambda_S^{\mathrm{tree}}\Bigg[(\beta-4)\Big(-4h_1 - 2\mathrm{i}zq_\mu h_2 + |z|\left(h_4 + m_1 m_2 h_5 - q^2 h_7\right)\Big) \\ & + \beta\left(q^2 - m_1 m_2\right)\Big[\frac{1}{2}z^2\left(h_2 - q^2 h_3\right) + |z|\Big(\mathrm{i}zq_\mu\left(h_5 - h_6 - h_7\right) \\ & - \left(h_5 - 2h_6 + q^2 h_8\right)\Big)\Big]\Bigg] \\ & + \Lambda_S^{\mathrm{tree}} \not{q}\,\mathrm{i}\left(m_1 + m_2\right)\Big[\beta\Big(|z|\left(h_5 - q^2 h_8\right) - \frac{1}{2}z^2\left(h_2 + q^2 h_3\right)\Big) \\ & - 2|z|\left(h_5 - h_6\right)\Big] \\ & + \Lambda_{V_\mu}^{\mathrm{tree}}\left(m_1 + m_2\right) z\Big[(\beta+2)h_1 - \beta\Big(|z|\, q^2\left(h_5 - h_6 - h_7\right) - \mathrm{i}zq_\mu h_2\Big)\Big]\Bigg\},\end{aligned} \tag{3.23}$$

$$\Lambda_P^{\mathrm{d_1}} = \gamma_5\ \Lambda_S^{\mathrm{d_1}}\{m_2 \mapsto -m_2\}, \tag{3.24}$$

$$\begin{aligned}\Lambda^{\mathrm{d_1}}_{V_\mu} = \frac{g^2 C_f}{16\pi^2}\Bigg\{ & \Lambda^{\mathrm{tree}}_{V_\mu}\Bigg[-4\,(\beta-1)\,h_1 + |z|\,\Big[\,(\beta+2)\,h_4 - (\beta-2)\,\big(m_1 m_2 h_5 + q^2 h_7\big)\,\Big] \\ & \qquad + 2\beta z q_\mu \Big[z q_\mu h_2 - \mathrm{i}\,(h_1+h_2) + \mathrm{i}\,|z|\,(h_5-h_6-h_7)\,\Big] \\ & \qquad + \beta\,\big(q^2+m_1 m_2\big)\,\Big[\,|z|\,\big(h_6 - q^2 h_8\big) - \frac{1}{2} z^2\,\big(h_2 + q^2 h_3\big)\,\Big]\Bigg] \\ & + \Big(\Lambda^{\mathrm{tree}}_{V_\mu} \not{q}\, m_1 + \not{q} \Lambda^{\mathrm{tree}}_{V_\mu}\, m_2\Big)\;\beta\Big[-|z|\,\Big(z q_\mu\,(h_5-h_6-h_7) - \mathrm{i}\,\big(h_6 - q^2 h_8\big)\Big) \\ & \qquad + \frac{1}{2}\mathrm{i} z^2\,\big(h_2 - q^2 h_3\big)\,\Big] \\ & + \Lambda^{\mathrm{tree}}_S\,(m_1+m_2)\,\Big[z(\beta-4) h_1 - 2\mathrm{i}\,|z|\,q_\mu(\beta-2)\,(h_5-h_6)\,\Big] \\ & + \Lambda^{\mathrm{tree}}_S \not{q}\Big[2\,|z|\,q_\mu\Big(\beta\,(h_5 - h_6 + m_1 m_2 h_8) - 2h_7\Big) - \beta z^2 q_\mu\,(h_2 - m_1 m_2 h_3) \\ & \qquad + 2\mathrm{i} z\,(\beta h_1 - 2h_2) - \mathrm{i}\beta z\,|z|\,\big(q^2 + m_1 m_2\big)\,(h_5 - h_6 - h_7)\,\Big]\Bigg\}, \end{aligned} \tag{3.25}$$

$$\begin{aligned}\Lambda^{\mathrm{d_1}}_{V_\nu} = \frac{g^2 C_f}{16\pi^2}\Bigg\{ & \Lambda^{\mathrm{tree}}_{V_\nu}\Bigg[-2\Big(2\,(\beta-1)\,h_1 + (\beta-2)\,\mathrm{i} z q_\mu h_2\Big) \\ & \qquad - (\beta-2)\,|z|\,\big(m_1 m_2 h_5 + q^2 h_7 - h_4\big) \\ & \qquad + \big(q^2 + m_1 m_2\big)\,\beta\Big[\,|z|\,\Big(\mathrm{i} z q_\mu\,(h_5 - h_6 - h_7) + \big(h_6 - q^2 h_8\big)\Big) \\ & \qquad\qquad + \frac{1}{2} z^2\,\big(h_2 - q^2 h_3\big)\,\Big]\Bigg] \\ & + \big(\Lambda^{\mathrm{tree}}_{V_\nu} \not{q}\, m_1 + \not{q}\Lambda^{\mathrm{tree}}_{V_\nu}\, m_2\big)\,\mathrm{i}\beta\Big[\,|z|\,\big(h_6 - q^2 h_8\big) - \frac{1}{2} z^2\,\big(h_2 + q^2 h_3\big)\,\Big] \\ & + \Lambda^{\mathrm{tree}}_{T_{\mu\nu}}\,(m_1 - m_2)\,\beta z\Big[-h_1 + |z|\,q^2\,(h_5 - h_6 - h_7) - \mathrm{i} z q_\mu h_2\Big] \\ & + \Lambda^{\mathrm{tree}}_{V_\mu} z q_\nu\Big[\beta\Big(\mathrm{i}\,|z|\,\big(q^2 - m_1 m_2\big)\,(h_5 - h_6 - h_7) + 2\,(z q_\mu h_2 - \mathrm{i} h_1)\Big) - 4\mathrm{i} h_2\Big] \\ & - \Big(\Lambda^{\mathrm{tree}}_{V_\mu} \not{q}\, m_1 + \not{q}\Lambda^{\mathrm{tree}}_{V_\mu}\, m_2\Big)\,\beta z\,|z|\,q_\nu\,(h_5 - h_6 - h_7) \\ & + \Lambda^{\mathrm{tree}}_S\,(m_1+m_2)\,\mathrm{i} q_\nu\Big[-2(\beta-2)\,|z|\,(h_5 - h_6) + \beta z^2 h_2\Big] \\ & + \Lambda^{\mathrm{tree}}_S \not{q} q_\nu\Big[\beta\Big(2\,|z|\,(h_5 - h_6 + m_1 m_2 h_8) - z^2\,(h_2 - m_1 m_2 h_3)\Big) - 4\,|z|\,h_7\Big]\Bigg\} \end{aligned} \tag{3.26}$$

$$\Lambda^{\mathrm{d_1}}_{A_{\mu(\nu)}} = \gamma_5\;\Lambda^{\mathrm{d_1}}_{V_{\mu(\nu)}}\{m_2 \mapsto -m_2\}, \tag{3.27}$$

$$
\begin{aligned}
\Lambda^{\mathrm{d_1}}_{T_{\mu\nu}} = \frac{g^2 C_f}{16\pi^2}\Bigg\{ & \Lambda^{\mathrm{tree}}_{T_{\mu\nu}}\beta\Bigg[-2\left(2h_1 - z^2 q_\mu^2 h_2\right) + |z|\left[h_4 + q^2\Big(h_5 - h_7 + 2\mathrm{i}zq_\mu\left(h_5 - h_6 - h_7\right)\Big)\right] \\
& \qquad - 2\mathrm{i}zq_\mu(h_1+h_2) - \left(q^2 - m_1 m_2\right)\Big(|z|\,q^2 h_8 + \frac{1}{2}z^2\left(h_2 + q^2 h_3\right)\Big)\Bigg] \\
& + \Big(\Lambda^{\mathrm{tree}}_{T_{\mu\nu}} \not{q}\, m_1 + \not{q}\Lambda^{\mathrm{tree}}_{T_{\mu\nu}}\, m_2\Big)\Bigg[\beta\Big[\frac{1}{2}\mathrm{i}z^2\left(h_2 - q^2 h_3\right) - |z|\Big(zq_\mu\left(h_5 - h_6 - h_7\right) \\
& \qquad + \mathrm{i}\left(h_5 - 2h_6 + q^2 h_8\right)\Big)\Big] + 2\mathrm{i}\,|z|\left(h_5 - h_6\right)\Bigg] \\
& - \Lambda^{\mathrm{tree}}_{V_\nu}(\beta - 2)z\left(m_1 - m_2\right)h_1 \\
& + \Lambda^{\mathrm{tree}}_{V_\nu}\not{q}\beta\Bigg[2\left(|z|\,q_\mu m_1 m_2 h_8 - \mathrm{i}zh_1\right) + \mathrm{i}z\,|z|\left(q^2 - m_1 m_2\right)\left(h_5 - h_6 - h_7\right) \\
& \qquad + z^2 q_\mu\left(h_2 + m_1 m_2 h_3\right)\Bigg] \\
& - \Lambda^{\mathrm{tree}}_{V_\mu}\mathrm{i}\beta z^2 q_\nu(m_1 - m_2)h_2 + \Lambda^{\mathrm{tree}}_{V_\mu}\not{q}\beta q_\nu\Big[z^2\left(h_2 - m_1 m_2 h_3\right) - 2\,|z|\,m_1 m_2 h_8\Big] \\
& + \Lambda^{\mathrm{tree}}_{S}\beta z q_\nu\Big[2\left(\mathrm{i}h_1 - zq_\mu h_2\right) - \mathrm{i}\,|z|\left(q^2 - m_1 m_2\right)\left(h_5 - h_6 - h_7\right)\Big] \\
& + \Lambda^{\mathrm{tree}}_{S}\not{q}\beta z\,|z|\,q_\nu\left(m_1 - m_2\right)\left(h_5 - h_6 - h_7\right)\Bigg\}, \qquad (3.28)
\end{aligned}
$$

$$
\begin{aligned}
\Lambda^{\mathrm{d_1}}_{T_{\nu\rho}} = \frac{g^2 C_f}{16\pi^2}\Bigg\{ & \Lambda^{\mathrm{tree}}_{T_{\nu\rho}}\beta\Bigg[-2\left(2h_1 + \mathrm{i}zq_\mu h_2\right) + |z|\Big(h_4 + q^2\left(h_5 - h_7\right)\Big) \\
& \qquad + \left(q^2 - m_1 m_2\right)\Big[\frac{1}{2}z^2\left(h_2 - q^2 h_3\right) - |z|\Big(q^2 h_8 - \mathrm{i}zq_\mu\left(h_5 - h_6 - h_7\right)\Big)\Big]\Bigg] \\
& + \Big(\Lambda^{\mathrm{tree}}_{T_{\nu\rho}} \not{q}\, m_1 + \not{q}\Lambda^{\mathrm{tree}}_{T_{\nu\rho}} m_2\Big)\mathrm{i}\Big[-\beta\Big(\frac{1}{2}z^2\left(h_2 + q^2 h_3\right) + |z|\left(h_5 - 2h_6 + q^2 h_8\right)\Big) \\
& \qquad + 2\,|z|\left(h_5 - h_6\right)\Big] \\
& + \varepsilon_{\mu\nu\rho\sigma}\,\Lambda^{\mathrm{tree}}_{A_\sigma}\left(m_1 + m_2\right)\Big[-\beta z\,|z|\,q^2\left(h_5 - h_6 - h_7\right) + (\beta - 2)\,z h_1 + \mathrm{i}\beta z^2 q_\mu h_2\Big] \\
& + \Big(\Lambda^{\mathrm{tree}}_{T_{\mu\nu}} q_\rho - \Lambda^{\mathrm{tree}}_{T_{\mu\rho}} q_\nu\Big)\beta z\Big[2\left(\mathrm{i}h_1 - zh_2 q_\mu\right) - \mathrm{i}\,|z|\left(q^2 + m_1 m_2\right)\left(h_5 - h_6 - h_7\right)\Big] \\
& + \Big[\Big(\Lambda^{\mathrm{tree}}_{T_{\mu\nu}} q_\rho - \Lambda^{\mathrm{tree}}_{T_{\mu\rho}} q_\nu\Big)\not{q}\, m_1 + \not{q}\Big(\Lambda^{\mathrm{tree}}_{T_{\mu\nu}} q_\rho - \Lambda^{\mathrm{tree}}_{T_{\mu\rho}} q_\nu\Big) m_2\Big]\beta z\,|z|\left(h_5 - h_6 - h_7\right) \\
& + \Big(\Lambda^{\mathrm{tree}}_{V_\nu} q_\rho - \Lambda^{\mathrm{tree}}_{V_\rho} q_\nu\Big)\mathrm{i}\beta z^2\left(m_1 - m_2\right)h_2 \\
& - \Big(\Lambda^{\mathrm{tree}}_{V_\nu} q_\rho - \Lambda^{\mathrm{tree}}_{V_\rho} q_\nu\Big)\not{q}\beta\Big[z^2\left(h_2 + m_1 m_2 h_3\right) + 2\,|z|\,m_1 m_2 h_8\Big]\Bigg\}, \qquad (3.29)
\end{aligned}
$$

$$\Lambda_S^{\mathrm{d}_2} = \frac{g^2 C_f}{16\pi^2}\Bigg\{\Lambda_S^{\mathrm{tree}}\Bigg[(\beta-1)\Big[2f_{11}-2-\frac{1}{\varepsilon}-\log\left(\frac{\overline{\mu}^2}{q^2+m_1^2}\right)+\frac{m_1^2}{q^2}\log\left(1+\frac{q^2}{m_1^2}\right)\Big] + \beta q^2\Big(\mathrm{i}q_\mu\left(g_{31}-zf_{31}\right)+\left(q^2+m_1^2\right)g_{41}-\left(q^2-q_\mu^2\right)g_{51}\Big)-2\mathrm{i}q_\mu g_{21}\Bigg] + \Lambda_S^{\mathrm{tree}}\not{q}\beta m_1\Big[-q_\mu\left(g_{31}-zf_{31}\right)+\mathrm{i}g_{41}\left(q^2+m_1^2\right)-\mathrm{i}g_{51}\left(q^2-q_\mu^2\right)\Big] + \Lambda_{V_\mu}^{\mathrm{tree}}m_1\left(2g_{11}-\beta z f_{21}\right)+\Lambda_{V_\mu}^{\mathrm{tree}}\not{q}\mathrm{i}\Big(\beta z f_{21}-2\left(g_{11}-g_{21}\right)\Big)\Bigg\}, \tag{3.30}$$

$$\Lambda_\Gamma^{\mathrm{d}_2} = \Lambda_S^{\mathrm{d}_2}\,\Gamma, \tag{3.31}$$

$$\Lambda_S^{\mathrm{d}_3} = \frac{g^2 C_f}{16\pi^2}\Bigg\{\Lambda_S^{\mathrm{tree}}\Bigg[(\beta-1)\Big[2f_{12}-2-\frac{1}{\varepsilon}-\log\left(\frac{\overline{\mu}^2}{q^2+m_2^2}\right)+\frac{m_2^2}{q^2}\log\left(1+\frac{q^2}{m_2^2}\right)\Big] + \beta q^2\Big(\mathrm{i}q_\mu\left(g_{32}-zf_{32}\right)+\left(q^2+m_2^2\right)g_{42}-\left(q^2-q_\mu^2\right)g_{52}\Big)-2\mathrm{i}q_\mu g_{22}\Bigg] + \Lambda_S^{\mathrm{tree}}\not{q}\beta m_2\Big[-q_\mu\left(g_{32}-zf_{32}\right)+\mathrm{i}g_{42}\left(q^2+m_2^2\right)-\mathrm{i}g_{52}\left(q^2-q_\mu^2\right)\Big] + \Lambda_{V_\mu}^{\mathrm{tree}}m_2\left(2g_{12}-\beta z f_{22}\right)+\not{q}\Lambda_{V_\mu}^{\mathrm{tree}}\mathrm{i}\Big(\beta z f_{22}-2\left(g_{12}-g_{22}\right)\Big)\Bigg\}, \tag{3.32}$$

$$\Lambda_\Gamma^{\mathrm{d}_3} = \Gamma\,\Lambda_S^{\mathrm{d}_3}, \tag{3.33}$$

$$\Lambda_\Gamma^{\mathrm{d}_4} = \frac{g^2 C_f}{16\pi^2}\Lambda_\Gamma^{\mathrm{tree}}\Big[4+(\beta+2)\Big(2\gamma_E+\frac{1}{\varepsilon}+\log\left(\frac{1}{4}z^2\overline{\mu}^2\right)\Big)\Big]. \tag{3.34}$$

UV-divergent terms of order $\mathcal{O}(1/\varepsilon)$ arise from the last three diagrams. These terms are multiples of the tree-level values of Green's functions and therefore do not lead to any mixing. However, there are finite terms for each $\mathcal{O}_\Gamma$ with different Dirac structures than the original operator; some of these terms are responsible for the finite mixing which occurs in RI′. In particular, they lead to the expected mixing within the pairs $(\Gamma, \Gamma\gamma_\mu)$ or equivalently $(\Gamma, \gamma_\mu\Gamma)$. This is a consequence of the violation of chiral symmetry by the mass term in the fermion action, as well as the flavor-symmetry breaking when masses have different values. For the case of equal masses (no flavor-symmetry breaking) $m_1 = m_2$, the mixing pattern reduces to $(\Gamma, \frac{1}{2}\{\Gamma, \gamma_\mu\})$, which is the same as the pattern for massless quarks on the lattice. Our findings are expected to be valid also on the lattice.

The one-loop Green's functions exhibit a nontrivial dependence on dimensionless quantities involving the Wilson-line length z, the external quark momentum q, and the quark masses m_i $(i = 1, 2)$: zq_μ, zm_i. This dependence is in addition to the standard logarithmic dependence on $\bar{\mu}$: $\log(\bar{\mu}^2/q^2)$. Also, we note that our results are not analytic functions of z near $z = 0$; this was expected due to the appearance of contact terms beyond tree level. For the case $z = 0$, the nonlocal operators are replaced by local massive fermion bilinear operators; their renormalization is addressed in Ref. [185], using a generalization of the RI-SMOM scheme, called RI-mSMOM. Further, the Green's functions of Feynman diagrams satisfy the following reflection relations, with respect to z:

$$\Lambda_\Gamma^{d_1}(z, m_1, m_2) = \frac{1}{4}\mathrm{tr}(\Gamma^2)\ \left[\Lambda_\Gamma^{d_1}(-z, -m_2, -m_1)\right]^\dagger, \tag{3.35}$$

$$\Lambda_\Gamma^{d_2}(z, m) = \frac{1}{4}\mathrm{tr}(\Gamma^2)\ \left[\Lambda_\Gamma^{d_3}(-z, -m)\right]^\dagger, \tag{3.36}$$

$$\Lambda_\Gamma^{d_4}(z) = \frac{1}{4}\mathrm{tr}(\Gamma^2)\ \left[\Lambda_\Gamma^{d_4}(-z)\right]^\dagger. \tag{3.37}$$

[Note that $(1/4)\ \mathrm{tr}(\Gamma^2) = \pm 1$, depending on Γ.] The total one-loop bare Green's functions of operators $\mathcal{O}_\Gamma$ are given by the sum over the contributions of the four diagrams:

$$\Lambda_\Gamma^{\text{1-loop}} = \sum_{i=1}^{4} \Lambda_\Gamma^{d_i}. \tag{3.38}$$

3.3.3 Renormalization factors

3.3.3.1 Renormalization factors of fermion field and mass

The perturbative determination of Z_ψ and Z_m proceeds in textbook fashion by calculating the bare fermion self-energy in DR to one loop; we present it here for completeness. The Feynman diagram contributing to this two-point Green's function is shown in Fig. 3.2. Denoting by Σ the higher-order terms $\mathcal{O}(g^2)$ of the 1-PI

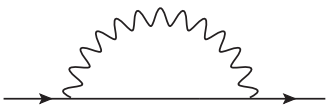

FIGURE 3.2: Feynman diagram contributing to the one-loop calculation of the fermion self-energy. The straight (wavy) lines represent fermions (gluons).

amputated Green's function of the fermion field, the inverse full fermion propagator

takes the following form: $\langle\psi\bar{\psi}\rangle^{-1} = i\not{q} + m\mathbb{1} - \Sigma$. Writing Σ in the more useful form: $\Sigma = i\not{q}\,\Sigma_1(q^2,m) \;+\; m\;\mathbb{1}\;\Sigma_2(q^2,m)$, we present the one-loop results for the functions Σ_1, Σ_2:

$$\Sigma_1(q^2,m) = \frac{g^2 C_f}{16\pi^2}(\beta-1)\left\{1+\frac{1}{\varepsilon}+\log\left(\frac{\overline{\mu}^2}{q^2+m^2}\right)-\frac{m^2}{q^2}\left[1-\frac{m^2}{q^2}\log\left(1+\frac{q^2}{m^2}\right)\right]\right\} + \mathcal{O}(g^4), \tag{3.39}$$

$$\Sigma_2(q^2,m) = \frac{g^2 C_f}{16\pi^2}\left\{2+(\beta-4)\left[2+\frac{1}{\varepsilon}+\log\left(\frac{\overline{\mu}^2}{q^2+m^2}\right)-\frac{m^2}{q^2}\log\left(1+\frac{q^2}{m^2}\right)\right]\right\} + \mathcal{O}(g^4). \tag{3.40}$$

The renormalization conditions for Z_ψ and Z_m in the RI′ scheme, using the above notation, take the following perturbative forms:

$$Z_\psi^{DR,RI'} = \frac{1}{1-\Sigma_1}\Big|_{q_\nu=\bar{q}_\nu}, \tag{3.41}$$

$$Z_m^{DR,RI'} = \frac{1-\Sigma_1}{1-\Sigma_2}\Big|_{q_\nu=\bar{q}_\nu}. \tag{3.42}$$

Thus, in the presence of finite fermion masses, the results for the renormalization factors of the fermion field and mass are given below:

$$Z_\psi^{DR,RI'} = 1+\frac{g^2 C_f}{16\pi^2}(\beta-1)\left[\frac{1}{\varepsilon}+1+\log\left(\frac{\overline{\mu}^2}{\bar{q}^2+m^2}\right)-\frac{m^2}{\bar{q}^2}\left(1-\frac{m^2}{\bar{q}^2}\log\left(1+\frac{\bar{q}^2}{m^2}\right)\right)\right] + \mathcal{O}(g^4), \tag{3.43}$$

$$Z_m^{DR,RI'} = 1+\frac{g^2 C_f}{16\pi^2}\left[-\frac{3}{\varepsilon}+\beta-5-3\log\left(\frac{\overline{\mu}^2}{\bar{q}^2+m^2}\right)-(\beta-4)\frac{m^2}{\bar{q}^2}\log\left(1+\frac{\bar{q}^2}{m^2}\right) + (\beta-1)\frac{m^2}{\bar{q}^2}\left(1-\frac{m^2}{\bar{q}^2}\log\left(1+\frac{\bar{q}^2}{m^2}\right)\right)\right] + \mathcal{O}(g^4). \tag{3.44}$$

We recall that the mass appearing in the above expressions is the renormalized mass, which coincides with the bare mass to this order. The results for Z_ψ and Z_m are in agreement with Ref. [186], in the massless limit and for $\bar{q} = \bar{\mu}$.

The renormalization factors in the $\overline{\text{MS}}$ scheme can be readily inferred from Eqs. (3.43) and (3.44) by taking only the pole part in epsilon:

$$Z_{\psi}^{DR,\overline{\text{MS}}} = 1 + \frac{g^2 C_f}{16\pi^2}\frac{1}{\varepsilon}(\beta - 1) + \mathcal{O}(g^4), \tag{3.45}$$

$$Z_{m}^{DR,\overline{\text{MS}}} = 1 + \frac{g^2 C_f}{16\pi^2}\frac{1}{\varepsilon}(-3) + \mathcal{O}(g^4). \tag{3.46}$$

3.3.3.2 Renormalization factors of Wilson-line operators

Now, we have all the ingredients for the extraction of renormalization factors of Wilson-line operators in the RI′ and $\overline{\text{MS}}$ schemes. By writing Z_{ψ_f} and Λ_Γ in the form:

$$Z_{\psi_f}^{DR,Y} = 1 + g^2 z_{\psi_f}^{Y} + \mathcal{O}(g^4), \tag{3.47}$$

$$\Lambda_{\Gamma_i} = \Lambda_{\Gamma_i}^{\text{tree}} + \Lambda_{\Gamma_i}^{\text{1-loop}} + \mathcal{O}(g^4), \qquad (i = 1, 2), \tag{3.48}$$

where[5]

$$\Lambda_{\Gamma_i}^{\text{1-loop}} = g^2 \sum_{j=1}^{2} \lambda_{ij}\ \Lambda_{\Gamma_j}^{\text{tree}} + \cdots, \qquad \lambda_{ij} = \frac{1}{4N_c}\frac{1}{g^2}\,\text{Tr}\Big[\Lambda_{\Gamma_i}^{\text{1-loop}}\,(\Lambda_{\Gamma_j}^{tree})^{\dagger}\Big], \tag{3.49}$$

the condition for the renormalization of Wilson-line operators in the RI′ scheme, up to one loop, reads

$$\Big[Z_{\Gamma_1,\Gamma_2}^{DR,RI'}\Big]_{ij} = \delta_{ij} + g^2\delta_{ij}\Big(\frac{1}{2}z_{\psi_f}^{RI'} + \frac{1}{2}z_{\psi_{f'}}^{RI'} + \lambda_{ii}\Big|_{q_\nu=\bar{q}_\nu}\Big) + g^2(1-\delta_{ij})\lambda_{ij}\Big|_{q_\nu=\bar{q}_\nu}. \tag{3.50}$$

The equivalent expression for $Z_{\Gamma}^{DR,\overline{\text{MS}}}$ follows from Eq. (3.50), by keeping in λ_{ij} only pole parts in epsilon; the latter appear only for $i = j$, leading to

$$Z_{\Gamma_i}^{DR,\overline{\text{MS}}} = 1 + g^2\Big(\frac{1}{2}z_{\psi_f}^{\overline{\text{MS}}} + \frac{1}{2}z_{\psi_{f'}}^{\overline{\text{MS}}} + \lambda_{ii}\Big|_{1/\varepsilon}\Big). \tag{3.51}$$

[5]The Green's functions $\Lambda_{\Gamma_i}^{\text{1-loop}}$ also contain additional Dirac structures [see Eqs. (3.23) - (3.34)], which do not contribute to the evaluation of renormalization factors Z_Γ in the $\overline{\text{MS}}$ scheme, as they are $\mathcal{O}(\varepsilon^0)$ terms, nor in RI′, as the trace in Eq. (3.11) gives zero.

Our final results are presented below. In the $\overline{\text{MS}}$ scheme, the renormalization factors of operators have the form:

$$Z_{\Gamma}^{DR,\overline{\text{MS}}} = 1 + \frac{g^2\, C_f}{16\,\pi^2}\,\frac{3}{\varepsilon} + \mathcal{O}(g^4), \tag{3.52}$$

in agreement with Refs. [146, 147, 155]. As we observe, they are independent of operator Γ, fermion masses, Wilson-line length z, and gauge parameter β. In RI′, the renormalization factors are given with respect to the conversion factors, which are presented in the next section:

$$\left[Z_{\Gamma_1,\Gamma_2}^{DR,RI'}\right]_{ij} = \left[\mathcal{C}_{\Gamma_1,\Gamma_2}^{\overline{\text{MS}},\text{R}I'}\right]_{ij} + \frac{g^2\, C_f}{16\,\pi^2}\,\frac{3}{\varepsilon}\delta_{ij} + \mathcal{O}(g^4). \tag{3.53}$$

The above relation stems from the one-loop expression of Eq. (3.13).

3.3.4 Conversion factors

We present below our results for all the matrix elements of 2×2 conversion factors in a compact way. We use the same notation as in Sec. 3.3.2 for bare Green's functions; the only difference is that the Feynman parameter integrals, appearing here, depend on the RI′ scale $\bar{q}$ instead of the external momentum q:

$$
\begin{aligned}
\big[C_{S,V_\mu}\big]_{11} = \; 1 + \frac{g^2 C_f}{16\pi^2}\Bigg\{ & 7 - 3\beta + 2(\beta+2)\gamma_E + 2(\beta-1)\Big(f_{11}+f_{12}\Big) - (\beta-4)\Big(4h_1 - |z|\,h_4\Big) \\
& + 3\log\left(\frac{\overline{\mu}^2}{\bar{q}^2}\right) + (\beta+2)\log\left(\frac{1}{4}z^2\bar{q}^2\right) + \frac{1}{2}(\beta-1)\Bigg[- \frac{m_1^2}{\bar{q}^2} - \frac{m_2^2}{\bar{q}^2} \\
& + \frac{m_1^2}{\bar{q}^2}\left(2 + \frac{m_1^2}{\bar{q}^2}\right)\log\left(1 + \frac{\bar{q}^2}{m_1^2}\right) + \frac{m_2^2}{\bar{q}^2}\left(2 + \frac{m_2^2}{\bar{q}^2}\right)\log\left(1 + \frac{\bar{q}^2}{m_2^2}\right) \\
& + \log\left(1 + \frac{m_1^2}{\bar{q}^2}\right) + \log\left(1 + \frac{m_2^2}{\bar{q}^2}\right)\Bigg] + 2\,|z|\,m_1 m_2(\beta-2)h_5 \\
& + \beta\,|z|\left(\bar{q}^2 - m_1 m_2\right)\Big(2h_6 - \bar{q}^2 h_8\Big) - \bar{q}^2\,|z|\left(\beta h_5 + (\beta-4)h_7\right) \\
& + \beta\bar{q}^2\Big[(m_1^2 + \bar{q}^2)\; g_{41} + (m_2^2 + \bar{q}^2)\; g_{42} - (\bar{q}^2 - \bar{q}_\mu^2)\Big(g_{51} + g_{52}\Big)\Big] \\
& + \frac{1}{2}\beta z^2\Big(\bar{q}^2 - m_1 m_2\Big)\Big(h_2 - \bar{q}^2 h_3\Big) \\
& - 2\;\mathrm{i}\;\bar{q}_\mu\Big(g_{11} + g_{12}\Big) + \mathrm{i}z\bar{q}_\mu\Big[\beta\Big(f_{21} + f_{22}\Big) - 2(\beta-4)h_2\Big] \\
& + \mathrm{i}\beta\bar{q}^2\bar{q}_\mu\Big[g_{31} + g_{32} - z\Big(f_{31} + f_{32}\Big)\Big] \\
& + \mathrm{i}\beta z\,|z|\,\bar{q}_\mu\Big(\bar{q}^2 - m_1 m_2\Big)\Big(h_5 - h_6 - h_7\Big)\Bigg\} + \mathcal{O}(g^4),
\end{aligned}
\tag{3.54}
$$

$$
\begin{aligned}
\big[C_{S,V_\mu}\big]_{12} = \; \frac{g^2 C_f}{16\pi^2}\Bigg\{ & - \beta z\Big(m_1 f_{21} + m_2 f_{22}\Big) - \beta\bar{q}_\mu^2\Big[m_1\Big(g_{31} - z f_{31}\Big) + m_2\Big(g_{32} - z f_{32}\Big)\Big] \\
& + \mathrm{i}\beta\bar{q}_\mu\Big[m_1(m_1^2 + \bar{q}^2)g_{41} + m_2(m_2^2 + \bar{q}^2)g_{42} - (\bar{q}^2 - \bar{q}_\mu^2)\Big(m_1 g_{51} + m_2 g_{52}\Big)\Big] \\
& + 2\Big(m_1 g_{11} + m_2 g_{12}\Big) + \Big(m_1 + m_2\Big)\Bigg[(\beta+2)z h_1 - \mathrm{i}\beta\bar{q}^2\,|z|\,\bar{q}_\mu h_8 \\
& + \mathrm{i}\,|z|\,\bar{q}_\mu\Big((\beta-2)h_5 + 2h_6\Big) + \frac{1}{2}\mathrm{i}\beta z^2\bar{q}_\mu\Big(h_2 - \bar{q}^2 h_3\Big) \\
& - \beta\bar{q}^2 z\,|z|\,\Big(h_5 - h_6 - h_7\Big)\Bigg]\Bigg\} + \mathcal{O}(g^4),
\end{aligned}
\tag{3.55}
$$

$$\big[C_{S,V_\mu}\big]_{21} = \big[C_{S,V_\mu}\big]_{12} + \frac{g^2 C_f}{16\pi^2}\Big(m_1+m_2\Big)\Bigg\{ -6zh_1 - 3\mathrm{i}(\beta-2)\,|z|\,\bar{q}_\mu\Big(h_5-h_6\Big) + \beta z\,|z|\,\big(\bar{q}^2-\bar{q}_\mu^2\big)\,\Big(h_5-h_6-h_7\Big)\Bigg\} + \mathcal{O}(g^4), \tag{3.56}$$

$$\big[C_{S,V_\mu}\big]_{22} = \big[C_{S,V_\mu}\big]_{11} + \frac{g^2 C_f}{16\pi^2}\Bigg\{ -12h_1 - 12\mathrm{i}z\bar{q}_\mu h_2 + 3\,|z|\,\Big[2h_4 - m_1m_2\Big((\beta-2)h_5-\beta h_6\Big)\Big] - 2\beta\,|z|\,m_1m_2(\bar{q}^2-\bar{q}_\mu^2)h_8 + |z|\,(\bar{q}^2+2\bar{q}_\mu^2)\Big[\beta\Big(h_5-h_6\Big)-2h_7\Big] - \beta z^2\,\big(\bar{q}^2-\bar{q}_\mu^2\big)\,\Big(h_2+m_1m_2h_3\Big)\Bigg\} + \mathcal{O}(g^4), \tag{3.57}$$

$$[C_{P,A_\mu}]_{ij} = [C_{S,V_\mu}]_{ij}\{h_k \mapsto (-1)^{1+\delta_{ij}}h_k, m_1 \mapsto -m_1\} \quad (\text{where } i,j=1,2 \text{ and } k=1,2,\cdots,8), \tag{3.58}$$

$$\big[C_{V_\nu,T_{\mu\nu}}\big]_{11} = \big[C_{P,A_\mu}\big]_{11} + \frac{g^2 C_f}{16\pi^2}\Bigg\{ -12h_1 - 4\mathrm{i}z\bar{q}_\mu h_2 + |z|\,(\bar{q}^2+2\bar{q}_\nu^2)\Big[\beta\Big(h_5-h_6\Big)-2h_7\Big] + |z|\,\Big[2h_4 + m_1m_2\Big((\beta-2)h_5-\beta h_6+2\beta\bar{q}_\nu^2 h_8\Big)\Big] - \beta z^2\bar{q}_\nu^2\Big(h_2-m_1m_2h_3\Big)\Bigg\} + \mathcal{O}(g^4), \tag{3.59}$$

$$\big[C_{V_\nu,T_{\mu\nu}}\big]_{12} = -\big[C_{P,A_\mu}\big]_{12} + \frac{g^2 C_f}{16\pi^2}\Big(m_1-m_2\Big)\Bigg\{2zh_1 + \mathrm{i}(\beta-2)\,|z|\,\bar{q}_\mu\Big(h_5-h_6\Big) - \beta z\,|z|\,\bar{q}_\nu^2\Big(h_5-h_6-h_7\Big)\Bigg\} + \mathcal{O}(g^4), \tag{3.60}$$

$$\big[C_{V_\nu,T_{\mu\nu}}\big]_{21} = -\big[C_{P,A_\mu}\big]_{21} - \frac{g^2 C_f}{16\pi^2}\Big(m_1-m_2\Big)\Bigg\{2zh_1 + \mathrm{i}(\beta-2)\,|z|\,\bar{q}_\mu\Big(h_5-h_6\Big) - \beta z\,|z|\,\bar{q}_\nu^2\Big(h_5-h_6-h_7\Big)\Bigg\} + \mathcal{O}(g^4), \tag{3.61}$$

$$\begin{aligned}\left[C_{V_\nu,T_{\mu\nu}}\right]_{22} = \left[C_{P,A_\mu}\right]_{22} + \frac{g^2 C_f}{16\pi^2}\Bigg\{ &-4h_1 + 4\mathrm{i}z\bar{q}_\mu h_2 + |z|\,(\bar{q}^2 - 2\bar{q}_\nu^2)\Big[\beta\Big(h_5 - h_6\Big) - 2h_7\Big] \\ &- |z|\left[2h_4 + m_1 m_2\Big((\beta-2)h_5 - \beta h_6 + 2\beta\bar{q}_\nu^2 h_8\Big)\right] \\ &+ \beta z^2 \bar{q}_\nu^2\Big(h_2 - m_1 m_2 h_3\Big)\Bigg\} + \mathcal{O}(g^4),\end{aligned} \tag{3.62}$$

$$[C_{A_\nu,T_{\rho\sigma}}]_{ij} = (-\varepsilon_{\mu\nu\rho\sigma})^{1+\delta_{ij}}\ [C_{V_\nu,T_{\mu\nu}}]_{ij}\{h_k \mapsto (-1)^{1+\delta_{ij}} h_k, m_1 \mapsto -m_1\} \tag{3.63}$$

(where $i,j = 1,2$ and $k = 1,2,\cdots,8$; $\varepsilon_{\mu\nu\rho\sigma}$ is the Levi-Civita tensor, $\varepsilon_{1234} = 1$).

Our results are in agreement with Ref. [114] in the massless limit[6]. A consequence of the above relations is that, in the case of equal quark masses $m_1 = m_2$, the nondiagonal matrix elements of C_{P,A_μ} and $C_{V_\nu,T_{\mu\nu}}$ vanish. Also, the matrix elements of conversion factors satisfy the following reflection relation with respect to z:

$$[C_{\Gamma_1,\Gamma_2}(\bar{q},z,m_1,m_2)]_{ij} = (-1)^{1+\delta_{ij}}[C^*_{\Gamma_1,\Gamma_2}(\bar{q},-z,m_1,m_2)]_{ij}. \tag{3.64}$$

This means that the real part of diagonal (nondiagonal) matrix elements is an even (odd) function of z, while the imaginary part is odd (even).

3.4 Graphs

In this section, we illustrate our results for conversion factors by selecting certain values of the free parameters used in simulations. To this end, we plot the real and imaginary parts of the conversion factor matrix elements as a function of Wilson-line length, z. For input, we employ certain parameter values, used by ETMC in the ensemble of dynamical $N_f = 2+1+1$ twisted mass fermions of Ref. [110]; i.e., we set[7] $g^2 = 3.077$,

[6] Checking agreement is quite nontrivial; it requires the elimination of certain integrals over Feynman parameters, integration by parts, as well as the interchange of the limit operation with integration.

[7] A most natural choice for the coupling constant would be its $\overline{\mathrm{MS}}$ value, even though the choice of bare vs renormalized coupling constant should, in principle, be irrelevant for one-loop results, such as the ones we plot in this section. Nevertheless, these plots are meant to reveal some salient features of the conversion factors, which certainly are not affected by selecting $g^2 \sim 3.77$ ($\overline{\mathrm{MS}}$) rather than $g^2 = 3.077$ (lattice); indeed, given the simple linear dependence on g^2 of the quantities plotted, the effect of a change in g^2 can be inferred by inspection. For precise quantitative values of the conversion factors, one should of course refer to our results in algebraic form, presented in Sec. 3.3.

$\beta = 1$ (Landau gauge), $N_c = 3$, $\bar{\mu} = 2$ GeV, and $\bar{q} = \frac{2\pi}{32a}(n_z, 0, 0, \frac{n_t}{2} + \frac{1}{4})$, for $a = 0.082$ fm (lattice spacing), $n_z = 4$, and $n_t = 8$ (the Wilson line is taken to lie in the z direction, which, by convention, is denoted by $\mu = 1$). Expressed in GeV, $\bar{q} = (1.887, 0, 0, 2.048)$ GeV. To examine the impact of finite quark masses on the conversion factors, we plot six different cases of external quark masses:

1. massless quarks ($m_1 = m_2 = 0$)
2. $m_1 = m_2 = 13.2134$ MeV, corresponding to the bare twisted mass used in Ref. [110]
3. one up and one strange quark ($m_1 = 2.3$ MeV, $m_2 = 95$ MeV)
4. two strange quarks ($m_1 = m_2 = 95$ MeV)
5. one up and one charm quark ($m_1 = 2.3$ MeV, $m_2 = 1275$ MeV)
6. two charm quarks ($m_1 = m_2 = 1275$ MeV).

As regards the $\bar{q}$ dependence, we have not included further graphs for the sake of conciseness; however, using a variety of values for the components of $\bar{q}$, we find no significant difference. More quantitative assessments can be directly obtained from our algebraic results.

In Figs. 3.3 and 3.4, we present graphs of some representative conversion factors (C_{S,V_1}, C_{P,A_1}) for the six cases of external quark masses. The plots are given only for positive values of z, since the behavior of conversion factors for negative values follows the reflection relation of Eq.(3.64). We observe that the real part of the conversion factor matrix elements is an order of magnitude larger than the imaginary part and that the diagonal elements are an order of magnitude larger than the nondiagonal elements. Also, for increasing values of z, the real part of diagonal elements tends to increase, while the imaginary part as well as the real part of nondiagonal elements tend to stabilize. Diagonal elements are almost equal to each other, as regards both their real and imaginary parts; a similar behaviour is also exhibited by the nondiagonal elements. Further, the diagonal elements of C_{S,V_1} and C_{P,A_1} behave almost identically, while the nondiagonal elements have different behavior; this is to be expected, given that the cases of equal masses give zero nondiagonal elements for C_{P,A_1}. Comparing the six cases, we deduce that the impact of mass becomes significant when we include a strange or a charm quark; the presence of a strange quark causes changes of order $0.005 - 0.01$ for real parts, and $0.001 - 0.003$ for imaginary parts, while the presence of a charm quark causes changes of order $0.07 - 0.14$ for real parts and $0.015 - 0.03$ for imaginary parts. On the contrary, the cases of massless quarks and $m_1 = m_2 = 13.2134$ MeV are almost coincident. Therefore, we conclude that, for quark masses quite smaller than the strange quark mass, we may ignore the mass terms in our calculations, while

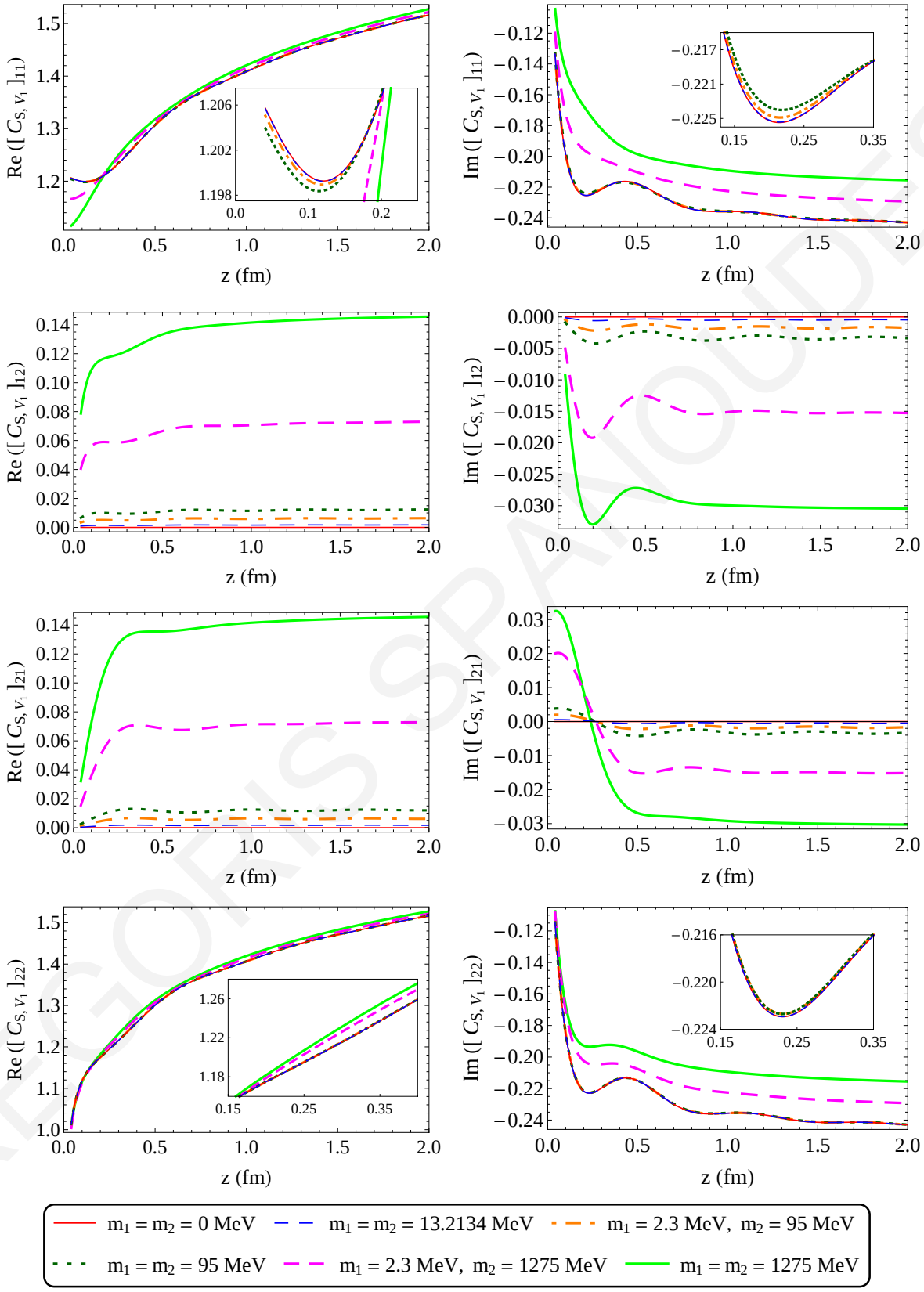

FIGURE 3.3: Real (left panels) and imaginary (right panels) parts of the conversion factor matrix elements for the operator pair (S, V_1) as a function of z, for different values of quark masses $[g^2 = 3.077, \quad \beta = 1, \quad N_c = 3, \quad \bar{\mu} = 2 \text{ GeV}, \quad \bar{q} = \frac{2\pi}{32\ (0.082\ \text{fm})}(4, 0, 0, \frac{17}{4})]$.

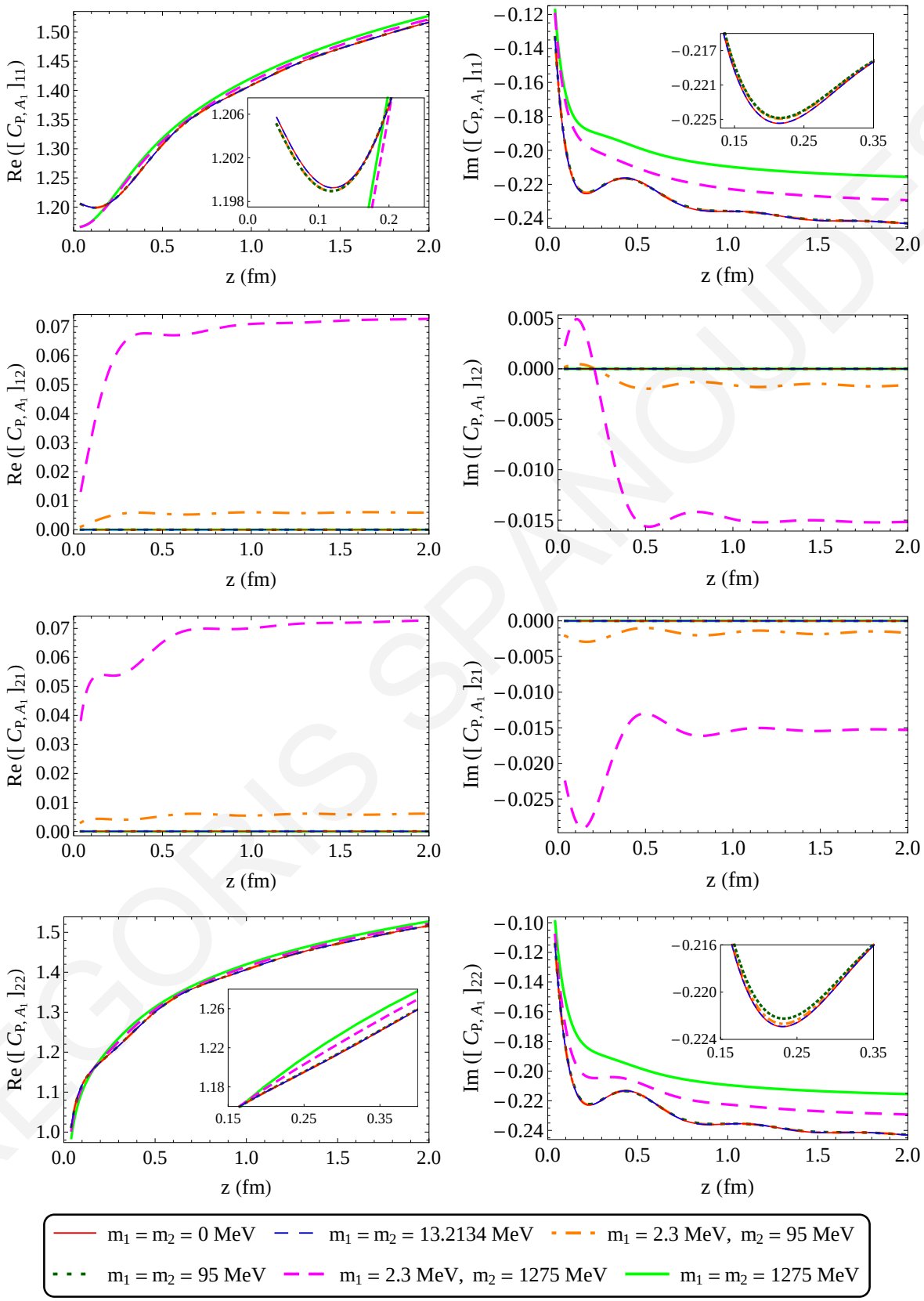

FIGURE 3.4: Real (left panels) and imaginary (right panels) parts of the conversion factor matrix elements for the operator pair $(P,\ A_1)$ as a function of z, for different values of quark masses $[g^2 = 3.077,\quad \beta = 1,\quad N_c = 3,\quad \bar{\mu} = 2$ GeV, $\bar{q} = \frac{2\pi}{32\ (0.082\ \text{fm})}(4, 0, 0, \frac{17}{4})]$.

for larger values, the mass terms are significant.

Regarding the convergence of the perturbative series, we note that one-loop contributions are a small fraction of the tree-level values, which is a desirable indication of stability. Nevertheless, given that these contributions are not insignificant, a two-loop calculation would be certainly welcome; this is further necessitated by the fact that the one-loop contributions for the real parts of the diagonal matrix elements of the conversion factors do not sufficiently stabilize for large values of z.

3.5 Summary

In this work, we have presented the one-loop calculation, in dimensional regularization, of the renormalization factors for nonlocal quark operators, including a straight Wilson line, which are involved in the definition of quasi-PDFs. The novel aspect of this work is the presence of nonzero quark masses in our computations, which results in mixing among these operators, both in the continuum and on the lattice.

The operator mixing, observed in Ref. [114] for massless fermions on the lattice, is extended into more operator pairs for massive fermions. More precisely, for operators with equal masses of external quark fields, the mixing pairs are the same as those of massless fermions; i.e., the unpolarized quasi-PDF in direction μ (parallel to the Wilson line) mixes with the twist-3 scalar operator, and the helicity quasi-PDF in direction ν (perpendicular to μ) mixes with the transversity quasi-PDF in directions perpendicular to μ and ν. However, for operators with different masses of external quark fields, there are additional pairs: the helicity quasi-PDF in direction μ mixes with the pseudoscalar operator, and the unpolarized quasi-PDF in direction ν mixes with the transversity quasi-PDF in the μ and ν directions. Thus, before matching to the physical massive PDFs, one must eliminate the mixing nonperturbatively. To this end, we extend the RI′ scheme suggested in Ref. [114] including the additional mixing pairs.

To convert the nonperturbative RI′ estimates of renormalization factors to the $\overline{\text{MS}}$ scheme, we have calculated the one-loop conversion factors between the two schemes in DR for massive quarks. Because of the operator-pair mixing in the continuum,

the conversion factors are generally nondiagonal 2×2 matrices. Comparing with the massless case, the impact of quark masses on the conversion factors becomes significant for values near or greater than the strange quark mass. Our findings can be used to the corresponding nonperturbative studies of heavy-quark quasi-PDFs.

Appendices

3.A List of Feynman parameter Integrals

In this appendix, we present a list of Feynman parameter integrals, which appear in the expressions of our results. They do not have a closed analytic form, but they are convergent and can be computed numerically in a straightforward manner, for any given value of their arguments. We can classify them into three types of integrals:
1. f_1 - f_3: integrals over the Feynman parameter x
2. g_1 - g_5: double integrals over the Feynman parameter x and variable ζ (the location of gluon fields along the Wilson line)
3. h_1 - h_8: double integrals over the Feynman parameters x_1 and x_2.
These integrals are functions of the external momentum 4-vector q_ν, the Wilson-line length z, and the external quark masses m_1 and/or m_2. Also, they involve a modified Bessel function of the second kind, K_0 or K_1. For the sake of brevity, we use the following notation:
$s \equiv \left(q^2\,(1-x)\,x + m^2 x\right)^{1/2}$ and $t \equiv \left(q^2\,(1-x_1-x_2)\,(x_1+x_2) + m_1^2\;x_1 + m_2^2\;x_2\right)^{1/2}$,

$$f_1\,(q,z,m) = \int_0^1 dx\;\; \exp\left(-\mathrm{i}q_\mu x z\right)\; K_0\left(|z|\,s\right), \tag{3.65}$$

$$f_2\,(q,z,m) = \int_0^1 dx\;\; \exp\left(-\mathrm{i}q_\mu x z\right)\; K_0\left(|z|\,s\right)\;\; (1-x), \tag{3.66}$$

$$f_3\,(q,z,m) = \int_0^1 dx\;\; \exp\left(-\mathrm{i}q_\mu x z\right)\; K_0\left(|z|\,s\right)\;\; (1-x)\;\frac{x^2}{s^2}, \tag{3.67}$$

$$g_1(q,z,m) = \int_0^1 dx \int_0^z d\zeta \ \exp\left(-\mathrm{i}q_\mu x\zeta\right) K_0\left(|\zeta|\, s\right), \tag{3.68}$$

$$g_2(q,z,m) = \int_0^1 dx \int_0^z d\zeta \ \exp\left(-\mathrm{i}q_\mu x\zeta\right) K_0\left(|\zeta|\, s\right) \ x, \tag{3.69}$$

$$g_3(q,z,m) = \int_0^1 dx \int_0^z d\zeta \ \exp\left(-\mathrm{i}q_\mu x\zeta\right) K_0\left(|\zeta|\, s\right) \ (1-x)\ \frac{x^2}{s^2}, \tag{3.70}$$

$$g_4(q,z,m) = \int_0^1 dx \int_0^z d\zeta \ \exp\left(-\mathrm{i}q_\mu x\zeta\right) K_0\left(|\zeta|\, s\right) \ (1-x)\ \frac{x^2}{s^2}\ \zeta, \tag{3.71}$$

$$g_5(q,z,m) = \int_0^1 dx \int_0^z d\zeta \ \exp\left(-\mathrm{i}q_\mu x\zeta\right) K_0\left(|\zeta|\, s\right) \ (1-x)\ \frac{x^3}{s^2}\ \zeta, \tag{3.72}$$

$$h_1(q,z,m_1,m_2) = \int_0^1 dx_1 \int_0^{1-x_1} dx_2 \ \exp\left(-\mathrm{i}q_\mu (x_1+x_2) z\right) K_0\left(|z|\, t\right), \tag{3.73}$$

$$h_2(q,z,m_1,m_2) = \int_0^1 dx_1 \int_0^{1-x_1} dx_2 \ \exp\left(-\mathrm{i}q_\mu (x_1+x_2) z\right) K_0\left(|z|\, t\right) \ (1-x_1-x_2), \tag{3.74}$$

$$h_3(q,z,m_1,m_2) = \int_0^1 dx_1 \int_0^{1-x_1} dx_2 \ \exp\left(-\mathrm{i}q_\mu (x_1+x_2) z\right) K_0\left(|z|\, t\right) \ (1-x_1-x_2)\cdot \frac{(x_1+x_2)^2}{t^2}, \tag{3.75}$$

$$h_4(q,z,m_1,m_2) = \int_0^1 dx_1 \int_0^{1-x_1} dx_2 \ \exp\left(-\mathrm{i}q_\mu (x_1+x_2) z\right) K_1\left(|z|\, t\right) \ t, \tag{3.76}$$

$$h_5(q,z,m_1,m_2) = \int_0^1 dx_1 \int_0^{1-x_1} dx_2 \ \exp\left(-\mathrm{i}q_\mu (x_1+x_2) z\right) K_1\left(|z|\, t\right) \ \frac{1}{t}, \tag{3.77}$$

$$h_6(q,z,m_1,m_2) = \int_0^1 dx_1 \int_0^{1-x_1} dx_2 \ \exp\left(-\mathrm{i}q_\mu (x_1+x_2) z\right) K_1\left(|z|\, t\right) \ \frac{(x_1+x_2)}{t}, \tag{3.78}$$

$$h_7(q,z,m_1,m_2) = \int_0^1 dx_1 \int_0^{1-x_1} dx_2 \ \exp\left(-\mathrm{i}q_\mu (x_1+x_2) z\right) K_1\left(|z|\, t\right) \ \frac{(1-x_1-x_2)^2}{t}, \tag{3.79}$$

$$h_8(q,z,m_1,m_2) = \int_0^1 dx_1 \int_0^{1-x_1} dx_2 \ \exp\left(-\mathrm{i}q_\mu (x_1+x_2) z\right) K_1\left(|z|\, t\right) \ (1-x_1-x_2)\cdot \frac{(x_1+x_2)^2}{t^3}. \tag{3.80}$$

Chapter 4

Perturbative renormalization of staple-shaped operators related to TMDs on the lattice

4.1 Introduction

In this work we generalize our calculations regarding Wilson-line operators (Ref. [114], Chapter 3) to include nonlocal operators with a staple-shaped Wilson line. We compute their Green's functions to one-loop level in perturbation theory using dimensional (DR) and lattice (LR) regularizations. The functional form of the Green's functions reveals the renormalization pattern and mixing among operators of different Dirac structure, in each regularization. We find that these operators renormalize multiplicatively in DR, but have finite mixing in LR. Results for both regularizations have been combined to extract the renormalization functions in the lattice $\overline{\text{MS}}$ scheme. In addition, the results in DR have been used to obtain the conversion factor between RI-type and $\overline{\text{MS}}$ schemes. We also present an extension to operators containing a Wilson line of arbitrary shape on the lattice, with n cusps.

Staple-shaped nonlocal operators (see Fig. 4.1) are crucial in studies of TMDs, which encode important details on the internal structure of hadrons. In particular, they give access to the intrinsic motion of partons with respect to the transverse momentum, through the formalism of QCD factorization, that can be used to link experimental data

to the three-dimensional partonic structure of hadrons. An operator with a staple of infinite length, $\eta \to \infty$, (see Fig. 4.1) enters the analysis of semi-inclusive deep inelastic scattering (SIDIS) processes[1] in a kinematical region where the photon virtuality is large and the measured transverse momentum of the produced hadron is of the order of $\Lambda_{\rm QCD}$ [187].

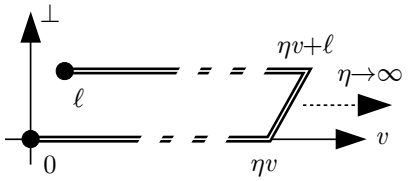

FIGURE 4.1: Staple-shaped gauge links as used in analyses of SIDIS and Drell-Yan processes. For notation, see Ref. [125].

To date, only limited studies of TMDs exist in lattice QCD (see, e.g., Refs. [125, 128, 188, 189] and references therein), such as the generalized Sivers and Boer-Mulders transverse momentum shifts for the SIDIS and Drell-Yan cases. These studies include staple links of finite length that is restricted by the spatial extent of the lattice volume. To recover the desired infinite length one checks for convergence as the length increases, and an extrapolation to $\eta \to \infty$ is applied. More recently, the connection between nonlocal operators with staple-shaped Wilson line and orbital angular momentum [190, 191] has been discussed. This relies on a comparison between straight and staple-shaped Wilson lines, with the staple-shaped path yielding the Jaffe-Manohar [192, 193] definition of quark orbital angular momentum, and the straight path yielding Ji's definition [193–195]. The difference between these two can be understood as the torque experienced by the struck quark as a result of final state interactions [193, 194].

An important aspect of calculations in lattice QCD is the renormalization that needs to be applied on the operators under study (unless conserved currents are used). As is known from older studies [143, 145–147, 196], the renormalization of Wilson-line operators in continuum theory (except DR) includes a divergent term $e^{-\delta m L}$, where δm is a dimensionful quantity whose magnitude diverges linearly with the regulator, and L is the total length of the contour. For staple-shaped operators, $L = (2|y| + |z|)$, where $y \lesseqgtr 0$ and $z \lesseqgtr 0$ define the extension of the staple in the $y-z$ plane, chosen to

[1] Staple-shaped operators appear also in Drell-Yan process, with the staple oriented in the opposite direction compared to SIDIS.

be spatial. The existing lattice calculations of staple-shaped operators assume that the lattice operators have the same renormalization properties as the continuum operators, in particular that there is no mixing present. This allows one to focus on ratios between such operators [125, 128, 188, 189] in order to cancel multiplicative renormalization, which is currently unknown[2]. However, as we show in this work, this is not the case for operators where finite mixing is present and must be taken into account.

One of the main goals of this study is to provide important information that may impact nonperturbative studies of TMDs and potentially lead to the development of a nonperturbative renormalization prescription similar to the case of quasi-PDFs discussed in Chapter 3. The chapter is organized in five sections including the following: In Sec. 4.2 we provide the set of operators under study, the lattice formulation, the renormalization prescription for nonlocal operators that mix under renormalization and the basics of the conversion to the $\overline{\text{MS}}$ scheme. Section 4.3 presents our main results in dimensional and lattice regularization. This includes both the renormalization functions and conversion factors between the RI′ and $\overline{\text{MS}}$ schemes. An extension of the work to include general nonlocal Wilson-line operators with n cusps is presented in Sec. 4.4, while in Sec. 4.5 we give a summary and conclusions. For completeness we include two appendices where we give a list of Feynman parameter integrals, which appear in the Green's functions of staple operators (Appendix 4.A), as well as the expressions related to the renormalization of the fermion fields (Appendix 4.B).

4.2 Calculation Setup

In this section we briefly introduce the setup of our calculation, along with the notation used in this chapter. We give the definitions of the operators and the lattice actions; we also provide the renormalization prescriptions that we use in the presence of operator mixing.

[2]The question of whether nonlocal operators with staple-shaped Wilson lines renormalize multiplicatively was raised in Ref. [128] after the work on straight Wilson-line operators [114].

4.2.1 Operator setup

The staple-shaped Wilson-line operators have the following form:

$$\mathcal{O}_\Gamma \equiv \bar{\psi}(x)\ \Gamma\ W(x, x+y\hat{\mu}_2, x+y\hat{\mu}_2+z\hat{\mu}_1, x+z\hat{\mu}_1)\ \psi(x+z\hat{\mu}_1), \tag{4.1}$$

where W denotes a staple with side lengths $|z|$ and $|y|$, which lies in the plane specified by the directions $\hat{\mu}_1$ and $\hat{\mu}_2$ (see Fig. 4.2); it is defined by

$$W(x, x+y\hat{\mu}_2, x+y\hat{\mu}_2+z\hat{\mu}_1, x+z\hat{\mu}_1) = \\ \mathcal{P}\Big\{ \left(e^{ig\int_0^y d\zeta A_{\mu_2}(x+\zeta\hat{\mu}_2)}\right) \cdot \left(e^{ig\int_0^z d\zeta A_{\mu_1}(x+y\hat{\mu}_2+\zeta\hat{\mu}_1)}\right) \cdot \left(e^{ig\int_0^y d\zeta A_{\mu_2}(x+z\hat{\mu}_1+\zeta\hat{\mu}_2)}\right)^\dagger \Big\}. \tag{4.2}$$

The symbol Γ can be one of the following Dirac matrices: $\mathbb{1}$, γ_5, γ_μ, $\gamma_5\gamma_\mu$, $\sigma_{\mu\nu}$ (where $\mu, \nu = 1, 2, 3, 4$ and $\sigma_{\mu\nu} = [\gamma_\mu, \gamma_\nu]/2$). For convenience, we adopt the following notation for each Dirac matrix: $S \equiv \mathbb{1}$, $P \equiv \gamma_5$, $V_\mu \equiv \gamma_\mu$, $A_\mu \equiv \gamma_5\gamma_\mu$, $T_{\mu\nu} \equiv \sigma_{\mu\nu}$ and the standard nomenclature for the corresponding operators: $\mathcal{O}_S$: scalar, $\mathcal{O}_P$: pseudoscalar, $\mathcal{O}_{V_\mu}$: vector, $\mathcal{O}_{A_\mu}$: axial-vector and $\mathcal{O}_{T_{\mu\nu}}$: tensor. Of particular interest is the study of vector, axial-vector and tensor operators, which correspond to the three types of TMDs: unpolarized, helicity and transversity, respectively.

The fermion and antifermion fields appearing in $\mathcal{O}_\Gamma$ can have different flavor indices. Operators with different flavor content cannot mix among themselves; further, for mass-independent renormalization schemes, flavor-nonsinglet operators which differ only in their flavor content will have the same renormalization factors and mixing coefficients. Results for the flavor-singlet case will be identical to those for the flavor-nonsinglet case at one loop, but they will differ beyond one loop and nonperturbatively; however, the setup described below [Eqs. (4.7 – 4.12)] will be identical in both cases.

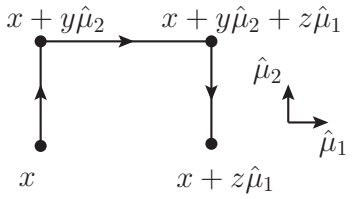

FIGURE 4.2: Staple-shaped Wilson line $W(x, x+y\hat{\mu}_2, x+y\hat{\mu}_2+z\hat{\mu}_1, x+z\hat{\mu}_1)$.

4.2.2 Lattice actions

In our lattice calculation we make use of the Wilson/clover fermion action [12]. In standard notation it reads

$$\begin{aligned} S_{\rm F} = &- \frac{a^3}{2} \sum_{x,f,\mu} \overline{\psi}_f(x) \Big[(r-\gamma_\mu) U_\mu(x)\ \psi_f(x+a\hat{\mu}) + (r+\gamma_\mu) U^\dagger_\mu(x-a\hat{\mu})\ \psi_f(x-a\hat{\mu}) \Big] \\ &+ a^3 \sum_{x,f} \overline{\psi}_f(x)\ (4r + a m_o^f)\ \psi_f(x) \\ &- \frac{a^3}{32} \sum_{x,f,\mu,\nu} c_{SW}\ \overline{\psi}_f(x)\ \sigma_{\mu\nu}\ \Big[Q_{\mu\nu}(x) - Q_{\nu\mu}(x) \Big]\ \psi_f(x)\,, \end{aligned} \tag{4.3}$$

where a is the lattice spacing and

$$\begin{aligned} Q_{\mu\nu} \ &= \ U_\mu(x)\ U_\nu(x+a\hat{\mu})\ U^\dagger_\mu(x+a\hat{\nu})\ U^\dagger_\nu(x) \\ &+ \ U_\nu(x)\ U^\dagger_\mu(x+a\hat{\nu}-a\hat{\mu})\ U^\dagger_\nu(x-a\hat{\mu})\ U_\mu(x-a\hat{\mu}) \\ &+ \ U^\dagger_\mu(x-a\hat{\mu})\ U^\dagger_\nu(x-a\hat{\mu}-a\hat{\nu})\ U_\mu(x-a\hat{\mu}-a\hat{\nu})\ U_\nu(x-a\hat{\nu}) \\ &+ \ U^\dagger_\nu(x-a\hat{\nu})\ U_\mu(x-a\hat{\nu})\ U_\nu(x+a\hat{\mu}-a\hat{\nu})\ U^\dagger_\mu(x). \end{aligned} \tag{4.4}$$

Following common practice, we henceforth set the Wilson parameter r equal to 1. The clover coefficient c_{SW} will be treated as a free parameter, for wider applicability of the results. The mass term ($\sim m_0^f$) will be irrelevant in our one-loop calculations, since we will apply mass-independent renormalization schemes. The above formulation, and thus our results, are also applicable to the twisted mass fermions [197] in the massless case. One should, however, keep in mind that, in going from the twisted basis to the physical basis, operator identifications are modified (e.g., the scalar density, under "maximal twist", turns into a pseudoscalar density, etc.).

For gluons, we employ a family of Symanzik improved actions [198], of the form,

$$\begin{aligned} S_G \ = \frac{2}{g_0^2} \Big[\ & c_0 \ \sum_{\rm plaq.} {\rm Re\,Tr}\,\{1 - U_{\rm plaq.}\} \ + \ c_1 \sum_{\rm rect.} {\rm Re\,Tr}\,\{1 - U_{\rm rect.}\} \\ + \ & c_2 \ \sum_{\rm chair} {\rm Re\,Tr}\,\{1 - U_{\rm chair}\} \ + \ c_3 \sum_{\rm paral.} {\rm Re\,Tr}\,\{1 - U_{\rm paral.}\} \Big]\,, \end{aligned} \tag{4.5}$$

where $U_{\rm plaq.}$ is the 4-link Wilson loop and $U_{\rm rect.}$, $U_{\rm chair}$, $U_{\rm paral.}$ are the three possible independent 6-link Wilson loops (see Fig. 4.3). The Symanzik coefficients c_i satisfy

the following normalization condition:

$$c_0 + 8c_1 + 16c_2 + 8c_3 = 1. \tag{4.6}$$

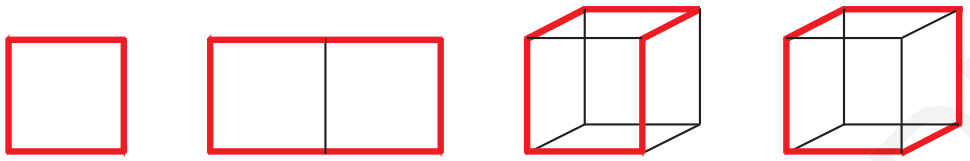

FIGURE 4.3: The four Wilson loops of the Symanzik improved gauge actions.

For the numerical integration over loop momenta we selected a variety of values for c_i, which are shown in Table 4.1; for the sake of compactness, in what follows we will present only results for some of the most frequently used sets of values: Wilson, Tree-level Symanzik and Iwasaki gluons.

Gluon action	c_0	c_1	c_2	c_3
Wilson	1	0	0	0
TL Symanzik	5/3	-1/12	0	0
TILW, βc_0 =8.60	2.3168064	-0.151791	0	-0.0128098
TILW, βc_0 =8.45	2.3460240	-0.154846	0	-0.0134070
TILW, βc_0 =8.30	2.3869776	-0.159128	0	-0.0142442
TILW, βc_0 =8.20	2.4127840	-0.161827	0	-0.0147710
TILW, βc_0 =8.10	2.4465400	-0.165353	0	-0.0154645
TILW, βc_0 =8.00	2.4891712	-0.169805	0	-0.0163414
Iwasaki	3.648	-0.331	0	0
DBW2	12.2688	-1.4086	0	0

TABLE 4.1: Values of the Symanzik coefficients for selected gluon actions: Wilson, Tree Level (TL) Symanzik, Tadpole Improved Lüscher-Weisz (TILW), Iwasaki, Doubly Blocked Wilson (DBW2). (Note: $\beta = 2N_c/g_0^2$).

4.2.3 Renormalization prescription

The renormalization of nonlocal operators is a nontrivial process. As shown in a previous study of straight-line operators in Ref. [114], a hidden operator mixing is present in chirality-breaking regularizations, such as the Wilson/clover fermions on

the lattice. This mixing does not involve any divergent terms; it stems from finite regularization-dependent terms, which are not present in the $\overline{\text{MS}}$ renormalization scheme, as defined in dimensional regularization (DR). Thus, our first goal is to compute perturbatively all renormalization functions and mixing coefficients which arise in going from the lattice regularization (LR) to the $\overline{\text{MS}}$ scheme. Ultimately, a nonperturbative evaluation of all these quantities is desirable; to this end, and given that the very definition of $\overline{\text{MS}}$ is perturbative, we must devise an appropriate, RI′-type renormalization prescription which reflects the operator mixing. We will proceed with the definition of the renormalization factors of operators, as mixing matrices, in textbook fashion. We modify the prescription described in Ref. [114] to correspond to the resulting operator-mixing pairs of the present calculation, which are different from those found in the straight-line operators. The reason behind this difference is explained in detail in Sec. 4.4. The mixing pairs found from our calculation on the lattice are (see Sec. 4.3.2.2): $(\mathcal{O}_P, \mathcal{O}_{A_{\mu_2}}), (\mathcal{O}_{V_i}, \mathcal{O}_{T_{i\mu_2}})$, where i can be any of the three orthogonal directions to the $\hat{\mu}_2$ direction. The remaining operators do not show any mixing, and thus their renormalization factors have the typical 1×1 form [see Eq. (4.9)]. Taking into account all the above, we define the renormalization factors which relate each bare operator $\mathcal{O}_\Gamma$ with the corresponding renormalized one via the following equations:

$$\begin{pmatrix} \mathcal{O}^Y_P \\ \mathcal{O}^Y_{A_{\mu_2}} \end{pmatrix} = \begin{pmatrix} Z^{X,Y}_P & Z^{X,Y}_{(P,A_{\mu_2})} \\ Z^{X,Y}_{(A_{\mu_2},P)} & Z^{X,Y}_{A_{\mu_2}} \end{pmatrix}^{-1} \begin{pmatrix} \mathcal{O}_P \\ \mathcal{O}_{A_{\mu_2}} \end{pmatrix}, \tag{4.7}$$

$$\begin{pmatrix} \mathcal{O}^Y_{V_i} \\ \mathcal{O}^Y_{T_{i\mu_2}} \end{pmatrix} = \begin{pmatrix} Z^{X,Y}_{V_i} & Z^{X,Y}_{(V_i,T_{i\mu_2})} \\ Z^{X,Y}_{(T_{i\mu_2},V_i)} & Z^{X,Y}_{T_{i\mu_2}} \end{pmatrix}^{-1} \begin{pmatrix} \mathcal{O}_{V_i} \\ \mathcal{O}_{T_{i\mu_2}} \end{pmatrix}, \quad (i \neq \mu_2) \tag{4.8}$$

$$\mathcal{O}^Y_\Gamma \;=\; \left(Z^{X,Y}_\Gamma\right)^{-1} \mathcal{O}_\Gamma, \qquad \Gamma = S, V_{\mu_2}, A_i, T_{ij}, \quad (i \neq j \neq \mu_2 \neq i), \tag{4.9}$$

where $X(Y)$ stands for the regularization (renormalization) scheme: $X = \text{DR}, \text{LR}, \ldots$, $Y = \overline{\text{MS}}, \text{RI}', \ldots$ As our one-loop calculations will show, in dimensional regularization there is no operator mixing and thus the mixing matrices are diagonal; this property is actually expected to hold to all loops, based on similar arguments as those of Refs. [143, 144, 146].

As is standard practice, the calculation of the renormalization factors of $\mathcal{O}_\Gamma$ stems from the evaluation of the corresponding one-particle-irreducible (1-PI) two-point amputated Green's functions $\Lambda_\Gamma \equiv \langle \psi_f \, \mathcal{O}_\Gamma \, \bar{\psi}_{f'} \rangle_{\text{amp}}$. According to the definitions of Eqs. (4.7 – 4.9),

the relations between the bare Green's functions and the renormalized ones are given by[3]

$$\begin{pmatrix} \Lambda^Y_P \\ \Lambda^Y_{A_{\mu_2}} \end{pmatrix} = \left(Z^{X,Y}_{\psi_f}\right)^{1/2} \left(Z^{X,Y}_{\psi_{f'}}\right)^{1/2} \begin{pmatrix} Z^{X,Y}_P & Z^{X,Y}_{(P,A_{\mu_2})} \\ Z^{X,Y}_{(A_{\mu_2},P)} & Z^{X,Y}_{A_{\mu_2}} \end{pmatrix}^{-1} \begin{pmatrix} \Lambda^X_P \\ \Lambda^X_{A_{\mu_2}} \end{pmatrix}, \tag{4.10}$$

$$\begin{pmatrix} \Lambda^Y_{V_i} \\ \Lambda^Y_{T_{i\mu_2}} \end{pmatrix} = \left(Z^{X,Y}_{\psi_f}\right)^{1/2} \left(Z^{X,Y}_{\psi_{f'}}\right)^{1/2} \begin{pmatrix} Z^{X,Y}_{V_i} & Z^{X,Y}_{(V_i,T_{i\mu_2})} \\ Z^{X,Y}_{(T_{i\mu_2},V_i)} & Z^{X,Y}_{T_{i\mu_2}} \end{pmatrix}^{-1} \begin{pmatrix} \Lambda^X_{V_i} \\ \Lambda^X_{T_{i\mu_2}} \end{pmatrix}, (i \neq \mu_2) \tag{4.11}$$

$$\Lambda^Y_\Gamma = \left(Z^{X,Y}_{\psi_f}\right)^{1/2} \left(Z^{X,Y}_{\psi_{f'}}\right)^{1/2} \left(Z^{X,Y}_\Gamma\right)^{-1} \Lambda^X_\Gamma, \quad \Gamma = S, V_{\mu_2}, A_i, T_{ij}, \ (i \neq j \neq \mu_2 \neq i), \tag{4.12}$$

where $Z^{X,Y}_{\psi_f}, Z^{X,Y}_{\psi_{f'}}$ are the renormalization factors of the external quark fields of flavors f and f' respectively, defined through the relation,

$$\psi^Y_{f(f')} = \left(Z^{X,Y}_{\psi_{f(f')}}\right)^{-1/2} \psi_{f(f')}. \tag{4.13}$$

We note that in the case of massless quarks, the flavor content does not affect the renormalization factors of fermion fields or the Green's functions of $\mathcal{O}_\Gamma$, and thus we omit the flavor index in the sequel. We also note that for regularizations which break chiral symmetry (such as Wilson/clover fermions), an additive mass renormalization is also needed, beyond one loop; however, this is irrelevant for our one-loop calculations. The expressions of Λ_Γ depend on the coupling constant g_0, whose renormalization factor is defined through

$$g^Y = \mu^{(D-4)/2} \left(Z^{X,Y}_g\right)^{-1} g_0, \tag{4.14}$$

where μ is related to the $\overline{\text{MS}}$ renormalization scale $\bar{\mu}$ ($\bar{\mu} \equiv \mu(4\pi/e^{\gamma_E})^{1/2}$, γ_E is Euler's constant) and D is the number of Euclidean spacetime dimensions (in DR: $D \equiv 4 - 2\varepsilon$, in LR: $D = 4$). For our one-loop calculations, $Z^{X,Y}_g$ is set to 1 (tree-level value).

There are four one-loop Feynman diagrams contributing to Λ_Γ, shown in Fig. 4.4. Diagrams $d_2 - d_4$ are further divided into subdiagrams, shown in Fig. 4.5, depending on the side of the staple from which gluons emanate.

In our computations we make use of two renormalization schemes: the modified minimal-subtraction scheme ($\overline{\text{MS}}$) and a variant of the modified

[3] In the right-hand sides of Eqs. (4.10 – 4.12) it is, of course, understood that the regulators must be set to their limit values.

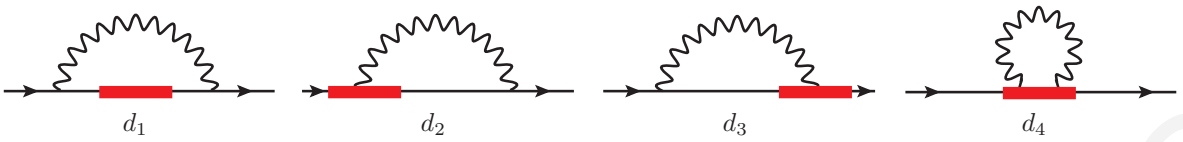

FIGURE 4.4: Feynman diagrams contributing to the one-loop calculation of the Green's functions of staple operator $\mathcal{O}_\Gamma$. The straight (wavy) lines represent fermions (gluons). The operator insertion is denoted by a filled rectangle.

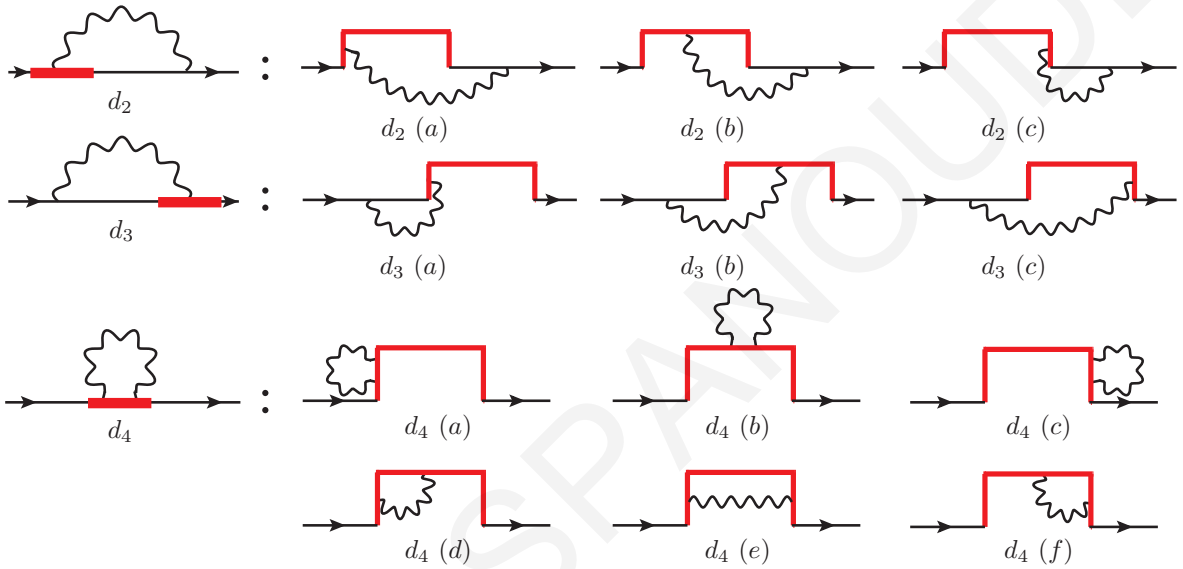

FIGURE 4.5: Subdiagrams contributing to the one-loop calculation of the Green's functions of staple operator $\mathcal{O}_\Gamma$. The straight (wavy) lines represent fermions (gluons). The operator insertion is denoted by a staple-shaped line.

regularization-independent scheme (RI′). The second one is needed for the nonperturbative evaluations of the renormalized Green's functions Λ_Γ on the lattice, which will be converted to $\overline{\text{MS}}$, through appropriate conversion factors. For our perturbative lattice calculations, the renormalization factors of $\mathcal{O}_\Gamma$ in the $\overline{\text{MS}}$ scheme can be derived by calculating Eqs. (4.10 – 4.12) for both $X = \text{LR}$ and $X = \text{DR}$, and demanding that their left-hand sides are X-independent and, thus, identical in the two regularizations.

For the RI′ scheme, we extend the standard renormalization conditions for the bilinear operators, consistently with the definitions of Eqs. (4.10 – 4.12),

$$\text{tr}\Big[\begin{pmatrix}\Lambda_P^{\text{RI}'}\\ \Lambda_{A_{\mu_2}}^{\text{RI}'}\end{pmatrix}\Big((\Lambda_P^{\text{tree}})^\dagger \;\; (\Lambda_{A_{\mu_2}}^{\text{tree}})^\dagger\Big)\Big]\Big|_{\substack{q_\nu=\bar{q}_\nu\\(\forall\nu)}} = \text{tr}\Big[\begin{pmatrix}\Lambda_P^{\text{tree}}\\ \Lambda_{A_{\mu_2}}^{\text{tree}}\end{pmatrix}\Big((\Lambda_P^{\text{tree}})^\dagger \;\; (\Lambda_{A_{\mu_2}}^{\text{tree}})^\dagger\Big)\Big] = 4N_c\mathbb{1}_{2\times 2},$$

$$\mathrm{tr}\Big[\begin{pmatrix}\Lambda^{\mathrm{RI}'}_{V_i}\\ \\ \Lambda^{\mathrm{RI}'}_{T_{i\mu_2}}\end{pmatrix}\Big((\Lambda^{\mathrm{tree}}_{V_i})^\dagger \;\; (\Lambda^{\mathrm{tree}}_{T_{i\mu_2}})^\dagger\Big)\Big]\Big|_{\substack{q_\nu=\bar{q}_\nu\\(\forall\nu)}} = \mathrm{tr}\Big[\begin{pmatrix}\Lambda^{\mathrm{tree}}_{V_i}\\ \\ \Lambda^{\mathrm{tree}}_{T_{i\mu_2}}\end{pmatrix}\Big((\Lambda^{\mathrm{tree}}_{V_i})^\dagger \;\; (\Lambda^{\mathrm{tree}}_{T_{i\mu_2}})^\dagger\Big)\Big] = 4N_c\mathbb{1}_{2\times 2},$$

$$(i\neq\mu_2), \quad (4.15)$$

$$\mathrm{tr}\Big[\Lambda^{\mathrm{RI}'}_\Gamma(\Lambda^{\mathrm{tree}}_\Gamma)^\dagger\Big]\Big|_{\substack{q_\nu=\bar{q}_\nu\\(\forall\nu)}} = \mathrm{tr}\Big[\Lambda^{\mathrm{tree}}_\Gamma(\Lambda^{\mathrm{tree}}_\Gamma)^\dagger\Big] = 4N_c, \quad \Gamma = S, V_{\mu_2}, A_i, T_{ij},\ (i\neq j\neq\mu_2\neq i), \quad (4.16)$$

where $\Lambda^{\mathrm{tree}}_\Gamma \equiv \Gamma\exp(iq_{\mu_1}z)$ is the tree-level value of the Green's functions of $\mathcal{O}_\Gamma$, $\bar{q}$ is the RI′ renormalization scale four-vector, and N_c is the number of colors. Note that the traces appearing in Eqs. (4.15 – 4.16) regard only Dirac and color indices; in particular, Eqs. (4.15) and (4.15) retain their 2×2 matrix form, and thus they each correspond to four conditions. We mention that an alternative definition of the RI′ scheme can be adopted so that the renormalization factors depend only on a minimal set of parameters, $(\bar{q}^2, \bar{q}_{\mu_1}, \bar{q}_{\mu_2})$, rather than all the individual components of $\bar{q}$; this can be achieved by taking the average over all allowed values of the indices i, j, in conditions (4.15) and (4.16), whenever i, j are present. This alternative scheme is not so useful in lattice simulations, where, besides the two special directions of the plane in which the staple lies, the temporal direction stands out from the remaining spatial directions; this leaves us with only one nonspecial direction, and thus this choice of normalization is not particularly advantageous in this case.

The RI′ renormalization factors of fermion fields can be derived by imposing the massless normalization condition,

$$\mathrm{tr}\Big[S^{\mathrm{RI}'}(S^{\mathrm{tree}})^{-1}\Big]\Big|_{q^2=\bar{q}^2} = \mathrm{tr}\Big[S^{\mathrm{tree}}(S^{\mathrm{tree}})^{-1}\Big] = 4N_c, \quad (4.17)$$

where $S^{\mathrm{RI}'} \equiv \langle\psi^{\mathrm{RI}'}\bar{\psi}^{\mathrm{RI}'}\rangle$ is the RI′-renormalized quark propagator and $S^{\mathrm{tree}} \equiv (i\not{q})^{-1}$ is its tree-level value.

4.2.4 Conversion to the $\overline{\mathrm{MS}}$ scheme

The conversion of the nonperturbative RI′-renormalized Green's functions $\Lambda^{\mathrm{RI}'}_\Gamma$ to the $\overline{\mathrm{MS}}$ scheme can be performed only perturbatively, since the definition of $\overline{\mathrm{MS}}$ is perturbative in nature. The corresponding one-loop conversion factors between the

two schemes are extracted from our calculations, and their explicit expressions are presented in Sec. 4.3. As a consequence of the observed operator-pair mixing, some of the conversion factors will be 2×2 matrices, just as the renormalization factors of the operators. Following the definitions of Eqs. (4.7 – 4.8), they are defined as

$$\begin{pmatrix} C_{P}^{\overline{\text{MS}},\text{RI}'} & C_{(P,A_{\mu_2})}^{\overline{\text{MS}},\text{RI}'} \\ C_{(A_{\mu_2},P)}^{\overline{\text{MS}},\text{RI}'} & C_{A_{\mu_2}}^{\overline{\text{MS}},\text{RI}'} \end{pmatrix} = \begin{pmatrix} Z_{P}^{X,\overline{\text{MS}}} & Z_{(P,A_{\mu_2})}^{X,\overline{\text{MS}}} \\ Z_{(A_{\mu_2},P)}^{X,\overline{\text{MS}}} & Z_{A_{\mu_2}}^{X,\overline{\text{MS}}} \end{pmatrix}^{-1} \begin{pmatrix} Z_{P}^{X,\text{RI}'} & Z_{(P,A_{\mu_2})}^{X,\text{RI}'} \\ Z_{(A_{\mu_2},P)}^{X,\text{RI}'} & Z_{A_{\mu_2}}^{X,\text{RI}'} \end{pmatrix}, \tag{4.18}$$

$$\begin{pmatrix} C_{V_i}^{\overline{\text{MS}},\text{RI}'} & C_{(V_i,T_{i\mu_2})}^{\overline{\text{MS}},\text{RI}'} \\ C_{(T_{i\mu_2},V_i)}^{\overline{\text{MS}},\text{RI}'} & C_{T_{i\mu_2}}^{\overline{\text{MS}},\text{RI}'} \end{pmatrix} = \begin{pmatrix} Z_{V_i}^{X,\overline{\text{MS}}} & Z_{(V_i,T_{i\mu_2})}^{X,\overline{\text{MS}}} \\ Z_{(T_{i\mu_2},V_i)}^{X,\overline{\text{MS}}} & Z_{T_{i\mu_2}}^{X,\overline{\text{MS}}} \end{pmatrix}^{-1} \begin{pmatrix} Z_{V_i}^{X,\text{RI}'} & Z_{(V_i,T_{i\mu_2})}^{X,\text{RI}'} \\ Z_{(T_{i\mu_2},V_i)}^{X,\text{RI}'} & Z_{T_{i\mu_2}}^{X,\text{RI}'} \end{pmatrix}, (i \neq \mu_2), \tag{4.19}$$

$$C_{\Gamma}^{\overline{\text{MS}},\text{RI}'} = (Z_{\Gamma}^{X,\overline{\text{MS}}})^{-1} (Z_{\Gamma}^{X,\text{RI}'}), \quad \Gamma = S, V_{\mu_2}, A_i, T_{ij}, \ (i \neq j \neq \mu_2 \neq i). \tag{4.20}$$

Being regularization independent, they can be evaluated more easily in $X = \text{DR}$; in this regularization there is no operator mixing, and thus the conversion factors of $\mathcal{O}_\Gamma$ turn out to be diagonal. We note in passing that the definition of the $\overline{\text{MS}}$ scheme depends on the prescription used for extending γ_5 to D dimensions[4]; this, in particular, will affect conversion factors for the pseudoscalar and axial-vector operators. However, such a dependence will only appear beyond one loop.

Given that the conversion factors are diagonal, the Green's functions of $\mathcal{O}_\Gamma$ in the RI′ scheme can be directly converted to the $\overline{\text{MS}}$ scheme through the following relation, valid for all Γ:

$$\Lambda_{\Gamma}^{\overline{\text{MS}}} = (C_{\psi}^{\overline{\text{MS}},\text{RI}'})^{-1} C_{\Gamma}^{\overline{\text{MS}},\text{RI}'} \Lambda_{\Gamma}^{\text{RI}'}, \tag{4.21}$$

where $\mathcal{C}_{\psi}^{\overline{\text{MS}},\text{RI}'} \equiv (Z_{\psi}^{X,\overline{\text{MS}}})^{-1} Z_{\psi}^{X,\text{RI}'}$ is the conversion factor for fermion fields.

4.3 Calculation procedure and Results

In this section we proceed with the one-loop calculation of the renormalization factors of the staple operators in the RI′ and $\overline{\text{MS}}$ renormalization schemes, both in dimensional and lattice regularizations. We apply the prescription described above, and we present our final results. We also include the one-loop expressions for the conversion factors between the two schemes.

[4]See, e.g., Refs. [50, 179–183] for a discussion of four relevant prescriptions and some conversion factors among them.

4.3.1 Calculation in dimensional regularization

4.3.1.1 Methodology

We calculate the bare Green's functions of the staple operators in D Euclidean spacetime dimensions (where $D \equiv 4 - 2\varepsilon$ and ε is the regulator), in which momentum-loop integrals are well-defined. The methodology for calculating these integrals is briefly described in the work of Ref. [183] regarding straight Wilson-line operators, as well as on Chapter 3 section 3.3, and it is summarized below: We follow the standard procedure of introducing Feynman parameters. The momentum-loop integrals depend on exponential functions of the μ_1- and/or μ_2-component of the internal momentum [e.g., $\exp(ip_{\mu_1}z)$, $\exp(ip_{\mu_1}\zeta)$]. The integration over the components of momentum without an exponential dependence is performed using standard D-dimensional formulae (e.g., [184]), followed by a subsequent nontrivial integration over the remaining components p_{μ_1} and/or p_{μ_2}. The resulting expressions contain a number of Feynman parameter integrals and/or integrals over ζ-variables stemming from the definition of $\mathcal{O}_\Gamma$, which depend on modified Bessel functions of the second kind, K_n and which do not have a closed analytic form; they are listed in Appendix 4.A. We expand these expressions as Laurent series in ε and we keep only terms up to $\mathcal{O}(\varepsilon^0)$. The full expressions of the bare Green's functions of $\mathcal{O}_\Gamma$ are given in the following subsection.

4.3.1.2 Green's functions in dimensional regularization

In this subsection, the full expressions for the one-loop amputated Green's functions of the staple operators $\Lambda_\Gamma^{1-\text{loop}}$, calculated in dimensional regularization (DR), are presented in a compact form [Eqs. (4.22 – 4.31)]. From these expressions it is straightforward to derive the renormalized Green's functions, both in the $\overline{\text{MS}}$ scheme [by removing the $\mathcal{O}(1/\varepsilon)$ terms] and in any variant of the RI′ scheme, as described in Sec. 4.2.3; the corresponding conversion factors [Eqs. (4.18 – 4.20)] also follow immediately. The functions $\Lambda_\Gamma^{1-\text{loop}}$ depend on integrals of modified Bessel functions of the second kind, K_n, over Feynman parameters and/or over ζ-variables stemming from the definition of the staple operators. These integrals are denoted by $P_i \equiv P_i(q^2, q_{\mu_1}, z)$, $Q_i \equiv Q_i(q^2, q_{\mu_1}, q_{\mu_2}, z, y)$ and $R_i \equiv R_i(q^2, q_{\mu_1}, q_{\mu_2}, z, y)$; they are listed in Appendix 4.A [Eqs. (4.67 – 4.84)].

$$\begin{aligned}\Lambda_S^{\text{1-loop}} = \frac{g^2 C_F}{16\pi^2}\Bigg\{ \Lambda_S^{\text{tree}}\Bigg[&(8-\beta)\left(2+\frac{1}{\varepsilon}+\log\left(\frac{\overline{\mu}^2}{q^2}\right)\right) + 2(\beta+6)\gamma_E + (\beta+2)\log\left(\frac{q^2z^2}{4}\right) \\ &+ 4\log\left(\frac{q^2y^2}{4}\right) + 4\left(2\,\frac{y}{z}\tan^{-1}\left(\frac{y}{z}\right) - \log\left(1+\frac{y^2}{z^2}\right)\right) + 2(\beta+2)P_1 \\ &- 2\beta\sqrt{q^2}\,|z|\,P_4 + 2q_{\mu_1}\Big(2Q_4 - i\Big(2Q_1 - \beta z(P_1-P_2)\Big)\Big) \\ &+ 4q_{\mu_2}\Big(R_6 - R_2 + i(R_1-R_4)\Big)\Bigg] \\ &+ \Lambda_{T_{\mu_1\mu_2}}^{\text{tree}}\Big[4\sqrt{q^2}(yQ_3+zR_5)\Big] + \Lambda_{V_{\mu_1}}^{\text{tree}} \not{q}\Big[-4Q_4\Big] + \Lambda_{V_{\mu_2}}^{\text{tree}} \not{q}\Big[4i(R_4-R_1)\Big]\Bigg\},\end{aligned} \tag{4.22}$$

$$\Lambda_P^{\text{1-loop}} = \gamma_5 \Lambda_S^{\text{1-loop}}, \tag{4.23}$$

$$\begin{aligned}\Lambda_{V_{\mu_1}}^{\text{1-loop}} = \frac{g^2 C_F}{16\pi^2}\Bigg\{ \Lambda_{V_{\mu_1}}^{\text{tree}}\Bigg[&\beta + (8-\beta)\left(2+\frac{1}{\varepsilon}+\log\left(\frac{\overline{\mu}^2}{q^2}\right)\right) + 2(\beta+6)\gamma_E + (\beta+2)\log\left(\frac{q^2z^2}{4}\right) \\ &+ 4\log\left(\frac{q^2y^2}{4}\right) + 4\left(2\,\frac{y}{z}\tan^{-1}\left(\frac{y}{z}\right) - \log\left(1+\frac{y^2}{z^2}\right)\right) + 2(\beta P_1 - 2P_2) \\ &- \frac{1}{2}\beta q^2 z^2 (P_1-P_2) - 2iq_{\mu_1}\Big(2(Q_1+Q_2+zP_3) - \beta z(P_1-P_2)\Big) \\ &- 2\sqrt{q^2}\,|z|\,(\beta P_4 - 2P_5) + 4q_{\mu_2}\Big(R_6 - R_2 + i(R_1-R_4)\Big)\Bigg] \\ &+ \Lambda_{V_{\mu_2}}^{\text{tree}}\Bigg[4i\Big(\sqrt{q^2}(yQ_5+zR_8) + q_{\mu_1}\Big(R_4 - R_1 + i(R_3-R_7)\Big)\Big)\Bigg] \\ &+ \Lambda_S^{\text{tree}} \not{q}\Bigg[i\Big(4(Q_2 - zP_3) - \beta\sqrt{q^2}z\,|z|\,(P_4-P_5)\Big) \\ &\qquad + q_{\mu_1}\left(2\frac{|z|}{\sqrt{q^2}}\Big((\beta-2)P_4 + 2P_5\Big) + \beta z^2 P_3\right)\Bigg] \\ &+ \Lambda_{T_{\mu_1\mu_2}}^{\text{tree}} \not{q}\Big[4i(R_4-R_1)\Big]\Bigg\},\end{aligned} \tag{4.24}$$

$$\begin{aligned}\Lambda^{\text{1-loop}}_{V_{\mu_2}} = \frac{g^2 C_F}{16\pi^2}\Bigg\{ & \Lambda^{\text{tree}}_{V_{\mu_2}}\Bigg[(8-\beta)\left(2+\frac{1}{\varepsilon}+\log\left(\frac{\overline{\mu}^2}{q^2}\right)\right) + 2(\beta+6)\gamma_E + (\beta+2)\log\left(\frac{q^2z^2}{4}\right) \\ & + 4\log\left(\frac{q^2y^2}{4}\right) + 4\left(2\,\frac{y}{z}\tan^{-1}\left(\frac{y}{z}\right) - \log\left(1+\frac{y^2}{z^2}\right)\right) + 2(\beta P_1 - 2P_2) \\ & - \beta\sqrt{q^2}\,|z|\,P_4 + 2q_{\mu_1}\Big(2Q_4 - i\Big(2Q_1 - \beta z(P_1-P_2)\Big)\Big) \\ & - 4q_{\mu_2}(R_2+R_3-R_6-R_7)\Bigg] \\ & + \Lambda^{\text{tree}}_{V_{\mu_1}}\Bigg[-i\Bigg(4\sqrt{q^2}(yQ_5+zR_8) \\ & \quad + q_{\mu_2}\left(4(Q_2+zP_3-iQ_4) - \beta\sqrt{q^2}z\,|z|\,(P_4-P_5)\right)\Bigg)\Bigg] \\ & + \Lambda^{\text{tree}}_{S}\not{q}\Bigg[4(R_3-R_7) + q_{\mu_2}\Big(2\frac{|z|}{\sqrt{q^2}}\Big((\beta-2)P_4+2P_5\Big) - \beta z^2 P_3\Big)\Bigg] \\ & + \Lambda^{\text{tree}}_{T_{\mu_1\mu_2}}\not{q}\Big[4Q_4\Big]\Bigg\}, \end{aligned} \tag{4.25}$$

$$\begin{aligned}\Lambda^{\text{1-loop}}_{V_{\nu}} = \frac{g^2 C_F}{16\pi^2}\Bigg\{ & \Lambda^{\text{tree}}_{V_{\nu}}\Bigg[(8-\beta)\left(2+\frac{1}{\varepsilon}+\log\left(\frac{\overline{\mu}^2}{q^2}\right)\right) + 2(\beta+6)\gamma_E + (\beta+2)\log\left(\frac{q^2z^2}{4}\right) \\ & + 4\log\left(\frac{q^2y^2}{4}\right) + 4\left(2\,\frac{y}{z}\tan^{-1}\left(\frac{y}{z}\right) - \log\left(1+\frac{y^2}{z^2}\right)\right) + 2(\beta P_1 - 2P_2) \\ & - \beta\sqrt{q^2}\,|z|\,P_4 + 2q_{\mu_1}\Big(2Q_4 - i\Big(2Q_1 - \beta z(P_1-P_2)\Big)\Big) \\ & + 4q_{\mu_2}\Big(R_6 - R_2 + i(R_1-R_4)\Big)\Bigg] \\ & + \Lambda^{\text{tree}}_{V_{\mu_1}} q_\nu\Bigg[-i\left(4(Q_2+zP_3-iQ_4) - \beta\sqrt{q^2}\;z\,|z|\,(P_4-P_5)\right)\Bigg] \\ & + \Lambda^{\text{tree}}_{V_{\mu_2}} q_\nu\Big[4i\Big(R_4 - R_1 + i(R_3-R_7)\Big)\Big] + \varepsilon_{\mu_1\mu_2\nu\rho}\;\Lambda^{\text{tree}}_{A_\rho}\Big[4\sqrt{q^2}(yQ_3+zR_5)\Big] \\ & + \Lambda^{\text{tree}}_{S}\not{q}q_\nu\Big[2\frac{|z|}{\sqrt{q^2}}\Big((\beta-2)P_4+2P_5\Big) - \beta z^2 P_3\Big] + \Lambda^{\text{tree}}_{T_{\mu_1\nu}}\not{q}\Big[4Q_4\Big] \\ & + \Lambda^{\text{tree}}_{T_{\mu_2\nu}}\not{q}\Big[4i(R_1-R_4)\Big]\Bigg\}, \qquad (\nu\neq\mu_1,\mu_2) \end{aligned} \tag{4.26}$$

$$\Lambda^{\text{1-loop}}_{A_{\mu_1}} = \gamma_5\Lambda^{\text{1-loop}}_{V_{\mu_1}}, \quad \Lambda^{\text{1-loop}}_{A_{\mu_2}} = \gamma_5\Lambda^{\text{1-loop}}_{V_{\mu_2}} \quad \Lambda^{\text{1-loop}}_{A_{\nu}} = \gamma_5\Lambda^{\text{1-loop}}_{V_{\nu}}, \qquad (\nu\neq\mu_1,\mu_2) \tag{4.27}$$

$$\Lambda^{\text{1-loop}}_{T_{\mu_1\mu_2}} = \frac{g^2 C_F}{16\pi^2}\Bigg\{\Lambda^{\text{tree}}_{T_{\mu_1\mu_2}}\Bigg[\beta + (8-\beta)\left(2+\frac{1}{\varepsilon}+\log\left(\frac{\overline{\mu}^2}{q^2}\right)\right) + 2(\beta+6)\gamma_E + (\beta+2)\log\left(\frac{q^2z^2}{4}\right) + 4\log\left(\frac{q^2y^2}{4}\right) + 4\left(2\,\frac{y}{z}\tan^{-1}\left(\frac{y}{z}\right) - \log\left(1+\frac{y^2}{z^2}\right)\right) + 2(\beta-2)P_1 - \frac{1}{2}\beta q^2 z^2 (P_1-P_2) - 2iq_{\mu_1}\Big(2(Q_1+Q_2) - \beta z(P_1-P_2)\Big) - \beta\sqrt{q^2}\,|z|\,P_4 - 4q_{\mu_2}(R_2+R_3-R_6-R_7)\Bigg] + \Lambda^{\text{tree}}_{S}\Bigg[-4\sqrt{q^2}(yQ_3+zR_5) + 4iq_{\mu_1}\Big(R_4-R_1+i(R_3-R_7)\Big) + iq_{\mu_2}\Big(4(Q_2-iQ_4) - \beta\sqrt{q^2}\;z\,|z|\,(P_4-P_5)\Big)\Bigg] + \Lambda^{\text{tree}}_{V_{\mu_1}}\not{q}\Big[4(R_3-R_7) + \beta q_{\mu_2} z^2 P_3\Big] + \Lambda^{\text{tree}}_{V_{\mu_2}}\not{q}\Bigg[-i\Big(4Q_2 - \beta\sqrt{q^2}\;z\,|z|\,(P_4-P_5)\Big) - \beta q_{\mu_1} z^2 P_3\Bigg]\Bigg\}, \tag{4.28}$$

$$\Lambda^{\text{1-loop}}_{T_{\mu_1\nu}} = \frac{g^2 C_F}{16\pi^2}\Bigg\{\Lambda^{\text{tree}}_{T_{\mu_1\nu}}\Bigg[\beta + (8-\beta)\left(2+\frac{1}{\varepsilon}+\log\left(\frac{\overline{\mu}^2}{q^2}\right)\right) + 2(\beta+6)\gamma_E + (\beta+2)\log\left(\frac{q^2z^2}{4}\right) + 4\log\left(\frac{q^2y^2}{4}\right) + 4\left(2\,\frac{y}{z}\tan^{-1}\left(\frac{y}{z}\right) - \log\left(1+\frac{y^2}{z^2}\right)\right) + 2(\beta-2)P_1 - \frac{1}{2}\beta q^2 z^2 (P_1-P_2) - 2iq_{\mu_1}\Big(2(Q_1+Q_2) - \beta z(P_1-P_2)\Big) - \beta\sqrt{q^2}\,|z|\,P_4 + 4q_{\mu_2}\Big(R_6-R_2+i(R_1-R_4)\Big)\Bigg] + \Lambda^{\text{tree}}_{T_{\mu_1\mu_2}}\Big[4iq_\nu(R_4-R_1+i(R_3-R_7))\Big] + \Lambda^{\text{tree}}_{T_{\mu_2\nu}}\Big[4i\Big(\sqrt{q^2}(yQ_5+zR_8) + q_{\mu_1}(R_4-R_1+i(R_3-R_7))\Big)\Big] + \Lambda^{\text{tree}}_{S} q_\nu\Big[i\Big(4(Q_2-iQ_4) - \beta\sqrt{q^2}\;z\,|z|\,(P_4-P_5)\Big)\Big] + \Lambda^{\text{tree}}_{V_{\mu_1}}\not{q}\Big[\beta q_\nu z^2 P_3\Big] + \Lambda^{\text{tree}}_{V_\nu}\not{q}\Big[-i\Big(4Q_2 - \beta\sqrt{q^2}\;z\,|z|\,(P_4-P_5)\Big) - \beta q_{\mu_1} z^2 P_3\Big] + \epsilon_{\mu_1\mu_2\nu\rho}\,\Lambda^{\text{tree}}_{A_\rho}\not{q}\Big[4i(R_1-R_4)\Big]\Bigg\}, \qquad (\nu \neq \mu_1,\mu_2) \tag{4.29}$$

$$\Lambda^{\text{1-loop}}_{T_{\mu_2\nu}} = -\gamma_5\;\varepsilon_{\mu_1\mu_2\nu\rho}\;\Lambda^{\text{1-loop}}_{T_{\mu_1\rho}}, \qquad (\nu \neq \mu_1,\mu_2) \tag{4.30}$$

$$\Lambda^{\text{1-loop}}_{T_{\nu\rho}} = -\gamma_5\, \varepsilon_{\mu_1\mu_2\nu\rho}\, \Lambda^{\text{1-loop}}_{T_{\mu_1\mu_2}}, \qquad (\nu,\rho \neq \mu_1,\mu_2). \tag{4.31}$$

In Eqs. (4.30, 4.31), $\varepsilon_{\mu_1\mu_2\nu\rho}$ is the Levi-Civita tensor, $\varepsilon_{1234} = 1$.

4.3.1.3 Renormalization factors

Our one-loop results for the renormalization factors of the staple operators in both $\overline{\text{MS}}$ and RI′ schemes are presented below.

In the $\overline{\text{MS}}$ scheme, only the pole parts [$\mathcal{O}(1/\varepsilon)$ terms] contribute to the renormalization factors. Diagram d_1 has no $1/\varepsilon$ terms, as it is finite in $D = 4$ dimensions. Also, it gives the same expressions with the corresponding straight-line operators, because it involves only the zero-gluon operator vertex. This statement is true in any regularization. As we expected, the divergent terms arise from the remaining diagrams $d_2 - d_4$, in which end point [Eq. (4.33)], contact [Eq. 4.34)] and cusp divergences [Eq. (4.35)] arise. We provide below the pole parts for each subdiagram:

$$\Lambda_\Gamma^{d_1}|_{1/\varepsilon} = \Lambda_\Gamma^{d_2(a)}|_{1/\varepsilon} = \Lambda_\Gamma^{d_2(b)}|_{1/\varepsilon} = \Lambda_\Gamma^{d_3(b)}|_{1/\varepsilon} = \Lambda_\Gamma^{d_3(c)}|_{1/\varepsilon} = \Lambda_\Gamma^{d_4(e)}|_{1/\varepsilon} = 0, \tag{4.32}$$

$$\Lambda_\Gamma^{d_2(c)}|_{1/\varepsilon} = \Lambda_\Gamma^{d_3(a)}|_{1/\varepsilon} = \frac{g^2 C_F}{16\pi^2}\Lambda_\Gamma^{\text{tree}}\frac{1}{\varepsilon}(1-\beta), \tag{4.33}$$

$$\Lambda_\Gamma^{d_4(a)}|_{1/\varepsilon} = \Lambda_\Gamma^{d_4(b)}|_{1/\varepsilon} = \Lambda_\Gamma^{d_4(c)}|_{1/\varepsilon} = \frac{g^2 C_F}{16\pi^2}\Lambda_\Gamma^{\text{tree}}\frac{1}{\varepsilon}(2+\beta), \tag{4.34}$$

$$\Lambda_\Gamma^{d_4(d)}|_{1/\varepsilon} = \Lambda_\Gamma^{d_4(f)}|_{1/\varepsilon} = \frac{g^2 C_F}{16\pi^2}\Lambda_\Gamma^{\text{tree}}\frac{1}{\varepsilon}(-\beta), \tag{4.35}$$

where $C_F = (N_c^2 - 1)/(2N_c)$ and β is the gauge fixing parameter, defined such that $\beta = 0$ (1) corresponds to the Feynman (Landau) gauge. It is deduced that diagrams d_2, d_3 give the same pole terms as in the case $y = 0$, since only end points affect these diagrams (no cusps). Also, the result for the cusp divergences of angle $\pi/2$ agrees with previous studies of nonsmooth Wilson-line operators for a general cusp angle θ [144, 148, 149]: it follows from these studies that the one-loop result corresponding to each of the diagrams $d_4(d)$ and $d_4(f)$ is given by $-(g^2C_F)/(16\pi^2\varepsilon)\,(2\theta\cot\theta+\beta)$, which is indeed in agreement with Eq. (4.35). By imposing that the $\overline{\text{MS}}$-renormalized Green's functions of $\mathcal{O}_\Gamma$ are equal to the finite parts (exclude pole terms) of the corresponding bare Green's functions, we derive the renormalization factors of $\mathcal{O}_\Gamma$ in $\overline{\text{MS}}$, using Eqs.

(4.10 – 4.12); the result is given below,

$$Z_\Gamma^{\mathrm{DR},\overline{\mathrm{MS}}} = 1 + \frac{g^2 C_F}{16\pi^2}\frac{7}{\varepsilon} + \mathcal{O}(g^4), \tag{4.36}$$

where we make use of the one-loop expression for the renormalization factor $Z_\psi^{\mathrm{DR},\overline{\mathrm{MS}}}$, given in Appendix 4.B [Eq. (4.85)]. Since the pole parts are multiples of the tree-level values $\Lambda_\Gamma^{\mathrm{tree}}$, the nondiagonal elements of the $\overline{\mathrm{MS}}$ renormalization factors, defined in Eqs. (4.7, 4.8), are equal to zero. The diagonal elements, shown in Eq. (4.36), depend neither on the Dirac structure, nor on the lengths of the staple segments; further, they are gauge invariant.

In the RI′ scheme, there are additional finite terms, which contribute to the renormalization factors of $\mathcal{O}_\Gamma$ [according to the conditions of Eqs. (4.15 – 4.16)]. These terms depend on the external momentum, and they stem from all Feynman diagrams. They are also multiples of the tree-level values of the Green's functions. As a consequence, the RI′ mixing matrices, defined in Eqs. (4.7, 4.8), are also diagonal. Therefore, there is no operator mixing in DR. The results for $Z_\Gamma^{\mathrm{DR},\mathrm{RI}'}$, together with $Z_\Gamma^{\mathrm{DR},\overline{\mathrm{MS}}}$ [Eq. (4.36)], lead directly to the conversion factors $C_\Gamma^{\overline{\mathrm{MS}},\mathrm{RI}'}$ through the relation,

$$Z_\Gamma^{\mathrm{DR},\mathrm{RI}'} = C_\Gamma^{\overline{\mathrm{MS}},\mathrm{RI}'} + \frac{g^2 C_F}{16\pi^2}\frac{7}{\varepsilon} + \mathcal{O}(g^4). \tag{4.37}$$

Our resulting expressions for the conversion factors are given in the following subsection [Eqs. (4.38 – 4.42)].

4.3.1.4 Conversion factors

We present below our results for the conversion factors of staple operators between the RI′ and $\overline{\mathrm{MS}}$ schemes. Since the renormalization factors of $\mathcal{O}_\Gamma$ are diagonal in both $\overline{\mathrm{MS}}$ and RI′ schemes, the conversion factors will also be diagonal. Our expressions depend on integrals of modified Bessel functions of the second kind K_n, over one Feynman parameter and possibly over one of the variables ζ appearing in Eq. (4.2). These integrals are denoted by $P_i \equiv P_i(\bar{q}^2, \bar{q}_{\mu_1}, z)$, $Q_i \equiv Q_i(\bar{q}^2, \bar{q}_{\mu_1}, \bar{q}_{\mu_2}, z, y)$ and $R_i \equiv R_i(\bar{q}^2, \bar{q}_{\mu_1}, \bar{q}_{\mu_2}, z, y)$; they are defined in Eqs. (4.67 – 4.84) of Appendix 4.A.

$$C_S^{\mathrm{RI}',\overline{\mathrm{MS}}} = 1 + \frac{g^2 C_F}{16\pi^2}\Bigg\{(15-\beta) + 2(\beta+6)\gamma_E + 7\log\left(\frac{\overline{\mu}^2}{\overline{q}^2}\right) + (\beta+2)\log\left(\frac{\overline{q}^2 z^2}{4}\right) + 4\log\left(\frac{\overline{q}^2 y^2}{4}\right) + 4\left(2\,\frac{y}{z}\tan^{-1}\left(\frac{y}{z}\right) - \log\left(1+\frac{y^2}{z^2}\right)\right) + 2(\beta+2)P_1 - 2\beta\sqrt{\overline{q}^2}\,|z|\,P_4 - 2i\overline{q}_{\mu_1}\Big(2Q_1 - \beta z(P_1-P_2)\Big) + 4\overline{q}_{\mu_2}(R_6-R_2)\Bigg\} + \mathcal{O}(g^4), \tag{4.38}$$

$$C_{V_{\mu_1}}^{\mathrm{RI}',\overline{\mathrm{MS}}} = 1 + \frac{g^2 C_F}{16\pi^2}\Bigg\{15 + 2(\beta+6)\gamma_E + 7\log\left(\frac{\overline{\mu}^2}{\overline{q}^2}\right) + (\beta+2)\log\left(\frac{\overline{q}^2 z^2}{4}\right) + 4\log\left(\frac{\overline{q}^2 y^2}{4}\right) + 4\left(2\,\frac{y}{z}\tan^{-1}\left(\frac{y}{z}\right) - \log\left(1+\frac{y^2}{z^2}\right)\right) + 2(\beta P_1 - 2P_2) - 2\sqrt{\overline{q}^2}\,|z|\,(\beta P_4 - 2P_5) - \frac{1}{2}\beta\overline{q}^2 z^2(P_1-P_2) + 4\overline{q}_{\mu_2}(R_6-R_2) - i\overline{q}_{\mu_1}\Big(4Q_1 - 2z\Big(\beta(P_1-P_2) - 4P_3\Big) + \beta\sqrt{\overline{q}^2}\;z\,|z|\,(P_4-P_5)\Big) + \overline{q}_{\mu_1}^2\Big(2\frac{|z|}{\sqrt{q^2}}\Big((\beta-2)P_4 + 2P_5\Big) + \beta z^2 P_3\Big)\Bigg\} + \mathcal{O}(g^4), \tag{4.39}$$

$$C_{V_\nu}^{\mathrm{RI}',\overline{\mathrm{MS}}} = 1 + \frac{g^2 C_F}{16\pi^2}\Bigg\{(15-\beta) + 2(\beta+6)\gamma_E + 7\log\left(\frac{\overline{\mu}^2}{\overline{q}^2}\right) + (\beta+2)\log\left(\frac{\overline{q}^2 z^2}{4}\right) + 4\log\left(\frac{\overline{q}^2 y^2}{4}\right) + 4\left(2\,\frac{y}{z}\tan^{-1}\left(\frac{y}{z}\right) - \log\left(1+\frac{y^2}{z^2}\right)\right) + 2(\beta P_1 - 2P_2) - \beta\sqrt{\overline{q}^2}\,|z|\,P_4 - 2i\overline{q}_{\mu_1}\Big(2Q_1 - \beta z(P_1-P_2)\Big) + 4\overline{q}_{\mu_2}(R_6-R_2) + \overline{q}_\nu^2\Big(2\frac{|z|}{\sqrt{q^2}}\Big((\beta-2)P_4 + 2P_5\Big) - \beta z^2 P_3\Big)\Bigg\} + \mathcal{O}(g^4), \quad (\nu \neq \mu_1), \tag{4.40}$$

$$C^{\mathrm{RI}',\overline{\mathrm{MS}}}_{T_{\mu_1\nu}} = 1 + \frac{g^2 C_F}{16\pi^2}\Bigg\{15 + 2(\beta+6)\gamma_E + 7\log\left(\frac{\overline{\mu}^2}{\overline{q}^2}\right) + (\beta+2)\log\left(\frac{\overline{q}^2 z^2}{4}\right)$$
$$+ 4\log\left(\frac{\overline{q}^2 y^2}{4}\right) + 4\left(2\,\frac{y}{z}\tan^{-1}\left(\frac{y}{z}\right) - \log\left(1+\frac{y^2}{z^2}\right)\right)$$
$$+ 2(\beta-2)P_1 - \beta\sqrt{\overline{q}^2}\,|z|\,P_4 - \frac{1}{2}\beta\overline{q}^2 z^2(P_1-P_2) + 4\overline{q}_{\mu_2}(R_6-R_2)$$
$$- i\overline{q}_{\mu_1}\Big(4Q_1 - 2\beta z(P_1-P_2) + \beta\sqrt{\overline{q}^2}\;z\,|z|\,(P_4-P_5)\Big)$$
$$+ \beta z^2\left(\overline{q}^2_{\mu_1} + \overline{q}^2_{\nu}\right)P_3\Bigg\} + \mathcal{O}(g^4), \quad (\nu \neq \mu_1), \tag{4.41}$$

$$C_P = C_S, \quad C_{A_{\mu_1}} = C_{V_{\mu_1}}, \quad C_{A_\nu} = C_{V_\nu}, \quad C_{T_{\rho\sigma}} = C_{T_{\mu_1\nu}}, \quad (\mu_1,\nu,\rho,\sigma \text{ are all different}). \tag{4.42}$$

We note that the real parts of the above expressions, as well as the bare Green's functions, are not analytic functions of z (y) near $z \to 0$ ($y \to 0$); in particular, the limit $z \to 0$ leads to quadratic divergences, while the limit $y \to 0$ leads to logarithmic divergences. The singular limits were expected, due to the appearance of contact terms beyond tree level. In the case $y = 0$, the staple operators are replaced by straight-line operators of length $|z|$, the renormalization of which is addressed in our work of Ref. [114]. In the case $z = 0$, the nonlocal operators are replaced by local bilinear operators, the renormalization of which is studied, e.g., in Refs. [49, 50, 182, 186].

Since our results for the conversion factors will be combined with nonperturbative data, it is useful to employ certain values of the free parameters mostly used in simulations. To this end, we set: $\bar{\mu} = 2$ GeV and $\beta = 1$ (Landau gauge). For the RI′ scale we employ values which are relevant for simulations by ETMC [110], as follows: $a\bar{q} = (\frac{2\pi}{L}n_1, \frac{2\pi}{L}n_2, \frac{2\pi}{L}n_3, \frac{2\pi}{T}(n_4+\frac{1}{2}))$, where a is the lattice spacing, $(L^3 \times T)$ is the lattice size and (n_1, n_2, n_3, n_4) is a 4-vector defined on the lattice. A standard choice of values for n_i is the case $n_1 = n_2 = n_3 \neq n_4$, in which the temporal component n_4 stands out from the remaining equal spatial components. As an example we apply $(n_1, n_2, n_3, n_4) = (4, 4, 4, 9)$, $L = 32$, $T = 64$ and $a = 0.09$ fm. For a better assessment of our results, we plot in Fig. 4.6 the real and imaginary parts of the quantities $\overline{C}_\Gamma$, defined through $C^{RI',\overline{\mathrm{MS}}}_\Gamma = 1 + \frac{g^2 C_F}{16\pi^2}\,\overline{C}_\Gamma + \mathcal{O}(g^4)$, as functions of the dimensionless variables z/a and y/a, using the above parameter values. In the case $y = 0$, we use the expressions of the conversion factors for straight-line operators, calculated in Ref. [114], while in the case $z = 0$, we use the one-loop expressions of the conversion factors for local bilinear operators, written in Refs. [49, 50]. For definiteness, we choose $\mu_1 = 1$ and $\mu_2 = 2$.

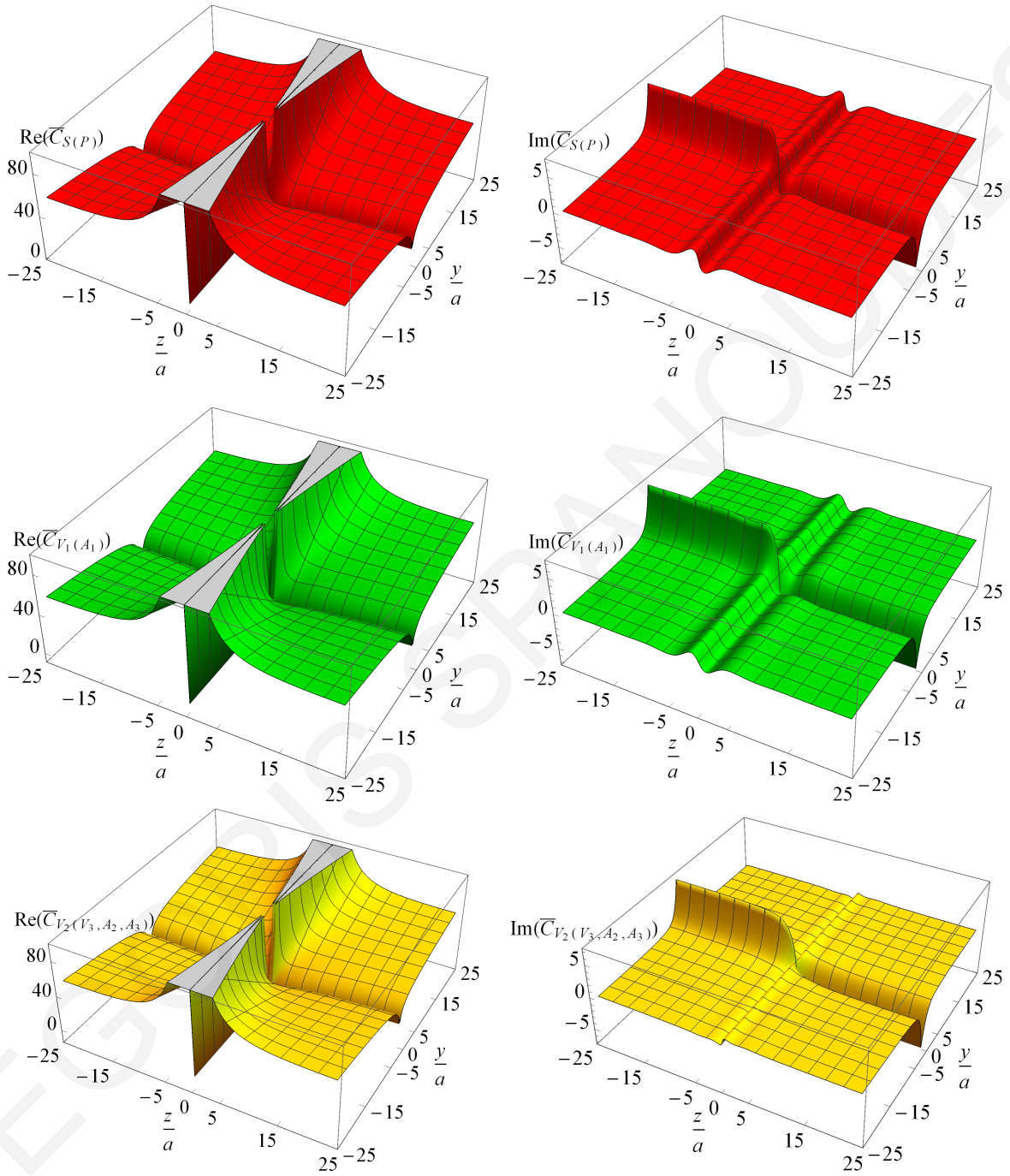

FIGURE 4.6: Real (left panels) and imaginary (right panels) parts of the quantities $\overline{C}_S = \overline{C}_P$, $\overline{C}_{V_1} = \overline{C}_{A_1}$ and $\overline{C}_{V_2} = \overline{C}_{V_3} = \overline{C}_{A_2} = \overline{C}_{A_3}$, involved in the one-loop expressions of the conversion factors: $C_\Gamma^{\mathrm{RI}',\overline{\mathrm{MS}}} = 1 + \frac{g^2 C_F}{16\pi^2}\,\overline{C}_\Gamma + \mathcal{O}(g^4)$, as functions of z/a and y/a [for $\beta = 1$, $\bar{\mu} = 2\ GeV$, $a = 0.09$ fm, $a\bar{q} = (\frac{2\pi}{L}n_1, \frac{2\pi}{L}n_2, \frac{2\pi}{L}n_3, \frac{2\pi}{T}(n_4 + \frac{1}{2}))$, $L = 32$, $T = 64$, $(n_1, n_2, n_3, n_4) = (4, 4, 4, 9)$]. Here, we choose $\mu_1 = 1$ and $\mu_2 = 2$.

Graphs for $\overline{C}_{V_4} = \overline{C}_{A_4}$, $\overline{C}_{T_{12}} = \overline{C}_{T_{13}} = \overline{C}_{T_{42}} = \overline{C}_{T_{34}}$ and $\overline{C}_{T_{14}} = \overline{C}_{T_{32}}$ are not included in Fig. 4.6, as their resulting values are very close to those of $\overline{C}_{V_2}$ (fractional differences: $\lesssim 10^{-3}$).

The real parts of $\overline{C}_\Gamma$ are even functions of both z/a and y/a. In Fig. 4.6, one observes that, for large values of z/a, they tend to stabilize, while for large values of y/a they tend to increase; thus, a two-loop calculation of the conversion factors is essential for more sufficiently convergent results. Further, the dependence on the choice of Γ becomes milder for increasing values of z/a and y/a. Regarding the imaginary parts of $\overline{C}_\Gamma$, they are odd functions of z/a and even functions of y/a. For large values of z/a or y/a, they tend to converge to a positive value. In particular, when both z/a and y/a take large values, the imaginary parts tend to zero. For large values of y/a and, simultaneously, small values of z/a, the imaginary parts of $\overline{C}_\Gamma$ demonstrate a small fluctuation around zero, which differs for each Γ, either in form (e.g., $\overline{C}_{V_2}$ and $\overline{C}_S$ have opposite signs for given values of z/a, y/a) or in magnitude (e.g., the fluctuation of $\overline{C}_S$ is bigger and sharper than the fluctuation of $\overline{C}_{V_1}$). As regards the $\bar{q}$ dependence, we have not included further graphs for the sake of conciseness; however, testing a variety of values for the components of $a\bar{q}$, used in simulations, we find no significant difference, especially for large values of z/a and y/a.

4.3.2 Calculation in lattice regularization

4.3.2.1 Methodology

At first, let us give the lattice version of the staple operators,

$$\mathcal{O}_\Gamma^{\text{latt.}} \equiv \bar{\psi}(x)\ \Gamma\ W(x, x + ma\hat{\mu}_2, x + ma\hat{\mu}_2 + na\hat{\mu}_1, x + na\hat{\mu}_1)\ \psi(x + na\hat{\mu}_1), \tag{4.43}$$

$$\begin{aligned} &W(x, x + ma\hat{\mu}_2, x + ma\hat{\mu}_2 + na\hat{\mu}_1, x + na\hat{\mu}_1) \equiv \\ &\Big(\prod_{\ell=0}^{m\mp1} U_{\pm\mu_2}(x + \ell a\hat{\mu}_2)\Big) \cdot \Big(\prod_{\ell=0}^{n\mp1} U_{\pm\mu_1}(x + ma\hat{\mu}_2 + \ell a\hat{\mu}_1)\Big) \cdot \\ &\Big(\prod_{\ell=0}^{m\mp1} U_{\pm\mu_2}(x + na\hat{\mu}_1 + \ell a\hat{\mu}_2)\Big)^\dagger, \quad n \equiv z/a,\ m \equiv y/a, \end{aligned} \tag{4.44}$$

where upper (lower) signs of the first and third parenthesis correspond to $m > 0$ ($m < 0$) and upper (lower) signs of the second parenthesis correspond to $n > 0$ ($n < 0$). The calculation of the bare Green's functions of such nonlocal operators on the lattice is more complicated than the corresponding calculation of local operators; the products of gluon links lead to expressions whose summands, taken individually, contain possible additional IR singularities along a whole hyperplane, instead of a single point [terms $\sim 1/\sin(p_\mu/2)$ or $1/\sin^2(p_\mu/2)$]. Also, the UV-regulator limit, $a \to 0$, is more delicate in this case, as the Green's functions depend on a through the additional combinations z/a, y/a, besides the combination aq (where q is the external quark momentum). Thus, we have to modify the standard methods of evaluating Feynman diagrams on the lattice [199], in order to apply them in the case of nonlocal operators.

The procedure that we used for the calculation of the bare Green's functions of $\mathcal{O}_\Gamma^{\text{latt.}}$ is briefly described in the work of Ref. [114] regarding straight Wilson-line operators, and it is summarized below: The main task is to write the lattice expressions, in terms of continuum integrals, which are easier to calculate, plus lattice integrals independent of aq; however, the latter will still have a nontrivial dependence on z/a and y/a. To this end, we perform a series of additions and subtractions to the original integrands: we extend the standard procedure of Kawai *et al.* [199], in order to isolate the possible IR divergences stemming from the integration over the p_μ component, which appears on the integrals' denominators [$\sim 1/\sin(p_\mu/2)$ or $1/\sin^2(p_\mu/2)$]. To accomplish this, we add and subtract to the original integrands the lowest order of their Laurent expansion in p_μ. Also, in order to end up with continuum integrals, we add and subtract the continuum counterparts of the integrands; then, the integration region can be split up into two parts: the whole domain of the real numbers minus the region outside the Brillouin zone. The above operations allow us to separate the original expressions into a sum of two parts: one part contains integrals which can be evaluated explicitly for nonzero values of a, leading to linear or logarithmic divergences, and a second part for which a naive $a \to 0$ limit can be taken, e.g.,

$$\int dp f(p) e^{i(z/a)p} \to 0, \quad \int dp f(p) \sin^2(\frac{z}{a}p) \to \frac{1}{2}\int dp f(p). \tag{4.45}$$

The numerical integrations entail a very small systematic error, which is smaller than the last digit presented in all results shown in the sequel.

4.3.2.2 Green's functions and operator mixing

The results for the bare lattice Green's functions of the staple operators are presented below in terms of the $\overline{\text{MS}}$-renormalized Green's functions, derived by the corresponding calculation in DR,

$$\Lambda_{\Gamma}^{\text{LR}} \ = \Lambda_{\Gamma}^{\overline{\text{MS}}} - \frac{g^2\, C_F}{16\,\pi^2}\, e^{i\, q_{\mu_1} z} \cdot \mathcal{F} \ + \ \mathcal{O}(g^4), \tag{4.46}$$

$$\mathcal{F} = \Big[\Gamma\Big(\alpha_1 + 3.7920\,\beta + \alpha_2\,\frac{|z| + 2\ |y|}{a} + \log\left(a^2\bar{\mu}^2\right)(8-\beta)\Big) + \text{sgn}(y)\Big[\Gamma, \gamma_{\mu_2}\Big]\Big(\alpha_3 + \alpha_4\, c_{\text{SW}}\Big)\Big], \tag{4.47}$$

where α_i are numerical constants which depend on the gluon action in use; their values are given in Table 4.2 for the Wilson, Tree-level Symanzik and Iwasaki gluon actions[5]. We note that α_2, α_3, and α_4 have the same values (up to a sign) as the corresponding coefficients in the straight-line operators [114].

Gluon action	$\boldsymbol{\alpha_1}$	$\boldsymbol{\alpha_2}$	$\boldsymbol{\alpha_3}$	$\boldsymbol{\alpha_4}$
Wilson	-22.5054	19.9548	7.2250	-4.1423
Tree-level Symanzik	-22.0931	17.2937	6.3779	-3.8368
Iwasaki	-18.2456	12.9781	4.9683	-3.2638

TABLE 4.2: Numerical values of the coefficients $\alpha_1 - \alpha_4$ appearing in the one-loop bare lattice Green's functions $\Lambda_{\Gamma}^{\text{LR}}$.

In Eqs. (4.46, 4.47), we observe that there is a linear divergence [$\mathcal{O}(1/a)$], which depends on the length of the staple line ($|z| + 2\ |y|$); this was expected according to the studies of closed Wilson-loop operators in regularizations other than DR [143]. This divergence arises from the tadpolelike diagram d_4 and in particular from the subdiagrams $d_4(a)$, $d_4(b)$, $d_4(c)$. We note that the coefficient α_2 entering the strength of the linear divergence, is given by

$$\alpha_2 \ = -\frac{1}{2}\ \int_{-\pi}^{\pi} \frac{d^3p}{(2\pi)^3}\ D(\bar{p})_{\nu\nu}, \tag{4.48}$$

where $D(p)_{\mu\nu}$ is the gluon propagator, $\hat{\nu}$ is the direction parallel to each straight-line segment of the Wilson line and $\bar{p}$ equals the four-vector momentum p with $p_\nu \to 0$. Moreover, additional contributions of different Dirac structures than the original operators appear ($[\Gamma, \gamma_{\mu_2}]$ terms); these contributions arise from the "sail" diagrams

[5] A more precise result for the numerical constant 3.7920, which multiplies the β parameter, is $16\pi^2 P_2$, where $P_2 = 0.02401318111946489(1)$ [39].

d_2, d_3 and in particular from the subdiagrams $d_2(c)$, $d_3(a)$. In order to obtain on the lattice the same results for the $\overline{\text{MS}}$-renormalized Green's functions as those obtained in DR, we have to subtract such regularization dependent terms in the renormalization process. A simple multiplicative renormalization cannot eliminate these terms; the introduction of mixing matrices is therefore necessary. However, for the operators with $\Gamma = S, V_{\mu_2}, A_i, T_{ij}$, where $i \neq j \neq \mu_2 \neq i$, the contribution $[\Gamma, \gamma_{\mu_2}]$ is zero, and, thus, there is no mixing for these operators. In conclusion, there is mixing between the operators $(\mathcal{O}_P, \mathcal{O}_{A_{\mu_2}}), (\mathcal{O}_{V_i}, \mathcal{O}_{T_{i\mu_2}})$, where $i \neq \mu_2$, as we have mentioned previously. This feature must be taken into account in the nonperturbative renormalization of TMDs.

4.3.2.3 Renormalization factors

The $\overline{\text{MS}}$ renormalization factors can be derived by the requirement that the terms in Eq. (4.47) vanish in the renormalized Green's functions. Thus, through Eqs. (4.10 – 4.12), one obtains the following results for the diagonal and nondiagonal elements of the renormalization factors:

$$Z_{\Gamma}^{\text{LR},\overline{\text{MS}}} = 1 + \frac{g^2 C_F}{16\pi^2}\Big[(e_1^{\psi} + 1 - \alpha_1) - \alpha_2 \frac{|z| + 2\,|y|}{a} + e_2^{\psi} c_{SW} + e_3^{\psi} c_{SW}^2 - 7\log\left(a^2\bar{\mu}^2\right)\Big] + \mathcal{O}(g^4), \tag{4.49}$$

$$Z_{(P,A_{\mu_2})}^{\text{LR},\overline{\text{MS}}} = Z_{(A_{\mu_2},P)}^{\text{LR},\overline{\text{MS}}} = Z_{(V_i,T_{i\mu_2})}^{\text{LR},\overline{\text{MS}}} = Z_{(T_{i\mu_2},V_i)}^{\text{LR},\overline{\text{MS}}} = \frac{g^2 C_F}{16\pi^2}\text{sgn}(y)(-2)\Big[\alpha_3 + \alpha_4 c_{SW}\Big] + \mathcal{O}(g^4), \tag{4.50}$$

where the coefficients e_i^{ψ} stem from the renormalization factor of the fermion field $Z_{\psi}^{\text{LR},\overline{\text{MS}}}$, given in Appendix 4.B [Eq. (4.89)].

A number of observations are in order, regarding the above one-loop results: both diagonal and nondiagonal elements of the renormalization factors are operator independent, just as the corresponding renormalization factors in DR. Also, the dependence of the diagonal elements on the clover coefficient c_{SW} is entirely due to the renormalization factor of fermion fields; on the contrary, the dependence of the nondiagonal elements on c_{SW} is derived from the Green's functions of the operators, and in particular it is different for each choice of gluon action. Consequently, tuning the clover coefficient we can set the nondiagonal elements of the renormalization factors to zero and, thus, suppress the operator mixing. At one-loop level, this can be

done by choosing $c_{SW} = -\alpha_3/\alpha_4$. For the gluon actions given in this paper, the values of the coefficient c_{SW}, which lead to no mixing at one loop, are 1.7442 for Wilson action, 1.6623 for tree-level Symanzik action and 1.5222 for Iwasaki action; these values are the same as those, which eliminate the mixing in the case of straight-line operators [114].

In the RI′ scheme, the renormalization factors can be read off our expressions for the conversion factors, given in Eqs. (4.38 – 4.42), in a rather straightforward way,

$$Z_\Gamma^{\mathrm{LR,RI'}} = C_\Gamma^{\overline{\mathrm{MS}},\mathrm{RI'}} + \frac{g^2 C_F}{16\pi^2}\Big[(e_1^\psi + 1 - \alpha_1) - \alpha_2\,\frac{|z| + 2\,|y|}{a} + e_2^\psi c_{SW} + e_3^\psi c_{SW}^2 - 7\log\left(a^2\bar{\mu}^2\right)\Big] + \mathcal{O}(g^4), \tag{4.51}$$

$$Z^{\mathrm{LR,RI'}}_{(P,A_{\mu_2})} = Z^{\mathrm{LR,RI'}}_{(A_{\mu_2},P)} = Z^{\mathrm{LR,RI'}}_{(V_i,T_{i\mu_2})} = Z^{\mathrm{LR,RI'}}_{(T_{i\mu_2},V_i)} = \frac{g^2 C_F}{16\pi^2}\mathrm{sgn}(y)(-2)\Big[\alpha_3 + \alpha_4 c_{SW}\Big] + \mathcal{O}(g^4). \tag{4.52}$$

Since the conversion factors are diagonal, the one-loop nondiagonal elements of the RI′ renormalization factors are equal to the corresponding $\overline{\mathrm{MS}}$ expressions.

4.4 Extension to general Wilson-line lattice operators with n cusps

This work on staple operators, along with studies on straight-line operators ([114], Chapter 3), lead us to some interesting conclusions about nonlocal operators. From these two cases, we can completely deduce the renormalization coefficients of a general Wilson-line operator with n cusps, defined on the lattice; in particular, we determine both the divergent (linear and logarithmic) and the finite parts of multiplicative renormalizations, as well as all mixing coefficients. We can also justify the nature of the mixing in each case.

All the above coefficients can be deduced from the difference between the bare Green's functions on the lattice and the corresponding $\overline{\mathrm{MS}}$-renormalized Green's functions, obtained in DR: $\Delta\Lambda_\Gamma \equiv \Lambda_\Gamma^{\mathrm{LR}} - \Lambda_\Gamma^{\overline{\mathrm{MS}}}$. Below we have gathered results for these differences, in the case of both straight-line (Ref. [114]) and staple (this work) operators, presented separately for each Feynman diagram:

Straight-line operators,

$$\left(\Lambda_\Gamma^{\text{straight}}\right)_{d_i}^{\text{LR}} - \left(\Lambda_\Gamma^{\text{straight}}\right)_{d_i}^{\overline{\text{MS}}} \equiv -\frac{g^2 C_F}{16\pi^2}\, e^{iq_{\mu_1} z} \cdot \mathcal{F}_{d_i}^{\text{straight}} + \mathcal{O}(g^4), \qquad (i = 1, 2, 3, 4), \tag{4.53}$$

where

$$\mathcal{F}_{d_1}^{\text{straight}} = 0, \tag{4.54}$$

$$\mathcal{F}_{d_2+d_3}^{\text{straight}} = 2\,\Gamma\left[\alpha_5 + 3.7920\,\beta + (1-\beta)\log(a^2\bar{\mu}^2)\right] + \text{sgn}(z)(\Gamma\gamma_{\mu_1} + \gamma_{\mu_1}\Gamma)(\alpha_3 + \alpha_4 c_{SW}), \tag{4.55}$$

$$\mathcal{F}_{d_4}^{\text{straight}} = \Gamma\left[\alpha_6 - 3.7920\,\beta + (2+\beta)\log(a^2\bar{\mu}^2) + \alpha_2\frac{|z|}{a}\right]. \tag{4.56}$$

Staple operators,

$$\left(\Lambda_\Gamma^{\text{staple}}\right)_{d_i}^{\text{LR}} - \left(\Lambda_\Gamma^{\text{staple}}\right)_{d_i}^{\overline{\text{MS}}} \equiv -\frac{g^2 C_F}{16\pi^2}\, e^{iq_{\mu_1} z} \cdot \mathcal{F}_{d_i}^{\text{staple}} + \mathcal{O}(g^4), \qquad (i = 1, 2, 3, 4), \tag{4.57}$$

where

$$\mathcal{F}_{d_1}^{\text{staple}} = 0, \tag{4.58}$$

$$\mathcal{F}_{d_2+d_3}^{\text{staple}} = 2\,\Gamma\left[\alpha_5 + 3.7920\,\beta + (1-\beta)\log(a^2\bar{\mu}^2)\right] + \text{sgn}(y)(\Gamma\gamma_{\mu_2} - \gamma_{\mu_2}\Gamma)(\alpha_3 + \alpha_4 c_{SW}), \tag{4.59}$$

$$\mathcal{F}_{d_4}^{\text{staple}} = \Gamma\Big\{3\left[\alpha_6 - 3.7920\,\beta + (2+\beta)\log(a^2\bar{\mu}^2)\right] + \alpha_2\frac{|z|+2|y|}{a} + 2\left[\alpha_7 + 3.7920\,\beta - \beta\log(a^2\bar{\mu}^2)\right]\Big\}. \tag{4.60}$$

The coefficients α_i are numerical constants, which depend on the Symanzik coefficients of the gluon action in use; their values for Wilson, tree-level Symanzik and Iwasaki gluons are given in Tables 4.2 and 4.3. Comparing the above results for the two types

Gluon action	$\boldsymbol{\alpha_5}$	$\boldsymbol{\alpha_6}$	$\boldsymbol{\alpha_7}$
Wilson	-4.4641	-4.5258	0
Tree-level Symanzik	-4.3413	-3.9303	-0.8099
Iwasaki	-4.1637	-1.9053	-2.1011

TABLE 4.3: Numerical values of the coefficients $\alpha_5 - \alpha_7$ appearing in the one-loop bare lattice Green's functions of Wilson-line operators (straight line and staple).

of operators, we come to the following conclusions which can be generalized to Wilson-line lattice operators of arbitrary shape:

- The linear divergence [$\mathcal{O}(1/a)$] depends on the Wilson line's length.

- Diagram d_1 gives a finite, regulator-independent result in all cases.

- The only contribution of sail diagrams (d_2 and d_3) to $\Delta\Lambda_\Gamma$ comes from their end points. This is because any parts of a segment which do not include the end points will give finite contributions to $\Lambda_\Gamma^{\mathrm{LR}}$, in which the naïve continuum limit $a \to 0$ can be taken, leading to the same result as in DR and thus to a vanishing contribution in $\Delta\Lambda_\Gamma$. Consequently the shape of the Wilson line is largely irrelevant and, indeed, all numerical coefficients in Eq. (4.59) coincide with those in Eq. (4.55). The only dependence on the shape regards the Dirac structure of the operator which mixes with $\mathcal{O}_\Gamma$. The mixing terms depend on the direction of the Wilson line in the end points. For the straight Wilson line, the direction in both end points is $\mathrm{sgn(z)}\hat{\mu}_1$, which leads to the appearance of the additional Dirac structure $\mathrm{sgn(z)}(\Gamma\gamma_{\mu_1} + \gamma_{\mu_1}\Gamma)$ upon adding together sail diagrams d_2 and d_3. For the staple Wilson line, the direction in the left end point is $\mathrm{sgn(y)}\hat{\mu}_2$ and in the right end point is $-\mathrm{sgn(y)}\hat{\mu}_2$; thus, the additional Dirac structure which appears upon adding the two sail diagrams is $\mathrm{sgn(y)}(\Gamma\gamma_{\mu_2} - \gamma_{\mu_2}\Gamma)$.

  The mixing pairs for each type of nonlocal operator can be also explained (partially) by symmetry arguments. For straight-line operators, there is a residual rotational (or cubic, on the lattice) symmetry (including reflections) with respect to the three transverse directions to the $\hat{\mu}$ direction parallel to the Wilson line. As a consequence, operators which transform in the same way under this residual symmetry can mix among themselves, under renormalization; i.e., mixing can occur only among the pairs of operators ($\mathcal{O}_\Gamma$, $\mathcal{O}_{\Gamma\gamma_\mu}$). This argument can now be applied to a general Wilson line: given that only end points contribute, mixing can occur only with $\mathcal{O}_{\Gamma\gamma_\mu}$, where $\hat{\mu}$ refers to the directions of the two end points of the line. Clearly, the subsets of operators which finally mix depend on the commutation properties between Γ and γ_μ. We note that, if the fermion action in use preserves chiral symmetry, then none of the operators will mix with each other.

- The tadpole diagram (d_4) for the staple operators gives, aside from the linearly divergent terms, two types of contributions: one corresponds to each of the three straight-line segments [first square bracket in Eq. (4.60)], which is identical to the corresponding contribution from the straight Wilson line, multiplied by a factor

of 3, and another contribution for each of the two cusps [second square bracket in Eq. (4.60)], multiplied by a factor of 2, which cannot be obtained from the study of straight-line operators.

As a consequence of the above, it follows that the difference $\Lambda_\Gamma^{\rm LR} - \Lambda_\Gamma^{\overline{\rm MS}}$ for a general Wilson-line operator with n cusps (and, hence, $n+1$ segments), defined on the lattice, can be fully extracted from the combination of our results for the straight-line and the staple operators: the contributions of each straight-line segment and each cusp, appearing in the general operators, are obtained from Eqs. (4.53 – 4.60). Therefore, without performing any new calculations, the result for the Green's functions of general Wilson-line lattice operators with n cusps, is determined below,

$$\left(\Lambda_\Gamma^{\rm general}\right)_{d_i}^{\rm LR} - \left(\Lambda_\Gamma^{\rm general}\right)_{d_i}^{\overline{\rm MS}} \equiv -\frac{g^2 C_F}{16\pi^2}\, e^{iq_{\mu_1} z}\cdot \mathcal{F}_{d_i}^{\rm general} + \mathcal{O}(g^4), \qquad (i=1,2,3,4), \quad (4.61)$$

where

$$\mathcal{F}_{d_1}^{\rm general} = 0, \quad (4.62)$$

$$\mathcal{F}_{d_2+d_3}^{\rm general} = 2\,\Gamma\left[\alpha_5 + 3.7920\,\beta + (1-\beta)\log(a^2\bar{\mu}^2)\right] + (\Gamma\hat{\not{\mu}}_i + \hat{\not{\mu}}_f\Gamma)(\alpha_3 + \alpha_4 c_{SW}), \quad (4.63)$$

$$\mathcal{F}_{d_4}^{\rm general} = \Gamma\Big\{(n+1)\alpha_6 - 3.7920\,\beta + [2(n+1)+\beta]\log(a^2\bar{\mu}^2) + \frac{L}{a}\alpha_2 + n\alpha_7\Big\}, \quad (4.64)$$

L is the Wilson line's length and $\hat{\mu}_i$ ($\hat{\mu}_f$) is the direction of the Wilson line in the initial (final) end point. In the above relations, it is explicit that there is mixing between the pairs of operators $(\mathcal{O}_\Gamma, \mathcal{O}_{\Gamma\hat{\not{\mu}}_i + \hat{\not{\mu}}_f\Gamma})$. Proceeding further with the renormalization of these operators, we extract the renormalization factors in the $\overline{\rm MS}$ scheme,

$$Z_{\Gamma(diag.)}^{\rm LR,\overline{MS}} = 1 + \frac{g^2 C_F}{16\pi^2}\Big[e^\Gamma - \alpha_2\frac{L}{a} + e_2^\psi c_{SW} + e_3^\psi c_{SW}^2 - (2n+3)\log\left(a^2\bar{\mu}^2\right)\Big] + \mathcal{O}(g^4), \quad (4.65)$$

$$Z_{\Gamma(nondiag./mix.)}^{\rm LR,\overline{MS}} = \frac{g^2 C_F}{16\pi^2}(-1)\Big[\alpha_3 + \alpha_4 c_{SW}\Big] + \mathcal{O}(g^4), \quad (4.66)$$

where $e^\Gamma = \Big[e_1^\psi + 1 - 2\alpha_5 - (n+1)\alpha_6 - n\alpha_7\Big]$ and e_i^ψ are given in Appendix 4.B. It is worth noting that the results in Eqs. (4.65, 4.66) are both gauge invariant, as was expected.

4.5 Summary and Conclusions

In this work, we have studied the one-loop renormalization of the nonlocal staple-shaped Wilson-line quark operators, both in dimensional regularization (DR) and on the lattice (Wilson/clover massless fermions and Symanzik-improved gluons). This is a follow-up calculation of Ref. [114], in which straight-line nonlocal operators are studied. These perturbative studies are parts of a wider community effort for investigating the renormalization of nonlocal operators employed in lattice computations of parton distributions (PDFs, GPDs, TMDs) of hadronic Physics. A novel aspect of this calculation is the presence of cusps in the Wilson line included in the definition of the nonlocal operators under study, which results in the appearance of additional logarithmic divergences. Perturbative studies of such nonsmooth operators had not been carried out previously on the lattice. As in the case of the straight-line operators, certain pairs of these nonlocal operators mix under renormalization, for chirality-breaking lattice actions, such as the Wilson/clover fermion action. The path structure of each type of nonlocal operator (straight-line, staple, ...) leads to different mixing pairs. The results of the present study provide additional information on the renormalization of general nonlocal operators on the lattice.

Particular novel outcomes of our calculation are:

- The one-loop results for the amputated two-point one-particle-irreducible (1-PI) Green's functions of the staple operators both in DR [Eqs. (4.22 – 4.31)] and on the lattice [Eqs. (4.46, 4.47)].
- The mixing pairs of the staple operators: $(\mathcal{O}_P, \mathcal{O}_{A_{\mu_2}}), (\mathcal{O}_{V_i}, \mathcal{O}_{T_{i\mu_2}})$, $i \neq \mu_2$ (for notation, see Sec. 4.2.1). We propose a minimal RI′-like condition [Eqs. (4.15 – 4.16)], which disentangles this mixing and which is appropriate for nonperturbative calculations of parton-distribution functions on the lattice.
- The one-loop expressions for the renormalization factors of the staple operators in both dimensional and lattice regularizations, in the $\overline{\text{MS}}$ scheme and the proposed RI′ scheme [Eqs. (4.36, 4.37, 4.49 – 4.52)].
- The one-loop conversion factors between the RI′ and $\overline{\text{MS}}$ schemes [Eqs. (4.38 – 4.42)].

- An extension of our calculations to general Wilson-line lattice operators with n cusps; we have provided results for their renormalization factors [Eqs. (4.65, 4.66)].

Our results are useful for improving the nonperturbative investigations of transverse momentum-dependent distribution functions (TMDs) on the lattice. Such an example is the calculation of the generalized g_{1T} worm-gear shift in the TMD limit ($|\eta|\to\infty$); this quantity involves a ratio between the axial and vector operators. A recent study of TMDs on the lattice [128] reveals tension between results for g_{1T} in the clover and domain-wall formulations. This is not observed in other structures and is an indication of nonmultiplicative renormalization. Our proposed RI′-type scheme can be applied to the nonperturbative evaluation of renormalization factors and mixing coefficients of the unpolarized, helicity and transversity quasi-TMDs; this is expected to fix the inconsistency between the two calculations of g_{1T}. Also, our one-loop conversion factors can be used to convert the RI′ nonperturbative results to the $\overline{\text{MS}}$ scheme. Our results for general Wilson-line lattice operators with n cusps can be used in the nonperturbative renormalization of more general continuum nonlocal operators.

Comparing our results for the staple operators with the corresponding ones for the straight-line operators, we deduce that the strength of the linear divergences is the same for both types of operators; the presence of cusps lead to additional logarithmic divergences in the staple operators. Also, the observed mixing pairs among operators with different Dirac structures depend on the direction of Wilson line in the end points, and thus, they are different between the two types of operators: the straight-line operator $\mathcal{O}_\Gamma$ mixes with $\mathcal{O}_{\{\Gamma,\gamma_{\mu_1}\}}$, while the staple operator $\mathcal{O}_\Gamma$ mixes with $\mathcal{O}_{[\Gamma,\gamma_{\mu_2}]}$ (for notation, see Sec. 4.2.1). However, the values of the mixing coefficients are the same in the two cases.

Appendices

4.A List of Feynman Parameter Integrals

In this appendix, we present a list of Feynman parameter integrals, which appear in the expressions of our results. In what follows, we use the notation: $s \equiv \sqrt{q^2(1-x)x}$.

$$P_1(q^2, q_{\mu_1}, z) \equiv \int_0^1 dx\ e^{-iq_{\mu_1}xz}\ K_0\left(s\,|z|\right), \tag{4.67}$$

$$P_2(q^2, q_{\mu_1}, z) \equiv \int_0^1 dx\ e^{-iq_{\mu_1}xz}\ K_0\left(s\,|z|\right) x, \tag{4.68}$$

$$P_3(q^2, q_{\mu_1}, z) \equiv \int_0^1 dx\ e^{-iq_{\mu_1}xz}\ K_0\left(s\,|z|\right) x(1-x), \tag{4.69}$$

$$P_4(q^2, q_{\mu_1}, z) \equiv \int_0^1 dx\ e^{-iq_{\mu_1}xz}\ K_1\left(s\,|z|\right) \sqrt{(1-x)x}, \tag{4.70}$$

$$P_5(q^2, q_{\mu_1}, z) \equiv \int_0^1 dx\ e^{-iq_{\mu_1}xz}\ K_1\left(s\,|z|\right) \sqrt{(1-x)x}\ x, \tag{4.71}$$

$$Q_1(q^2, q_{\mu_1}, q_{\mu_2}, z, y) \equiv \int_0^1 dx \int_0^z d\zeta\ e^{-iq_{\mu_1}x\zeta} \cos(q_{\mu_2}xy) K_0\left(s\sqrt{y^2+\zeta^2}\right), \tag{4.72}$$

$$Q_2(q^2, q_{\mu_1}, q_{\mu_2}, z, y) \equiv \int_0^1 dx \int_0^z d\zeta\ e^{-iq_{\mu_1}x\zeta} \cos(q_{\mu_2}xy) K_0\left(s\sqrt{y^2+\zeta^2}\right)(1-x), \tag{4.73}$$

$$Q_3(q^2, q_{\mu_1}, q_{\mu_2}, z, y) \equiv \int_0^1 dx \int_0^z d\zeta\ e^{-iq_{\mu_1}x\zeta} \cos(q_{\mu_2}xy) K_1\left(s\sqrt{y^2+\zeta^2}\right) \frac{\sqrt{(1-x)x}}{\sqrt{y^2+\zeta^2}}, \tag{4.74}$$

$$Q_4(q^2, q_{\mu_1}, q_{\mu_2}, z, y) \equiv \int_0^1 dx \int_0^z d\zeta\ e^{-iq_{\mu_1}x\zeta} \sin(q_{\mu_2}xy) K_0\left(s\sqrt{y^2+\zeta^2}\right)(1-x), \tag{4.75}$$

$$Q_5(q^2, q_{\mu_1}, q_{\mu_2}, z, y) \equiv \int_0^1 dx \int_0^z d\zeta\ e^{-iq_{\mu_1}x\zeta} \sin(q_{\mu_2}xy) K_1\left(s\sqrt{y^2+\zeta^2}\right) \frac{\sqrt{(1-x)x}}{\sqrt{y^2+\zeta^2}}, \tag{4.76}$$

$$R_1(q^2, q_{\mu_2}, y) \equiv \int_0^1 dx \int_0^y d\zeta \ \cos(q_{\mu_2} x\zeta) \ K_0\left(s\,|\zeta|\right)(1-x), \tag{4.77}$$

$$R_2(q^2, q_{\mu_2}, y) \equiv \int_0^1 dx \int_0^y d\zeta \ \sin(q_{\mu_2} x\zeta) \ K_0\left(s\,|\zeta|\right), \tag{4.78}$$

$$R_3(q^2, q_{\mu_2}, y) \equiv \int_0^1 dx \int_0^y d\zeta \ \sin(q_{\mu_2} x\zeta) \ K_0\left(s\,|\zeta|\right)(1-x), \tag{4.79}$$

$$R_4(q^2, q_{\mu_1}, q_{\mu_2}, z, y) \equiv \int_0^1 dx \int_0^y d\zeta \ e^{-iq_{\mu_1} xz} \ \cos(q_{\mu_2} x\zeta) \ K_0\left(s\sqrt{z^2+\zeta^2}\right)(1-x), \tag{4.80}$$

$$R_5(q^2, q_{\mu_1}, q_{\mu_2}, z, y) \equiv \int_0^1 dx \int_0^y d\zeta \ e^{-iq_{\mu_1} xz} \ \cos(q_{\mu_2} x\zeta) \ K_1\left(s\sqrt{z^2+\zeta^2}\right) \frac{\sqrt{(1-x)x}}{\sqrt{z^2+\zeta^2}}, \tag{4.81}$$

$$R_6(q^2, q_{\mu_1}, q_{\mu_2}, z, y) \equiv \int_0^1 dx \int_0^y d\zeta \ e^{-iq_{\mu_1} xz} \ \sin(q_{\mu_2} x\zeta) \ K_0\left(s\sqrt{z^2+\zeta^2}\right), \tag{4.82}$$

$$R_7(q^2, q_{\mu_1}, q_{\mu_2}, z, y) \equiv \int_0^1 dx \int_0^y d\zeta \ e^{-iq_{\mu_1} xz} \ \sin(q_{\mu_2} x\zeta) \ K_0\left(s\sqrt{z^2+\zeta^2}\right)(1-x), \tag{4.83}$$

$$R_8(q^2, q_{\mu_1}, q_{\mu_2}, z, y) \equiv \int_0^1 dx \int_0^y d\zeta \ e^{-iq_{\mu_1} xz} \ \sin(q_{\mu_2} x\zeta) \ K_1\left(s\sqrt{z^2+\zeta^2}\right) \frac{\sqrt{(1-x)x}}{\sqrt{z^2+\zeta^2}}. \tag{4.84}$$

4.B Renormalization of fermion fields

In this appendix, we have gathered useful expressions regarding the renormalization of fermion fields in both dimensional (DR) and lattice (LR) regularizations, taken from, e.g., Refs. [186] and [200], respectively. We give the one-loop expressions for the renormalization factors in the $\overline{\text{MS}}$ and RI′ schemes, as well as the conversion factors between the two schemes,

$$Z_\psi^{\text{DR},\overline{\text{MS}}} = 1 + \frac{g^2 C_F}{16\pi^2}(\beta - 1)\frac{1}{\varepsilon} + \mathcal{O}(g^4), \tag{4.85}$$

$$Z_\psi^{\text{DR,RI}'} = 1 + \frac{g^2 C_F}{16\pi^2}(\beta - 1)\left(\frac{1}{\varepsilon} + 1 + \log\left(\frac{\bar{\mu}^2}{\bar{q}^2}\right)\right) + \mathcal{O}(g^4), \tag{4.86}$$

$$C_\psi^{\text{RI}',\overline{\text{MS}}} = \frac{Z_\psi^{\text{DR,RI}'}}{Z_\psi^{\text{DR},\overline{\text{MS}}}} = \frac{Z_\psi^{\text{LR,RI}'}}{Z_\psi^{\text{LR},\overline{\text{MS}}}} = 1 + \frac{g^2 C_F}{16\pi^2}(\beta - 1)\left(1 + \log\left(\frac{\bar{\mu}^2}{\bar{q}^2}\right)\right) + \mathcal{O}(g^4), \tag{4.87}$$

$$Z_\psi^{\mathrm{LR,RI'}} = 1 + \frac{g^2 C_F}{16\pi^2}\left[e_1^\psi + 4.7920\,\beta + e_2^\psi c_{SW} + e_3^\psi c_{SW}^2 + (1-\beta)\log\left(a^2\bar{q}^2\right)\right] + \mathcal{O}(g^4), \tag{4.88}$$

$$Z_\psi^{\mathrm{LR},\overline{\mathrm{MS}}} = \frac{Z_\psi^{\mathrm{LR,RI'}}}{C_\psi^{\mathrm{RI'},\overline{\mathrm{MS}}}} = 1 + \frac{g^2 C_F}{16\pi^2}\Big[(e_1^\psi + 1) + 3.7920\,\beta + e_2^\psi c_{SW} + e_3^\psi c_{SW}^2 + (1-\beta)\log\left(a^2\bar{\mu}^2\right)\Big] + \mathcal{O}(g^4). \tag{4.89}$$

The numerical constants e_i^ψ depend on the gluon action in use; their values for Wilson, tree-level Symanzik and Iwasaki improved gluon actions are given in Table 4.4.

Gluon action	$\boldsymbol{e_1^\psi}$	$\boldsymbol{e_2^\psi}$	$\boldsymbol{e_3^\psi}$
Wilson	11.8524	-2.2489	-1.3973
Tree-level Symanzik	8.2313	-2.0154	-1.2422
Iwasaki	3.3246	-1.6010	-0.9732

TABLE 4.4: Numerical values of the coefficients e_1^ψ-e_3^ψ appearing in the one-loop renormalization factors of fermion fields on the lattice.

Chapter 5

Higher-loop renormalization of Wilson-line operators related to quasi- PDFs

5.1 Introduction

In this work we extend our studies on Wilson-line operators to two-loop order. In particular, we calculate the two-loop renormalization factors of straight Wilson-line operators in the RI′ and $\overline{\text{MS}}$ schemes using dimensional regularization; the computation considers only massless fermions. We also extract the conversion factors between the two schemes. The motivation behind this study is mainly based on an argument in Ref.[99] about the truncation effects coming from the one-loop conversion factors. In this paper, it is claimed that two-loop corrections of the conversion factors are expected to eliminate the unphysical feature of the real part of the nonperturbative renormalized matrix elements becoming negative for large Wilson-line lengths. In particular, numerical experiments indicate that a natural change of the conversion factor by two-loop contributions ($\sim 10-20$ %), should be enough to suppress the unwanted effect. A by-product of this two-loop calculation is the anomalous dimension of the Wilson-line operators to next order in g^2 (also found in Refs. [155, 201, 202] in the context of HQET); this is useful for improving the method for eliminating the linear divergences, nonperturbatively (see Ref.[114]).

In the rest of this chapter, we provide the setup of our calculation (Sec. 5.2) and our preliminary results on the calculation of two-loop contributions to the bare Green's functions of Wilson-line operators (Sec. 5.3).

5.2 Setup

The theoretical setup related to the definition of the straight Wilson-line operators $\mathcal{O}_\Gamma$, along with the necessary prescription of the renormalization schemes is provided in Chapter 3. We note that, as we use massless fermions, the mixing pattern reduces to the following pairs[1]: $(\Gamma_1, \Gamma_2) = (\mathbb{1}, \gamma_1)$, $(\gamma_5\gamma_2, \gamma_3\gamma_4)$, $(\gamma_5\gamma_3, \gamma_4\gamma_2)$, and $(\gamma_5\gamma_4, \gamma_2\gamma_3)$, where by convention 1 is the direction of the straight Wilson line and 2, 3, and 4 are directions perpendicular to it.

For the extraction of the two-loop renormalization factors of operators, the two-loop expression for the renormalization function of the fermion field Z_ψ, as well as, the one-loop expression for the renormalization function of the coupling constant Z_g are involved (besides the two-loop expression for the bare two-point Green's function of $\mathcal{O}_\Gamma$, Λ_Γ). By writing Z_ψ, Z_g, and Λ_Γ in the form[2]:

$$Z_\psi = 1 + g_0^2 z_\psi^{(1)} + g_0^4 z_\psi^{(2)} + \mathcal{O}(g_0^6), \tag{5.1}$$

$$Z_g = 1 + g_0^2 z_g^{(1)} + \mathcal{O}(g_0^4), \tag{5.2}$$

$$\begin{aligned}\Lambda_{\Gamma_i} &= \Lambda_{\Gamma_1}^{\text{tree}}\left[\delta_{i1} + g_0^2 \lambda_{i1}^{(1)} + g_0^4 \lambda_{i1}^{(2)} + \mathcal{O}(g_0^6)\right] \\ &+ \Lambda_{\Gamma_2}^{\text{tree}}\left[\delta_{i2} + g_0^2 \lambda_{i2}^{(1)} + g_0^4 \lambda_{i2}^{(2)} + \mathcal{O}(g_0^6)\right] + \cdots, (i = 1, 2),\end{aligned} \tag{5.3}$$

the renormalization factors of $\mathcal{O}_\Gamma$ in RI′, reads:

[1] originally found in Ref. [114].

[2] The Green's functions Λ_{Γ_i} may also contain additional Dirac structures, which do not contribute to Z_{Γ_i} defined in RI′ or $\overline{\text{MS}}$.

$$\begin{aligned}\left[Z^{\mathrm{DR,RI'}}_{\Gamma_1,\Gamma_2}\right]_{ij} &= \delta_{ij}\Bigg\{1+g^2_{\mathrm{RI'}}\left[\left(z^{(1)}_\psi\right)^{\mathrm{DR,RI'}}+\lambda^{(1)}_{ii}\right]+g^4_{\mathrm{RI'}}\Bigg[\left(z^{(2)}_\psi\right)^{\mathrm{DR,RI'}}+\lambda^{(2)}_{ii}\\ &\quad+\left(z^{(1)}_\psi\right)^{\mathrm{DR,RI'}}\lambda^{(1)}_{ii}+2\left(z^{(1)}_\psi\right)^{\mathrm{RI'}}\left(z^{(1)}_g\right)^{\mathrm{DR,RI'}}+2\left(z^{(1)}_g\right)^{\mathrm{DR,RI'}}\lambda^{(1)}_{ii}\Bigg]\\ &\quad+\mathcal{O}(g^6_{\mathrm{RI'}})\Bigg\}\Bigg|_{q_\nu=\bar{q}_\nu}\\ &+ (1-\delta_{ij})\Bigg\{g^2_{\mathrm{RI'}}\lambda^{(1)}_{ij}+g^4_{\mathrm{RI'}}\left[\lambda^{(2)}_{ij}+\left(z^{(1)}_\psi\right)^{\mathrm{DR,RI'}}\lambda^{(1)}_{ij}+2\left(z^{(1)}_g\right)^{\mathrm{DR,RI'}}\lambda^{(1)}_{ij}\right]\\ &\quad+\mathcal{O}(g^6_{\mathrm{RI'}})\Bigg\}\Bigg|_{q_\nu=\bar{q}_\nu}\end{aligned} \tag{5.4}$$

The equivalent expression for $Z^{DR,\overline{\mathrm{MS}}}_{\Gamma}$ follows from Eq. (5.4), by keeping in $\lambda^{(1)}_{ij},\lambda^{(2)}_{ij}$ only pole parts in ε; the latter appears only for $i=j$, leading to

$$\begin{aligned}Z^{DR,\overline{\mathrm{MS}}}_{\Gamma_i} &= \Bigg\{1+g^2_{\overline{\mathrm{MS}}}\left[\left(z^{(1)}_\psi\right)^{\mathrm{DR},\overline{\mathrm{MS}}}+\lambda^{(1)}_{ii}\right]+g^4_{\overline{\mathrm{MS}}}\Bigg[\left(z^{(2)}_\psi\right)^{\mathrm{DR},\overline{\mathrm{MS}}}+\lambda^{(2)}_{ii}+\left(z^{(1)}_\psi\right)^{\mathrm{DR},\overline{\mathrm{MS}}}\lambda^{(1)}_{ii}\\ &\quad+2\left(z^{(1)}_\psi\right)^{\mathrm{DR},\overline{\mathrm{MS}}}\left(z^{(1)}_g\right)^{\mathrm{DR},\overline{\mathrm{MS}}}+2\left(z^{(1)}_g\right)^{\mathrm{DR},\overline{\mathrm{MS}}}\lambda^{(1)}_{ii}\Bigg]+\mathcal{O}(g^6_{\overline{\mathrm{MS}}})\Bigg\}\Bigg|_{1/\varepsilon^2,1/\varepsilon}\end{aligned} \tag{5.5}$$

The expressions of Z_ψ and Z_g are well-known beyond one loop [186].

5.3 Calculation and results

There are fifty-six two-loop Feynman diagrams contributing to the two-point Green's function of operators, shown in Figs. 5.1, 5.2. The methodology for calculating the momentum-loop integrals corresponding to these Feynman diagrams is briefly described in our previous work in Chapter 3. Here we extend this methodology to two loops.

Firstly, we follow the standard procedure of introducing Feynman parameters. Then, the momentum-loop integrals take the following general form:

$$\int\frac{d^Dp_1}{(2\pi)^D}\int\frac{d^Dp_2}{(2\pi)^D}\frac{e^{ip_{1\mu}z_1}\;e^{ip_{2\mu}z_2}\;(p_{1\nu_1}\cdots p_{1\nu_n})\;(p_{1\rho_1}\cdots p_{1\rho_m})f(\{\alpha_i\})}{\left[\alpha_1p_1^2+\alpha_2p_2^2+\alpha_3p_1\cdot p_2+\alpha_4p_1\cdot q+\alpha_5p_2\cdot q+\alpha_6\right]^\beta}, \tag{5.6}$$

FIGURE 5.1: Feynman diagrams contributing to the two-loop calculation of the Green's functions of straight-line operator $\mathcal{O}_\Gamma$. The straight (wavy, dashed) lines represent fermions (gluons, qhosts). The operator insertion is denoted by a filled rectangle. (1/2)

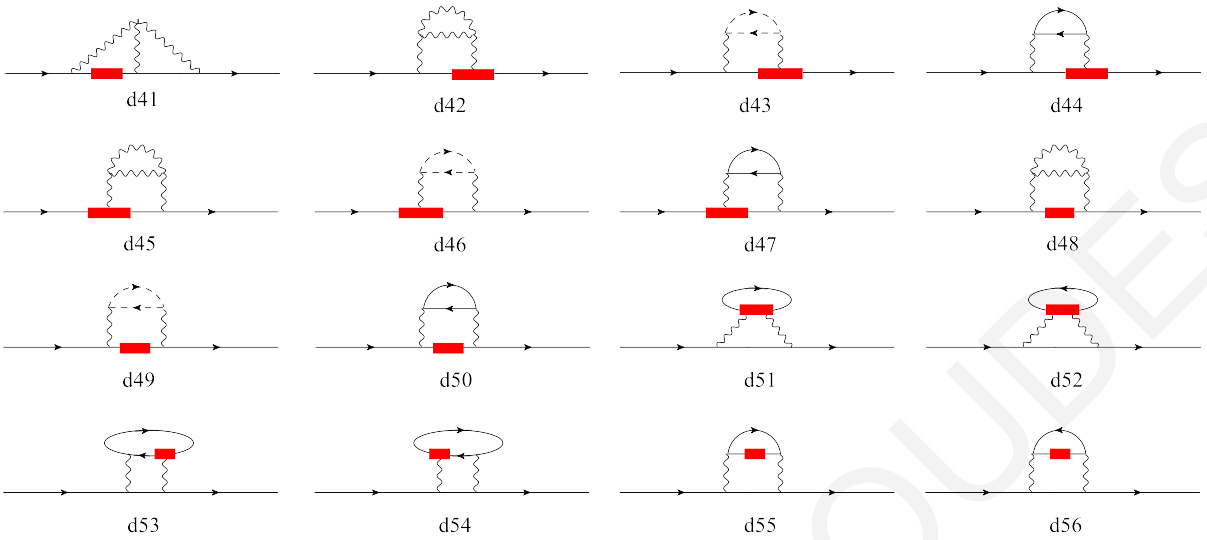

FIGURE 5.2: Feynman diagrams contributing to the two-loop calculation of the Green's functions of straight-line operator $\mathcal{O}_\Gamma$. The straight (wavy, dashed) lines represent fermions (gluons, qhosts). The operator insertion is denoted by a filled rectangle. (2/2)

where α_i $(i = 1{-}6)$ depends on Feynman parameters, $f(\{\alpha_i\})$ is a function of α_i and q is the external momentum. The integration over the components of momentum without an exponential dependence is performed using standard D-dimensional formulae (e.g., [184]), followed by a subsequent nontrivial integration over the remaining components p_{1_μ} and p_{2_μ}. This procedure leads to the following two-loop formulae:

$$\begin{aligned} A(\beta) \;\equiv\; & \int \frac{d^D p_1}{(2\pi)^D} \int \frac{d^D p_2}{(2\pi)^D} \frac{e^{ip_{1_\mu} z_1}\; e^{ip_{2_\mu} z_2}}{\left[\alpha_1 p_1^2 + \alpha_2 p_2^2 + \alpha_3 p_1\cdot p_2 + \alpha_4 p_1\cdot k_1 + \alpha_5 p_2\cdot k_2 + \alpha_6\right]^\beta} \\ =\; & \frac{2^{1-\beta}\alpha_1^{D-\beta} s_2^{(D-\beta)/2}}{\pi^D \Gamma(\beta) s_1^{D/2}} K_{D-\beta}(\sqrt{s_2}) \exp\left[\frac{-ik_{1_\mu}\alpha_4(2\alpha_2 z_1 - \alpha_3 z_2)}{s_1}\right] \cdot \\ & \exp\left[\frac{-ik_{2_\mu}\alpha_5(2\alpha_1 z_2 - \alpha_3 z_1)}{s_2}\right], \end{aligned} \tag{5.7}$$

$$\begin{aligned} & \int \frac{d^D p_1}{(2\pi)^D} \int \frac{d^D p_2}{(2\pi)^D} \frac{e^{ip_{1_\mu} z_1}\; e^{ip_{2_\mu} z_2}\; (p_{1_{\nu_1}} \cdots p_{1_{\nu_n}})\; (p_{1_{\rho_1}} \cdots p_{1_{\rho_m}})}{\left[\alpha_1 p_1^2 + \alpha_2 p_2^2 + \alpha_3 p_1\cdot p_2 + \alpha_4 p_1\cdot k_1 + \alpha_5 p_2\cdot k_2 + \alpha_6\right]^\beta} = \\ & \frac{(-1)^{n+m}\;\Gamma(\beta - n - m)}{\alpha_4^n \alpha_5^m\;\Gamma(\beta)} \frac{\partial}{\partial k_{1_{\nu_1}}} \cdots \frac{\partial}{\partial k_{1_{\nu_n}}} \frac{\partial}{\partial k_{2_{\rho_1}}} \cdots \frac{\partial}{\partial k_{2_{\rho_m}}} A(\beta - n - m), \end{aligned} \tag{5.8}$$

where $s_1 \equiv 4a_1 a_2 - a_3^2$,
$s_2 \equiv \left[(\alpha_6/\alpha_1) - (\alpha_2\alpha_4^2 k_1^2 + \alpha_1\alpha_5^2 k_2^2 - \alpha_3\alpha_4\alpha_5 k_1 k_2)/(\alpha_1 s_1)\right] \cdot \left[z_1^2 + (\alpha_3 z_1 - 2\alpha_1 z_2)^2/s_1\right]$,
and $K_\nu(z)$ is a modified Bessel function of the second kind. We note that the formula

in Eq. (5.7) is only valid for $s_1 > 0$, $s_2 > 0$, $\alpha_1 \neq 0$, $D < (3/4+\beta)$; the same conditions for s_1, s_2, α_1 are also valid for the formula in Eq. (5.8), while the condition for D is modified as $D < (3/4 + \beta - n/2 - m/2)$. In order to perform Laurent expansion in ε, it might be necessary to make subtractions in the original integrand so that possible poles (in the integration region of Feynman parameters and/or ζ-variables stemming from the definition of $\mathcal{O}_\Gamma$) be isolated and interchange between integration and limit (of vanishing regulator) operations can be applied in the remaining convergent part (see 3.3.1).

So far we have completed the calculation of the Green's functions of straight Wilson-line operators for the first twenty diagrams ($d_1 - d_{20}$), including some of the most delicate ones, such as diagrams with up to four gluons stemming from the definition of the operators, which result in multiple integrations over the position of gluons along the Wilson line, combined with overlapping divergences (e.g., d_{18}). Preliminary results of our calculations are presented below. We provide only a small part of our current results because the length of the expression for each diagram is very large. The expressions for the bare Green's functions of Wilson-line operators for the "tadpole"-like diagrams $d_1 - d_7$ are:

$$\begin{aligned}\Lambda_\Gamma^{d_1} &= \frac{g^4 C_F^2}{(16\pi^2)^2}\Lambda_\Gamma^{\text{tree}}\Big\{(\beta+2)^2\frac{1}{\varepsilon^2} + \Big[2(\beta+2)\Big(4+(\beta+2)(2\gamma_E+\log\left(\frac{\bar{\mu}^2 z^2}{4}\right))\Big)\Big]\frac{1}{\varepsilon} \\ &\quad +4(\beta+2)\log\left(\frac{\bar{\mu}^2 z^2}{4}\right)\left((\beta+2)\log\left(\frac{\bar{\mu}^2 z^2}{4}\right)+4\gamma_E(\beta+2)+8\right) \\ &\quad -\pi^2(\beta+2)^2+16\left(\gamma_E^2(\beta+2)^2+4\gamma_E(\beta+2)+2(\beta+3)\right)\Big\}, \quad (5.9)\end{aligned}$$

$$\begin{aligned}\Lambda_\Gamma^{d_2} &= \frac{g^4 C_F}{(16\pi^2)^2 N_c}\Lambda_\Gamma^{\text{tree}}\Bigg\{\frac{(\beta+2)^2}{2}\frac{1}{\varepsilon^2} + \Big[\frac{(\beta+2)}{2}\Big(2(\beta+2)\left(2\gamma_E+\log\left(\frac{\bar{\mu}^2 z^2}{4}\right)\right) \\ &\quad +\beta+10\Big)\Big]\frac{1}{\varepsilon} + \frac{1}{4}\Bigg(8\Big(\beta^2+10\beta+2\gamma_E^2(\beta+2)^2 \\ &\quad +\gamma_E(\beta+2)(\beta+10)+20\Big)+4(\beta+2)\log\left(\frac{\bar{\mu}^2 z^2}{4}\right) \\ &\quad \left((\beta+2)\log\left(\frac{\bar{\mu}^2 z^2}{4}\right)+\beta+4\gamma_E(\beta+2)+10\right) \\ &\quad -\pi^2(\beta+2)^2\Bigg)\Bigg\}, \quad (5.10)\end{aligned}$$

$$\Lambda_\Gamma^{d_3} = \frac{g^4 C_F^2}{(16\pi^2)^2}\Lambda_\Gamma^{\text{tree}}\Bigg\{\frac{(\beta+2)^2}{2}\frac{1}{\varepsilon^2}+\Big[(\beta+2)\Bigg((\beta+2)\left(2\gamma_E+\log\left(\frac{\bar{\mu}^2 z^2}{4}\right)\right) +\beta+6\Bigg)\Big]\frac{1}{\varepsilon}+\frac{1}{12}\Bigg(48\Big(\beta^2+8\beta+\gamma_E^2(\beta+2)^2 +\gamma_E(\beta+2)(\beta+6)+14\Big)+12(\beta+2)\log\left(\frac{\bar{\mu}^2 z^2}{4}\right)\left((\beta+2)\log\left(\frac{\bar{\mu}^2 z^2}{4}\right)+2(\beta+2\gamma(\beta+2)+6)\right) +\pi^2(\beta+2)^2\Bigg)\Bigg\}, \tag{5.11}$$

$$\Lambda_\Gamma^{d_4} = \frac{g^4 C_F N_c}{(16\pi^2)^2}\Lambda_\Gamma^{\text{tree}}\Bigg\{-\frac{3}{4}\beta(\beta+2)\frac{1}{\varepsilon^2}-\frac{\beta}{2}\Bigg[3(\beta+2)\left(2\gamma_E+\log\left(\frac{\bar{\mu}^2 z^2}{4}\right)\right) +2(\beta+5)\Bigg]\frac{1}{\varepsilon}-\frac{1}{24}\beta\Bigg(36(\beta+2)\log^2\left(\frac{\bar{\mu}^2 z^2}{4}\right) +48(\beta+3\gamma_E(\beta+2)+5)\log\left(\frac{\bar{\mu}^2 z^2}{4}\right)+48\Big(2\beta+3\gamma_E^2(\beta+2) +2\gamma_E(\beta+5)+9\Big)-5\pi^2(\beta+2)\Bigg)\Bigg\}, \tag{5.12}$$

$$\Lambda_\Gamma^{d_5+d_6} = \frac{g^4 C_F N_c}{(16\pi^2)^2}\Lambda_\Gamma^{\text{tree}}\Bigg\{\frac{(3\beta+10)}{4}\frac{1}{\varepsilon^2}+\frac{1}{8}\Big[4(3\beta+10)\log\left(\frac{\bar{\mu}^2 z^2}{4}\right) +(\beta(3\beta+24\gamma_E+2)+80\gamma_E+88)\Big]\frac{1}{\varepsilon}+\frac{1}{24}\Bigg(6\log\left(\frac{\bar{\mu}^2 z^2}{4}\right) +\Big((6\beta+20)\log\left(\frac{\bar{\mu}^2 z^2}{4}\right)+(\beta(3\beta+24\gamma_E+2)+80\gamma_E+88)\Big) +3(\beta(13\beta+14)+400)+12\gamma_E(\beta(3\beta+12\gamma_E+2)+40\gamma_E +88)+\pi^2(3\beta+10)\Bigg)\Bigg\}, \tag{5.13}$$

$$\Lambda_\Gamma^{d_7} = \frac{g^4 C_F N_f}{(16\pi^2)^2}\Lambda_\Gamma^{\rm tree}\Bigg\{ -\frac{1}{\varepsilon^2} + -2\left[\log\left(\frac{\bar\mu^2 z^2}{4}\right) + 2(1+\gamma_E)\right]\frac{1}{\varepsilon} + \frac{1}{6}\Bigg(-12\log\left(\frac{\bar\mu^2 z^2}{4}\right)\left(\log\left(\frac{\bar\mu^2 z^2}{4}\right) + 4(1+\gamma_E)\right) - \pi^2 - 48\gamma_E(2+\gamma_E) - 108\Bigg)\Bigg\}, \tag{5.14}$$

where $C_F \equiv (N_c^2-1)/(2N_c)$, N_c (N_f) is the number of colors (flavors) and β is the gauge parameter [$\beta = 0$ (1) in Feynman (Landau) gauge]. Diagrams which are not tadpole-like present a highly nontrivial dependence on z and on the external momentum q, extending the one-loop expressions shown in Chapter 3. As an example, we provide the resulting expression for diagram d_{18} (for simplicity) in the Feynman gauge ($\beta = 0$):

$$\begin{aligned}\Lambda_\Gamma^{d_{18}} = {} & \frac{g^4 C_F}{(16\pi^2)^2 N_c}\Lambda_\Gamma^{\rm tree}\int_0^z \zeta_1 \int_0^{\zeta 1} d\zeta_2 \int_0^1 dx_1 \int_0^1 dx_2 \Bigg\{ -\frac{2\; e^{-iq_\mu \zeta_2}}{(1-x_1)x_1\zeta_1^2 + x_2(\zeta_2 - x_1\zeta_1)^2} \\ & + \int_0^{1-x_2} dx_3 \Bigg[K_0\left(\sqrt{q^2(1-x_2-x_3)(x_2+x_3)[(1-x_1)x_1\zeta_1^2 + x_3(\zeta_2 - x_1\zeta_1)^2]/x_3}\right)\cdot \\ & e^{-iq_\mu x_1(1-x_2-x_3)\zeta_1}\; e^{-iq_\mu(x_2+x_3)\zeta_2}\; \frac{q^2}{x_3}\Bigg(-1 + x_1(1-x_2-x_3) + 2(x_2+x_3)^2 \\ & + \frac{(1-x_1)x_1(1-x_2-x_3)(x_2+x_3)\zeta_1(2\;\zeta_1 - \zeta_2)}{(1-x_1)x_1\zeta_1^2 + x_3(\zeta_2 - x_1\zeta_1)^2}\Bigg) \\ & - K_1\left(\sqrt{q^2(1-x_2-x_3)(x_2+x_3)[(1-x_1)x_1\zeta_1^2 + x_3(\zeta_2 - x_1\zeta_1)^2]/x_3}\right)\cdot \\ & e^{-iq_\mu x_1(1-x_2-x_3)\zeta_1}\; e^{-iq_\mu(x_2+x_3)\zeta_2}\; 2\sqrt{\frac{q^2(1-x_2-x_3)(x_2+x_3)}{x_3\;[(1-x_1)x_1\zeta_1^2 + x_3(\zeta_2 - x_1\zeta_1)^2]}}\cdot \\ & \left(1 - 2x_1 + iq_\mu(x_2+x_3)(\zeta_2 - x_1\zeta_1) + \frac{(1-x_1)x_1\zeta_1(2\;\zeta_1 - \zeta_2)}{(1-x_1)x_1\zeta_1^2 + x_3(\zeta_2 - x_1\zeta_1)^2}\right)\Bigg]\Bigg\}. \end{aligned} \tag{5.15}$$

Calculations for the remaining diagrams $d_{21} - d_{56}$ are still in progress. Our work will continue beyond the completion of this Thesis. The full results will be produced and published in the near future.

Chapter 6

Two-loop renormalization of staggered fermion bilinears: singlet vs nonsinglet operators

6.1 Introduction

In this work we study the renormalization of fermion bilinears $\mathcal{O}_\Gamma = \bar{\psi}\Gamma\psi$ on the lattice, where $\Gamma = \mathbb{1}$, γ_5, γ_μ, $\gamma_5\,\gamma_\mu$, $\gamma_5\,\sigma_{\mu\,\nu}$ ($\sigma_{\mu\nu} = [\gamma_\mu, \gamma_\nu]/2i$). We consider flavor singlet ($\sum_f \bar{\psi}_f\Gamma\psi_f$, f: flavor index) as well as nonsinglet ($\bar{\psi}_{f_1}\Gamma\psi_{f_2}, f_1 \neq f_2$) operators, to two loops in perturbation theory. More specifically, we compute the difference between the renormalization functions of singlet and nonsinglet operators. Our calculations were performed making use of a class of improved lattice actions: Symanzik improved gluons and staggered fermions with twice stout-smeared links. Previous calculations of this difference have been performed in Refs. [49, 50], using Wilson gluons and clover fermions, and also in Ref. [203], using the SLiNC action.

The most demanding part of this study is the computation of the two-point Green's functions of $\mathcal{O}_\Gamma$, up to two loops. From these Green's functions we extract the renormalization functions for $\mathcal{O}_\Gamma$: $Z_\Gamma^{L,Y}$ (L: lattice regularization, Y (= RI', $\overline{\text{MS}}$): renormalization schemes). As a check on our results, we have computed them in an arbitrary covariant gauge. Our expressions can be generalized, in a straightforward manner, to fermionic fields in an arbitrary representation.

Flavor singlet operators are relevant for a number of hadronic properties including, e.g., topological features or the spin structure of hadrons. Matrix elements of such operators are notoriously difficult to study via numerical simulations, due to the presence of (fermion line) disconnected diagrams, which in principle require evaluation of the full fermion propagator. In recent years there has been some progress in the numerical study of flavor singlet operators; furthermore, for some of them, a nonperturbative estimate of their renormalization has been obtained using the Feynman-Hellmann relation [65]. Perturbation theory can give an important cross check for these estimates, and provide a prototype for other operators which are more difficult to renormalize nonperturbatively.

Given that for the renormalization of flavor nonsinglet operators one can obtain quite accurate nonperturbative estimates, we will focus on the perturbative evaluation of the *difference* between the flavor singlet and nonsinglet renormalization; this difference first shows up at two loops.

Perturbative computations beyond one loop for Green's functions with nonzero external momenta are technically quite involved, and their complication is greatly increased when improved gluon and fermion actions are employed. For fermion bilinear operators, the only two-loop computations in standard perturbation theory thus far have been performed by our group [49, 50], employing Wilson gluons and Wilson/clover fermions. Similar investigations have been carried out in the context of stochastic perturbation theory [204].

Staggered fermions entail additional complications as compared to Wilson fermions. In particular, the fact that fermion degrees of freedom are distributed over neighbouring lattice points requires the introduction of link variables in the definition of gauge invariant fermion bilinears, with a corresponding increase in the number of Feynman diagrams. In addition, the appearance of 16 (rather than 1) poles in the fermion propagator leads to a rather intricate structure of divergent contributions in two-loop diagrams.

A novel aspect of the calculations is that the gluon links, which appear both in the staggered fermion action and in the definition of the bilinear operators in the staggered basis, are improved by applying a stout smearing procedure up to two times, iteratively. Compared to most other improved formulations of staggered

fermions, the stout smearing action leads to smaller taste violating effects [205–207]. Application of stout improvement on staggered fermions thus far has been explored, by our group, only to one-loop computations [183]; a two-loop computation had never been investigated before.

Further composite fermion operators of interest, to which one can apply our perturbative techniques, are higher dimension bilinears such as: $\bar{\psi}\Gamma\, D^{\mu}\psi$ (appearing in hadron structure functions) and four-fermion operators such as: $(\bar{s}\,\Gamma_1\, d)\,(\bar{s}\,\Gamma_2\, d)$ (appearing in $\Delta S = 2$ transitions, etc.); in these cases, complications such as operator mixing greatly hinder nonperturbative methods of renormalization, making a perturbative approach all that more essential.

The outline of this chapter is as follows: Sec. 6.2 presents a brief theoretical background in which we introduce the formulation of the staggered fermion action and the bilinear operators in the staggered basis, as well as all necessary definitions of renormalization schemes and of the quantities to compute. Sec. 6.3 contains the calculational procedure and the results which are obtained. A method for the evaluation of a list of nontrivial divergent two-loop integrals, which stem from the staggered formalism, is briefly described in this section. In Sec. 6.4 we discuss our results and we plot several graphs for certain values of free parameters, like the stout and clover coefficients.

6.2 Formulation

6.2.1 Lattice actions

In our calculation we made use of the staggered formulation of the fermion action on the lattice [13], applying a twice stout smearing procedure on the gluon links. In standard notation, it reads:

$$S_{\rm SF} = a^4 \sum_{x,\mu} \frac{1}{2a}\, \overline{\chi}(x)\, \eta_{\mu}(x) \left[\widetilde{\widetilde{U}}_{\mu}(x)\, \chi(x+a\hat{\mu}) - \widetilde{\widetilde{U}}^{\dagger}_{\mu}(x-a\hat{\mu})\, \chi(x-a\hat{\mu})\right] + a^4 \sum_{x} m\, \overline{\chi}(x)\, \chi(x) \tag{6.1}$$

where $\chi(x)$ is a one-component fermion field, and $\eta_{\mu}(x) = (-1)^{\sum_{\nu<\mu} n_{\nu}}$ $[x = (a\,n_1, a\,n_2, a\,n_3, a\,n_4), \quad n_i\, \epsilon\, \mathbb{Z}]$. The relation between the staggered field $\chi(x)$

and the standard fermion field $\psi(x)$, is given by:

$$\psi(x) \;= \gamma_x\, \chi(x) \quad , \qquad \bar{\psi}(x) \;= \bar{\chi}(x)\, \gamma_x^{\dagger},$$

$$\gamma_x \;= \gamma_1^{n_1}\, \gamma_2^{n_2}\, \gamma_3^{n_3}\, \gamma_4^{n_4} \quad , \qquad x \;= (a\, n_1, a\, n_2, a\, n_3, a\, n_4), \quad n_i \,\epsilon\, \mathbb{Z} \tag{6.2}$$

The mass term will be irrelevant, since we will apply mass-independent renormalization schemes (RI', $\overline{\rm MS}$). The gluon links $\widetilde{\widetilde{U}}_\mu(x)$, appearing above, are doubly stout links, defined as:

$$\widetilde{\widetilde{U}}_\mu(x) \;= e^{i\, \widetilde{Q}_\mu(x)}\, \widetilde{U}_\mu(x) \tag{6.3}$$

where $\widetilde{U}_\mu(x)$ is the singly stout link, defined as [24]:

$$\widetilde{U}_\mu(x) \;= e^{i\, Q_\mu(x)}\, U_\mu(x) \tag{6.4}$$

where

$$Q_\mu(x) \;= \frac{\omega}{2\, i}\left[V_\mu(x) U_\mu^\dagger(x) - U_\mu(x) V_\mu^\dagger(x) - \frac{1}{N_c}{\rm Tr}\left(V_\mu(x) U_\mu^\dagger(x) - U_\mu(x) V_\mu^\dagger(x)\right)\right] \tag{6.5}$$

$V_\mu(x)$ represents the sum over all staples associated with the link $U_\mu(x)$ and N_c is the number of colors. Correspondingly, $\widetilde{Q}_\mu(x)$ is defined as in Eq.(6.5), but using $\widetilde{U}_\mu$ as links (also in the construction of V_μ). To obtain results that are as general as possible, we use different stout parameters, ω, in the first (ω_1) and the second (ω_2) smearing iteration.

For gluons, we employ the Symanzik improved action S_G, defined in Eq. (4.5). The algebraic part of our computation was carried out for generic values of Symanzik coefficients c_i; for the numerical integration over loop momenta we selected a number of commonly used sets of values, which are shown in Table 4.1.

6.2.2 Definition of bilinear operators in the staggered basis

The absence of Dirac indices in the staggered action leads to the assigning of a single fermion field component to each lattice site. Hence, the action contains only four rather than sixteen fermion doublers, which are called "tastes". So, in the staggered formalism a physical fermion field $\psi(x)$ with taste components is defined as a linear combination

of the single-component fermion fields $\chi(x)$ that live on the corners of 4-dimensional elementary hypercubes of the lattice. In standard notation:

$$\psi_{\alpha,t}(y) \;= \frac{1}{2}\sum_{C} (\gamma_C)_{\,\alpha,t}\, \chi(y)_C\,, \quad \chi(y)_C = \frac{1}{2}\sum_{\alpha,t} (\xi_C)_{\,\alpha,t}\, \psi_{\alpha,t}(y) \tag{6.6}$$

where $\chi(y)_C \equiv \chi(y + aC)/4$, y denotes the position of a hypercube inside the lattice ($y_\mu \in 2\mathbb{Z}$), C denotes the position of a fermion field component within a specific hypercube ($C_\mu \in \{0,1\}$), $\gamma_C = \gamma_1^{C_1}\,\gamma_2^{C_2}\,\gamma_3^{C_3}\,\gamma_4^{C_4}$, $\xi_C = \xi_1^{C_1}\,\xi_2^{C_2}\,\xi_3^{C_3}\,\xi_4^{C_4}$, $\xi_\mu = \gamma_\mu^*$, α is a Dirac index and t is a taste index. In terms of fermion fields with taste components one can now define fermion bilinear operators as:

$$\mathcal{O}_{\Gamma,\xi} \;= \bar{\psi}(x)\; (\Gamma \otimes \xi)\; \psi(x) \tag{6.7}$$

where Γ and ξ are arbitrary 4×4 matrices acting on the Dirac and taste indices of $\psi_{\alpha,t}(x)$, respectively. After transforming to the staggered basis via Eq. (6.6), the operator $\mathcal{O}_{\Gamma,\xi}$ can be written as [180]:

$$\mathcal{O}_{\Gamma,\xi} \;=\; \sum_{C,D} \bar{\chi}(y)_C\; \big(\overline{\Gamma \otimes \xi}\big)_{\,CD}\, U_{C,D}\, \chi(y)_D\,, \tag{6.8}$$

$$\big(\overline{\Gamma \otimes \xi}\big)_{\,CD} \;\equiv \frac{1}{4}\,\mathrm{Tr}\left[\gamma_C^\dagger\,\Gamma\,\gamma_D\,\xi\right] \tag{6.9}$$

In order to ensure the gauge invariance of the above operators, one inserts the quantity $U_{C,D}$, which is the average of products of gauge link variables along all possible shortest paths connecting the sites $y + C$ and $y + D$. In this work we focus on taste-singlet operators, thus $\xi = \mathbb{1}$. Using the relations $\gamma_\mu\gamma_C = \eta_\mu(C)\gamma_{C+\hat{\mu}}$ and $\mathrm{tr}(\gamma_C^\dagger\gamma_D) = 4\delta_{C,D}$, we calculate the quantity $\big(\overline{\Gamma \otimes \mathbb{1}}\big)_{CD}$ for each operator Γ:

$$\begin{aligned}
\frac{1}{4}\mathrm{Tr}\left[\gamma_C^\dagger\,\mathbb{1}\,\gamma_D\right] &= \delta_{C,D}\,,\\
\frac{1}{4}\,\mathrm{Tr}\left[\gamma_C^\dagger\,\gamma_\mu\,\gamma_D\right] &= \delta_{C,D+_2\hat{\mu}}\;\eta_\mu(D)\,,\\
\frac{1}{4}\mathrm{Tr}\left[\gamma_C^\dagger\,\sigma_{\mu\nu}\,\gamma_D\right] &= \frac{1}{i}\,\delta_{C,D+_2\hat{\mu}+_2\hat{\nu}}\;\eta_\nu(D)\;\eta_\mu(D+_2\hat{\nu})\,,\\
\frac{1}{4}\,\mathrm{Tr}\left[\gamma_C^\dagger\,\gamma_5\,\gamma_\mu\,\gamma_D\right] &= \delta_{C,D+_2\hat{\mu}+_2(1,1,1,1)}\;\cdot\\
&\quad\;\eta_\mu(D)\,\eta_1(D+_2\hat{\mu})\,\eta_2(D+_2\hat{\mu})\,\eta_3(D+_2\hat{\mu})\,\eta_4(D+_2\hat{\mu})\,,\\
\frac{1}{4}\,\mathrm{Tr}\left[\gamma_C^\dagger\,\gamma_5\,\gamma_D\right] &= \delta_{C,D+_2(1,1,1,1)}\;\eta_1(D)\,\eta_2(D)\,\eta_3(D)\,\eta_4(D)
\end{aligned} \tag{6.10}$$

where $a +_2 b \equiv (a+b) \bmod 2$. Now, the operators can be written as:

$$\mathcal{O}_S(y) = \sum_D \bar{\chi}(y)_D \, \chi(y)_D \tag{6.11}$$

$$\mathcal{O}_V(y) = \sum_D \bar{\chi}(y)_{D+_2\hat{\mu}} \, U_{D+_2\hat{\mu},D} \, \chi(y)_D \, \eta_\mu(D) \tag{6.12}$$

$$\mathcal{O}_T(y) = \frac{1}{i} \sum_D \bar{\chi}(y)_{D+_2\hat{\mu}+_2\hat{\nu}} \, U_{D+_2\hat{\mu}+_2\hat{\nu},D} \, \chi(y)_D \, \eta_\nu(D) \, \eta_\mu(D +_2 \hat{\nu}) \, , \mu \neq \nu \tag{6.13}$$

$$\mathcal{O}_A(y) = \sum_D \bar{\chi}(y)_{D+_2\hat{\mu}+_2(1,1,1,1)} \, U_{D+_2\hat{\mu}+_2(1,1,1,1),D} \, \chi(y)_D \, \eta_\mu(D) \cdot \eta_1(D +_2 \hat{\mu}) \, \eta_2(D +_2 \hat{\mu}) \, \eta_3(D +_2 \hat{\mu}) \, \eta_4(D +_2 \hat{\mu}) \tag{6.14}$$

$$\mathcal{O}_P(y) = \sum_D \bar{\chi}(y)_{D+_2(1,1,1,1)} \, U_{D+_2(1,1,1,1),D} \, \chi(y)_D \, \eta_1(D) \, \eta_2(D) \, \eta_3(D) \, \eta_4(D) \tag{6.15}$$

where S(Scalar), P(Pseudoscalar), V(Vector), A(Axial Vector), T(Tensor) correspond to: $\Gamma = \mathbb{1}, \gamma_5, \gamma_\mu, \gamma_5\gamma_\mu, \gamma_5 \, \sigma_{\mu\nu}$. With the exception of the Scalar operator, the remaining operators contain averages of products of up to 4 gluon links (in orthogonal directions) between the fermion and the antifermion fields. For example, the average entering the tensor operator of Eq. (6.14) is:

$$U_{D+_2\hat{\mu}+_2\hat{\nu},D} = \frac{1}{2} \left[U^\dagger_\nu(y + aD +_2 a\hat{\mu}) \, U^\dagger_\mu(y + aD) + \{\mu \leftrightarrow \nu\} \right] \tag{6.16}$$

(Eq. 6.16 is valid when $(D +_2 \hat{\mu} +_2 \hat{\nu})_i \geq D_i$, $i = 1, 2, 3, 4$, and takes a similar form for all other cases.)

Just as in the staggered fermion action, the gluon links used in the operators, are doubly stout links. We have kept the stout parameters of the action $(\omega_{A_1}, \omega_{A_2})$ distinct from the stout parameters of the operators $(\omega_{O_1}, \omega_{O_2})$, for wider applicability of the results. The presence of gluon links in the definition of bilinear operators creates new Feynman diagrams which do not appear in the Wilson-like fermion actions, leading to nontrivial contributions in our two-loop calculation.

6.2.3 Momentum representation of fermion action and bilinear operators in the staggered formulation

In order to express the staggered action and bilinear operators in momentum space, we use some useful relations, such as the following equivalent expression of $\eta_\mu(x)$:

$$\eta_\mu(x) \ = e^{i\pi\bar{\mu}\, n}\,, \quad x = an\,, \quad \bar{\mu} = \sum_{\nu=1}^{\mu-1} \hat{\nu} \tag{6.17}$$

Also, the summation over the position of $\mathcal{O}_\Gamma$, followed by Fourier transformation leads to expressions of the form:

$$\sum_{y_\mu \,\epsilon\, 2\mathbb{Z}} e^{i\, y\cdot k} \ = \frac{1}{16}(2\pi)^4 \sum_C \delta_{2\pi}^{(4)}\,(k + \pi\, C) \tag{6.18}$$

where $\delta_{2\pi}^{(4)}\,(k)$ stands for the standard periodic δ-function with nonvanishing support at $k \,\mathrm{mod} 2\pi = 0$. In addition, the summation over the index D in the definition of $\mathcal{O}_\Gamma$, after Fourier transformation, may give expressions such as:

$$\sum_D e^{-i\pi(C-E)\cdot D} \ = 16\ \delta_{C,E} \tag{6.19}$$

where $E = (E_1, E_2, E_3, E_4),\ E_\mu \in \{0, 1\}$. Furthermore, expressions like $e^{ik(D+_2\hat{\mu})a}$ (for Vector and similar expressions for all other operators), which arise through Fourier transformations of the fermion and the antifermion fields, can be written in the following useful form:

$$e^{ik(D+_2\hat{\mu})a} \ = e^{ikDa}[\cos(k_\mu a) + ie^{i\pi D\cdot\hat{\mu}}\sin(k_\mu a)] \tag{6.20}$$

Finally, since contributions to the continuum limit come from the neighbourhood of each of the 16 poles of the external momenta q, at $q_\mu = (\pi/a)C_\mu$, it is useful to define q'_μ and C_μ through

$$q_\mu \ = q'_\mu + \frac{\pi}{a}C_\mu \quad (\,\mathrm{mod}(\frac{2\pi}{a})\,), \quad (C_\mu\ \epsilon\ \{0, 1\}) \tag{6.21}$$

where the "small" (physical) part q' has each of its components restricted to one half of the Brillouin zone: $-\pi/(2a) \le q'_\mu \le \pi/(2a)$. Thus, conservation of external momenta

takes the form:

$$\delta^{(4)}_{2\pi}(a\,q_1 - a\,q_2 + \pi D) \;= \frac{1}{a}\delta^{(4)}(q'_1 - q'_2)\prod_{\mu}\delta_{C_{1\mu}+_2 C_{2\mu}+_2 D_\mu,0} \tag{6.22}$$

6.2.4 Renormalization of fermion bilinear operators

The renormalization functions Z_Γ for lattice fermion bilinear operators, relate the bare operators $\mathcal{O}_{\Gamma_0} = \bar{\psi}\Gamma\psi$ to their corresponding renormalized continuum operators $\mathcal{O}_\Gamma$ via:

$$\mathcal{O}_\Gamma \;= Z_\Gamma\,\mathcal{O}_{\Gamma_0} \tag{6.23}$$

Renormalization functions of such lattice operators are necessary ingredients in the prediction of physical probability amplitudes from lattice matrix elements. In order to calculate the renormalization functions Z_Γ, it is essential to compute the 2-point amputated Green's functions of the operators $\mathcal{O}_{\Gamma_0}$; they can be written in the following form:

$$\Sigma_{\rm S}(aq) \;=\; \mathbb{1}\;\Sigma^{(1)}_{\rm S}(aq) \tag{6.24}$$

$$\Sigma_{\rm P}(aq) \;=\; \gamma_5\;\Sigma^{(1)}_{\rm P}(aq) \tag{6.25}$$

$$\Sigma_{\rm V}(aq) \;=\; \gamma_\mu\;\Sigma^{(1)}_{\rm V}(aq) + \frac{q^\mu \not{q}}{q^2}\;\Sigma^{(2)}_{\rm V}(aq) \tag{6.26}$$

$$\Sigma_{\rm A}(aq) \;=\; \gamma_5\;\gamma_\mu\;\Sigma^{(1)}_{\rm A}(aq) + \gamma_5\;\frac{q^\mu \not{q}}{q^2}\;\Sigma^{(2)}_{\rm AA}(aq) \tag{6.27}$$

$$\Sigma_{\rm TT}(aq) \;=\; \gamma_5\;\sigma_{\mu\nu}\;\Sigma^{(1)}_{\rm T}(aq) + \gamma_5\;\frac{\not{q}}{q^2}(\gamma_\mu q_\nu - \gamma_\nu q_\mu)\;\Sigma^{(2)}_{\rm T}(aq) \tag{6.28}$$

where $\Sigma^{(1)}_\Gamma = 1 + \mathcal{O}(g_0^2)$, $\Sigma^{(2)}_\Gamma = \mathcal{O}(g_0^2)$, g_0: bare coupling constant.

The RI' renormalization scheme is defined by imposing renormalization conditions on matrix elements at a scale $\bar{\mu}$. The renormalization condition giving $Z^{L,RI'}_\Gamma$ (L: Lattice) is:

$$\lim_{a\,\to 0}\left[Z^{L,RI'}_\psi\;Z^{L,RI'}_\Gamma\;\Sigma^{(1)}_\Gamma(aq)\right]_{\substack{q^2=\bar{\mu}^2,\\ m=0}} = 1 \tag{6.29}$$

where Z_ψ is the renormalization function for the fermion field ($\psi = Z_\psi^{-1/2}\;\psi_0$, $\psi(\psi_0)$: renormalized (bare) fermion field). Such a condition guarantees that the renormalized Green's function of $\mathcal{O}_\Gamma$ (the quantity in brackets in Eq. 6.29) will be a finite function of the renormalized coupling constant g for all values of the momenta ($g = \mu^{-\epsilon}Z_g^{-1}g_0$

where μ is the mass scale introduced to ensure that g_0 has the correct dimensionality in $D = 4-2\varepsilon$ dimensions). Comparison between the RI' and the $\overline{\rm MS}$ schemes is normally performed at the same scale $\bar{\mu} = \mu(4\pi/e^{\gamma_E})^{1/2}$.

The RI' renormalization prescription, as given above, does not involve $\Sigma_\Gamma^{(2)}$; nevertheless, renormalizability of the theory implies that $Z_\Gamma^{L,RI'}$ will render the entire Green's function finite. An alternative prescription, more appropriate for nonperturbative renormalization, is:

$$\lim_{a\to 0}\left[Z_\psi^{L,RI'} Z_\Gamma^{L,RI'(\rm alter)}\ \frac{{\rm tr}(\Gamma\Sigma_\Gamma(aq))}{{\rm tr}(\Gamma\Gamma)}\right]_{\substack{q^2=\bar{\mu}^2,\\ m=0}} = 1 \tag{6.30}$$

where a summation over repeated indices μ and ν is understood. This scheme has the advantage of taking into account the whole bare Green's function and therefore is useful for numerical simulations where the arithmetic data for Σ_Γ cannot be separated into two different structures. The two prescriptions differ between themselves (for V, A, T) by a finite amount which can be deduced from lower loop calculations combined with continuum results.

Conversion of renormalization functions from RI' to the $\overline{\rm MS}$ scheme is facilitated by the fact that renormalized Green's functions are regularization independent; thus the finite conversion factors:

$$C_\Gamma(g,\alpha)\ \equiv \frac{Z_\Gamma^{L,RI'}}{Z_\Gamma^{L,\overline{\rm MS}}} = \frac{Z_\Gamma^{DR,RI'}}{Z_\Gamma^{DR,\overline{\rm MS}}} \tag{6.31}$$

(DR: Dimensional Regularization, α: gauge parameter) can be evaluated in DR, leading to $Z_\Gamma^{L,\overline{\rm MS}} = Z_\Gamma^{L,RI'}/C_\Gamma(g,\alpha)$. For the Pseudoscalar and Axial Vector operators, in order to satisfy Ward identities, additional finite factors $Z_5^{\rm P}(g)$ and $Z_5^{\rm A}(g)$, calculable in DR, are required:

$$Z_{\rm P}^{L,\overline{\rm MS}} = \frac{Z_{\rm P}^{L,RI'}}{C_{\rm S} Z_5^{\rm P}}, \qquad Z_{\rm A}^{L,\overline{\rm MS}} = \frac{Z_{\rm A}^{L,RI'}}{C_{\rm V} Z_5^{\rm A}}. \tag{6.32}$$

The inclusion of these factors in the definitions of Z_P and Z_A amount to a variant convention on the $\overline{\rm MS}$ scheme. These factors are gauge independent; we also note that the value of Z_5^A for the flavor singlet operator differs from that of the nonsinglet one.

The values of Z_5^P, $Z_5^{A(\text{singlet})}$ and $Z_5^{A(\text{nonsinglet})}$, calculated in Ref. [182], are:

$$Z_5^P(g) = 1 - \frac{g^2}{(4\pi)^2}(8C_F) + \frac{g^4}{(4\pi)^4}\Big(\frac{2}{9}C_F N_c + \frac{4}{9}C_F N_f\Big) + \mathcal{O}(g^6) \tag{6.33}$$

$$Z_5^{A(\text{singlet})}(g) = 1 - \frac{g^2}{(4\pi)^2}(4C_F) + \frac{g^4}{(4\pi)^4}\Big(22C_F^2 - \frac{107}{9}C_F N_c + \frac{31}{18}C_F N_f\Big) + \mathcal{O}(g^6) \tag{6.34}$$

$$Z_5^{A(\text{nonsinglet})}(g) = 1 - \frac{g^2}{(4\pi)^2}(4C_F) + \frac{g^4}{(4\pi)^4}\Big(22C_F^2 - \frac{107}{9}C_F N_c + \frac{2}{9}C_F N_f\Big) + \mathcal{O}(g^6) \tag{6.35}$$

where $C_F \equiv (N_c^2-1)/(2N_c)$ and N_f is the number of flavors.

We list below all relevant conversion factors relating the *RI′*, *RI′-alternative* and $\overline{\text{MS}}$ schemes. Given that the conversion factors are regularization independent, the renormalization functions Z_Γ appearing below may be evaluated in any regularization scheme.

Conversion factors between *RI′* and $\overline{\text{MS}}$ schemes

$$C_\Gamma^{\overline{\text{MS}},RI'} \equiv C_\Gamma \equiv \frac{Z_\Gamma^{RI'}}{Z_\Gamma^{\overline{\text{MS}}}} \tag{6.36}$$

$$\begin{aligned} C_{S(singlet)}^{\overline{\text{MS}},RI'} &= 1 + \frac{g_{RI'}^2}{(4\pi)^2}\, C_F\, (\alpha_{\overline{\text{MS}}} + 4) \\ &+ \frac{g_{RI'}^4}{24(4\pi)^4} C_F \Big[\Big(24\, \alpha_{\overline{\text{MS}}}^2 + 96\, \alpha_{\overline{\text{MS}}} - 288\, \zeta(3) + 57\Big)\, C_F + 166\, N_f \\ &\qquad - \Big(18\, \alpha_{\overline{\text{MS}}}^2 + 84\, \alpha_{\overline{\text{MS}}} - 432\, \zeta(3) + 1285\Big)\, N_c\Big] \\ &+ \mathcal{O}(g_{RI'}^6) \end{aligned} \tag{6.37}$$

$$\begin{aligned} C_{P(singlet)}^{\overline{\text{MS}},RI'} &= 1 + \frac{g_{RI'}^2}{(4\pi)^2}\, C_F\, (\alpha_{\overline{\text{MS}}} - 4) \\ &+ \frac{g_{RI'}^4}{24(4\pi)^4} C_F \Big[\Big(24\, \alpha_{\overline{\text{MS}}}^2 - 96\, \alpha_{\overline{\text{MS}}} - 288\, \zeta(3) - 711\Big)\, C_F + \frac{530}{3}\, N_f \\ &\qquad - \Big(18\, \alpha_{\overline{\text{MS}}}^2 + 84\, \alpha_{\overline{\text{MS}}} - 432\, \zeta(3) + \frac{3839}{3}\Big)\, N_c\Big] \\ &+ \mathcal{O}(g_{RI'}^6) \end{aligned} \tag{6.38}$$

$$C_{V(singlet)}^{\overline{\text{MS}},RI'} = 1 + \mathcal{O}(g_{RI'}^8) \tag{6.39}$$

$$C_{A(singlet)}^{\overline{\text{MS}},RI'} = 1 - \frac{g_{RI'}^2}{(4\pi)^2}(4C_F) + \frac{g_{RI'}^4}{(4\pi)^4}\Big(22C_F^2 - \frac{107}{9}C_F N_c + \frac{31}{18}C_F N_f\Big) + \mathcal{O}(g_{RI'}^6) \tag{6.40}$$

$$
\begin{aligned}
C^{\overline{\rm MS},RI'}_{T(singlet)} &= 1 \;+\; \frac{g^2_{RI'}}{(4\pi)^2}\, C_F\, \alpha_{\overline{\rm MS}} \\
&+\; \frac{g^4_{RI'}}{216(4\pi)^4}\, C_F \Big[\Big(216\, \alpha^2_{\overline{\rm MS}} + 4320\, \zeta(3) - 4815\Big)\, C_F + 626\, N_f \\
&\qquad + \Big(162\, \alpha^2_{\overline{\rm MS}} + 756\, \alpha_{\overline{\rm MS}} - 3024\, \zeta(3) + 5987\Big)\, N_c\Big] \\
&+\; \mathcal{O}(g^6_{RI'}) \qquad (6.41)\\
C^{\overline{\rm MS},RI'}_{\Gamma(nonsinglet)} &= C^{\overline{\rm MS},RI'}_{\Gamma(singlet)}, \quad \Gamma \neq A_\mu \qquad (6.42)\\
C^{\overline{\rm MS},RI'}_{A(nonsinglet)} &= 1 \;-\; \frac{g^2_{RI'}}{(4\pi)^2}(4C_F) + \frac{g^4_{RI'}}{(4\pi)^4}\Big(22C_F^2 - \frac{107}{9}C_F N_c + \frac{2}{9}C_F N_f\Big) + \mathcal{O}(g^6_{RI'}) \qquad (6.43)
\end{aligned}
$$

where $\zeta(x)$ is the Riemann's zeta function. The conversion of gauge parameter α between the two schemes is given by:

$$\alpha_{RI'} = \frac{\alpha_{\overline{\rm MS}}}{C^{\overline{\rm MS},RI'}_{A_\mu}} \qquad (6.44)$$

where the conversion factor $C^{\overline{\rm MS},RI'}_{A_\mu}$ for the gluon field A_μ is given by [1]:

$$C^{\overline{\rm MS},RI'}_{A_\mu} \equiv \frac{Z^{RI'}_{A_\mu}}{Z^{\overline{\rm MS}}_{A_\mu}} = 1 + \frac{g^2_{RI'}}{36(4\pi)^2}\Big[\Big(9\, \alpha^2_{\overline{\rm MS}} + 18\, \alpha_{\overline{\rm MS}} + 97\Big)\, N_c - 40\, N_f\Big] + \mathcal{O}(g^4_{RI'}) \qquad (6.45)$$

Conversion factors between RI' and $RI'alternative$ schemes

$$C^{RI',RI'alter}_{\Gamma} \equiv \frac{Z^{RI'alter}_{\Gamma}}{Z^{RI'}_{\Gamma}} \qquad (6.46)$$

$$
\begin{aligned}
C^{RI',RI'alter}_{S(singlet)} &= C^{RI',RI'alter}_{S(nonsinglet)} = C^{RI',RI'alter}_{P(singlet)} = C^{RI',RI'alter}_{P(nonsinglet)} = 1 \qquad (6.47)\\
C^{RI',RI'alter}_{V(singlet)} &= C^{RI',RI'alter}_{V(nonsinglet)} = C^{RI',RI'alter}_{A(nonsinglet)} = \\
&\quad 1 - \frac{g^4_{RI'}}{(4\pi)^4}\, C_F\, \Big(\frac{3}{4}C_F - \frac{251}{36}N_c + \frac{19}{18}N_f\Big) + \mathcal{O}(g^6_{RI'}) \qquad (6.48)\\
C^{RI',RI'alter}_{A(singlet)} &= 1 - \frac{g^4_{RI'}}{(4\pi)^4}\, C_F\, \Big(\frac{3}{4}C_F - \frac{251}{36}N_c + \frac{1}{18}N_f\Big) + \mathcal{O}(g^6_{RI'}) \qquad (6.49)\\
C^{RI',RI'alter}_{T(singlet)} &= C^{RI',RI'alter}_{T(nonsinglet)} = 1 + \mathcal{O}(g^6_{RI'}) \qquad (6.50)
\end{aligned}
$$

[1] Not to be confused with the conversion factor $C^{\overline{\rm MS},RI'}_{A}$ for the axial vector operator!

Conversion factors between *RI′alternative* and $\overline{\text{MS}}$ schemes

$$C_{\Gamma}^{\overline{\text{MS}},RI'alter} \equiv \frac{Z_{\Gamma}^{RI'alter}}{Z_{\Gamma}^{\overline{\text{MS}}}} \tag{6.51}$$

$$C_{\Gamma(singlet/nonsinglet)}^{\overline{\text{MS}},RI'alter} = C_{\Gamma(singlet/nonsinglet)}^{\overline{\text{MS}},RI'} \; C_{\Gamma(singlet/nonsinglet)}^{RI',RI'alter} \tag{6.52}$$

6.3 Computation and Results

In the previous section, the calculation setup was presented in rather general terms. Here we focus on the two-loop difference between flavor singlet and nonsinglet operator renormalization. Given that this difference first arises at two loops, we only need the tree-level values of Z_ψ, Z_g and of the conversion factors C_Γ, Z_5^P ($Z_\psi = Z_g = C_\Gamma = Z_5^P = 1$). Since $C_\Gamma = 1$, the difference up to two loops will not depend on the renormalization scheme for all operators Γ, except for the axial vector case. There are two factors contributing to this scheme dependence: On one hand, the conversion factor Z_5^A between RI' and $\overline{\text{MS}}$ differs for the singlet and nonsinglet operators (see Eqs. 6.32, 6.34, 6.35); on the other hand, non-identical contributions of the form $\gamma_5 q_\mu \not{q}/q^2$ in the Green's functions for the singlet and nonsinglet axial vector operators lead to a nontrivial conversion between the RI' and *RI′-alternative* schemes, as shown in Eq. (6.54). In addition, for our computations we will use mass-independent renormalization schemes; this means that the renormalized mass of quarks will be taken to be zero.

6.3.1 Results on the two-loop difference between flavor singlet and nonsinglet operator renormalization

In this subsection, we present the computational procedure and results on the two-loop difference between flavor singlet and nonsinglet operator renormalization using the staggered formulation of the fermion action (Eq. 6.1). There are 10 two-loop Feynman diagrams contributing to this difference in the evaluation of the Green's functions (Eqs. 6.24 - 6.28), shown in Fig. 6.1. They all contain an operator insertion inside a closed fermion loop, and therefore vanish in the flavor nonsinglet case. Note that only diagrams 6 and 7 appear in the continuum. Furthermore, diagrams 3, 4, 8, 9 and 10 appear only in the staggered formulation (and not in Wilson-like fermion actions), due

to the presence of some new vertices with gluon lines stemming from the definition of bilinear operators (from the product $U_{C,D}$ in Eq. 6.8). These diagrams involve operator vertices (the cross in the diagram) with up to two gluons. For $\mathcal{O}_{\rm S}$ only diagrams 1, 2, 5, 6 and 7 contribute, since $U_{C,D} = \mathbb{1}$. In order to simplify our calculations of Z_Γ, we worked with $\sum_y \mathcal{O}_\Gamma(y)$ so that no momentum enters the diagrams at the operator insertion point.

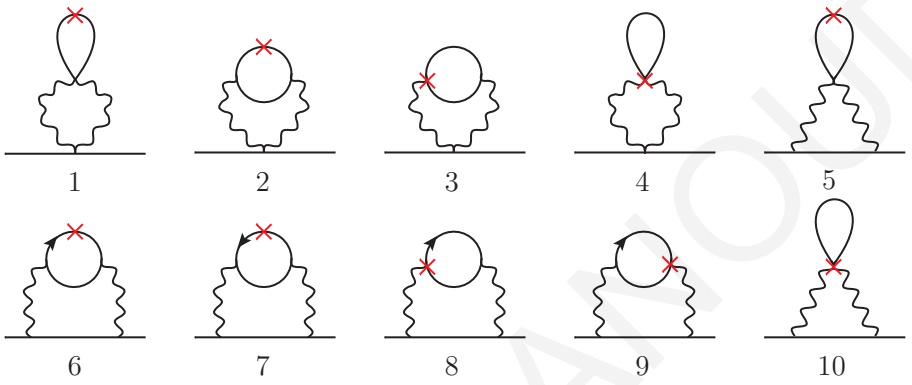

FIGURE 6.1: Diagrams (in staggered formulation) contributing to the difference between flavor singlet and nonsinglet values of Z_Γ. Solid (wavy) lines represent fermions (gluons). A cross denotes insertion of the operator $\mathcal{O}_\Gamma$.

The evaluation of the above diagrams using the improved staggered action is more complicated than the evaluation of the corresponding diagrams in Wilson-like actions (Wilson gluons and clover fermions: [49, 50], SLiNC: [203]). One reason for this is the appearance of divergences in nontrivial corners of the Brillouin zone. Also, the presence of operator vertices with gluon lines, besides increasing the number of diagrams, gives terms with unusual offsets in momentum conservation delta functions (e.g., $\delta^{(4)}_{2\pi}(p_1 + p_2 + \pi\hat{\mu})$); it turns out that these terms vanish in the final expression of each diagram. In addition, the two (rather than one) smearing steps of gluon links in the fermion action, as well as in the operators, lead to extremely lengthy vertices; the lengthiest cases which appeared in our computation are the operator vertices with two gluons ($\sim$ 800000 terms for the Axial Vector). Since these vertices appear only with their fermion lines contracted among themselves (diagrams: 4 and 10), we do not need to compute them as individual objects; we have used this fact in order to simplify the expression for diagrams 4 and 10. Also, the gluon propagator must now be inverted numerically for every choice of values for the Symanzik coefficients and for each value of the loop momentum 4-vector; an inversion in closed form exists, but it is not efficient. Comparing to our previous evaluation of these diagrams with Wilson gluons and clover

fermions [49, 50] and with SLiNC action [203], we will find neither any new superficial divergences ($\ln^2(a^2\bar{\mu}^2)$ terms) nor any new subdivergences ($\ln(a^2\bar{\mu}^2)$ terms).

Another important issue for the above diagrams is exploiting the underlying symmetries. For example in the Wilson-like actions, the denominator of the fermion propagator satisfies the symmetry $p_\mu \rightarrow -p_\mu, \forall\mu$; in the staggered case there is another symmetry: $p_\mu \rightarrow p_\mu + \pi\hat{\nu}$, where μ, ν can be in the same or in different directions. This is a consequence of the semi-periodicity of the function $\sin^2(p_\mu)$, which appears in the denominator of the staggered propagator (rather than $\sin^2(p_\mu/2)$). These symmetries help us to reduce the number of terms in the diagrams, eliminating odd integrands.

The contribution of the diagrams in Fig. 6.1 to $Z_{\rm S}$, $Z_{\rm P}$, $Z_{\rm V}$, $Z_{\rm T}$ vanishes identically just as in continuum regularizations. The closed fermion loop of the diagrams which contribute to $Z_{\rm S}$, $Z_{\rm P}$, $Z_{\rm T}$, gives an odd number of exponentials of the inner momentum; this leads to odd integrands, which equal zero, due to the symmetry of the staggered propagator mentioned above. So, for the cases of $Z_{\rm S}$, $Z_{\rm P}$, $Z_{\rm T}$, the contribution vanishes diagram by diagram. Conversely, for the case of $Z_{\rm V}$, each diagram vanishes when we add its symmetric diagram (diagrams 6+7, 8+9). Therefore, only $Z_{\rm A}$ is affected. In particular, only diagrams 6 - 9 contribute to $Z_{\rm A}$; the remaining diagrams vanish. Then, for the Axial Vector operator, our result can be written in the following form:

$$
\begin{aligned}
&Z_{\rm A}^{\rm RI'(singlet)}(a\bar{\mu}) - Z_{\rm A}^{\rm RI'(nonsinglet)}(a\bar{\mu}) \;=\\
&- \frac{g_0^4}{(4\pi)^4}\, C_F\, N_f \Big\{ \mathbf{6\ ln(a^2\bar{\mu}^2)} + \alpha_1 + \alpha_2\, (\omega_{A_1} + \omega_{A_2}) + \alpha_3\, (\omega_{A_1}^2 + \omega_{A_2}^2)\\
&+ \alpha_4\, \omega_{A_1}\, \omega_{A_2} + \alpha_5\, (\omega_{A_1}^3 + \omega_{A_2}^3) + \alpha_6\, \omega_{A_1}\, \omega_{A_2}\, (\omega_{A_1} + \omega_{A_2}) + \alpha_7\, (\omega_{A_1}^4 + \omega_{A_2}^4)\\
&+ \alpha_8\, \omega_{A_1}^2\, \omega_{A_2}^2 + \alpha_9\, \omega_{A_1}\, \omega_{A_2}\, (\omega_{A_1}^2 + \omega_{A_2}^2) + \alpha_{10}\, \omega_{A_1}^2\, \omega_{A_2}^2\, (\omega_{A_1} + \omega_{A_2})\\
&+ \alpha_{11}\, \omega_{A_1}\, \omega_{A_2}\, (\omega_{A_1}^3 + \omega_{A_2}^3) + \alpha_{12}\, \omega_{A_1}^3\, \omega_{A_2}^3 + \alpha_{13}\, \omega_{A_1}^2\, \omega_{A_2}^2\, (\omega_{A_1}^2 + \omega_{A_2}^2)\\
&+ \alpha_{14}\, \omega_{A_1}^3\, \omega_{A_2}^3\, (\omega_{A_1} + \omega_{A_2}) + \alpha_{15}\, \omega_{A_1}^4\, \omega_{A_2}^4 + \alpha_{16}\, (\omega_{O_1} + \omega_{O_2}) + \alpha_{17}\, \omega_{O_1}\, \omega_{O_2}\\
&+ \alpha_{18}\, (\omega_{A_1} + \omega_{A_2})\, (\omega_{O_1} + \omega_{O_2}) + \alpha_{19}\, \omega_{A_1}\, \omega_{A_2}\, (\omega_{O_1} + \omega_{O_2})\\
&+ \alpha_{20}\, \Big[(\omega_{A_1}^2 + \omega_{A_2}^2)\, (\omega_{O_1} + \omega_{O_2}) + (\omega_{A_1} + \omega_{A_2})\, \omega_{O_1}\, \omega_{O_2}\Big]\\
&+ \alpha_{21}\, (\omega_{A_1}^2 + \omega_{A_2}^2)\, \omega_{O_1}\, \omega_{O_2} + \alpha_{22}\, (\omega_{A_1}^3 + \omega_{A_2}^3)\, (\omega_{O_1} + \omega_{O_2})\\
&+ \alpha_{23}\, \omega_{A_1}\, \omega_{A_2}\, \Big[(\omega_{A_1} + \omega_{A_2})\, (\omega_{O_1} + \omega_{O_2}) + \omega_{O_1}\, \omega_{O_2}\Big]\\
&+ \alpha_{24}\, (\omega_{A_1}^3 + \omega_{A_2}^3)\, \omega_{O_1}\, \omega_{O_2} + \alpha_{25}\, \omega_{A_1}\, \omega_{A_2}\, (\omega_{A_1}^2 + \omega_{A_2}^2)\, (\omega_{O_1} + \omega_{O_2})\\
&+ \alpha_{26}\, \omega_{A_1}\, \omega_{A_2}\, \Big[\omega_{A_1}\, \omega_{A_2}\, (\omega_{O_1} + \omega_{O_2}) + (\omega_{A_1} + \omega_{A_2})\omega_{O_1}\, \omega_{O_2}\Big]\\
&+ \alpha_{27}\, \omega_{A_1}^2\, \omega_{A_2}^2\, \omega_{O_1}\, \omega_{O_2}\\
&+ \alpha_{28}\, \omega_{A_1}\, \omega_{A_2}\, \Big[\omega_{A_1}\, \omega_{A_2}\, (\omega_{A_1} + \omega_{A_2})\, (\omega_{O_1} + \omega_{O_2}) + (\omega_{A_1}^2 + \omega_{A_2}^2)\, \omega_{O_1}\, \omega_{O_2}\Big]\\
&+ \alpha_{29}\, \omega_{A_1}^3\, \omega_{A_2}^3\, (\omega_{O_1} + \omega_{O_2}) + \alpha_{30}\, \omega_{A_1}^2\, \omega_{A_2}^2\, (\omega_{A_1} + \omega_{A_2})\, \omega_{O_1}\, \omega_{O_2}\\
&+ \alpha_{31}\, \omega_{A_1}^3\, \omega_{A_2}^3\, \omega_{O_1}\, \omega_{O_2} \Big\} + \mathcal{O}(g_0^6)
\end{aligned}
\tag{6.53}
$$

The numerical constants α_i have been computed for various sets of values of the Symanzik coefficients; their values are listed in Table 6.1 for the Wilson, Tree-level Symanzik and Iwasaki gluon actions. The errors quoted stem from extrapolation of the results of numerical integration over loop momenta for different lattice sizes. The extrapolation methods that we used are described in Ref. [208]. The computation was performed in a general covariant gauge, confirming that the result is gauge independent, as it should be in $\overline{\rm MS}$. The computation with staggered fermions gives rise to some nontrivial divergent integrals, which cannot be present in the Wilson formulation due to the different pole structure of the fermion propagator. In the following subsection, we provide a brief description of the manipulations performed to evaluate such divergent terms. We note that the result for the Axial Vector operator, as we expected, has a scale dependence; it has the same divergent behaviour just as in the Wilson case and in the continuum, i.e. $6\ln(a^2\bar{\mu}^2)$. This is related to the axial

	Wilson	TL Symanzik	Iwasaki
α_1	17.420(1)	16.000(1)	14.610(1)
α_2	-116.049(7)	-81.342(5)	-41.583(2)
α_3	839.788(9)	539.121(6)	230.050(1)
α_4	2175.14(3)	1394.12(2)	591.88(1)
α_5	-3462.830(1)	-2098.136(5)	-801.633(3)
α_6	-19565.9(1)	-11858.6(1)	-4528.6(1)
α_7	6424.33(2)	3740.18(1)	1337.93(1)
α_8	200966.5(4)	117179.7(4)	41977.1(1)
α_9	92171.5(3)	53720.8(1)	19237.6(1)
α_{10}	-1026448(1)	-580271(2)	-198722(1)
α_{11}	-183998.3(3)	-103929.7(3)	-35561.1(1)
α_{12}	5517230(30)	3037110(10)	1003641(1)
α_{13}	2145810(10)	1180684(4)	389979(1)
α_{14}	-11889300(40)	-6386950(30)	-2046240(10)
α_{15}	26137700(200)	13729010(10)	4278680(10)
α_{16}	24.9873(2)	18.0489(4)	9.9571(2)
α_{17}	-97.4550(2)	-62.2675(1)	-26.5359(1)
α_{18}	-292.3650(5)	-186.8025(4)	-79.6078(2)
α_{19}	4864.513(9)	2921.876(6)	1107.333(2)
α_{20}	1621.504(3)	973.959(2)	369.111(1)
α_{21}	-10617.81(2)	-6122.11(1)	-2169.30(1)
α_{22}	-3539.269(6)	-2040.705(4)	-723.099(1)
α_{23}	-31853.42(5)	-18366.34(3)	-6507.89(1)
α_{24}	25847.14(3)	14435.59(2)	4881.52(1)
α_{25}	77541.41(1)	43306.78(6)	14644.54(2)
α_{26}	232624.2(3)	129920.3(2)	43933.6(1)
α_{27}	-1844375(1)	-1002465(1)	-326727(1)
α_{28}	-614791.6(6)	-334155.0(4)	-108909.0(2)
α_{29}	1736048.1(8)	920956.7(7)	290916.1(3)
α_{30}	5208144(2)	2762870(2)	872748(1)
α_{31}	-15545543(1)	-8065557(2)	-2478207(1)

TABLE 6.1: Numerical coefficients for the Axial Vector operator using staggered fermions.

anomaly. As was expected, this logarithmic divergence originates in diagrams 6 and 7, which are the only ones present in the continuum.

Finally, the presence of a term of the form $\gamma_5\ q_\mu\ \not{q}/q^2$ in the Green's function of the Axial Vector operator (Eq. 6.27) implies that, in the alternative RI' scheme mentioned

in Sec. 6.2.4, the above result is modified by a finite term, as below:

$$\begin{aligned} &Z_{\rm A}^{{\rm RI}'{\rm alter(singlet)}}(a\bar{\mu}) - Z_{\rm A}^{{\rm RI}'{\rm alter(nonsinglet)}}(a\bar{\mu}) \;= \\ &Z_{\rm A}^{{\rm RI}'{\rm (singlet)}}(a\bar{\mu}) - Z_{\rm A}^{{\rm RI}'{\rm (nonsinglet)}}(a\bar{\mu}) + \frac{g_0^4}{(4\pi)^4}\; C_F\; N_f + \mathcal{O}(g_0^6) \end{aligned} \tag{6.54}$$

Furthermore, according to the conversion relations between RI' and $\overline{\rm MS}$ schemes (6.40 - 6.43), in the $\overline{\rm MS}$ scheme we must also add a finite term, as below:

$$\begin{aligned} &Z_A^{\overline{\rm MS}(singlet)} - Z_A^{\overline{\rm MS}(nonsinglet)} \;= \\ &Z_A^{RI'(singlet)} - Z_A^{RI'(nonsinglet)} + \frac{g_0^4}{(4\pi)^4}(-\frac{3}{2}C_F N_f) + \mathcal{O}(g_0^6) \end{aligned} \tag{6.55}$$

6.3.2 Evaluation of a basis of nontrivial divergent two-loop Feynman diagrams in the staggered formalism

In this subsection we present the procedure that we used to evaluate nontrivial divergent integrals which appeared in our two-loop computation using staggered fermions. In the Wilson-like actions, the two-loop divergent integrals can be expressed in terms of a basis of standard integrals found in Ref. [39], along with manipulations found in Ref. [50]. However, in the staggered case, the divergent integrals are not related to those standard integrals in an obvious way. Some further steps are needed to this end.

In our computation, there appeared 4 types of nontrivial divergent 2-loop integrals, using staggered fermions; they are listed below:

$$I_{1\mu\nu} = \int_{-\pi}^{\pi}\frac{d^4k}{(2\pi)^4}\frac{\mathring{k}_\mu\,\mathring{k}_\nu}{(\widehat{k}^2)^2\;(\widehat{k+aq})^2}\int_{-\pi}^{\pi}\frac{d^4p}{(2\pi)^4}\frac{1}{\mathring{p}^2\;(\mathring{p+k})^2} \tag{6.56}$$

$$I_{2\mu\nu} = \int_{-\pi}^{\pi}\frac{d^4k}{(2\pi)^4}\frac{\mathring{k}_\mu\;\sin(aq_\nu)}{(\widehat{k}^2)^2\;(\widehat{k+aq})^2}\int_{-\pi}^{\pi}\frac{d^4p}{(2\pi)^4}\frac{1}{\mathring{p}^2\;(\mathring{p+k})^2} \tag{6.57}$$

$$I_{3\mu\nu\rho\sigma} = \int_{-\pi}^{\pi}\frac{d^4k}{(2\pi)^4}\frac{\mathring{k}_\mu\,\mathring{k}_\nu}{(\widehat{k}^2)^2\;(\widehat{k+aq})^2}\int_{-\pi}^{\pi}\frac{d^4p}{(2\pi)^4}\frac{\sin(2p_\rho)\;\sin(2p_\sigma)}{(\mathring{p}^2)^2\;(\mathring{p+k})^2} \tag{6.58}$$

$$I_{4\mu\nu\rho\sigma} = \int_{-\pi}^{\pi}\frac{d^4k}{(2\pi)^4}\frac{\mathring{k}_\mu\;\sin(aq_\nu)}{(\widehat{k}^2)^2\;(\widehat{k+aq})^2}\int_{-\pi}^{\pi}\frac{d^4p}{(2\pi)^4}\frac{\sin(2p_\rho)\;\sin(2p_\sigma)}{(\mathring{p}^2)^2\;(\mathring{p+k})^2} \tag{6.59}$$

where $\widehat{p}^2 = \sum_\mu \widehat{p}_\mu^2$, $\widehat{p}_\mu = 2\sin(p_\mu/2)$, $\overset{\circ}{p}^2 = \sum_\mu \overset{\circ}{p}_\mu^2$, $\overset{\circ}{p}_\mu = \sin(p_\mu)$ and q is an external momentum. The crucial point is the presence of expressions like $\overset{\circ}{p}^2$ or $(\overset{\circ}{p+k})^2$ rather than $\widehat{p}^2$ or $\widehat{(p+k)}^2$ in the denominators of the above integrals. This behaviour comes from the tree-level staggered fermion propagator. Also, the other crucial point is the fact that we cannot manipulate these integrals via subtractions of the form:

$$\frac{1}{\overset{\circ}{p}^2} = \frac{1}{\widehat{p}^2} + \Big(\frac{1}{\overset{\circ}{p}^2} - \frac{1}{\widehat{p}^2}\Big) \tag{6.60}$$

in order to express them in terms of a standard tabulated integral plus additional terms which are more convergent; such a procedure is applicable, e.g., in the case of the Wilson fermion propagator $\Big[1/\Big(\overset{\circ}{p}^2 + r^2(\widehat{p}^2)^2/4\Big)\Big]$ or in other less divergent integrals with staggered fermion propagators. The reason for which such a subtraction cannot be applied is the existence of potential IR singularities at all corners of the Brillouin zone (not only at zero momentum), in the staggered fermion propagator. Therefore, such a subtraction will not alleviate the divergent behaviour at the remaining corners of the Brillouin zone.

For the above integrals we followed a different approach. At first, we perform the substitution $p_\mu \to p'_\mu + \pi\, C_\mu$, where $-\pi/2 < p'_\mu < \pi/2$ and $C_\mu \in \{0, 1\}$, which is the same substitution that we applied to external momenta. Now the integration region for the innermost integral breaks up into 16 regions with range $[-\pi/2, \pi/2]$; the contributions from these regions are identical. To restore the initial range $[-\pi, \pi]$, we apply the following change of variables: $p'_\mu \to p''_\mu = 2p'_\mu$. Then we obtain:

$$I_{1\mu\nu} = 16 \int_{-\pi}^{\pi} \frac{d^4k}{(2\pi)^4} \frac{\overset{\circ}{k}_\mu \overset{\circ}{k}_\nu}{(\widehat{k}^2)^2\ \widehat{(k+aq)}^2} \int_{-\pi}^{\pi} \frac{d^4p}{(2\pi)^4} \frac{1}{\widehat{p}^2\ \widehat{(p+2k)}^2} \tag{6.61}$$

$$I_{2\mu\nu} = 16 \int_{-\pi}^{\pi} \frac{d^4k}{(2\pi)^4} \frac{\overset{\circ}{k}_\mu\ \sin(aq_\nu)}{(\widehat{k}^2)^2\ \widehat{(k+aq)}^2} \int_{-\pi}^{\pi} \frac{d^4p}{(2\pi)^4} \frac{1}{\widehat{p}^2\ \widehat{(p+2k)}^2} \tag{6.62}$$

$$I_{3\mu\nu\rho\sigma} = 64 \int_{-\pi}^{\pi} \frac{d^4k}{(2\pi)^4} \frac{\overset{\circ}{k}_\mu \overset{\circ}{k}_\nu}{(\widehat{k}^2)^2\ \widehat{(k+aq)}^2} \int_{-\pi}^{\pi} \frac{d^4p}{(2\pi)^4} \frac{\overset{\circ}{p}_\rho \overset{\circ}{p}_\sigma}{(\widehat{p}^2)^2\ \widehat{(p+2k)}^2} \tag{6.63}$$

$$I_{4\mu\nu\rho\sigma} = 64 \int_{-\pi}^{\pi} \frac{d^4k}{(2\pi)^4} \frac{\overset{\circ}{k}_\mu\ \sin(aq_\nu)}{(\widehat{k}^2)^2\ \widehat{(k+aq)}^2} \int_{-\pi}^{\pi} \frac{d^4p}{(2\pi)^4} \frac{\overset{\circ}{p}_\rho \overset{\circ}{p}_\sigma}{(\widehat{p}^2)^2\ \widehat{(p+2k)}^2} \tag{6.64}$$

where we omit the double prime from p. The above integrals are similar to standard divergent integrals, computed in Ref. [39]. The only difference is the presence of a

factor of 2 in the denominators, i.e. $1/(\widehat{p+2k})^2$. This can be treated via subtraction methods. We define:

$$A(k) = \int_{-\pi}^{\pi} \frac{d^4p}{(2\pi)^4} \frac{1}{\widehat{p}^2\ (\widehat{p+k})^2} \tag{6.65}$$

$$A_{\rm as}(k) \equiv \frac{1}{(4\pi)^2}[-\ln(k^2)+2] + P_2 \tag{6.66}$$

$$B_{\rho\sigma}(k) = \int_{-\pi}^{\pi} \frac{d^4p}{(2\pi)^4} \frac{\mathring{p}_\rho\ \mathring{p}_\sigma}{(\widehat{p}^2)^2\ (\widehat{p+k})^2} \tag{6.67}$$

$$\widetilde{B}_{\rho\sigma}(2k) \equiv \frac{1}{2(4\pi)^2} \frac{\mathring{k}_\rho\ \mathring{k}_\sigma}{\widehat{k}^2} + \delta_{\rho\sigma}[\frac{1}{4}A(2k) - \frac{1}{32}P_1] \tag{6.68}$$

where the values of the numerical constants P_1 and P_2 are noted in Ref. [39]. $A_{\rm as}(k)$ and $\widetilde{B}_{\rho\sigma}(2k)$ are asymptotic values of $A(k)$ and $B_{\rho\sigma}(2k)$, respectively:

$$A(k) = A_{\rm as}(k) + \mathcal{O}(k^2), \qquad B_{\rho\sigma}(2k) = \widetilde{B}_{\rho\sigma}(2k) + \mathcal{O}(k^2) \tag{6.69}$$

The first two integrals $I_{1\mu\nu}$ and $I_{2\mu\nu}$ contain the quantity $A(2k)$ and the remaining two integrals $I_{3\mu\nu\rho\sigma}$ and $I_{4\mu\nu\rho\sigma}$ the quantity $B_{\rho\sigma}(2k)$. We apply the following subtractions:

$$A(2k) = A(k) + [A_{\rm as}(2k) - A_{\rm as}(k)] + [A(2k) - A(k) - A_{\rm as}(2k) + A_{\rm as}(k)] \tag{6.70}$$

$$B_{\rho\sigma}(2k) = \widetilde{B}_{\rho\sigma}(2k) + [B_{\rho\sigma}(2k) - \widetilde{B}_{\rho\sigma}(2k)] \tag{6.71}$$

Integrals $I_{1\mu\nu}$ and $I_{2\mu\nu}$ separate into 3 sub-integrals. The first sub-integral with the quantity $A(k)$ is already computed in Ref. [39] (for $I_{1\mu\nu}$) or can be converted into standard divergent integrals of Ref. [39] using integration by parts (for $I_{2\mu\nu}$). The second sub-integral with the quantity $[A_{\rm as}(2k) - A_{\rm as}(k)] = -\ln 4/(4\pi)^2$ is a one loop divergent integral computed in Ref. [39] or [209]. The third sub-integral with the quantity $[A(2k)-A(k)-A_{\rm as}(2k)+A_{\rm as}(k)] = \mathcal{O}(k^2)$ is convergent and so we can integrate it numerically for $a \to 0$ (In particular, it gives zero for $I_{2\mu\nu}$). Also, integrals $I_{3\mu\nu\rho\sigma}$ and $I_{4\mu\nu\rho\sigma}$ separate into 2 sub-integrals. The first sub-integral with the quantity $\widetilde{B}_{\rho\sigma}(2k)$ gives expressions which can be converted into standard integrals of Refs. [39, 209–211] or into the above $I_{1\mu\nu}$, $I_{2\mu\nu}$ integrals. The second sub-integral with the quantity $[B_{\rho\sigma}(2k) - \widetilde{B}_{\rho\sigma}(2k)] = \mathcal{O}(k^2)$ is convergent and so we can integrate it numerically for $a \to 0$ (In particular, it gives zero for $I_{4\mu\nu\rho\sigma}$). Therefore, according to the above

manipulations, the final expressions for the four integrals are given by:

$$\begin{aligned} I_{1\mu\nu} &= \Big\{\frac{2}{(2\pi)^4}\Big[-\ln(a^2q^2)+\frac{3}{2}-\ln 4\Big]+\frac{1}{2\pi^2}P_2\Big\}\frac{q_\mu q_\nu}{q^2} \\ &+ \delta_{\mu\nu}\Big\{\frac{2}{(4\pi)^4}\Big[\ln(a^2q^2)\Big]^2-\frac{1}{4\pi^2}\Big[P_2+\frac{1}{(4\pi)^2}\Big(\frac{5}{2}-\ln 4\Big)\Big]\ln(a^2q^2) \\ &\qquad -\frac{1}{4\pi^2}\Big[P_2+\frac{3}{2(4\pi)^2}\ln 4\Big]+4X_2+G_1\Big\} \\ &+ \mathcal{O}(a^2q^2) \end{aligned} \tag{6.72}$$

$$I_{2\mu\nu} = \Big\{\frac{1}{(2\pi)^4}\Big[\ln(a^2q^2)-2+\ln 4\Big]-\frac{1}{\pi^2}P_2\Big\}\frac{q_\mu q_\nu}{q^2}+\mathcal{O}(a^2q^2) \tag{6.73}$$

$$\begin{aligned} I_{3\mu\nu\rho\sigma} &= \frac{1}{3(2\pi)^4}\frac{q_\mu q_\nu q_\rho q_\sigma}{q^4}+\delta_{\rho\sigma}\Big\{\frac{2}{(2\pi)^4}\Big[-\ln(a^2q^2)+\frac{5}{3}-\ln 4\Big]-\frac{1}{(4\pi)^2}(P_1-8P_2)\Big\}\frac{q_\mu q_\nu}{q^2} \\ &+ \frac{1}{12(2\pi)^4}\Big\{\delta_{\mu\nu}\frac{q_\rho q_\sigma}{q^2}+\delta_{\mu\rho}\frac{q_\nu q_\sigma}{q^2}+\delta_{\mu\sigma}\frac{q_\nu q_\rho}{q^2}+\delta_{\nu\rho}\frac{q_\mu q_\sigma}{q^2}+\delta_{\nu\sigma}\frac{q_\mu q_\rho}{q^2}\Big\} \\ &+ \delta_{\mu\nu}\delta_{\rho\sigma}\Big\{\frac{2}{(4\pi)^4}\Big[\ln(a^2q^2)\Big]^2-\frac{1}{4\pi^2}\Big[P_2-\frac{1}{8}P_1+\frac{1}{(4\pi)^2}\Big(\frac{51}{2}-\ln 4\Big)\Big]\ln(a^2q^2) \\ &\qquad -\frac{1}{4\pi^2}\Big[\Big(\frac{1}{3}-\ln 4\Big)P_2-\frac{11}{144}P_1+\frac{3}{2(4\pi)^2}\Big(\frac{1}{27}-\ln 4\Big)\Big] \\ &\qquad -\frac{1}{2}P_1\ P_2+4X_2+G_1+G_3\Big\} \\ &+ (\delta_{\mu\rho}\delta_{\nu\sigma}+\delta_{\mu\sigma}\delta_{\nu\rho})\Big\{\frac{1}{(12\pi)^4}\Big[-\ln(a^2q^2)+\frac{1}{6}\Big]+\frac{1}{6\pi^2}(P_1+3P_2)+G_2\Big\} \\ &+ \delta_{\mu\nu\rho\sigma}\Big\{\frac{1}{(2\pi)^4}+\frac{1}{2(4\pi)^2}-\frac{1}{3\pi^2}P_1+G_4\Big\}+\mathcal{O}(a^2q^2) \end{aligned} \tag{6.74}$$

$$\begin{aligned} I_{4\mu\nu\rho\sigma} &= -\frac{1}{2(2\pi)^4}\frac{q_\mu q_\nu q_\rho q_\sigma}{q^4}-\frac{4}{(4\pi)^4}\Big\{\delta_{\mu\rho}\frac{q_\nu q_\sigma}{q^2}+\delta_{\mu\sigma}\frac{q_\nu q_\rho}{q^2}\Big\} \\ &+ \delta_{\rho\sigma}\Big\{\frac{1}{(2\pi)^4}\Big[\ln(a^2q^2)-\frac{9}{4}\Big]-\frac{1}{2(2\pi)^2}(P_1-8P_2)\Big\}\frac{q_\mu q_\nu}{q^2}+\mathcal{O}(a^2q^2) \end{aligned} \tag{6.75}$$

where P_1, P_2, X_2 are given in Ref. [39] and $G_1 - G_4$ are given below:

$$G_1 = 0.000803016(6) \tag{6.76}$$

$$G_2 = -0.0006855532(7) \tag{6.77}$$

$$G_3 = 0.00098640(7) \tag{6.78}$$

$$G_4 = 0.00150252(2) \tag{6.79}$$

6.4 Discussion

The numerical value of the difference between singlet and nonsinglet renormalization functions can be very significant, depending on the values of the parameters employed in the action. In order to assess the importance of this difference, we present here several graphs of the results for certain values of c_i, ω_{A_1}, ω_{A_2}, ω_{O_1} and ω_{O_2}.

Firstly, we note that the result (6.53) is symmetric under the exchange of ω_As as well as under the exchange of ω_Os. This fact is consistent with the requirement that the results for $(\omega_{O_1}=0, \omega_{O_2}=\omega)$ and $(\omega_{O_1}=\omega, \omega_{O_2}=0)$ should coincide, since they both correspond to a single smearing step; similarly for the coefficients ω_{A_1} and ω_{A_2}. These properties provide nontrivial consistency checks of our computation.

In Fig. 6.2 we present 2D graphs of our results by selecting the following parameter values:

1. $\omega_{A_1}=\omega_{A_2}=\omega_{O_1}=\omega_{O_2}=\omega$
2. $\omega_{A_1}=\omega_{A_2}=\omega$, $\omega_{O_1}=\omega_{O_2}=0$ (No smearing procedure in the links of operators)
3. $\omega_{A_1}=\omega$, $\omega_{A_2}=\omega_{O_1}=\omega_{O_2}=0$ (One smearing step only in the links of fermion action)
4. $\omega_{A_1}=\omega_{O_1}=\omega$, $\omega_{A_2}=\omega_{O_2}=0$ (One smearing step in the links of fermion action and operators).

The vertical axis of theses plots corresponds to $Z_A^{\text{diff.}} \equiv \left[Z_A^{(\text{singlet})}(a\bar{\mu}) - Z_A^{(\text{nonsinglet})}(a\bar{\mu})\right]\left(-\frac{g_o^4}{(4\pi)^4}N_f C_F\right)^{-1}$ for $\bar{\mu}=1/a$. We plot the results for gluon actions: Wilson, tree-level Symanzik, Iwasaki in the same graph. We notice that the plots for the Iwasaki action are flatter than for the remaining actions but the Wilson action has the smallest values of Z_A^{diff}.

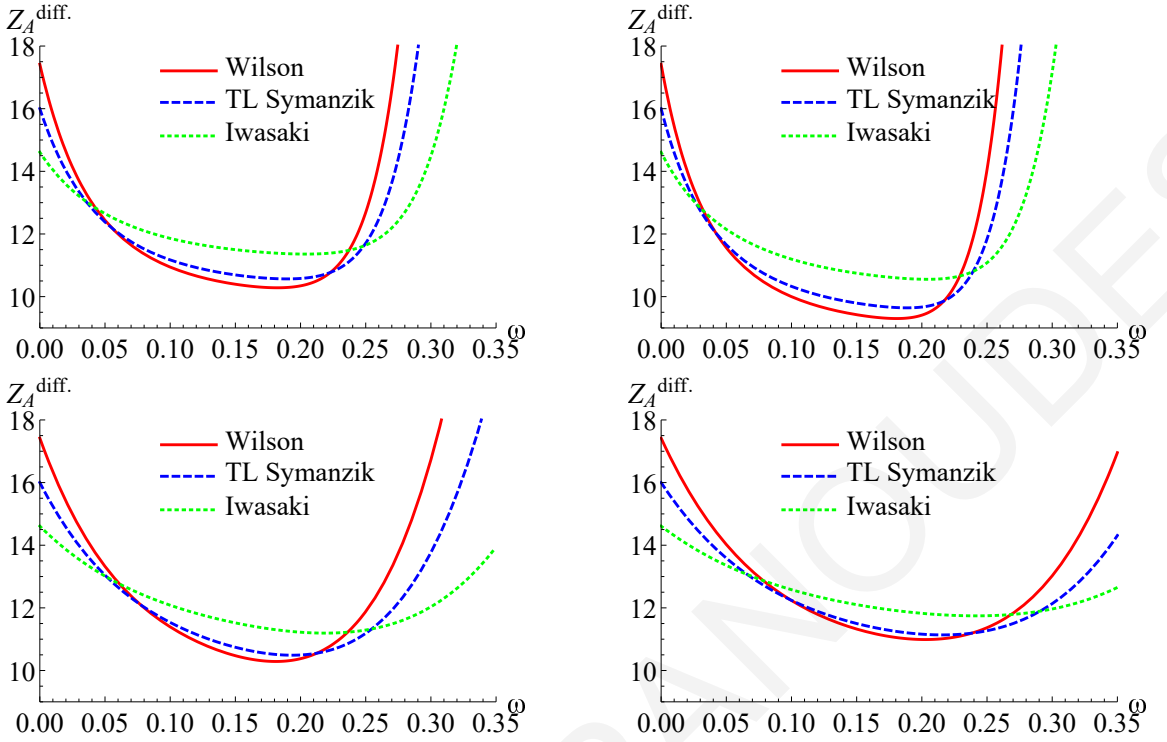

FIGURE 6.2: Plots of $Z_A^{\text{diff.}} \equiv \left[Z_A^{(\text{singlet})} - Z_A^{(\text{nonsinglet})}\right] \left(-\frac{g_o^4}{(4\pi)^4} N_f C_F\right)^{-1}$, as a function of ω for the parameter values: upper left: $\omega_{A_1} = \omega_{A_2} = \omega_{O_1} = \omega_{O_2} = \omega$, upper right: $\omega_{A_1} = \omega_{A_2} = \omega$, $\omega_{O_1} = \omega_{O_2} = 0$, lower left: $\omega_{A_1} = \omega$, $\omega_{A_2} = \omega_{O_1} = \omega_{O_2} = 0$, lower right: $\omega_{A_1} = \omega_{O_1} = \omega$, $\omega_{A_2} = \omega_{O_2} = 0$.

In Figs. (6.3 - 6.5) we present 3D graphs of our results by selecting the following parameter values:

Fig. 6.3: $\omega_{A_1}, \omega_{A_2}$: free parameters and $\omega_{O_1} = \omega_{O_2} = 0$ (No smearing procedure in the links of operators)

Fig. 6.4: $\omega_{A_1}, \omega_{O_1}$: free parameters and $\omega_{A_2} = \omega_{O_2} = 0$ (One smearing step in the links of fermion action and operators)

Fig. 6.5: $\omega_{A_1} = \omega_{A_2}$, $\omega_{O_1} = \omega_{O_2}$.

Just as in 2D graphs, the vertical axis of theses plots corresponds to $Z_A^{\text{diff.}}$ for $\bar{\mu} = 1/a$. We notice again that the plots for the Iwasaki action are flatter than the remaining actions. Also, from the first trio of graphs (Fig. 6.3), we notice that there is only one minimum, on the 45° axis. Therefore, the two smearing steps of the fermion action give better results than only one smearing step. Also, in Fig. 6.4, as well as in Fig. 6.5, we observe that the stout smearing of the action is more effective in minimizing $Z_A^{\text{diff.}}$ than the stout smearing of operators.

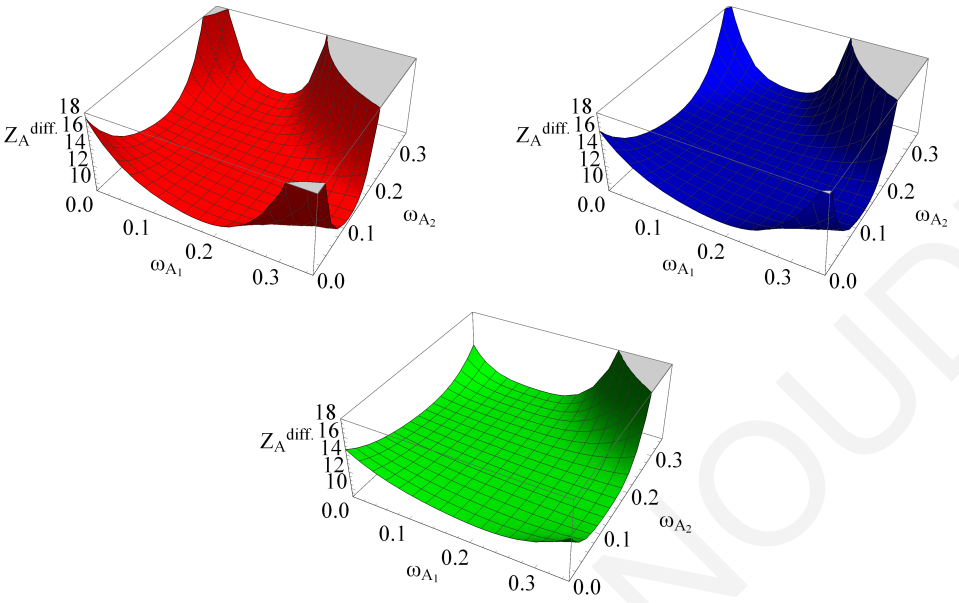

FIGURE 6.3: Plots of $Z_A^{\text{diff.}} \equiv \left[Z_A^{(\text{singlet})} - Z_A^{(\text{nonsinglet})}\right] \left(-\frac{g_o^4}{(4\pi)^4} N_f C_F\right)^{-1}$, as a function of ω_{A_1} and ω_{A_2} for $\omega_{O_1} = \omega_{O_2} = 0$ (upper left: Wilson action, upper right: TL Symanzik action, lower: Iwasaki action).

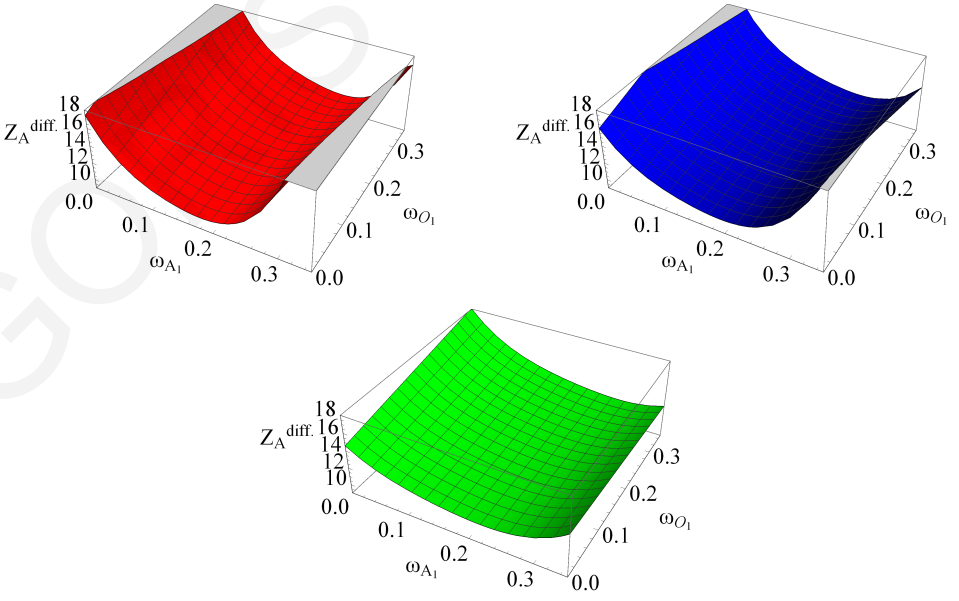

FIGURE 6.4: Plots of $Z_A^{\text{diff.}} \equiv \left[Z_A^{(\text{singlet})} - Z_A^{(\text{nonsinglet})}\right] \left(-\frac{g_o^4}{(4\pi)^4} N_f C_F\right)^{-1}$, as a function of ω_{A_1} and ω_{O_1} for $\omega_{A_2} = \omega_{O_2} = 0$ (upper left: Wilson action, upper right: TL Symanzik action, lower: Iwasaki action).

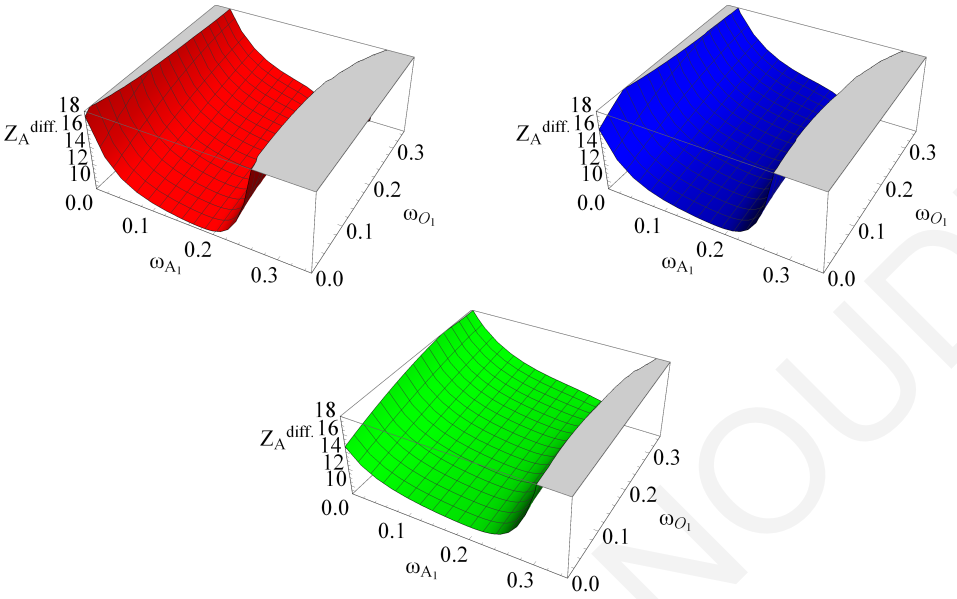

FIGURE 6.5: Plots of $Z_A^{\text{diff.}} \equiv \left[Z_A^{(\text{singlet})} - Z_A^{(\text{nonsinglet})}\right] \left(-\frac{g_o^4}{(4\pi)^4} N_f C_F\right)^{-1}$, as a function of ω_{A_1} and ω_{O_1} for $\omega_{A_2} = \omega_{A_1}$ and $\omega_{O_2} = \omega_{O_1}$ (upper left: Wilson action, upper right: TL Symanzik action, lower: Iwasaki action).

Chapter 7

Strong running coupling on the lattice

7.1 Introduction

In an interacting field theory, coupling constants λ are the fundamental parameters (along with the particles' masses) in terms of which predictions for observables are expressed. They encode the underlying dynamics of a field theory, as they describe the strength of the forces among the particles of the theory in different momentum regions. The denomination of "coupling constants" is actually misleading; they are not really constants, but they depend on a momentum renormalization scale μ. When μ takes values close to the scale of the momentum transfer Q in a given process then $\lambda(\mu^2 \simeq Q^2)$ is indicative of the effective strength of the underlying interactions in that process. Thus, we also refer to them as "running couplings" (they "run" with the momentum scale).

In nonabelian gauge theories, such as QCD, the evolution of the running coupling as a function of μ is of fundamental interest, especially at regions where scaling is verified. In particular, the strong interactions of quarks have totally different behavior from low to high momentum regions; at high momentum scales, QCD acts as an asymptotically free field theory, while it is confining at low momentum scales. Therefore, the strong coupling decreases with increasing momentum transfer, and vanishes at asymptotically high momentum scales. This means that the study of particle reactions at high energies

can be worked out using a perturbative expansion in powers of coupling constant. However, at low energies the strong coupling is so large that the perturbative expansion is not reliable. In this case, a nonperturbative treatment of the theory, such as lattice discretization, is required in order to reach a low momentum regime.

In lattice formulations of QCD, bare parameters depend on the lattice spacing a. Measurable quantities must not be affected by the variation of the theory's regulator; thus, bare parameters must be tuned with a in an appropriate way so that observables are fixed to their physical values. However, for sufficiently small values of lattice spacing, the a-dependence of bare parameters must be universal, i.e., independent of the observable considered. In order to ensure the finiteness of any observable, the bare coupling constant must vanish in the continuum limit corresponding to asymptotic freedom. However, numerical simulations on the lattice are performed at finite values of the bare parameters. Since the values of the bare lattice coupling are rather large, there are additional unwanted contributions to $\alpha_s = g^2/(4\pi)$, which are numerically significant. This is not, however, useful for comparing to results for α_s obtained from experiment. This is because the latter results give α_s in the $\overline{\text{MS}}$ scheme, which is commonly used in analysis of experimental data, and the conversion factor between these two schemes is known to converge extremely poorly in perturbation theory. Instead one must use a method which directly determines α_s in a scheme closer to $\overline{\text{MS}}$.

Different computational strategies are being pursued and several nonperturbative definitions of the stong coupling constant have been considered. Such a method regards the definition of α_s using the Schrödinger functional (SF) [212–215], in which one can nonperturbatively control the evolution of α_s to high-energy scales (using step-scaling functions), where the perturbative expansion converges. In this scheme, results for α_s can be produced not only for a wide range of low energies, but also in high energies where comparisons with perturbation theory can be made. A similar (more recent) method, which uses also step-scaling functions, regards the definition of α_s using the gradient flow (GF) scheme [216–218]. This scheme is more promising than SF because GF couplings have small statistical errors at large values of bare couplings, in contrast to the SF couplings, which have small statistical errors at small values of bare couplings. In both methods, conversion of the coupling to the $\overline{\text{MS}}$ scheme is required; however, this can be done only perturbatively.

7.2 β-function and Λ-parameter

The coupling constant satisfies the following renormalization group (RG) equation:

$$\mu \frac{dg}{d\mu}\Big|_{\substack{\text{bare}\\ \text{parameters}}} = \beta(g) = -(b_0 g^3 + b_1 g^5 + b_2 g^7 + \cdots), \tag{7.1}$$

where $\beta(g)$ is called beta-function and it is involved in the Callan-Symanzik equation:

$$\left[\mu \frac{\partial}{\partial \mu} + \beta(g)\frac{\partial}{\partial g} + n\gamma_1(g) + m\gamma_2(g)\right] G^{(n,m)}(\{x_i\}; \mu, g) = 0, \tag{7.2}$$

where n, m are the number of quark and gluon fields in the Green's function $G^{(n,m)}$ and γ_1 and γ_2 are the anomalous dimensions of the quark and gluon fields. The coefficients b_0, b_1 are universal, regularization independent constants, and they have been already known in the literature from calculations in dimensional regularization (DR) [219]. On the contrary, $b_i (i \geq 2)$ depends on the regulator. The minus sign in Eq. (7.1) implies the asymptotically free behavior of the strong interactions for processes involving large momentum transfers (hard processes).

Knowledge of the β-function leads to the solution of Eq. (7.1):

$$\Lambda = \mu (b_0 g^2)^{-b_1/(2b_0^2)} e^{-1/(2b_0 g^2)} \exp\left\{ -\int_0^g dg' \left[\frac{1}{\beta(g')} + \frac{1}{b_0 g'^3} - \frac{b_1}{b_0^2 g'} \right] \right\}, \tag{7.3}$$

where Λ is an integration constant, which corresponds to the scale where the perturbatively-defined coupling would diverge ($\mu \sim \Lambda$), i.e., its value is indicative of the momentum range where nonperturbative dynamics dominates; it is the nonperturbative scale of QCD, which characterizes the low momentum Physics. For large μ ($\mu \gg \Lambda$), the asymptotic solution of the RG equation reads:

$$\begin{aligned} \alpha_s(\mu^2) \simeq \frac{1}{b_0 t}\Big[1 &- \frac{b_1}{b_0^2}\frac{\ln t}{t} + \frac{b_1^2(\ln^2 t - \ln t - 1) + b_0 b_2}{b_0^4 t^2} \\ &- \frac{b_1^3(\ln^3 t - \tfrac{5}{2}\ln^2 t - 2\ln t + \tfrac{1}{2}) + 3 b_0 b_1 b_2 \ln t - \tfrac{1}{2} b_0^2 b_3}{b_0^6 t^3}\Big], \end{aligned} \tag{7.4}$$

where $t \equiv \ln(\mu^2/\Lambda^2)$.

On the lattice, the corresponding RG equation for the bare coupling g_0 is:

$$-a\frac{\partial g_0}{da}\Big|_{\substack{\text{physical}\\ \text{quantities}}} = \beta_L(g_0) = -(b_0 g_0^3 + b_1 g_0^5 + b_2^L g_0^7 + \cdots), \tag{7.5}$$

where β_L is the lattice form of β-function and it dictates the asymptotic dependence of the bare coupling constant g_0 on the lattice spacing a, required to maintain fixed the renormalized coupling at a given scale. The asymptotic solution of Eq. (7.5) is given by:

$$a\Lambda_L = \exp\Big(-\frac{1}{2b_0 g_\circ^2}\Big)(b_0 g_0^2)^{-b_1/(2b_0^2)}[1 + q g_0^2 + \mathcal{O}(g_0^4)] \tag{7.6}$$

where $q = (b_1^2 - b_0 b_2^L)/(2b_0^3)$ and Λ_L is the lattice form of Λ-parameter which corresponds to the conversion unit of dimensionless quantities coming from numerical simulations into measurable predictions for physical observables.

It is important to calculate on the lattice higher-order corrections of β-function, such as the coefficient b_2^L, for a given lattice formulation, in order to verify the two-loop asymptotic prediction of Λ_L. We recall that Monte Carlo simulations are actually performed at $g_0 \simeq 1$, and so deviations from the two-loop formula might not be negligible. Also the knowledge of b_2^L can be also used to improve the perturbative relation between the $\overline{\text{MS}}$-renormalized coupling and bare lattice coupling g_0, which is useful in calculations concerning running couplings [212, 213, 220–226]. The calculation of b_2^L is the main goal of our work in Chapter 8 using Symanzik-improved gluons and Wilson/clover fermions with a stout improvement.

7.3 The background field method

A useful technique in the evaluation of the matching between different couplings is the background field method [227–229]. The aim of this method is the simplification of quantum computations related to gauge and gravitational theories without losing explicit gauge invariance. Such calculations concerns the renormalization of nonabelian gauge theories; using dimensional regularization, the extended symmetry properties of the functional integral in the presence of a background gauge field have been exploited to establish the renormalizability of such theories to all orders of perturbation theory [230]. A particular example is the renormalization of the effective action: the introduction of a background field results in a gauge-invariant effective

action with respect to gauge transformations of the background field and it does not require any further counterterms besides those already needed in the absence of the background field.

The basic idea of the background field method is to write the gauge field in the action as the sum of two fields, the quantum field $Q_\mu(x)$ and the background field $B_\mu(x)$:

$$A_\mu(x) \ = B_\mu(x) + g_0 Q_\mu(x). \tag{7.7}$$

The quantum field is now the "fundamental" field of the theory (it is integrated in the path integral determination of Green's functions), while the background is just an arbitrary external source field, which is coupled to the dynamical fields of the theory. The gauge-fixing term, which breaks the gauge invariance with respect to transformations of the quantum field, is chosen in such a way that the invariance of the action under gauge transformations of the background field is preserved. The gauge-invariant effective action is just the background field effective action considered as a functional of $B_\mu(x)$, once the functional integration over the quantum field is performed. This effective action can be obtained from the calculation of the one-particle-irreducible two-point function of the background field.

The extension of the background field method to the lattice formulation of quantum field theories is really important for nonperturbative numerical studies. Lüscher and Weisz [231] have shown that pure lattice gauge theory with a background gauge field is renormalizable to all orders in perturbation theory. No additional counterterms are required besides those already needed in the absence of a background field, as it happens in the continuum case. Their argument, based on renormalizability of pure lattice gauge theory, BRS, background gauge and shift symmetries of the lattice functional integral, can be extended to full lattice QCD in the Wilson formulation. An essential point is the renormalizability of lattice gauge theory with Wilson fermions proved by Reisz to all orders in perturbation theory [232].

On the lattice, the background field technique can be approached in more than one way. Different lattice actions may be chosen and the precise way in which the background field is introduced is arbitrary to some extent. However, the differences between the choices of lattice actions should be irrelevant in the continuum limit. The background

field on the lattice is introduced by decomposing the gauge link variable as follows [211]:

$$\begin{aligned} U_\mu(x) &= U^Q_\mu(x) U^B_\mu(x), \\ U^Q_\mu(x) &= e^{ig_0 a Q_\mu(x+a\hat{\mu}/2)}, \\ U^B_\mu(x) &= e^{iaB_\mu(x+a\hat{\mu}/2)} \end{aligned} \tag{7.8}$$

where $Q_\mu(x) = Q^a_\mu(x)T^a$, $B_\mu(x) = B^a_\mu(x)T^a$, $tr(T^aT^b) = \delta^{ab}/2$, T^a are the generators of SU(N). Since the gauge link is now a product of two different field links, there is a freedom in interpreting the gauge transformation:

$$[U_\mu(x)]^\Lambda = \Lambda(x)U_\mu(x)\Lambda^{-1}(x+a\hat{\mu}); \tag{7.9}$$

the latter can be viewed in two ways: The first one considers the quantum field as a matter field which transforms purely locally, while the background field transforms as a true gauge field:

$$\begin{aligned} [U^Q_\mu(x)]^\Lambda &= \Lambda(x)U^Q_\mu(x)\Lambda^{-1}(x) \\ [U^B_\mu(x)]^\Lambda &= \Lambda(x)U^B_\mu(x)\Lambda^{-1}(x+a\hat{\mu}) \end{aligned} \tag{7.10}$$

The second one considers the background field as invariant, while the quantum field is now the true gauge field:

$$\begin{aligned} [U^Q_\mu(x)]^\Lambda &= \Lambda(x)U^Q_\mu(x)\Lambda^{-1}(x+a\hat{\mu}) \\ [U^B_\mu(x)]^\Lambda &= U^B_\mu(x) \end{aligned} \tag{7.11}$$

Let us call the first interpretation of gauge transformations as "background gauge transformations" and the second one as "quantum gauge transformations". As the background is an external field, which is not involved in the path integration, the gauge-fixing term, which ensures the finiteness of path integrals, can be chosen to preserve the gauge invariance under background transformations.

The fact that exact gauge invariance is preserved in the background field formalism, leads to a relation between the renormalization factors of background field Z_B and of coupling constant Z_g [233]:

$$Z_B(g_0, a\mu)\ Z^2_g(g_0, a\mu) = 1. \tag{7.12}$$

Thus, the matching formula between the lattice bare coupling constant and a renormalized one can be extracted by the evaluation of Z_B, instead of Z_g^2, which is simpler as there is no need to evaluate any three-point Green's functions.

Chapter 8

Lattice study of QCD β-function with improved actions

8.1 Introduction

The study of the strong running coupling $\alpha(\mu) = g^2(\mu)/(4\pi)$ in nonperturbative renormalization schemes is very active in the latest years; a number of extensive numerical simulations have been performed by a number of groups, giving promising results [234–238]. Of particular interest is the computation of $\alpha(\mu)$ at low-momentum regions where scaling phenomena is verified (e.g., color confinement). Knowledge of the perturbative relation between the bare running coupling $\alpha_0 = g_0^2/(4\pi)$ and the $\overline{\rm MS}$-renormalized running coupling $\alpha_{\overline{\rm MS}} = g^2_{\overline{\rm MS}}/(4\pi)$ at high orders, is important in such estimations; it is combined with these simulations in order to reach a nonperturbative regime [239].

Another important quantity, which has attracted much attention, is the scale parameter Λ_L associated with a lattice formulation of QCD [225, 240]. Knowledge of the three-loop correction (linear in g_0^2) of Λ_L is important in order to verify asymptotic scaling predictions. To this end we need to compute the three-loop (linear in g_0^7) lattice bare Callan-Symanzik β-function. The bare β-function dictates the asymptotic dependence of the bare coupling constant g_0 on the lattice spacing a, required to maintain fixed the renormalized coupling at a given scale. The β-function can be derived from the

combination of the two-loop relation between $\alpha_{\overline{\rm MS}}$ and α_0 (mentioned above) and the knowledge of the three-loop $\overline{\rm MS}$-renormalized β-function [219][1].

The main objective of this work is the computation of the three-loop coefficient of the bare β-function, b_2^L, on the lattice for $SU(N_c)$ gauge group and N_f multiplets of fermions. The computation was performed with the use of the following improved lattice actions (which have small discretization errors): Symanzik improved gluons and SLiNC fermions in an arbitrary representation of the gauge group $SU(N_c)$. The SLiNC action [25] utilizes stout smeared links in order to suppress effects of finite lattice size. This action is being used by the QCDSF Collaboration, in simulations of QCD with dynamical quark flavors. An additional objective is the computation of the ratio of energy scales $\Lambda_L/\Lambda_{\overline{\rm MS}}$[2] , in an arbitrary representation.

Previous calculations of b_2^L and $\Lambda_L/\Lambda_{\overline{\rm MS}}$ have been carried out using various techniques and discretization prescriptions. Older results involving Wilson gluons [39, 242], Symnazik improved gluons (only $\Lambda_L/\Lambda_{\overline{\rm MS}}$) [243], Wilson fermions [44], clover fermions [45, 46], overlap fermions [47] can be found in the literature. Corresponding computations for the SLiNC action, which is widely used in recent simulations, have never been done before, due to their sheer difficulty. Our results can be used to confirm some of the existing results mentioned before.

Furthermore, the results of such calculations can be used to make contact with a low momentum-regime of QCD. In particular, our results will be combined with extensive simulations performed by members of QCDSF Collaboration who have several aims, among them: the precise determination of the QCD scale Λ_{QCD}, the non-perturbative running of the renormalized coupling constant and the determination of hadronic properties using the "Wilson gradient flow" scheme, which is being very actively investigated by a number of groups at present [244].

This chapter is organized as follows. In Sec. 8.2 we formulate the problem, giving some useful relations, and in general, the theoretical setup of our calculation, including also the definition of the lattice actions which are used. Sec. 8.3 contains our one- and

[1]The $\overline{\rm MS}$-renormalized β-function is now known up to five loops [241].

[2]The Λ_L parameter is a dimensionful quantity; as such it cannot be directly obtained from the lattice. Instead, the quantity which is calculable is the ratio between Λ_L and the scale parameter in some continuum renormalization scheme such as $\overline{\rm MS}$: $\Lambda_L/\Lambda_{\overline{\rm MS}}$.

two-loop results for the β-function. The two-loop calculation is still ongoing, and we consider here only a part of this.

8.2 Formulation

8.2.1 Preliminaries

As mentioned in Chapter 7, for the lattice regularization a bare β-function is defined as:

$$\beta_L(g_0) \ = -a\frac{dg_0}{da}|_{\ g,\bar{\mu}} \tag{8.1}$$

where $\bar{\mu} = \mu(4\pi/e^{\gamma_E})^{1/2}$ is the renormalization momentum scale used in the $\overline{\rm MS}$ scheme of dimensional regularization (the currently most widely used scheme for the analysis of experimental data in high-energy Physics), γ_E is the Euler constant, a is the lattice spacing and $g(g_0)$ is the renormalized (bare) coupling constant. It is well known that in the asymptotic limit for QCD ($g_0 \to 0$), one can write the expansion of the β-function in powers of g_0, that is:

$$\beta_L(g_0) \ = -b_0{g_0}^3 - b_1{g_0}^5 - b_2^L{g_0}^7 + \mathcal{O}({g_0}^9) \tag{8.2}$$

The coefficients b_0, b_1 are universal, regularization independent constants, while $b_i^L (i \geq 2)$ depends on the regulator; it, generally, differs from one to another lattice action and it must be determined perturbatively.

The coefficient b_2^L can be extracted from the renormalization function Z_g, relating the bare coupling constant g_0 to the renormalized coupling constant $g_{\overline{\rm MS}}$:

$$g_0 \ = Z_g^{(L,\overline{\rm MS})}(g_0, a\bar{\mu}) \times g_{\overline{\rm MS}} \tag{8.3}$$

The combination of Eqs. (8.1) and (8.3) leads to the following relation:

$$\beta_L(g_0) \ = -g_0 a\frac{d}{da}\ln Z_g(g_0, a\bar{\mu})|_{\bar{\mu},g} \tag{8.4}$$

where it is being perceivable that the evaluation of b_2^L requires the computation of the three-loop expression of Z_g.

However, the knowledge of the $\overline{\text{MS}}$-renormalized β-function (in dimensional regularization) up to three loops:

$$\beta(g_{\overline{\text{MS}}}) = \bar{\mu}\frac{dg_{\overline{\text{MS}}}}{d\bar{\mu}}|_{a,g_0} = -b_0 g^3_{\overline{\text{MS}}} - b_1 g^5_{\overline{\text{MS}}} - b_2 g^7_{\overline{\text{MS}}} + \mathcal{O}(g^9_{\overline{\text{MS}}}) \tag{8.5}$$

allows to calculate b_2^L using only the two-loop expression of Z_g^2. Indeed comparing Eq. (8.4) with the definition of $\beta(g_{\overline{\text{MS}}})$ written in the form:

$$\beta(g_{\overline{\text{MS}}}) = -g_{\overline{\text{MS}}}\bar{\mu}\frac{d}{d\bar{\mu}}\ln Z_g(g_0, a\bar{\mu})|_{a,g_0}, \tag{8.6}$$

one can derive an exact relation, valid to all orders of perturbation theory:

$$\beta^L(g_0) = \Big(1 - g_0^2\frac{\partial}{\partial g_0^2}\ln Z_g^2\Big)^{-1} Z_g \beta(g_0 Z_g^{-1}) \tag{8.7}$$

Writing Z_g^2 as:

$$\Big(Z_g^{(L,\overline{\text{MS}})}(g_0, a\bar{\mu})\Big)^2 = 1 + {g_0}^2(b_0\ln(a^2\bar{\mu}^2) + l_0) + {g_0}^4(b_1\ln(a^2\bar{\mu}^2) + l_1) + \mathcal{O}({g_0}^6) \tag{8.8}$$

and inserting it in Eq. (8.7), we extract the relation:

$$b_2^L = b_2 - b_1 l_0 + b_0 l_1. \tag{8.9}$$

The quantities b_0, b_1 and b_2 have been known in the literature for quite some time [219]:

$$b_0 = \tfrac{1}{(4\pi)^2}\Big(\tfrac{11}{3}N_c - \tfrac{2}{3}N_f\Big), \tag{8.10}$$

$$b_1 = \tfrac{1}{(4\pi)^4}\Big[\tfrac{34}{3}N_c^2 - N_f\Big(\tfrac{13}{3}N_c - \tfrac{1}{N_c}\Big)\Big], \tag{8.11}$$

$$b_2 = \tfrac{1}{(4\pi)^6}\Big[\tfrac{2857}{54}N_c^3 + N_f\Big(-\tfrac{1709}{54}N_c^2 + \tfrac{187}{36} + \tfrac{1}{4N_c^2}\Big) + N_f^2\Big(\tfrac{56}{27}N_c - \tfrac{11}{18N_c}\Big)\Big] \tag{8.12}$$

Thus, the evaluation of b_2^L requires the determination of the 2-loop quantity l_1 and the 1-loop quantity l_0. The constant l_0 is further related to the ratio of the Λ parameters associated with the particular lattice regularization and the $\overline{\text{MS}}$ renormalization scheme:

$$\frac{\Lambda_L}{\Lambda_{\overline{\text{MS}}}} = \exp\Big(\frac{l_0}{2b_0}\Big) \tag{8.13}$$

Furthermore, using the asymptotic relation of $\beta^L(g_0)$ (8.2) and the fact that Λ_L is a particular solution of the RG (Renormalization Group) equation

$\Big(- a\frac{\partial}{\partial a} + \beta^L(g_0)\frac{\partial}{\partial g_0}\Big)\Lambda_L = 0$, one can derive the 2-loop corrected asymptotic scaling relation between a and g_0:

$$a\Lambda_L = \exp\Big[- \int^{g_0} \frac{dg}{\beta^L(g)}\Big] = \exp\Big(- \frac{1}{2b_0 g_0^2}\Big)(b_0 g_0^2)^{-b_1/(2b_0^2)}[1 + q g_0^2 + \mathcal{O}(g_0^4)] \quad (8.14)$$

where

$$q = \frac{b_1^2 - b_0 b_2^L}{2b_0^3} \quad (8.15)$$

8.2.2 Using the background field formulation

The most convenient and economical way to proceed with calculating Z_g^2 is to use the background field technique [211, 231, 233], described in Chapter 7, section 7.3. In this technique, the following relation is valid:

$$Z_B^{(L,\overline{\rm MS})}(g_0, a\mu) \times \Big(Z_g^{(L,\overline{\rm MS})}(g_0, a\mu)\Big)^2 = 1, \quad (8.16)$$

where Z_B is the background field renormalization function: $B_{\mu_0}(x) = [Z_B^{(L,\overline{\rm MS})}(g_0, a\bar{\mu})]^{1/2} B_\mu^{\overline{\rm MS}}(x)$, where $B_{\mu_0}(B_\mu^{\overline{\rm MS}})$ is the bare ($\overline{\rm MS}$-renormalized) background field. In this framework, instead of Z_g^2, one needs to compute Z_B, with no need to evaluate any 3-point Green's functions. For this purpose, we consider the 1-particle-irreducible 2-point Green's function of background gluon field, both in the continuum ($\Gamma_R^{BB}(p)_{\mu\nu}^{ab}$) and on the lattice ($\Gamma_L^{BB}(p)_{\mu\nu}^{ab}$).

We have adopted the notation of Ref.[39],where these functions can be expressed in terms of scalar amplitudes $\nu_R(p)$, $\nu(p)$:

$$\Gamma_R^{BB}(p)_{\mu\nu}^{ab} = -\delta^{ab}(\delta_{\mu\nu}p^2 - p_\mu p_\nu)(1 - \nu_R(p))/g^2_{\overline{\rm MS}}, \quad (8.17)$$

$$\sum_\mu \Gamma_L^{BB}(p)_{\mu\mu}^{ab} = -\delta^{ab} 3\hat{p}^2(1 - \nu(p))/g_0^2, \quad (8.18)$$

$$\nu_R(p) = \sum_{\ell=1}^{\infty} g^{2\ell}_{\overline{\rm MS}} \nu_R^{(\ell)}(p), \quad (8.19)$$

$$\nu(p) = \sum_{\ell=1}^{\infty} g_0^{2\ell} \nu^{(\ell)}(p). \quad (8.20)$$

where $\hat{p}^2 = \sum_\mu \hat{p}_\mu^2$, $\hat{p}_\mu = (2/a)sin(ap_\mu/2)$. The tensor structure of these Green's functions, as given above, is implied by the symmetries of the theory. Using the relation

between the background-field 2-point functions: $\Gamma_R^{BB}(p)^{ab}_{\mu\nu} = \Gamma_L^{BB}(p)^{ab}_{\mu\nu} + \mathcal{O}(a)$, as well as Eqs. (8.3, 8.17 - 8.20), we can express Z_g^2 in terms of $\nu_R(p)$, $\nu(p)$:

$$Z_g^2 = \frac{1-\nu(p)}{1-\nu_R(p)} \tag{8.21}$$

A similar relation is obtained for the renormalization factor Z_λ ($\lambda_0 = Z_\lambda\ \lambda_{\overline{\rm MS}}$, where $\lambda_0(\lambda_{\overline{\rm MS}})$ is the inverse bare ($\overline{\rm MS}$-renormalized) gauge parameter), where the scalar terms $\nu_R(p)$, $\nu(p)$ are replaced with the scalar terms $\omega_R(p)$, $\omega(p)$, which are stemming from the definition of quantum field self-energy in the continuum ($\Gamma_R^{QQ}(p)^{ab}_{\mu\nu}$) and on the lattice ($\Gamma_L^{QQ}(p)^{ab}_{\mu\nu}$) respectively. That is:

$$\Gamma_R^{QQ}(p)^{ab}_{\mu\nu} = -\delta^{ab}[(\delta_{\mu\nu}p^2 - p_\mu p_\nu)(1-\omega_R(p)) + \lambda_{\overline{\rm MS}}\ p_\mu p_\nu], \tag{8.22}$$

$$\sum_\mu \Gamma_L^{QQ}(p)^{ab}_{\mu\mu} = -\delta^{ab}\hat{p}^2[3(1-\omega(p)) + \lambda_0], \tag{8.23}$$

$$\omega_R(p) = \sum_{\ell=1}^{\infty} g_{\overline{\rm MS}}^{2\ell}\omega_R^{(\ell)}(p), \tag{8.24}$$

$$\omega(p) = \sum_{\ell=1}^{\infty} g_0^{2\ell}\omega^{(\ell)}(p), \tag{8.25}$$

and

$$Z_\lambda = \frac{1-\omega(p)}{1-\omega_R(p)}. \tag{8.26}$$

Combining Eq. (8.21) with Eq. (8.26), we are led to the following expression for Z_g^2:

$$Z_g^2 = \Bigg\{1 + g_0^2\left[\nu_R^{(1)}(p) - \nu^{(1)}(p)\right] + g_0^4\left[\nu_R^{(2)}(p) - \nu^{(2)}(p) + \lambda_{\overline{\rm MS}}\frac{\partial\nu_R^{(1)}(p)}{\partial\lambda_{\overline{\rm MS}}} \times \left(\omega_R^{(1)}(p) - \omega^{(1)}(p)\right)\right] + \mathcal{O}(g_0^6)\Bigg\}_{\lambda_{\overline{\rm MS}}=\lambda_0} \tag{8.27}$$

The amplitudes $\nu_R^{(1)}(p), \omega_R^{(1)}(p), \nu_R^{(2)}(p)$ calculated in dimensional regularization, have been already known in the literature[3] [44, 245]:

$$\nu_R^{(1)}(p) = \frac{N_c}{16\pi^2}\left[-\frac{11}{3}\ln(\frac{p^2}{\bar{\mu}^2}) + \frac{205}{36} + \frac{3}{2}\lambda_{\overline{\rm MS}}^{-1} + \frac{1}{4}\lambda_{\overline{\rm MS}}^{-2}\right] + \frac{N_f}{16\pi^2}\left[\frac{2}{3}\ln(\frac{p^2}{\bar{\mu}^2}) - \frac{10}{9}\right], \tag{8.28}$$

[3]The fermionic part of $\nu_R^{(2)}(p)$ is given in the Feynman gauge ($\lambda_{\overline{\rm MS}} = 1$), since our calculations do not need this quantity in general gauge.

$$\omega_R^{(1)}(p) = \frac{N_c}{16\pi^2}\left[\Big(-\frac{13}{6}+\frac{1}{2}\lambda_{\overline{\rm MS}}^{-1}\Big)\ln(\frac{p^2}{\bar\mu^2})+\frac{97}{36}+\frac{1}{2}\lambda_{\overline{\rm MS}}^{-1}+\frac{1}{4}\lambda_{\overline{\rm MS}}^{-2}\right]+\frac{N_f}{16\pi^2}\left[\frac{2}{3}\ln(\frac{p^2}{\bar\mu^2})-\frac{10}{9}\right], \tag{8.29}$$

$$\begin{aligned}\nu_R^{(2)}(p) &= \frac{N_c^2}{(16\pi^2)^2}\left[\Big(\frac{34}{3}-\frac{13}{4}\lambda_{\overline{\rm MS}}^{-1}-\frac{1}{3}\lambda_{\overline{\rm MS}}^{-2}+\frac{1}{4}\lambda_{\overline{\rm MS}}^{-3}-\frac{1}{16}\lambda_{\overline{\rm MS}}^{-4}\Big)\ln(\frac{p^2}{\bar\mu^2})+\Big(\frac{2687}{72}-\frac{57}{8}\Big)\right.\\ &\left.+\Big(-\frac{187}{48}+\frac{5}{4}\zeta(3)\Big)\lambda_{\overline{\rm MS}}^{-1}+\Big(-\frac{161}{144}-\frac{1}{8}\Big)\lambda_{\overline{\rm MS}}^{-2}-\frac{3}{16}\lambda_{\overline{\rm MS}}^{-3}-\frac{1}{16}\lambda_{\overline{\rm MS}}^{-4}\right]\\ &+\underbrace{\frac{N_f}{(16\pi^2)^2}\left[N_c\Big(3\ln(\frac{p^2}{\bar\mu^2})-\frac{401}{36}\Big)+\frac{1}{N_c}\Big(-\ln(\frac{p^2}{\bar\mu^2})+\frac{55}{12}-4\zeta(3)\Big)\right]}_{\text{for }\lambda_{\overline{\rm MS}}=1}\end{aligned} \tag{8.30}$$

Therefore, we only have to calculate the amplitudes $\nu^{(1)}(p), \omega^{(1)}(p)$, and $\nu^{(2)}(p)$. The quantities ℓ_0 and ℓ_1 can be also expressed in terms of $\nu_R(p)$, $\nu(p)$, $\omega_R(p)$, $\omega(p)$:

$$\ell_0 = -b_0\ln(a^2\bar\mu^2)+\left[\nu_R^{(1)}(p)-\nu^{(1)}(p)\right]_{\lambda_{\overline{\rm MS}}=\lambda_0}, \tag{8.31}$$

$$\ell_1 = -b_1\ln(a^2\bar\mu^2)+\left[\nu_R^{(2)}(p)-\nu^{(2)}(p)+\lambda_{\overline{\rm MS}}\,\frac{\partial\nu_R^{(1)}(p)}{\partial\lambda_{\overline{\rm MS}}}\,\Big(\omega_R^{(1)}(p)-\omega^{(1)}(p)\Big)\right]_{\lambda_{\overline{\rm MS}}=\lambda_0} \tag{8.32}$$

Finally, the relation between the $\overline{\rm MS}$-renormalized running coupling $\alpha_{\overline{\rm MS}}$ and the bare running coupling α_0 can be easily read from Eq. (8.27):

$$\begin{aligned}\alpha_{\overline{\rm MS}} &= \alpha_0+\alpha_0^2\,d_1(a\bar\mu)+\alpha_0^3\,d_2(a\bar\mu)+\mathcal{O}(\alpha_0^4),\\ d_1(a\bar\mu) &= \left[-4\pi\,\Big(\nu_R^{(1)}(p)-\nu^{(1)}(p)\Big)\right]_{\lambda_{\overline{\rm MS}}=\lambda_0},\\ d_2(a\bar\mu) &= (4\pi)^2\left[\Big(\nu_R^{(1)}(p)-\nu^{(1)}(p)\Big)^2-\Big(\nu_R^{(2)}(p)-\nu^{(2)}(p)\right.\\ &\left.+\lambda_{\overline{\rm MS}}\,\frac{\partial\nu_R^{(1)}(p)}{\partial\lambda_{\overline{\rm MS}}}\,\Big(\omega_R^{(1)}(p)-\omega^{(1)}(p)\Big)\Big)\right]_{\lambda_{\overline{\rm MS}}=\lambda_0}.\end{aligned} \tag{8.33}$$

Given that the effective action is gauge invariant, we can choose to perform our computations in the Feynman gauge; Eq. (8.33) then implies that $\nu^{(2)}(p)$, $\nu_R^{(2)}(p)$ and $\omega^{(1)}(p)$, $\omega_R^{(1)}(p)$ can be computed directly in the Feynman gauge $\lambda_0 = 1$, and only $\nu_R^{(1)}(p)$ needs to be computed in a general gauge.

8.2.3 Lattice actions

In our calculation we used the SLiNC fermion action [25]. This action is similar to the Wilson/clover action, defined in Eq. (4.3), with the following modification: the gluon links appearing in the Wilson part (not in the clover term; i.e., the first two lines in Eq. (4.3)) are replaced by stout-smeared links, $\widetilde{U}_\mu(x)$, as defined in Eq. (6.4)). Following common practice, we henceforth set the Wilson parameter r equal to 1. Both the stout coefficient ω and the clover coefficient c_{SW} will be treated as free parameters, for wider applicability of the results. As is customarily done, one may restrict attention to "mass-independent" renormalization schemes, in which normalization conditions on Green's functions are placed at zero renormalized mass. We note that the $\overline{\text{MS}}$ scheme is automatically mass independent, since pole terms do not contain masses. Thus, by adopting such a scheme, the β-function will be independent of the renormalized fermionic masses.

For gluons, we employ the Symanzik improved action S_G, defined in (4.5). We use a number of commonly used sets of values for the Symanzik coefficients c_i, given in Table 4.1.

Furthermore, a choice of gauge is required. We introduce the following gauge-fixing term [211]:

$$S_{gf} = \lambda_0 a^4 \sum_{x,\mu,\nu} \text{Tr}\left\{ D^-_\mu Q_\mu(x) D^-_\nu Q_\nu(x) \right\} \tag{8.34}$$

where

$$D^-_\mu Q_\nu(x) = \frac{1}{a}\Big[Q_\nu(x) - U^{B^{-1}}_\mu(x - a\hat{\mu})\; Q_\nu(x - a\hat{\mu})\; U^B_\mu(x - a\hat{\mu}) \Big] \tag{8.35}$$

Although this term breaks gauge invariance of quantum field, it succeeds in preserving gauge invariance of background field.

From the variation of the gauge-fixing term under a gauge transformation of the type (7.11), $\delta\left[D^-_\mu Q_\mu(x))\right]/\delta\Lambda(x)$, we are led to the Faddeev-Popov action; only terms necessary for our computation, i.e. up to $\mathcal{O}(g_0^2)$, are shown here:

$$S_{FP} = 2a^4 \sum_{x,\mu} \mathrm{Tr} \Big\{ (D^+_\mu \omega(x))^\dagger \Big(D^+_\mu \omega(x) + ig_0 \left[Q_\mu(x), \omega(x) \right] + \frac{1}{2} ig_0 a \left[Q_\mu(x), D^+_\mu \omega(x) \right] - \frac{1}{12} g_0^2 a^2 \left[Q_\mu(x), \left[Q_\mu(x), D^+_\mu \omega(x) \right] \right] + \cdots \Big) \Big\} \quad (8.36)$$

where $\omega(\omega^\dagger)$ is the ghost (antighost) field and

$$D^+_\mu \omega(x) = \frac{1}{a} \Big[U^B_\mu(x) \omega(x + a\hat{\mu}) U^{B^{-1}}_\mu(x) - \omega(x) \Big] \quad (8.37)$$

Finally, the change of integration variables from links to vector fields yields a Jacobian that can be rewritten as the usual measure term $S_{meas.}$ in the action:

$$S_{meas} = \frac{1}{12} N_c g_0^2 a^2 \sum_{x,\mu} \mathrm{Tr} \Big\{ Q_\mu(x) Q_\mu(x) + \cdots \Big\} \quad (8.38)$$

Therefore, the full action is:

$$S = S_F + S_G + S_{gf} + S_{FP} + S_{meas.}. \quad (8.39)$$

8.3 Calculations, results and discussion

The computation is broken into the following tasks: Firstly, we construct a total of twenty-five vertices stemming from the total action. Some of the more complicated vertices, such as the one containing 2 background and 4 quantum gluon fields, contain several thousands of terms. Secondly, we calculate all relevant one- and two-loop Feynman diagrams contributing to the amplitudes $\nu^{(1)}(p)$, $\omega^{(1)}(p)$, and $\nu^{(2)}(p)$ (see below). Upon contraction of the corresponding vertices we obtain huge algebraic expressions (many millions of terms for two-loop diagrams). Thirdly, we extract the one-loop amplitudes $\nu^{(1)}(p)$, $\omega^{(1)}(p)$, and the two-loop amplitude $\nu^{(2)}(p)$. A very delicate and complicated task regards the extraction of the dependence of the Green's functions, on the external momentum p; this task is briefly described in the next subsection 8.3.1. Finally, we extract the quantities ℓ_0, ℓ_1, b_2^L, $\Lambda_L/\Lambda_{\overline{\mathrm{MS}}}$, q and the perturbative relation between $\alpha_{\overline{\mathrm{MS}}}$ and α_0, as defined previously.

8.3.1 Extraction of external momentum

In this subsection, we describe the methodology for calculating the lattice momentum-loop integrals appearing in the bare Green's functions of background and quantum fields. This task is to make explicit the functional dependence of Green's functions on the external momentum p. In particular, there arise terms of the form p^0, p^2, $p^2\ln(a^2p^2)$, $p^2[\ln(a^2p^2)]^2$, $\sum_\mu p_\mu^4/p^2$, whose coefficients can be expressed as integrals of lengthy algebraic expressions over the internal (loop) momenta. The general idea is to decompose the given expression (to be integrated over internal momenta) in terms of a limited set of potentially divergent integrands, plus other terms which can be evaluated by naïve Taylor expansion in the external momentum, to the desired order. To this end, we perform two kinds of subtractions among the (fermion, and/or gluon) propagators, both in one-loop calculations and beyond. The first kind reduces the number of divergent integrals to a mimimal set of familiar (in the literature) integrals; to give an example:

$$\frac{1}{\tilde{q}^2} = \frac{1}{\hat{q}^2} + \frac{\hat{q}^2-\tilde{q}^2}{\tilde{q}^2\hat{q}^2} \tag{8.40}$$

$$D_{\mu\nu}(q) = D_{\mu\nu}^{\text{plaq.}}(q) + \Big[D_{\mu\nu}(q) - D_{\mu\nu}^{\text{plaq.}}(q)\Big] \tag{8.41}$$

where q is the (internal) loop momentum, $\tilde{q}^2$ is the inverse fermionic propagator: $\tilde{q}^2 = (\hat{q}^2 r/2)^2 + \sum_\mu sin^2 q_\mu$, $D_{\mu,\nu}(q)$ is the Symanzik improved gluon propagator and $D_{\mu\nu}^{\text{plaq.}}(q)$ is the plaquette Wilson gluon propagator: $D_{\mu\nu}^{\text{plaq.}}(q) = \delta_{\mu\nu}/\hat{q}^2$. The second kind of subtractions is used in order to perform a Taylor expansion of convergent terms, in external momentum p to the desired order; it has the following general form (to be performed iteratively):

$$f(q+p) = f(q) + \Big[f(q+p) - f(q)\Big]. \tag{8.42}$$

The order of implementation of these two kinds of subtractions is not obvious, especially beyond one loop.

The completion of the above procedure leaves us with loop integrals having no dependence on external momenta, which must be integrated numerically. A number of technical issues must be dealt with before numerical integration: for example, it is necessary to keep the Lorentz indices of the trigonometric functions of internal momenta independent of those in the rest of the expression. Each integral is

expressed as a sum over the discrete Brillouin zone of a finite lattice. The integration is performed for an extensive range of lattice sizes. At the end, we extrapolate our results from finite lattices towards an infinite lattice; we also estimate the systematic errors which stem from such a procedure. The extrapolation methods that we used are described in Ref. [208].

8.3.2 One-loop computation

There are six one-loop Feynman diagrams contributing to $\nu^{(1)}(p)$ and 7 diagrams contributing to $\omega^{(1)}(p)$, shown in Figs. 8.1 and 8.2 respectively. During the

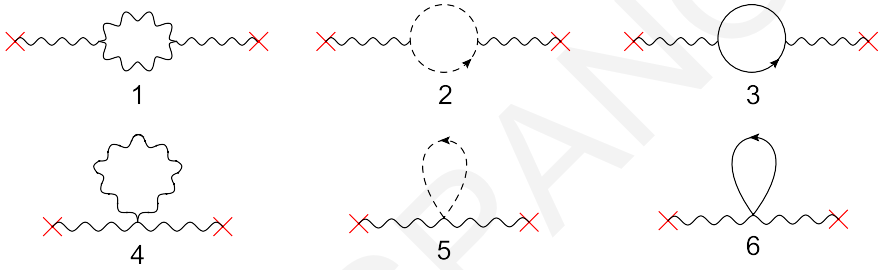

FIGURE 8.1: 1-loop diagrams contributing to $\nu^{(1)}(p)$. Wavy lines ending on a cross represent background gluons. Solid (dashed) lines represent fermions (ghosts).

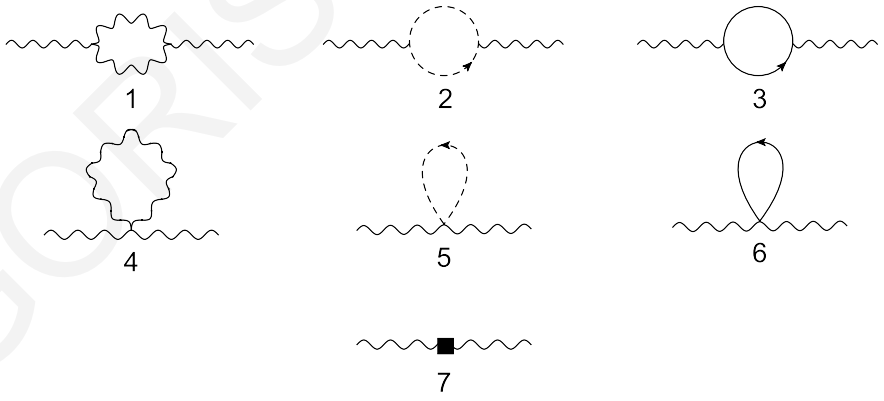

FIGURE 8.2: 1-loop diagrams contributing to $\omega^{(1)}(p)$. Wavy (solid, dashed) lines represent quantum gluons (fermions, ghosts). The solid box denotes a vertex stemming from the measure part of the action.

computation of the above diagrams, there arise terms of the form $\hat{p}^0$, $\hat{p}_\mu$, $\hat{p}_\mu^2$, $\hat{p}_\mu\hat{p}_\nu$, $\hat{p}^2$. Some forms are inconvenient; there are quadratically divergent terms ($\hat{p}^0$), linearly divergent terms ($\hat{p}_\mu$) and terms which break Lorentz invariance in the continuum limit ($\hat{p}_\mu^2$). These troublesome terms cancel in the sum of all diagrams or they are excluded by symmetry. Therefore, we are left with the terms $\hat{p}_\mu\hat{p}_\nu$, $\hat{p}^2$, as we expected.

Our results for $\nu^{(1)}(p)$ and $\omega^{(1)}(p)$ are presented below, in general gauge λ_0:

$$\nu^{(1)}(p) = \frac{N_c}{16\pi^2}\left[-\frac{11}{3}\ln(a^2p^2) + \boldsymbol{c}^{\nu^{(1)}}_{\boldsymbol{N_c}} + \frac{3}{2}\lambda_0^{-1} + \frac{1}{4}\lambda_0^{-2}\right] + \frac{1}{N_c}\frac{1}{16\pi^2}\,\boldsymbol{c}^{\nu^{(1)}}_{\boldsymbol{1/N_c}} + \frac{N_f}{16\pi^2}\left[\frac{2}{3}\ln(a^2p^2) + \boldsymbol{c}^{\nu^{(1)}}_{\boldsymbol{N_f}}\right] + \mathcal{O}(a^2p^2), \tag{8.43}$$

$$\omega^{(1)}(p) = \frac{N_c}{16\pi^2}\left[\left(-\frac{13}{6} + \frac{1}{2}\lambda_0^{-1}\right)\ln(a^2p^2) + \boldsymbol{c}^{\omega^{(1)}}_{\boldsymbol{N_c}} + \boldsymbol{c}^{\omega^{(1)}}_{\boldsymbol{\lambda_0^{-1}N_c}}\lambda_0^{-1} + \frac{1}{4}\lambda_0^{-2}\right] + \frac{1}{N_c}\frac{1}{16\pi^2}\boldsymbol{c}^{\omega^{(1)}}_{\boldsymbol{1/N_c}} + \frac{N_f}{16\pi^2}\left[\frac{2}{3}\ln(a^2p^2) + \boldsymbol{c}^{\omega^{(1)}}_{\boldsymbol{N_f}}\right] + \mathcal{O}(a^2p^2), \tag{8.44}$$

where

$$c^{\omega^{(1)}}_{\lambda_0^{-1}N_c} = -0.88629444(4), \tag{8.45}$$

$$c^{\nu^{(1)}}_{N_f} = c^{\omega^{(1)}}_{N_f} = -2.16850086(2) + 0.79694512(11)\ c_{SW} - 4.712691443(4)\ c^2_{SW} \tag{8.46}$$

and the numerical constants $c_i^{\nu^{(1)}}$, $c_i^{\omega^{(1)}}$ $(i = N_c, 1/N_c)$ are listed in Table 8.1 for different gluon actions. We notice that the fermionic contributions in $\omega^{(1)}(p)$, as well as the

Gluon action	$c^{\nu^{(1)}}_{N_c}$	$c^{\nu^{(1)}}_{1/N_c} = c^{\omega^{(1)}}_{1/N_c}$	$c^{\omega^{(1)}}_{N_c}$
Wilson	32.5328199(5)	-19.7392089(2)	22.3156745(1)
TL Symanzik	18.860597(3)	-6.6594802(3)	10.308794(3)
TILW, βc_0 =8.60	10.5954557(3)	1.3040804(4)	3.06253640(3)
TILW, βc_0 =8.45	10.2868675(4)	1.5985007(6)	2.7923321(3)
TILW, βc_0 =8.30	9.8615392(2)	2.0038705(5)	2.4199523(3)
TILW, βc_0 =8.20	9.5977109(3)	2.2550514(4)	2.1889929(4)
TILW, βc_0 =8.10	9.2575332(5)	2.5786980(4)	1.8912290(2)
TILW, βc_0 =8.00	8.8354866(3)	2.9797868(4)	1.5218513(2)
Iwasaki	-1.152587(2)	11.888842(1)	-8.5190295(6)
DBW2	-25.693965(165)	32.281461(3)	-29.853124(130)

TABLE 8.1: Numerical coefficients for the quantities $\nu^{(1)}(p)$ and $\omega^{(1)}(p)$.

contributions of the form $1/N_c$, are identical to those in $\nu^{(1)}(p)$. Furthermore, we observe that the one-loop results are independent of the stout-smearing coefficient ω. The above results are in agreement (up to 5 - 6 decimal places) with previous results for Wilson/Symanzik gluons and Wilson/clover fermions [39, 44, 45, 243].

The resulting one-loop quantity ℓ_0, as well as the ratio $\Lambda_L/\Lambda_{\overline{\text{MS}}}$, and the first coefficient in the expansion of running coupling $d_1(a\bar{\mu})$, are given by:

$$\ell_0 = \frac{N_c}{16\pi^2}\boldsymbol{c}^{\ell_0}_{\boldsymbol{N_c}} + \frac{1}{N_c}\frac{1}{16\pi^2}\,\boldsymbol{c}^{\ell_0}_{\boldsymbol{1/N_c}} + \frac{N_f}{16\pi^2}\boldsymbol{c}^{\ell_0}_{\boldsymbol{N_f}}, \tag{8.47}$$

$$\frac{\Lambda_L}{\Lambda_{\overline{\rm MS}}} = \exp\left[\frac{N_c \boldsymbol{c^{\ell_0}_{N_c}} + \frac{1}{N_c}\,\boldsymbol{c^{\ell_0}_{1/N_c}} + N_f \boldsymbol{c^{\ell_0}_{N_f}}}{\frac{22}{3}\,N_c - \frac{4}{3}\,N_f}\right], \tag{8.48}$$

$$d_1(a\bar{\mu}) = -\frac{1}{4\pi}\left[\left(\frac{11}{3}N_c - \frac{2}{3}N_f\right)\ln(a^2\bar{\mu}^2) + N_c \boldsymbol{c^{\ell_0}_{N_c}} + \frac{1}{N_c}\boldsymbol{c^{\ell_0}_{1/N_c}} + N_f \boldsymbol{c^{\ell_0}_{N_f}}\right], \tag{8.49}$$

where

$$c^{\ell_0}_{N_c} = \frac{205}{306} - c^{\nu^{(1)}}_{N_c}, \tag{8.50}$$

$$c^{\ell_0}_{1/N_c} = -c^{\nu^{(1)}}_{1/N_c}, \tag{8.51}$$

$$c^{\ell_0}_{N_f} = -3.27961197(2) + 0.79694512(11)\; c_{SW} - 4.712691443(4)\; c^2_{SW} \tag{8.52}$$

8.3.3 Two-loop computation

There are fifty-one two-loop Feynman diagrams contributing to $\nu^{(2)}(p)$, shown in Figs. 8.3 - 8.4. Each diagram is meant to be symmetrized over the color indices, Lorentz indices and momenta of the two external background fields. Below, we present our preliminary results for the simpler diagrams, the tadpoles $d_{46} - d_{51}$:

$$\hat{p}^2 \nu^{(2)}_i(p) = \left[\sum_{j,k}\left(c^{(i)}_{G\;(j,k)}\right)p^{2j}N_c^{2k} + \sum_{\ell,m,n,r}\left(c^{(i)}_{F\;(\ell,m,n,r)}\right)p^{2\ell}c^m_{\rm SW}\omega^n N_f N_c^r\right] \tag{8.53}$$

where $(i = 46+47+48, 49+50+51)$, $(j = 0, 1)$, $(k = -1, 0, 1)$, $(\ell = 0, 1)$, $(m = 0, 1, 2)$, $(n = 0, 1, 2, 3, 4)$, $(r = -1, 1)$. The coefficients $c^{(i)}_{G\;(j,k)}$, and $c^{(i)}_{F\;(\ell,m,n,r)}$ are given in Tables (8.2, 8.3), for Wilson, tree-level Symanzik and Iwasaki gluons. Coefficients not appearing in this table are zero. The numerical integrations entail a small systematic error; we keep only the first five decimal digits in our results. Our results are in agreement with previous results for Wilson gluons and Wilson/clover fermions [39, 44, 45, 243].

Results for other diagrams are not included in this Thesis, as the calculation is ongoing. This work is extremely demanding in terms of conceptual and technical complexity, but also in terms of computational resources. In particular, extracting the external momentum up to the second order, as described in section 8.3.1, millions of terms are produced for each diagram. The size of these expressions often places special requirements on RAM. We intend to investigate some other arrangements, in order to complete the computation in the near future.

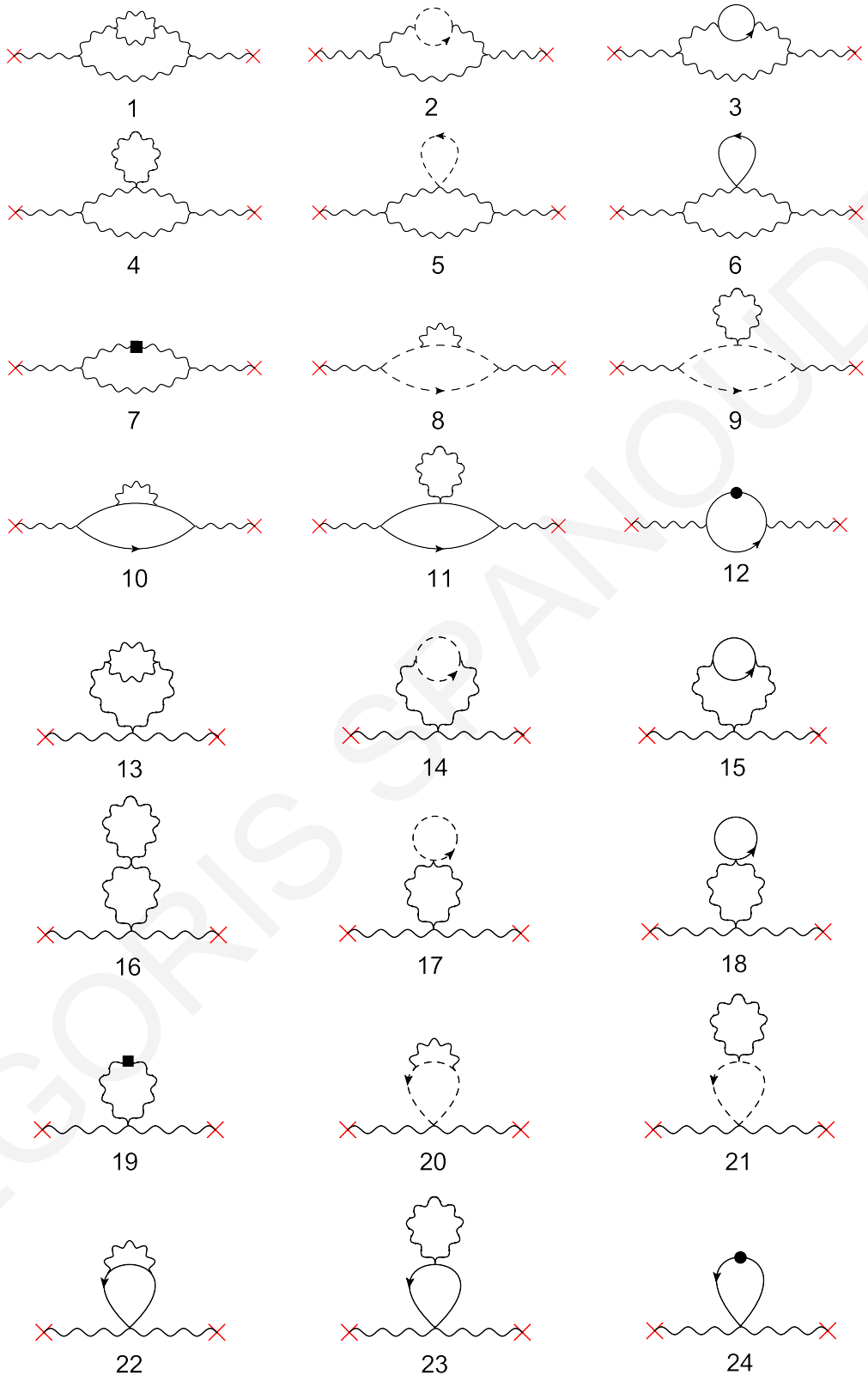

FIGURE 8.3: 2-loop diagrams contributing to $\nu^{(2)}(p)$. Wavy lines (without) ending on a cross represent (quantum) background gluons. Solid (dashed) lines represent fermions (ghosts). Solid boxes denote vertices stemming from the measure part of the action. A solid circle is a one-loop fermion mass counterterm. Both directions of the ghost (fermion) arrow in diagram 27 (29) must be considered. (1/2)

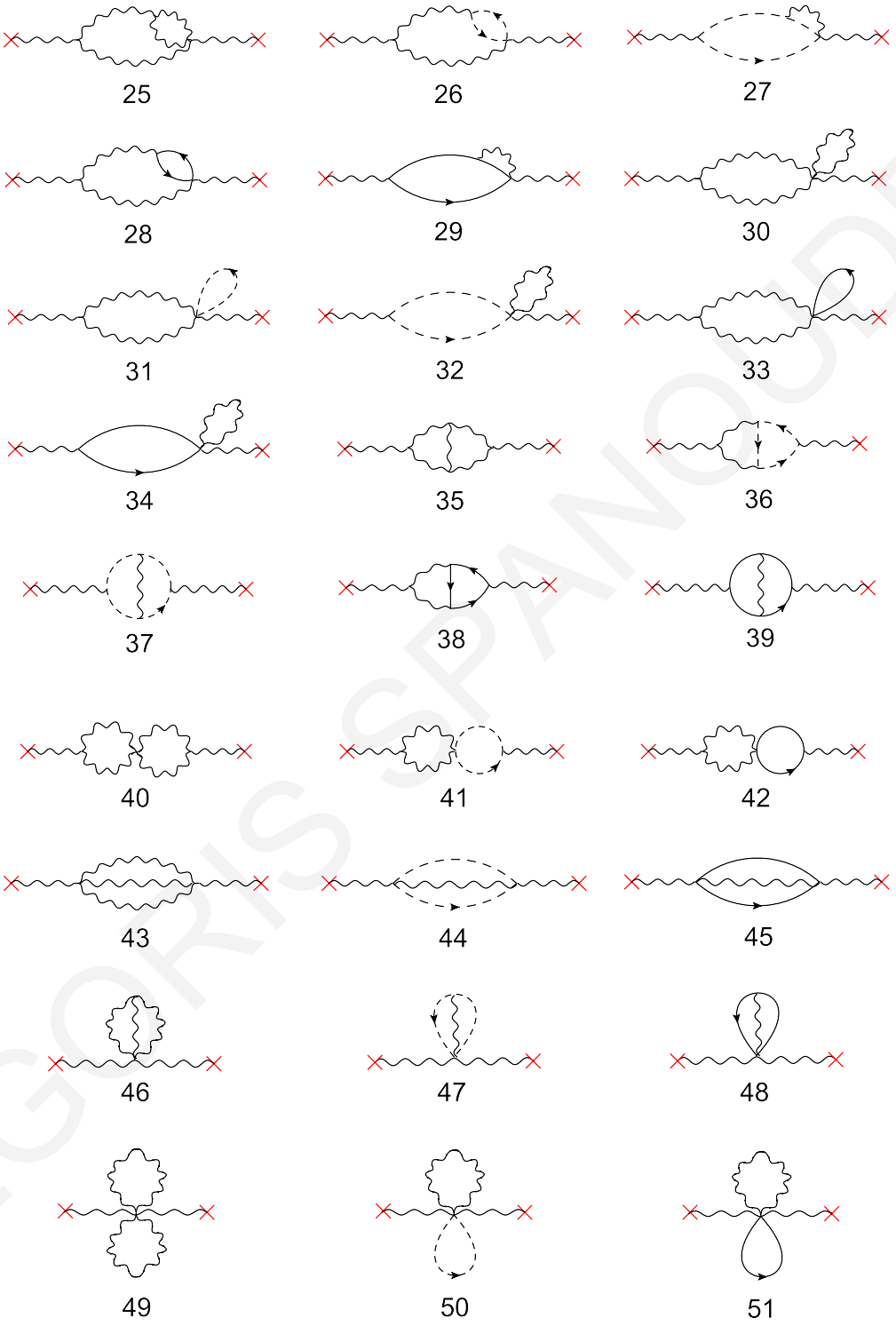

FIGURE 8.4: 2-loop diagrams contributing to $\nu^{(2)}(p)$. Wavy lines (without) ending on a cross represent (quantum) background gluons. Solid (dashed) lines represent fermions (ghosts). Solid boxes denote vertices stemming from the measure part of the action. A solid circle is a one-loop fermion mass counterterm. Both directions of the ghost (fermion) arrow in diagram 27 (29) must be considered. (2/2)

Coefficient	Wilson	Tree-level Symanzik	Iwasaki
$c_G^{46+47+48}{}_{(0,1)}$	2.40247(12)	0.16082(1)	0.17577(2)
$c_G^{46+47+48}{}_{(1,0)}$	-0.36158(2)	-0.01763(1)	-0.00607(1)
$c_G^{46+47+48}{}_{(1,1)}$	0.09040(1)	0.00564(1)	0.00534(1)
$c_F^{46+47+48}{}_{(0,0,0,-1)}$	0.06203(1)	0.00536(1)	0.00693(1)
$c_F^{46+47+48}{}_{(0,0,0,1)}$	0.06203(1)	0.00536(1)	0.00693(1)
$c_F^{46+47+48}{}_{(0,0,1,-1)}$	1.51384(31)	0.06582(1)	0.03475(1)
$c_F^{46+47+48}{}_{(0,0,1,1)}$	-3.10804(23)	-0.15790(1)	-0.11796(1)
$c_F^{46+47+48}{}_{(0,0,2,-1)}$	-7.40132(108)	-0.32062(5)	-0.17028(2)
$c_F^{46+47+48}{}_{(0,0,2,1)}$	11.48770(100)	0.49898(4)	0.26796(2)
$c_F^{46+47+48}{}_{(0,1,0,-1)}$	0.00635(1)	0.00034(1)	0.00024(1)
$c_F^{46+47+48}{}_{(0,1,0,1)}$	-0.02539(1)	-0.00134(1)	-0.00095(1)
$c_F^{46+47+48}{}_{(0,1,1,-1)}$	-0.02346(1)	-0.00119(1)	-0.00078(1)
$c_F^{46+47+48}{}_{(0,1,1,1)}$	0.05988(1)	0.00286(1)	0.00168(1)
$c_F^{46+47+48}{}_{(0,2,0,1)}$	1.13002(9)	0.05671(1)	0.03678(1)
$c_F^{46+47+48}{}_{(1,0,1,-1)}$	0.28544(3)	0.00841(1)	-0.00170(1)
$c_F^{46+47+48}{}_{(1,0,1,1)}$	0.00846(1)	0.00721(1)	0.01427(1)
$c_F^{46+47+48}{}_{(1,0,2,-1)}$	-5.97145(27)	-0.25905(1)	-0.13728(1)
$c_F^{46+47+48}{}_{(1,0,2,1)}$	3.96778(22)	0.17199(1)	0.09075(1)
$c_F^{46+47+48}{}_{(1,0,3,-1)}$	11.10200(63)	0.48093(1)	0.25543(1)
$c_F^{46+47+48}{}_{(1,0,3,1)}$	-5.55101(44)	-0.24046(1)	-0.12772(1)
$c_F^{46+47+48}{}_{(1,1,0,-1)}$	0.00317(1)	0.00017(1)	0.00012(1)
$c_F^{46+47+48}{}_{(1,1,0,1)}$	-0.00080(1)	-0.00004(1)	-0.00003(1)
$c_F^{46+47+48}{}_{(1,1,1,-1)}$	-0.03299(1)	-0.00169(1)	-0.00114(1)
$c_F^{46+47+48}{}_{(1,1,1,1)}$	0.02550(1)	0.00133(1)	0.00093(1)
$c_F^{46+47+48}{}_{(1,1,2,-1)}$	0.03519(1)	0.00178(1)	0.00117(1)
$c_F^{46+47+48}{}_{(1,1,2,1)}$	-0.01760(1)	-0.00089(1)	-0.00058(1)
$c_F^{46+47+48}{}_{(1,2,0,-1)}$	-0.18833(1)	-0.00945(1)	-0.00613(1)
$c_F^{46+47+48}{}_{(1,2,0,1)}$	0.04708(1)	0.00236(1)	0.00153(1)

TABLE 8.2: Numerical coefficients for the quantity $\nu^{(2)}(p)$ for the diagrams $d_{46} + d_{47} + d_{48}$.

Coefficient	Wilson	Tree-level Symanzik	Iwasaki
$c_G^{49+50+51}{}_{(0,-1)}$	-2.20769(1)	-0.17004(1)	-0.18512(1)
$c_G^{49+50+51}{}_{(0,0)}$	2.36345(1)	0.164452(1)	0.137555(1)
$c_F^{49+50+51}{}_{(0,0,0,-1)}$	0.24985(1)	0.01293(1)	0.00955(1)
$c_F^{49+50+51}{}_{(0,0,0,1)}$	-0.24985(1)	-0.01293(1)	-0.00955(1)
$c_F^{49+50+51}{}_{(0,0,1,-1)}$	-2.41898(1)	-0.110748(1)	-0.06358(1)
$c_F^{49+50+51}{}_{(0,0,1,1)}$	0.10192(1)	-0.05751(1)	-0.12111(1)
$c_F^{49+50+51}{}_{(0,0,2,-1)}$	9.67591(1)	0.43068(1)	0.23758(1)
$c_F^{49+50+51}{}_{(0,0,2,1)}$	-3.99855(1)	-0.02995(1)	0.16921(1)
$c_G^{49+50+51}{}_{(1,-1)}$	1.23370(1)	-0.02132(1)	-0.08316(1)
$c_G^{49+50+51}{}_{(1,0)}$	-2.67389(1)	0.04611(1)	0.20856(1)
$c_G^{49+50+51}{}_{(1,1)}$	1.44106(1)	-0.02306(1)	-0.12579(1)
$c_F^{49+50+51}{}_{(1,0,1,-1)}$	-2.79376(1)	-0.13014(1)	-0.07790(1)
$c_F^{49+50+51}{}_{(1,0,1,1)}$	2.78102(1)	0.13733(1)	0.09304(1)
$c_F^{49+50+51}{}_{(1,0,2,-1)}$	13.30440(1)	0.59680(1)	0.33294(1)
$c_F^{49+50+51}{}_{(1,0,2,1)}$	-8.81439(1)	-0.37470(1)	-0.18050(1)
$c_F^{49+50+51}{}_{(0,0,3,-1)}$	-14.51390(1)	-0.64602(1)	-0.35636(1)
$c_F^{49+50+51}{}_{(0,0,3,1)}$	9.67591(1)	0.43068(1)	0.23758(1)

TABLE 8.3: Numerical coefficients for the quantity $\nu^{(2)}(p)$ for the diagrams $d_{49} + d_{50} + d_{51}$.

Chapter 9

Conclusions

In this thesis, we study the perturbative renormalization of several quantum operators and other fundamental quantities, in the context of strong interaction Physics on the lattice. To this end, a number of higher-order calculations using a large family of improved lattice actions, which are currently used in numerical simulations by major international groups (e.g., ETMC, QCDSF, Wuppertal-Budapest Collaborations), are performed and presented in this dissertation. Our perturbative analysis of these calculations will be a guidance to the development of nonperturbative renormalization prescriptions. Also our results will give a cross check for nonperturbative estimates and will be combined with nonperturbative data in order to convert the lattice results to renormalized quantities in continuum renormalization schemes. Let us summarize our conclusions form these calculations.

In Chapter 3, we have evaluated the two-point bare Green's functions of straight Wilson-line operators, the renormalization factors in RI′ and $\overline{\text{MS}}$ schemes, as well as the conversion factors of these operators between the two renormalization schemes. The novel aspect of this work is the presence of nonzero quark masses in our computations, which results in mixing among these operators into pairs, both in the continuum and on the lattice. Finite mixing appears in the continuum, due to the chiral-symmetry breaking of mass terms in the fermion action. Comparing to the massless case on the lattice [14], the mixing pairs remain the same for flavor-singlet operators, i.e. $(\mathcal{O}_{\Gamma_1}, \mathcal{O}_{\Gamma_2})$, where $(\Gamma_1, \Gamma_2) = (\mathbb{1}, \gamma_1)$, $(\gamma_5\gamma_2, \gamma_3\gamma_4)$, $(\gamma_5\gamma_3, \gamma_4\gamma_2)$, $(\gamma_5\gamma_4, \gamma_2\gamma_3)$, where by convention 1 is the direction of the straight Wilson line and 2, 3, 4 are directions perpendicular to it. However, for the nonsinglet operators with

different masses of external quark fields, flavor-symmetry breaking leads to additional mixing pairs: $(\gamma_5, \gamma_5\gamma_1)$, $(\gamma_2, \gamma_1\gamma_2)$, $(\gamma_3, \gamma_1\gamma_3)$, $(\gamma_4, \gamma_1\gamma_4)$. As a consequence, the conversion factors are generally nondiagonal 2×2 matrices. This is relevant for disentangling the observed operator mixing on the lattice. Also, comparing the massive and the massless cases, the effect of finite mass on renormalization of Wilson-line operators becomes significant for strange quarks (the third lightest quark flavor), as well as for heavier quarks. These are features of heavy-quark quasi-PDFs, which must be taken into account in their future nonperturbative study.

In Chapter 4, we have studied the one-loop renormalization of the nonlocal staple-shaped Wilson-line quark operators, both in dimensional regularization (DR) and on the lattice (Wilson/clover massless fermions and Symanzik-improved gluons). A novel aspect of this calculation is the presence of cusps in the Wilson line included in the definition of the nonlocal operators under study, which results in the appearance of additional logarithmic divergences. Operator mixing also occurs for chirality-breaking lattice actions. The mixing pairs are: $(\mathcal{O}_{\Gamma_1}, \mathcal{O}_{\Gamma_2})$, where $(\Gamma_1, \Gamma_2) = (\gamma_5, \gamma_5\gamma_{\mu_2})$, $(\gamma_i, \gamma_i\gamma_{\mu_2})$, $i \neq \mu_2$ (for notation, see Sec. 4.2.1) which differ from those of straight-line operators. This study is relevant for the nonperturbative investigations of quasi-TMDs. Also, the results of the present study provide additional information on the renormalization of general nonlocal operators on the lattice. The observed mixing pairs among operators with different Dirac structures depend on the direction of Wilson line in the end points. Thus, for a Wilson-line operator with n cusps, the mixing pattern is $(\mathcal{O}_\Gamma, \mathcal{O}_{\Gamma\not{\hat{\mu}}_i + \not{\hat{\mu}}_f\Gamma})$, where $\hat{\mu}_i$ ($\hat{\mu}_f$) is the direction of the Wilson line in the initial (final) end point.

In Chapter 5, a natural continuation of the one-loop calculation for the conversion factors between RI′-renormalized and $\overline{\text{MS}}$-renormalized straight-line operators to two-loops is presented. Higher-loop corrections will eliminate large truncation effects from the nonperturbative results. Based on extensive studies for systematic uncertainties on the renormalization functions for the straight Wilson line [99, 246], we find empirically that the one-loop conversion factor is sufficient for lattice spacing satisfying $|z|/a \leq 7{-}8$ and $(a\mu)^2$ within the interval $2 \leq (a\mu)^2 \leq 4$. Outside these regions, a two-loop conversion factor would be called for; clearly, however, other systematic uncertainties will also become more relevant (lattice artifacts, volume effects, etc). We provide preliminary results regarding only a number of the two-loop Feynman diagrams that contribute to the Green's functions of straight-line operators.

In Chapter 6, we have computed the two-loop difference between the singlet and nonsinglet perturbative renormalization factors of all staggered quark bilinears. As we observed, the difference is nonzero only for the axial vector operator. Our result is presented in RI′ and $\overline{\text{MS}}$ renormalization schemes, as well as in an alternative RI′ scheme, more appropriate for nonperturbative calculations. A novel aspect of the calculation is that the gluon links, which appear both in the staggered fermion action and in the definition of the staggered bilinear operators, are improved by applying a stout smearing procedure up to two times, iteratively. Compared to most other improved formulations of staggered fermions, the stout smearing action leads to smaller taste violating effects [205, 206, 247]. Application of stout improvement on staggered fermions thus far has been explored, by our group, only to one-loop computations [47]; a two-loop computation had never been investigated before. Our result demonstrates that the two smearing steps of the fermion action give better results than only one smearing step. Also, the stout smearing of the action is more effective in minimizing the difference of singlet and nonsinglet renormalization factor of axial vector operator than the stout smearing of operators. A significant part of this work is the development of a method for treating new nontrivial divergent integrals stemming from the staggered formalism.

Finally, in Chapter 8, we have presented the one-loop calculation of the two-point Green's functions of background and quantum gluon fields, which are related to the definition of lattice β function. We observed that the one-loop results are independent of the stout-smearing coefficient. We extract the ratio of energy scales $\Lambda_L/\Lambda_{\overline{\text{MS}}}$, as well as the first coefficient $d_1(a\bar{\mu})$ in the perturbative expansion of the running coupling. The computation of two-loop Feynman diagrams contributing to the two-point Green's functions of background field, is still in progress. Such computations using the SLiNC action, which is widely used in recent simulations, have never been done before. The results of such calculations can be used to make contact with a low momentum-regime of QCD. In particular, our results will be combined with extensive simulations performed by members of QCDSF Collaboration in the "Wilson gradient flow" scheme, which is being very actively investigated by a number of groups at present.

There are several future plans in which our work can be extended:

- The first one is the one-loop evaluation of lattice artifacts to all orders in the lattice spacing, for a range of numerical values of the external quark momentum,

of the momentum renormalization scales, and of the action parameters, which are mostly used in simulations. Such a procedure has been successfully employed to local operators [53, 248, 249]. The subtraction of the unwanted contributions of the finite lattice spacing from the nonperturbative estimates is essential in order to reduce large cutoff effects in the renormalized Green's functions of the local and nonlocal operators studied in this dissertation and to guarantee a rapid convergence to the continuum limit.

- Secondly, we intend to add stout smearing on gluon links appearing in the definition of the straight-line and staple-shaped operators and to investigate its impact to the elimination of ultraviolet (UV) divergences and of operator mixing; modern simulations employ such smearing techniques for more convergent results.

- Thirdly, our perturbative analysis can be also applied to the study of further composite Wilson-line operators, relevant to different quasidistribution functions, e.g., gluon quasi-PDFs, etc.

- Moreover, a possible extension of the work regarding singlet and nonsinglet local operators is the application of other actions currently used in numerical simulations (e.g. several variants of staggered fermion action: HYP smearing [26], HEX smearing [27], Asqtad [250]), including actions with more steps of stout smearing. In these cases, additional contributions to the renormalization functions are more convergent, and thus their perturbative treatment is simpler; nevertheless, the sheer size of the vertices (already with two stout-smearing steps we have encountered $\sim 10^6$ terms) renders the computation quite cumbersome.

- Finally, extended versions of $\bar{\psi}\Gamma\psi$ may be studied; in this case the Feynman diagrams of Fig. 6.1 will apply also to Wilson fermions and loop integrands will typically contain a plethora of new terms, which however will be convergent.

Appendix A

Notation and Conventions

In this appendix we specify our notation and conventions adopted in the main body of the Thesis. The conventions regard the Euclidean formulation of QCD, the Dirac algebra, the Lie algebra of su(N_c) and D-dimensional definitions of fields, operators, momentum vectors, and other quantities.

A.1 The Euclidean formulation of QCD

In Euclidean spacetime[1], QCD action reads:

$$S_{\rm QCD} = \int d^4x \left[\sum_{f=1}^{N_f=6} \bar{\psi}_f(x) \Big(\gamma_\mu D_\mu(x) + m_f \mathbb{1} \Big) \psi_f(x) + \frac{1}{2} tr \Big(G_{\mu\nu}(x) G_{\mu\nu}(x) \Big) \right], \quad \text{(A.1)}$$

where the quark (antiquark) field $\psi_f(x)$, $[\bar{\psi}_f(x) \equiv \psi_f^\dagger(x)\gamma_4]$ is a 4-spinor in Dirac space and an SU(3) triplet in color space, for each flavor f; the gluon field strength tensor $G_{\mu\nu}(x)$ $[= -G_{\nu\mu}(x)]$, $(\mu, \nu = 1, 2, 3, 4)$ is defined by:

$$G_{\mu\nu}(x) = \frac{i}{g_0} [D_\mu(x), D_\nu(x)], \quad \text{(A.2)}$$

where g_0 is the bare coupling constant and $D_\mu(x)$ is the Euclidean covariant derivative:

$$D_\mu(x) = \partial_\mu - i g_0 A_\mu(x). \quad \text{(A.3)}$$

[1] A Wick rotation from real to imaginary times $x^0 \to -ix_4$ changes the geometry of spacetime from Lorentzian to Euclidean.

The trace in Eq. (A.1) is taken over color indices. The gluon field $A_\mu(x)$ is an $su(3)$ algebra element in color space, and thus, can be written as $A_\mu(x) = A^a_\mu(x)T^a$, where T^a are the generators of the algebra and $a = 1, \ldots, N_c^2 - 1$ ($N_c = 3$). Moreover, γ_μ is a 4×4 Euclidean Dirac matrix defined in Sec. A.2. Also, the bare quark mass m_f differs for quarks with different flavor.

A.2 Dirac Algebra

In Euclidean spacetime, the Dirac matrices γ_μ ($\mu = 1, 2, 3, 4$) obey the anticommutation relations:

$$\{\gamma_\mu, \gamma_\nu\} = 2\delta_{\mu\nu}\mathbb{1}, \tag{A.4}$$

where $\delta_{\mu\nu}$ is the Euclidean metric tensor and $\mathbb{1}$ is the 4×4 unit matrix. In addition, the γ_5 Dirac matrix is defined as the product:

$$\gamma_5 = \gamma_1\gamma_2\gamma_3\gamma_4, \tag{A.5}$$

which satisfies the following relations:

$$\{\gamma_5, \gamma_\mu\} = 0, \quad \gamma_5^2 = \mathbb{1}. \tag{A.6}$$

In chiral representation the Euclidean Dirac matrices have the following explicit 4×4 form:

$$\gamma_1 = \begin{pmatrix} 0 & 0 & 0 & -i \\ 0 & 0 & -i & 0 \\ 0 & i & 0 & 0 \\ i & 0 & 0 & 0 \end{pmatrix}, \ \gamma_2 = \begin{pmatrix} 0 & 0 & 0 & -1 \\ 0 & 0 & 1 & 0 \\ 0 & 1 & 0 & 0 \\ -1 & 0 & 0 & 0 \end{pmatrix}, \ \gamma_3 = \begin{pmatrix} 0 & 0 & -i & 0 \\ 0 & 0 & 0 & i \\ i & 0 & 0 & 0 \\ 0 & -i & 0 & 0 \end{pmatrix},$$
$$\gamma_4 = \begin{pmatrix} 0 & 0 & 1 & 0 \\ 0 & 0 & 0 & 1 \\ 1 & 0 & 0 & 0 \\ 0 & 1 & 0 & 0 \end{pmatrix}, \ \gamma_5 = \begin{pmatrix} 1 & 0 & 0 & 0 \\ 0 & 1 & 0 & 0 \\ 0 & 0 & -1 & 0 \\ 0 & 0 & 0 & -1 \end{pmatrix}. \tag{A.7}$$

It is obvious that $\gamma_\mu = \gamma_\mu^\dagger = \gamma_\mu^{-1}$, ($\mu = 1, 2, 3, 4, 5$).

A.3 su(N_c) Lie algebra

The fundamental representation of the SU(N_c) group is given by complex $N_c \times N_c$ matrices which are unitary and have their determinant equal to 1, i.e. if U_i are elements of SU(N_c) they obey $U_i^\dagger = U_i^{-1}$ and $\det(U_i) = 1$. A convenient way of representing a SU(N_c) matrix is to express it as an exponential of basis matrices T^a, the so-called generators of su(N_c) Lie algebra. In particular, an element U of SU(N_c) is written as:

$$U = \exp(i \sum_{a=1}^{N_c^2-1} \phi^a T^a) \tag{A.8}$$

where ϕ^a are used to parametrized U and $a = 1, \ldots (N_c^2 - 1)$ [$(N_c^2 - 1)$ is the number of independent parameters that are needed to describe the SU(N_c) matrices]. The generators T^a must be traceless, complex and hermitian $N_c \times N_c$ matrices obeying the commutation relations:

$$[T^a, T^b] = i f^{abc} T^c, \tag{A.9}$$

where f^{abc} is called structure constants and they are completely antisymmetric in an orthonormal basis of generators. A particular choice for the normalization condition, which is adopted in the Thesis, is:

$$tr(T^a T^b) = \frac{1}{2}\delta^{ab}. \tag{A.10}$$

Some useful identities of generators and structure constants are:

$$T^a T^a = C_F \mathbb{1}, \tag{A.11}$$

$$f^{acd} f^{bcd} = C_A \delta^{ab}, \tag{A.12}$$

where $C_F = (N_c^2 - 1)/(2N_c)$ and $C_A = N_c$ are the Casimir operators in the fundamental and adjoint representations, respectively.

A.4 D-dimensional quantities

Regarding the extension of 4-dimensional quantities to D-dimensional quantities in our calculations using the dimensional regularization, we adopt the following standard choices:

- The continuum Euclidean action has the same form as the 4-dimensional one, defined in Eq. (A.1), where the sums over vector indices μ, ν range from 1 to D rather than 1 to 4. We note that all D components of the quantum fields are nonzero. However, in the case of introducing background fields in the action, these fields have only 4 out of D components not equal to zero.

- The unit matrix in Dirac space obeys $\mathrm{tr}(\mathbb{1}) = 4$.

- A standard extension of γ_5 in D-dimensions satisfies the following relations [251]:

$$\{\gamma_5, \gamma_\mu\} = 0, \ (\mu = 1, 2, 3, 4), \tag{A.13}$$

$$[\gamma_5, \gamma_\mu] = 0, \ (\text{otherwise}). \tag{A.14}$$

  However, in our particular one-loop calculations, only the (anti)commutator of γ_5 with γ_μ, $(\mu = 1, 2, 3, 4)$ was needed and thus the corresponding results do not depend on the chosen extension of γ_5. Therefore, violations of chiral symmetry, coming from the choice of γ_5 extension to D dimensions are absent.

- External momentum vectors are considered as only 4-dimensional.

References

[1] K. G. Wilson, Confinement of Quarks, Phys. Rev. D10 (1974) 2445–2459, [,319(1974)]. doi:10.1103/PhysRevD.10.2445.

[2] M. Constantinou, Hadron Structure, PoS LATTICE2014 (2015) 001. arXiv:1411.0078, doi:10.22323/1.214.0001.

[3] M. Constantinou, Recent progress in hadron structure from Lattice QCD, PoS CD15 (2015) 009. arXiv:1511.00214, doi:10.22323/1.253.0009.

[4] J. Giedt, A. W. Thomas, R. D. Young, Dark matter, the CMSSM and lattice QCD, Phys. Rev. Lett. 103 (2009) 201802. arXiv:0907.4177, doi:10.1103/PhysRevLett.103.201802.

[5] C. Davies, P. Lepage, Lattice QCD meets experiment in hadron physics, AIP Conf. Proc. 717 (1) (2004) 615–624. arXiv:hep-ph/0311041, doi:10.1063/1.1799771.

[6] S. J. Brodsky, A. L. Deshpande, H. Gao, R. D. McKeown, C. A. Meyer, Z.-E. Meziani, R. G. Milner, J. Qiu, D. G. Richards, C. D. Roberts, QCD and Hadron PhysicsarXiv:1502.05728.

[7] E.-C. Aschenauer, et al., Pre-Town Meeting on Spin Physics at an Electron-Ion Collider, Eur. Phys. J. A53 (4) (2017) 71. arXiv:1410.8831, doi:10.1140/epja/i2017-12251-4.

[8] C. Alexandrou, M. Constantinou, K. Hadjiyiannakou, K. Jansen, C. Kallidonis, G. Koutsou, A. Vaquero Avilés-Casco, C. Wiese, Nucleon Spin and Momentum Decomposition Using Lattice QCD Simulations, Phys. Rev. Lett. 119 (14) (2017) 142002. arXiv:1706.02973, doi:10.1103/PhysRevLett.119.142002.

[9] M. Marinkovic, Leading hadronic contribution to muon g-2 from lattice QCD and the MUonE experiment , PoS LATTICE2018 (2018) 012.

[10] L. Jin, Review of Lattice Muon g-2 HLbL Calculation, PoS LATTICE2018 (2018) 011.

[11] W. Bietenholz, U. Gerber, M. Pepe, U. J. Wiese, Topological Lattice Actions, JHEP 12 (2010) 020. arXiv:1009.2146, doi:10.1007/JHEP12(2010)020.

[12] B. Sheikholeslami, R. Wohlert, Improved Continuum Limit Lattice Action for QCD with Wilson Fermions, Nucl. Phys. B259 (1985) 572. doi:10.1016/0550-3213(85)90002-1.

[13] J. B. Kogut, L. Susskind, Hamiltonian Formulation of Wilson's Lattice Gauge Theories, Phys. Rev. D11 (1975) 395–408. doi:10.1103/PhysRevD.11.395.

[14] R. Narayanan, H. Neuberger, Chiral fermions on the lattice, Phys. Rev. Lett. 71 (20) (1993) 3251. arXiv:hep-lat/9308011, doi:10.1103/PhysRevLett.71.3251.

[15] H. Neuberger, More about exactly massless quarks on the lattice, Phys. Lett. B427 (1998) 353–355. arXiv:hep-lat/9801031, doi:10.1016/S0370-2693(98)00355-4.

[16] H. Neuberger, Exact chiral symmetry on the lattice, Ann. Rev. Nucl. Part. Sci. 51 (2001) 23–52. arXiv:hep-lat/0101006, doi:10.1146/annurev.nucl.51.101701.132438.

[17] D. B. Kaplan, A Method for simulating chiral fermions on the lattice, Phys. Lett. B288 (1992) 342–347. arXiv:hep-lat/9206013, doi:10.1016/0370-2693(92)91112-M.

[18] V. Furman, Y. Shamir, Axial symmetries in lattice QCD with Kaplan fermions, Nucl. Phys. B439 (1995) 54–78. arXiv:hep-lat/9405004, doi:10.1016/0550-3213(95)00031-M.

[19] H. B. Nielsen, M. Ninomiya, Absence of Neutrinos on a Lattice. 1. Proof by Homotopy Theory, Nucl. Phys. B185 (1981) 20, [,533(1980)]. doi:10.1016/0550-3213(81)90361-8,10.1016/0550-3213(82)90011-6.

[20] R. Frezzotti, P. A. Grassi, S. Sint, P. Weisz, Lattice QCD with a chirally twisted mass term, JHEP 08 (2001) 058. arXiv:hep-lat/0101001.

[21] R. Frezzotti, G. C. Rossi, Chirally improving Wilson fermions. 1. O(a) improvement, JHEP 08 (2004) 007. arXiv:hep-lat/0306014, doi:10.1088/1126-6708/2004/08/007.

[22] R. Frezzotti, G. C. Rossi, Chirally improving Wilson fermions, Nucl. Phys. Proc. Suppl. 129 (2004) 880–882, [,880(2003)]. arXiv:hep-lat/0309157, doi:10.1016/S0920-5632(03)02741-5.

[23] R. Frezzotti, G. C. Rossi, Twisted mass lattice QCD with mass nondegenerate quarks, Nucl. Phys. Proc. Suppl. 128 (2004) 193–202, [,193(2003)]. arXiv:hep-lat/0311008, doi:10.1016/S0920-5632(03)02477-0.

[24] C. Morningstar, M. J. Peardon, Analytic smearing of SU(3) link variables in lattice QCD, Phys. Rev. D69 (2004) 054501. arXiv:hep-lat/0311018, doi:10.1103/PhysRevD.69.054501.

[25] R. Horsley, H. Perlt, P. E. L. Rakow, G. Schierholz, A. Schiller, Perturbative determination of c(SW) for plaquette and Symanzik gauge action and stout link clover fermions, Phys. Rev. D78 (2008) 054504. arXiv:arXiv:0807.0345, doi:10.1103/PhysRevD.78.054504.

[26] A. Hasenfratz, F. Knechtli, Flavor symmetry and the static potential with hypercubic blocking, Phys. Rev. D64 (2001) 034504. arXiv:hep-lat/0103029, doi:10.1103/PhysRevD.64.034504.

[27] S. Capitani, S. Durr, C. Hoelbling, Rationale for UV-filtered clover fermions, JHEP 11 (2006) 028. arXiv:hep-lat/0607006, doi:10.1088/1126-6708/2006/11/028.

[28] G. P. Lepage, Flavor symmetry restoration and Symanzik improvement for staggered quarks, Phys. Rev. D59 (1999) 074502. arXiv:hep-lat/9809157, doi:10.1103/PhysRevD.59.074502.

[29] E. Follana, Q. Mason, C. Davies, K. Hornbostel, G. P. Lepage, J. Shigemitsu, H. Trottier, K. Wong, Highly improved staggered quarks on the lattice, with applications to charm physics, Phys. Rev. D75 (2007) 054502. arXiv:hep-lat/0610092, doi:10.1103/PhysRevD.75.054502.

[30] M. Luscher, Exact chiral symmetry on the lattice and the Ginsparg-Wilson relation, Phys. Lett. B428 (1998) 342–345. arXiv:hep-lat/9802011, doi:10.1016/S0370-2693(98)00423-7.

[31] K. Symanzik, Continuum Limit and Improved Action in Lattice Theories. 1. Principles and phi**4 Theory, Nucl. Phys. B226 (1983) 187–204. doi:10.1016/0550-3213(83)90468-6.

[32] M. Luscher, P. Weisz, On-Shell Improved Lattice Gauge Theories, Commun. Math. Phys. 97 (1985) 59, [Erratum: Commun. Math. Phys.98,433(1985)]. doi:10.1007/BF01206178.

[33] M. Luscher, P. Weisz, Computation of the Action for On-Shell Improved Lattice Gauge Theories at Weak Coupling, Phys. Lett. 158B (1985) 250–254. doi:10.1016/0370-2693(85)90966-9.

[34] T. Takaishi, Heavy quark potential and effective actions on blocked configurations, Phys. Rev. D54 (1996) 1050–1053. doi:10.1103/PhysRevD.54.1050.

[35] Y. Iwasaki, Renormalization Group Analysis of Lattice Theories and Improved Lattice Action. II. Four-dimensional non-Abelian SU(N) gauge modelarXiv:1111.7054.

[36] M. Luscher, S. Sint, R. Sommer, P. Weisz, U. Wolff, Nonperturbative O(a) improvement of lattice QCD, Nucl. Phys. B491 (1997) 323–343. arXiv:hep-lat/9609035, doi:10.1016/S0550-3213(97)00080-1.

[37] G. Martinelli, S. Petrarca, C. T. Sachrajda, A. Vladikas, Nonperturbative renormalization of two quark operators with an improved lattice fermion action, Phys. Lett. B311 (1993) 241–248, [Erratum: Phys. Lett.B317,660(1993)]. doi:10.1016/0370-2693(93)90562-V.

[38] G. Martinelli, C. Pittori, C. T. Sachrajda, M. Testa, A. Vladikas, A General method for nonperturbative renormalization of lattice operators, Nucl. Phys. B445 (1995) 81–108. arXiv:hep-lat/9411010, doi:10.1016/0550-3213(95)00126-D.

[39] M. Lüscher, P. Weisz, Computation of the relation between the bare lattice coupling and the MS coupling in SU(N) gauge theories to two loops, Nucl. Phys. B452 (1995) 234–260. arXiv:hep-lat/9505011, doi:10.1016/0550-3213(95)00338-S.

[40] R. Narayanan, U. Wolff, Two loop computation of a running coupling lattice Yang-Mills theory, Nucl. Phys. B444 (1995) 425–446. arXiv:hep-lat/9502021, doi:10.1016/0550-3213(95)00170-W.

[41] A. Bode, U. Wolff, P. Weisz, Two loop computation of the Schrodinger functional in pure SU(3) lattice gauge theory, Nucl. Phys. B540 (1999) 491–499. arXiv:hep-lat/9809175, doi:10.1016/S0550-3213(98)00772-X.

[42] A. Bode, P. Weisz, U. Wolff, Two loop lattice expansion of the Schrodinger functional coupling in improved QCD, Nucl. Phys. Proc. Suppl. 83 (2000) 920–922. arXiv:hep-lat/9908044, doi:10.1016/S0920-5632(00)91845-0.

[43] A. Bode, P. Weisz, U. Wolff, Two loop computation of the Schrodinger functional in lattice QCD, Nucl. Phys. B576 (2000) 517–539, [Erratum: Nucl. Phys.B600,453(2001)]. arXiv:hep-lat/9911018, doi:10.1016/S0550-3213(00)00187-5,10.1016/S0550-3213(01)00045-1,10.1016/S0550-3213(01)00267-X.

[44] C. Christou, A. Feo, H. Panagopoulos, E. Vicari, The three loop β-function of $SU(N)$ lattice gauge theories with Wilson fermions, Nucl. Phys. B525 (1998) 387–400, [Erratum: Nucl. Phys.B608,479(2001)]. arXiv:hep-lat/9801007, doi:10.1016/S0550-3213(01)00268-1,10.1016/S0550-3213(98)00248-X.

[45] A. Bode, H. Panagopoulos, The Three loop beta function of QCD with the clover action, Nucl. Phys. B625 (2002) 198–210. arXiv:hep-lat/0110211, doi:10.1016/S0550-3213(02)00012-3.

[46] A. Bode, H. Panagopoulos, Y. Proestos, O(a) improved QCD: The Three loop beta function, and the critical hopping parameter, Nucl. Phys. Proc. Suppl. 106 (2002) 832–834. arXiv:hep-lat/0110225, doi:10.1016/S0920-5632(01)01858-8.

[47] M. Constantinou, H. Panagopoulos, QCD with overlap fermions: Running coupling and the 3-loop beta-function, Phys. Rev. D76 (2007) 114504. arXiv:0709.4368, doi:10.1103/PhysRevD.76.114504.

[48] Q. Mason, H. D. Trottier, R. Horgan, C. T. H. Davies, G. P. Lepage, High-precision determination of the light-quark masses from realistic lattice QCD, Phys. Rev. D73 (2006) 114501. arXiv:hep-ph/0511160, doi:10.1103/PhysRevD.73.114501.

[49] A. Skouroupathis, H. Panagopoulos, Two-loop renormalization of scalar and pseudoscalar fermion bilinears on the lattice, Phys. Rev. D76 (2007) 094514, [Erratum: Phys. Rev.D78,119901(2008)]. arXiv:0707.2906, doi:10.1103/PhysRevD.76.094514,10.1103/PhysRevD.78.119901.

[50] A. Skouroupathis, H. Panagopoulos, Two-loop renormalization of vector, axial-vector and tensor fermion bilinears on the lattice, Phys. Rev. D79 (2009) 094508. arXiv:0811.4264, doi:10.1103/PhysRevD.79.094508.

[51] M. Constantinou, P. Dimopoulos, R. Frezzotti, V. Lubicz, H. Panagopoulos, A. Skouroupathis, F. Stylianou, Perturbative renormalization factors and O(a^2) corrections for lattice 4-fermion operators with improved fermion/gluon actions, Phys. Rev. D83 (2011) 074503. arXiv:1011.6059, doi:10.1103/PhysRevD.83.074503.

[52] M. Constantinou, M. Costa, M. Göckeler, R. Horsley, H. Panagopoulos, H. Perlt, P. E. L. Rakow, G. Schierholz, A. Schiller, Perturbatively improving regularization-invariant momentum scheme renormalization constants, Phys. Rev. D87 (9) (2013) 096019. arXiv:1303.6776, doi:10.1103/PhysRevD.87.096019.

[53] C. Alexandrou, M. Constantinou, H. Panagopoulos, Renormalization functions for $N_f = 2$ and $N_f = 4$ twisted mass fermions, Phys. Rev. D95 (3) (2017) 034505. arXiv:1509.00213, doi:10.1103/PhysRevD.95.034505.

[54] M. Brambilla, F. Di Renzo, High-loop perturbative renormalization constants for Lattice QCD (II): three-loop quark currents for tree-level Symanzik improved gauge action and n_f=2 Wilson fermions, Eur. Phys. J. C73 (12) (2013) 2666. arXiv:1310.4981, doi:10.1140/epjc/s10052-013-2666-5.

[55] M. Dalla Brida, M. Lüscher, SMD-based numerical stochastic perturbation theory, Eur. Phys. J. C77 (5) (2017) 308. arXiv:1703.04396, doi:10.1140/epjc/s10052-017-4839-0.

[56] J. Ashman, et al., A Measurement of the Spin Asymmetry and Determination of the Structure Function g(1) in Deep Inelastic Muon-Proton Scattering, Phys. Lett. B206 (1988) 364, [,340(1987)]. doi:10.1016/0370-2693(88)91523-7.

[57] R. L. Jaffe, A. Manohar, The G(1) Problem: Fact and Fantasy on the Spin of the Proton, Nucl. Phys. B337 (1990) 509–546. doi:10.1016/0550-3213(90)90506-9.

[58] X.-D. Ji, Gauge-Invariant Decomposition of Nucleon Spin, Phys. Rev. Lett. 78 (1997) 610–613. arXiv:hep-ph/9603249, doi:10.1103/PhysRevLett.78.610.

[59] G. S. Bali, S. Collins, A. Schafer, Effective noise reduction techniques for disconnected loops in Lattice QCD, Comput. Phys. Commun. 181 (2010) 1570–1583. arXiv:0910.3970, doi:10.1016/j.cpc.2010.05.008.

[60] J. Green, N. Hasan, S. Meinel, M. Engelhardt, S. Krieg, J. Laeuchli, J. Negele, K. Orginos, A. Pochinsky, S. Syritsyn, Up, down, and strange nucleon axial form factors from lattice QCD, Phys. Rev. D95 (11) (2017) 114502. arXiv:1703.06703, doi:10.1103/PhysRevD.95.114502.

[61] C. Alexandrou, et al., Nucleon scalar and tensor charges using lattice QCD simulations at the physical value of the pion mass, Phys. Rev. D95 (11) (2017) 114514, [erratum: Phys. Rev.D96,no.9,099906(2017)]. arXiv:1703.08788, doi:10.1103/PhysRevD.96.099906,10.1103/PhysRevD.95.114514.

[62] N. Yamanaka, S. Hashimoto, T. Kaneko, H. Ohki, Nucleon charges with dynamical overlap fermions, Phys. Rev. D98 (5) (2018) 054516. arXiv:1805.10507, doi:10.1103/PhysRevD.98.054516.

[63] H.-W. Lin, R. Gupta, B. Yoon, Y.-C. Jang, T. Bhattacharya, Quark contribution to the proton spin from 2+1+1-flavor lattice QCD, Phys. Rev. D98 (9) (2018) 094512. arXiv:1806.10604, doi:10.1103/PhysRevD.98.094512.

[64] R. Gupta, B. Yoon, T. Bhattacharya, V. Cirigliano, Y.-C. Jang, H.-W. Lin, Flavor diagonal tensor charges of the nucleon from (2+1+1)-flavor lattice QCD, Phys. Rev. D98 (9) (2018) 091501. arXiv:1808.07597, doi:10.1103/PhysRevD.98.091501.

[65] A. J. Chambers, R. Horsley, Y. Nakamura, H. Perlt, P. E. L. Rakow, G. Schierholz, A. Schiller, J. M. Zanotti, A novel approach to nonperturbative renormalization of singlet and nonsinglet lattice operators, Phys. Lett. B740 (2015) 30–35. arXiv:1410.3078, doi:10.1016/j.physletb.2014.11.033.

[66] C. Bouchard, C. C. Chang, T. Kurth, K. Orginos, A. Walker-Loud, On the Feynman-Hellmann Theorem in Quantum Field Theory and the Calculation of Matrix Elements, Phys. Rev. D96 (1) (2017) 014504. arXiv:1612.06963, doi:10.1103/PhysRevD.96.014504.

[67] G. S. Bali, et al., Strangeness Contribution to the Proton Spin from Lattice QCD, Phys. Rev. Lett. 108 (2012) 222001. arXiv:1112.3354, doi:10.1103/PhysRevLett.108.222001.

[68] R. P. Feynman, Very high-energy collisions of hadrons, Phys. Rev. Lett. 23 (1969) 1415–1417, [,494(1969)]. doi:10.1103/PhysRevLett.23.1415.

[69] R. P. Feynman, The behavior of hadron collisions at extreme energies, Conf. Proc. C690905 (1969) 237–258.

[70] A. V. Radyushkin, Scaling limit of deeply virtual Compton scattering, Phys. Lett. B380 (1996) 417–425. arXiv:hep-ph/9604317, doi:10.1016/0370-2693(96)00528-X.

[71] M. Diehl, Generalized parton distributions, Phys. Rept. 388 (2003) 41–277. arXiv:hep-ph/0307382, doi:10.1016/j.physrep.2003.08.002,10.3204/DESY-THESIS-2003-018.

[72] X. Ji, Generalized parton distributions, Ann. Rev. Nucl. Part. Sci. 54 (2004) 413–450. doi:10.1146/annurev.nucl.54.070103.181302.

[73] A. V. Belitsky, A. V. Radyushkin, Unraveling hadron structure with generalized parton distributions, Phys. Rept. 418 (2005) 1–387. arXiv:hep-ph/0504030, doi:10.1016/j.physrep.2005.06.002.

[74] J. C. Collins, D. E. Soper, Back-To-Back Jets in QCD, Nucl. Phys. B193 (1981) 381, [Erratum: Nucl. Phys.B213,545(1983)]. doi:10.1016/0550-3213(81)90339-4.

[75] D. Boer, et al., Gluons and the quark sea at high energies: Distributions, polarization, tomography. arXiv:1108.1713.

[76] A. Accardi, et al., Electron Ion Collider: The Next QCD Frontier, Eur. Phys. J. A52 (9) (2016) 268. arXiv:1212.1701, doi:10.1140/epja/i2016-16268-9.

[77] R. Angeles-Martinez, et al., Transverse Momentum Dependent (TMD) parton distribution functions: status and prospects, Acta Phys. Polon. B46 (12) (2015) 2501–2534. arXiv:1507.05267, doi:10.5506/APhysPolB.46.2501.

[78] J. C. Collins, D. E. Soper, G. F. Sterman, Factorization of Hard Processes in QCD, Adv. Ser. Direct. High Energy Phys. 5 (1989) 1–91. arXiv:hep-ph/0409313, doi:10.1142/9789814503266_0001.

[79] R. Devenish, A. Cooper-Sarkar, Deep inelastic scattering, Oxford, UK: Univ. Pr., 2004.

[80] X.-D. Ji, Deeply virtual Compton scattering, Phys. Rev. D55 (1997) 7114–7125. arXiv:hep-ph/9609381, doi:10.1103/PhysRevD.55.7114.

[81] E. Perez, E. Rizvi, The Quark and Gluon Structure of the Proton, Rept. Prog. Phys. 76 (2013) 046201. arXiv:1208.1178, doi:10.1088/0034-4885/76/4/046201.

[82] A. De Roeck, R. S. Thorne, Structure Functions, Prog. Part. Nucl. Phys. 66 (2011) 727–781. arXiv:1103.0555, doi:10.1016/j.ppnp.2011.06.001.

[83] S. Alekhin, et al., The PDF4LHC Working Group Interim ReportarXiv:1101.0536.

[84] R. D. Ball, et al., Parton Distribution Benchmarking with LHC Data, JHEP 04 (2013) 125. arXiv:1211.5142, doi:10.1007/JHEP04(2013)125.

[85] S. Forte, G. Watt, Progress in the Determination of the Partonic Structure of the Proton, Ann. Rev. Nucl. Part. Sci. 63 (2013) 291–328. arXiv:1301.6754, doi:10.1146/annurev-nucl-102212-170607.

[86] P. Jimenez-Delgado, W. Melnitchouk, J. F. Owens, Parton momentum and helicity distributions in the nucleon, J. Phys. G40 (2013) 093102. arXiv:1306.6515, doi:10.1088/0954-3899/40/9/093102.

[87] J. Rojo, et al., The PDF4LHC report on PDFs and LHC data: Results from Run I and preparation for Run II, J. Phys. G42 (2015) 103103. arXiv:1507.00556, doi:10.1088/0954-3899/42/10/103103.

[88] J. Butterworth, et al., PDF4LHC recommendations for LHC Run II, J. Phys. G43 (2016) 023001. arXiv:1510.03865, doi:10.1088/0954-3899/43/2/023001.

[89] A. Accardi, et al., A Critical Appraisal and Evaluation of Modern PDFs, Eur. Phys. J. C76 (8) (2016) 471. arXiv:1603.08906, doi:10.1140/epjc/s10052-016-4285-4.

[90] J. Gao, L. Harland-Lang, J. Rojo, The Structure of the Proton in the LHC Precision Era, Phys. Rept. 742 (2018) 1–121. arXiv:1709.04922, doi:10.1016/j.physrep.2018.03.002.

[91] L. V. Gribov, E. M. Levin, M. G. Ryskin, Semihard Processes in QCD, Phys. Rept. 100 (1983) 1–150. doi:10.1016/0370-1573(83)90022-4.

[92] A. H. Mueller, J.-w. Qiu, Gluon Recombination and Shadowing at Small Values of x, Nucl. Phys. B268 (1986) 427–452. doi:10.1016/0550-3213(86)90164-1.

[93] L. D. McLerran, R. Venugopalan, Computing quark and gluon distribution functions for very large nuclei, Phys. Rev. D49 (1994) 2233–2241. arXiv:hep-ph/9309289, doi:10.1103/PhysRevD.49.2233.

[94] D. Dolgov, et al., Moments of nucleon light cone quark distributions calculated in full lattice QCD, Phys. Rev. D66 (2002) 034506. arXiv:hep-lat/0201021, doi:10.1103/PhysRevD.66.034506.

[95] D. Dolgov, et al., Moments of structure functions in full QCD, Nucl. Phys. Proc. Suppl. 94 (2001) 303–306, [,303(2000)]. arXiv:hep-lat/0011010, doi:10.1016/S0920-5632(01)00943-4.

[96] P. Dreher, et al., Continuum extrapolation of moments of nucleon quark distributions in full QCD, Nucl. Phys. Proc. Suppl. 119 (2003) 392–394, [,392(2002)]. arXiv:hep-lat/0211021, doi:10.1016/S0920-5632(03)01564-0.

[97] M. Gockeler, R. Horsley, D. Pleiter, P. E. L. Rakow, A. Schafer, G. Schierholz, Calculation of moments of structure functions, Nucl. Phys. Proc. Suppl. 119 (2003) 32–40, [,32(2002)]. arXiv:hep-lat/0209160, doi:10.1016/S0920-5632(03)01490-7.

[98] X. Ji, Parton Physics on a Euclidean Lattice, Phys. Rev. Lett. 110 (2013) 262002. arXiv:1305.1539, doi:10.1103/PhysRevLett.110.262002.

[99] C. Alexandrou, K. Cichy, M. Constantinou, K. Hadjiyiannakou, K. Jansen, H. Panagopoulos, F. Steffens, A complete non-perturbative renormalization prescription for quasi-PDFs, Nucl. Phys. B923 (2017) 394–415. arXiv:1706.00265, doi:10.1016/j.nuclphysb.2017.08.012.

[100] J.-W. Chen, T. Ishikawa, L. Jin, H.-W. Lin, Y.-B. Yang, J.-H. Zhang, Y. Zhao, Parton distribution function with nonperturbative renormalization from lattice QCD, Phys. Rev. D97 (1) (2018) 014505. arXiv:1706.01295, doi:10.1103/PhysRevD.97.014505.

[101] X. Xiong, X. Ji, J.-H. Zhang, Y. Zhao, One-loop matching for parton distributions: Nonsinglet case, Phys. Rev. D90 (1) (2014) 014051. arXiv:1310.7471, doi:10.1103/PhysRevD.90.014051.

[102] H.-W. Lin, J.-W. Chen, S. D. Cohen, X. Ji, Flavor Structure of the Nucleon Sea from Lattice QCD, Phys. Rev. D91 (2015) 054510. arXiv:1402.1462, doi:10.1103/PhysRevD.91.054510.

[103] C. Alexandrou, K. Cichy, V. Drach, E. Garcia-Ramos, K. Hadjiyiannakou, K. Jansen, F. Steffens, C. Wiese, First results with twisted mass fermions towards the computation of parton distribution functions on the lattice, PoS LATTICE2014 (2014) 135. arXiv:1411.0891, doi:10.22323/1.214.0135.

[104] L. Gamberg, Z.-B. Kang, I. Vitev, H. Xing, Quasi-parton distribution functions: a study in the diquark spectator model, Phys. Lett. B743 (2015) 112–120. arXiv:1412.3401, doi:10.1016/j.physletb.2015.02.021.

[105] C. Alexandrou, K. Cichy, V. Drach, E. Garcia-Ramos, K. Hadjiyiannakou, K. Jansen, F. Steffens, C. Wiese, Lattice calculation of parton distributions, Phys. Rev. D92 (2015) 014502. arXiv:1504.07455, doi:10.1103/PhysRevD.92.014502.

[106] I. Vitev, L. Gamberg, Z. Kang, H. Xing, A Study of Quasi-parton Distribution Functions in the Diquark Spectator Model, PoS QCDEV2015 (2015) 045. arXiv:1511.05242, doi:10.22323/1.249.0045.

[107] J.-W. Chen, S. D. Cohen, X. Ji, H.-W. Lin, J.-H. Zhang, Nucleon Helicity and Transversity Parton Distributions from Lattice QCD, Nucl. Phys. B911 (2016) 246–273. arXiv:1603.06664, doi:10.1016/j.nuclphysb.2016.07.033.

[108] A. Bacchetta, M. Radici, B. Pasquini, X. Xiong, Reconstructing parton densities at large fractional momenta, Phys. Rev. D95 (1) (2017) 014036. arXiv:1608.07638, doi:10.1103/PhysRevD.95.014036.

[109] C. Alexandrou, K. Cichy, K. Hadjiyiannakou, K. Jansen, F. Steffens, C. Wiese, A Lattice Calculation of Parton Distributions, PoS DIS2016 (2016) 042. arXiv:1609.00172, doi:10.22323/1.265.0042.

[110] C. Alexandrou, K. Cichy, M. Constantinou, K. Hadjiyiannakou, K. Jansen, F. Steffens, C. Wiese, Updated Lattice Results for Parton Distributions, Phys. Rev. D96 (1) (2017) 014513. arXiv:1610.03689, doi:10.1103/PhysRevD.96.014513.

[111] C. Alexandrou, K. Cichy, M. Constantinou, K. Hadjiyiannakou, K. Jansen, F. Steffens, C. Wiese, Parton Distributions from Lattice QCD with Momentum Smearing, PoS LATTICE2016 (2016) 151. arXiv:1612.08728, doi:10.22323/1.256.0151.

[112] C. E. Carlson, M. Freid, Lattice corrections to the quark quasidistribution at one-loop, Phys. Rev. D95 (9) (2017) 094504. arXiv:1702.05775, doi:10.1103/PhysRevD.95.094504.

[113] X. Xiong, T. Luu, U.-G. Meißner, Quasi-Parton Distribution Function in Lattice Perturbation Theory. arXiv:1705.00246.

[114] M. Constantinou, H. Panagopoulos, Perturbative renormalization of quasi-parton distribution functions, Phys. Rev. D96 (5) (2017) 054506. arXiv:1705.11193, doi:10.1103/PhysRevD.96.054506.

[115] Y.-Q. Ma, J.-W. Qiu, Extracting Parton Distribution Functions from Lattice QCD Calculations. arXiv:1404.6860.

[116] Y.-Q. Ma, J.-W. Qiu, QCD Factorization and PDFs from Lattice QCD Calculation, Int. J. Mod. Phys. Conf. Ser. 37 (2015) 1560041. arXiv:1412.2688, doi:10.1142/S2010194515600411.

[117] H.-n. Li, Nondipolar Wilson links for quasiparton distribution functions, Phys. Rev. D94 (7) (2016) 074036. arXiv:1602.07575, doi:10.1103/PhysRevD.94.074036.

[118] J.-W. Chen, X. Ji, J.-H. Zhang, Improved quasi parton distribution through Wilson line renormalization, Nucl. Phys. B915 (2017) 1–9. arXiv:1609.08102, doi:10.1016/j.nuclphysb.2016.12.004.

[119] W. Wang, S. Zhao, R. Zhu, Gluon quasidistribution function at one loop, Eur. Phys. J. C78 (2) (2018) 147. arXiv:1708.02458, doi:10.1140/epjc/s10052-018-5617-3.

[120] T. Izubuchi, X. Ji, L. Jin, I. W. Stewart, Y. Zhao, Factorization Theorem Relating Euclidean and Light-Cone Parton Distributions. arXiv:1801.03917.

[121] R. A. Briceño, M. T. Hansen, C. J. Monahan, Role of the Euclidean signature in lattice calculations of quasi-distributions and other nonlocal matrix elements,

Phys. Rev. D96 (1) (2017) 014502. arXiv:1703.06072, doi:10.1103/PhysRevD.96.014502.

[122] G. C. Rossi, M. Testa, Note on lattice regularization and equal-time correlators for parton distribution functions, Phys. Rev. D96 (1) (2017) 014507. arXiv:1706.04428, doi:10.1103/PhysRevD.96.014507.

[123] X. Ji, J.-H. Zhang, Y. Zhao, More On Large-Momentum Effective Theory Approach to Parton Physics, Nucl. Phys. B924 (2017) 366–376. arXiv:1706.07416, doi:10.1016/j.nuclphysb.2017.09.001.

[124] X. Ji, P. Sun, X. Xiong, F. Yuan, Soft factor subtraction and transverse momentum dependent parton distributions on the lattice, Phys. Rev. D91 (2015) 074009. arXiv:1405.7640, doi:10.1103/PhysRevD.91.074009.

[125] M. Engelhardt, P. Hägler, B. Musch, J. Negele, A. Schäfer, Lattice QCD study of the Boer-Mulders effect in a pion, Phys. Rev. D93 (5) (2016) 054501. arXiv:1506.07826, doi:10.1103/PhysRevD.93.054501.

[126] A. Radyushkin, Nonperturbative Evolution of Parton Quasi-Distributions, Phys. Lett. B767 (2017) 314–320. arXiv:1612.05170, doi:10.1016/j.physletb.2017.02.019.

[127] A. Radyushkin, Target Mass Effects in Parton Quasi-Distributions, Phys. Lett. B770 (2017) 514–522. arXiv:1702.01726, doi:10.1016/j.physletb.2017.05.024.

[128] B. Yoon, M. Engelhardt, R. Gupta, T. Bhattacharya, J. R. Green, B. U. Musch, J. W. Negele, A. V. Pochinsky, A. Schäfer, S. N. Syritsyn, Nucleon Transverse Momentum-dependent Parton Distributions in Lattice QCD: Renormalization Patterns and Discretization Effects, Phys. Rev. D96 (9) (2017) 094508. arXiv:1706.03406, doi:10.1103/PhysRevD.96.094508.

[129] W. Broniowski, E. Ruiz Arriola, Partonic quasidistributions of the proton and pion from transverse-momentum distributions, Phys. Rev. D97 (3) (2018) 034031. arXiv:1711.03377, doi:10.1103/PhysRevD.97.034031.

[130] X. Ji, L.-C. Jin, F. Yuan, J.-H. Zhang, Y. Zhao, Transverse Momentum Dependent Quasi-Parton-Distributions. arXiv:1801.05930.

[131] X. Ji, A. Schäfer, X. Xiong, J.-H. Zhang, One-Loop Matching for Generalized Parton Distributions, Phys. Rev. D92 (2015) 014039. arXiv:1506.00248, doi:10.1103/PhysRevD.92.014039.

[132] X. Xiong, J.-H. Zhang, One-loop matching for transversity generalized parton distribution, Phys. Rev. D92 (5) (2015) 054037. arXiv:1509.08016, doi:10.1103/PhysRevD.92.054037.

[133] Y. Jia, X. Xiong, Quasi-distribution amplitude of heavy quarkonia, Phys. Rev. D94 (9) (2016) 094005. arXiv:1511.04430, doi:10.1103/PhysRevD.94.094005.

[134] A. V. Radyushkin, Pion Distribution Amplitude and Quasi-Distributions, Phys. Rev. D95 (5) (2017) 056020. arXiv:1701.02688, doi:10.1103/PhysRevD.95.056020.

[135] J.-H. Zhang, J.-W. Chen, X. Ji, L. Jin, H.-W. Lin, Pion Distribution Amplitude from Lattice QCD, Phys. Rev. D95 (9) (2017) 094514. arXiv:1702.00008, doi:10.1103/PhysRevD.95.094514.

[136] W. Broniowski, E. Ruiz Arriola, Nonperturbative partonic quasidistributions of the pion from chiral quark models, Phys. Lett. B773 (2017) 385–390. arXiv:1707.09588, doi:10.1016/j.physletb.2017.08.055.

[137] J.-W. Chen, L. Jin, H.-W. Lin, A. Schäfer, P. Sun, Y.-B. Yang, J.-H. Zhang, R. Zhang, Y. Zhao, Kaon Distribution Amplitude from Lattice QCD and the Flavor SU(3) Symmetry. arXiv:1712.10025.

[138] X. Ji, J.-H. Zhang, Y. Zhao, Justifying the Naive Partonic Sum Rule for Proton Spin, Phys. Lett. B743 (2015) 180–183. arXiv:1409.6329, doi:10.1016/j.physletb.2015.02.054.

[139] H.-W. Lin, et al., Parton distributions and lattice QCD calculations: a community white paper, Prog. Part. Nucl. Phys. 100 (2018) 107–160. arXiv:1711.07916, doi:10.1016/j.ppnp.2018.01.007.

[140] S. Mandelstam, Feynman rules for electromagnetic and Yang-Mills fields from the gauge independent field theoretic formalism, Phys. Rev. 175 (1968) 1580–1623. doi:10.1103/PhysRev.175.1580.

[141] A. M. Polyakov, String Representations and Hidden Symmetries for Gauge Fields, Phys. Lett. 82B (1979) 247–250. doi:10.1016/0370-2693(79)90747-0.

[142] Yu. M. Makeenko, A. A. Migdal, Exact Equation for the Loop Average in Multicolor QCD, Phys. Lett. 88B (1979) 135. doi:10.1016/0370-2693(79)90131-X.

[143] V. S. Dotsenko, S. N. Vergeles, Renormalizability of Phase Factors in the Nonabelian Gauge Theory, Nucl. Phys. B169 (1980) 527–546. doi:10.1016/0550-3213(80)90103-0.

[144] R. A. Brandt, F. Neri, M.-a. Sato, Renormalization of Loop Functions for All Loops, Phys. Rev. D24 (1981) 879. doi:10.1103/PhysRevD.24.879.

[145] N. S. Craigie, H. Dorn, On the Renormalization and Short Distance Properties of Hadronic Operators in QCD, Nucl. Phys. B185 (1981) 204–220. doi:10.1016/0550-3213(81)90372-2.

[146] H. Dorn, Renormalization of Path Ordered Phase Factors and Related Hadron Operators in Gauge Field Theories, Fortsch. Phys. 34 (1986) 11–56. doi:10.1002/prop.19860340104.

[147] N. G. Stefanis, Gauge-invariant quark two-point Green's function through connector insertion to $\mathcal{O}(\alpha_s)$, Nuovo Cim. A83 (1984) 205. doi:10.1007/BF02902597.

[148] D. Knauss, K. Scharnhorst, Two Loop Renormalization of Nonsmooth String Operators in Yang-Mills Theory, Annalen Phys. 496 (1984) 331–344. doi:10.1002/andp.19844960413.

[149] G. P. Korchemsky, A. V. Radyushkin, Renormalization of the Wilson Loops Beyond the Leading Order, Nucl. Phys. B283 (1987) 342–364. doi:10.1016/0550-3213(87)90277-X.

[150] G. P. Korchemsky, A. V. Radyushkin, Infrared factorization, Wilson lines and the heavy quark limit, Phys. Lett. B279 (1992) 359–366. arXiv:hep-ph/9203222, doi:10.1016/0370-2693(92)90405-S.

[151] M. A. Shifman, M. B. Voloshin, On Annihilation of Mesons Built from Heavy and Light Quark and anti-B0 <---> B0 Oscillations, Sov. J. Nucl. Phys. 45 (1987) 292, [Yad. Fiz.45,463(1987)], https://inis.iaea.org/search/search.aspx?orig_q=RN:18034311.

[152] H. D. Politzer, M. B. Wise, Leading Logarithms of Heavy Quark Masses in Processes with Light and Heavy Quarks, Phys. Lett. B206 (1988) 681–684. doi:10.1016/0370-2693(88)90718-6.

[153] A. F. Falk, H. Georgi, B. Grinstein, M. B. Wise, Heavy Meson Form-factors From QCD, Nucl. Phys. B343 (1990) 1–13. doi:10.1016/0550-3213(90)90591-Z.

[154] X.-D. Ji, Order α_s corrections to heavy meson semileptonic decay form-factors, Phys. Lett. B264 (1991) 193–198. doi:10.1016/0370-2693(91)90726-7.

[155] K. G. Chetyrkin, A. G. Grozin, Three loop anomalous dimension of the heavy light quark current in HQET, Nucl. Phys. B666 (2003) 289–302. arXiv:hep-ph/0303113, doi:10.1016/S0550-3213(03)00490-5.

[156] X. Ji, J.-H. Zhang, Renormalization of quasi-parton distribution, Phys. Rev. D92 (2015) 034006. arXiv:1505.07699, doi:10.1103/PhysRevD.92.034006.

[157] T. Ishikawa, Y.-Q. Ma, J.-W. Qiu, S. Yoshida, Renormalizability of quasi-parton distribution functions, Phys. Rev. D96 (9) (2017) 094019. arXiv:1707.03107, doi:10.1103/PhysRevD.96.094019.

[158] X. Ji, J.-H. Zhang, Y. Zhao, Renormalization in Large Momentum Effective Theory of Parton Physics, Phys. Rev. Lett. 120 (11) (2018) 112001. arXiv:1706.08962, doi:10.1103/PhysRevLett.120.112001.

[159] W. Wang, S. Zhao, On the power divergence in quasi gluon distribution function. arXiv:1712.09247.

[160] J.-H. Zhang, X. Ji, A. Schäfer, W. Wang, S. Zhao, Renormalization of gluon quasi-PDF in large momentum effective theory. arXiv:1808.10824.

[161] Z.-Y. Li, Y.-Q. Ma, J.-W. Qiu, Multiplicative Renormalizability of Operators defining Quasiparton Distributions, Phys. Rev. Lett. 122 (6) (2019) 062002. arXiv:1809.01836, doi:10.1103/PhysRevLett.122.062002.

[162] G. Spanoudes, H. Panagopoulos, Renormalization of Wilson-line operators in the presence of nonzero quark masses, Phys. Rev. D98 (1) (2018) 014509. arXiv:1805.01164, doi:10.1103/PhysRevD.98.014509.

[163] M. Constantinou, Renormalization Issues on Long-Link Operators, in: 7th Workshop of the APS Topical Group on Hadronic Physics, Feb 1-3, 2017, https://www.jlab.org/indico/event/160/session/13/contribution/44.

[164] C. Alexandrou, K. Cichy, M. Constantinou, K. Jansen, A. Scapellato, F. Steffens, Light-Cone Parton Distribution Functions from Lattice QCD, Phys. Rev. Lett. 121 (11) (2018) 112001. arXiv:1803.02685, doi:10.1103/PhysRevLett.121.112001.

[165] C. Alexandrou, K. Cichy, M. Constantinou, K. Jansen, A. Scapellato, F. Steffens, Transversity parton distribution functions from lattice QCD, Phys. Rev. D98 (9) (2018) 091503. arXiv:1807.00232, doi:10.1103/PhysRevD.98.091503.

[166] T. Ishikawa, Y.-Q. Ma, J.-W. Qiu, S. Yoshida, Practical quasi parton distribution functions. arXiv:1609.02018.

[167] T. Ishikawa, Y.-Q. Ma, J.-W. Qiu, S. Yoshida, Matching issue in quasi parton distribution approach, PoS LATTICE2016 (2016) 177. arXiv:1703.08699, doi:10.22323/1.256.0177.

[168] C. Monahan, K. Orginos, Locally smeared operator product expansions in scalar field theory, Phys. Rev. D91 (7) (2015) 074513. arXiv:1501.05348, doi:10.1103/PhysRevD.91.074513.

[169] C. Monahan, K. Orginos, Quasi parton distributions and the gradient flow, JHEP 03 (2017) 116. arXiv:1612.01584, doi:10.1007/JHEP03(2017)116.

[170] C. Monahan, Smeared quasidistributions in perturbation theory, Phys. Rev. D97 (5) (2018) 054507. arXiv:1710.04607, doi:10.1103/PhysRevD.97.054507.

[171] J. Green, K. Jansen, F. Steffens, Nonperturbative renormalization of nonlocal quark bilinears for quasi-PDFs on the lattice using an auxiliary field, Phys. Rev. Lett. 121 (2) (2018) 022004. arXiv:1707.07152, doi:10.1103/PhysRevLett.121.022004.

[172] A. V. Radyushkin, Quasi-parton distribution functions, momentum distributions, and pseudo-parton distribution functions, Phys. Rev. D96 (3) (2017) 034025. arXiv:1705.01488, doi:10.1103/PhysRevD.96.034025.

[173] K. Orginos, A. Radyushkin, J. Karpie, S. Zafeiropoulos, Lattice QCD exploration of parton pseudo-distribution functions, Phys. Rev. D96 (9) (2017) 094503. arXiv:1706.05373, doi:10.1103/PhysRevD.96.094503.

[174] A. Radyushkin, One-loop evolution of parton pseudo-distribution functions on the lattice. arXiv:1801.02427.

[175] J.-H. Zhang, J.-W. Chen, C. Monahan, Parton distribution functions from reduced Ioffe-time distributions, Phys. Rev. D97 (7) (2018) 074508. arXiv:1801.03023, doi:10.1103/PhysRevD.97.074508.

[176] A. J. Chambers, R. Horsley, Y. Nakamura, H. Perlt, P. E. L. Rakow, G. Schierholz, A. Schiller, K. Somfleth, R. D. Young, J. M. Zanotti, Nucleon Structure Functions from Operator Product Expansion on the Lattice, Phys. Rev. Lett. 118 (24) (2017) 242001. arXiv:1703.01153, doi:10.1103/PhysRevLett.118.242001.

[177] Y.-Q. Ma, J.-W. Qiu, Exploring Partonic Structure of Hadrons Using ab initio Lattice QCD Calculations, Phys. Rev. Lett. 120 (2) (2018) 022003. arXiv:1709.03018, doi:10.1103/PhysRevLett.120.022003.

[178] K. Cichy, M. Constantinou, A guide to light-cone PDFs from Lattice QCD: an overview of approaches, techniques and results. arXiv:1811.07248.

[179] A. J. Buras, P. H. Weisz, QCD Nonleading Corrections to Weak Decays in Dimensional Regularization and 't Hooft-Veltman Schemes, Nucl. Phys. B333 (1990) 66–99. doi:10.1016/0550-3213(90)90223-Z.

[180] A. Patel, S. R. Sharpe, Perturbative corrections for staggered fermion bilinears, Nucl. Phys. B395 (1993) 701–732. arXiv:hep-lat/9210039, doi:10.1016/0550-3213(93)90054-S.

[181] S. A. Larin, J. A. M. Vermaseren, The Three loop QCD Beta function and anomalous dimensions, Phys. Lett. B303 (1993) 334–336. arXiv:hep-ph/9302208, doi:10.1016/0370-2693(93)91441-O.

[182] S. A. Larin, The Renormalization of the axial anomaly in dimensional regularization, Phys. Lett. B303 (1993) 113–118. arXiv:hep-ph/9302240, doi:10.1016/0370-2693(93)90053-K.

[183] M. Constantinou, M. Costa, H. Panagopoulos, Perturbative renormalization functions of local operators for staggered fermions with stout improvement, Phys. Rev. D88 (2013) 034504. arXiv:1305.1870, doi:10.1103/PhysRevD.88.034504.

[184] G. 't Hooft, M. J. G. Veltman, Diagrammar, Nato Sci. Ser. B 4 (1974) 177–322. doi:10.5170/CERN-1973-009.

[185] P. Boyle, L. Del Debbio, A. Khamseh, Massive momentum-subtraction scheme, Phys. Rev. D95 (5) (2017) 054505. arXiv:1611.06908, doi:10.1103/PhysRevD.95.054505.

[186] J. A. Gracey, Three loop anomalous dimension of nonsinglet quark currents in the RI-prime scheme, Nucl. Phys. B662 (2003) 247–278. arXiv:hep-ph/0304113, doi:10.1016/S0550-3213(03)00335-3.

[187] C. J. Bomhof, P. J. Mulders, F. Pijlman, The Construction of gauge-links in arbitrary hard processes, Eur. Phys. J. C47 (2006) 147–162. arXiv:hep-ph/0601171, doi:10.1140/epjc/s2006-02554-2.

[188] B. U. Musch, P. Hägler, J. W. Negele, A. Schäfer, Exploring quark transverse momentum distributions with lattice QCD, Phys. Rev. D83 (2011) 094507. arXiv:1011.1213, doi:10.1103/PhysRevD.83.094507.

[189] B. U. Musch, P. Hägler, M. Engelhardt, J. W. Negele, A. Schäfer, Sivers and Boer-Mulders observables from lattice QCD, Phys. Rev. D85 (2012) 094510. arXiv:1111.4249, doi:10.1103/PhysRevD.85.094510.

[190] M. Engelhardt, Quark orbital dynamics in the proton from Lattice QCD – from Ji to Jaffe-Manohar orbital angular momentum, Phys. Rev. D95 (9) (2017) 094505. arXiv:1701.01536, doi:10.1103/PhysRevD.95.094505.

[191] A. Rajan, M. Engelhardt, S. Liuti, Lorentz Invariance and QCD Equation of Motion Relations for Generalized Parton Distributions and the Dynamical Origin of Proton Orbital Angular Momentum, Phys. Rev. D98 (7) (2018) 074022. arXiv:1709.05770, doi:10.1103/PhysRevD.98.074022.

[192] Y. Hatta, Notes on the orbital angular momentum of quarks in the nucleon, Phys. Lett. B708 (2012) 186–190. arXiv:1111.3547, doi:10.1016/j.physletb.2012.01.024.

[193] M. Burkardt, Parton Orbital Angular Momentum and Final State Interactions, Phys. Rev. D88 (1) (2013) 014014. arXiv:1205.2916, doi:10.1103/PhysRevD.88.014014.

[194] X. Ji, X. Xiong, F. Yuan, Proton Spin Structure from Measurable Parton Distributions, Phys. Rev. Lett. 109 (2012) 152005. arXiv:1202.2843, doi:10.1103/PhysRevLett.109.152005.

[195] A. Rajan, A. Courtoy, M. Engelhardt, S. Liuti, Parton Transverse Momentum and Orbital Angular Momentum Distributions, Phys. Rev. D94 (3) (2016) 034041. arXiv:1601.06117, doi:10.1103/PhysRevD.94.034041.

[196] I. Ya. Aref'eva, Quantum Contour Field Equations, Phys. Lett. 93B (1980) 347–353. doi:10.1016/0370-2693(80)90529-8.

[197] A. Shindler, Twisted mass lattice QCD, Phys. Rept. 461 (2008) 37–110. arXiv:0707.4093, doi:10.1016/j.physrep.2008.03.001.

[198] R. Horsley, H. Perlt, P. E. L. Rakow, G. Schierholz, A. Schiller, One-loop renormalisation of quark bilinears for overlap fermions with improved gauge actions, Nucl. Phys. B693 (2004) 3–35, [Erratum: Nucl. Phys.B713,601(2005)]. arXiv:hep-lat/0404007, doi:10.1016/j.nuclphysb.2004.06.008,10.1016/j.nuclphysb.2005.01.044.

[199] H. Kawai, R. Nakayama, K. Seo, Comparison of the Lattice Λ Parameter with the Continuum Λ Parameter in Massless QCD, Nucl. Phys. B189 (1981) 40–62. doi:10.1016/0550-3213(81)90080-8.

[200] C. Alexandrou, M. Constantinou, T. Korzec, H. Panagopoulos, F. Stylianou, Renormalization constants of local operators for Wilson type improved fermions, Phys. Rev. D86 (2012) 014505. arXiv:1201.5025, doi:10.1103/PhysRevD.86.014505.

[201] X.-D. Ji, M. J. Musolf, Subleading logarithmic mass dependence in heavy meson form-factors, Phys. Lett. B257 (1991) 409–413. doi:10.1016/0370-2693(91)91916-J.

[202] D. J. Broadhurst, A. G. Grozin, Two loop renormalization of the effective field theory of a static quark, Phys. Lett. B267 (1991) 105–110. arXiv:hep-ph/9908362, doi:10.1016/0370-2693(91)90532-U.

[203] M. Constantinou, M. Hadjiantonis, H. Panagopoulos, Renormalization of Flavor Singlet and Nonsinglet Fermion Bilinear Operators, PoS LATTICE2014 (2014) 298. arXiv:1411.6990, doi:10.22323/1.214.0298.

[204] M. Brambilla, F. Di Renzo, M. Hasegawa, High-loop perturbative renormalization constants for Lattice QCD (III): three-loop quark currents for Iwasaki gauge action and n˙f=4 Wilson fermions, Eur. Phys. J. C74 (7) (2014) 2944. arXiv:1402.6581, doi:10.1140/epjc/s10052-014-2944-x.

[205] Y. Aoki, Z. Fodor, S. D. Katz, K. K. Szabo, The Equation of state in lattice QCD: With physical quark masses towards the continuum limit, JHEP 01 (2006) 089. arXiv:hep-lat/0510084, doi:10.1088/1126-6708/2006/01/089.

[206] S. Borsanyi, Z. Fodor, S. Katz, S. Krieg, C. Ratti, K. Szabo, Correlations and fluctuations from lattice QCD, J. Phys. G38 (2011) 124060. arXiv:1109.5030, doi:10.1088/0954-3899/38/12/124060.

[207] A. Bazavov, et al., Lattice QCD ensembles with four flavors of highly improved staggered quarks, Phys. Rev. D87 (5) (2013) 054505. arXiv:1212.4768, doi:10.1103/PhysRevD.87.054505.

[208] H. Panagopoulos, A. Skouroupathis, A. Tsapalis, Free energy and plaquette expectation value for gluons on the lattice, in three dimensions, Phys. Rev. D73 (2006) 054511. arXiv:hep-lat/0601009, doi:10.1103/PhysRevD.73.054511.

[209] K. G. Chetyrkin, F. V. Tkachov, Integration by Parts: The Algorithm to Calculate beta Functions in 4 Loops, Nucl. Phys. B192 (1981) 159–204. doi:10.1016/0550-3213(81)90199-1.

[210] H. Panagopoulos, E. Vicari, The Trilinear Gluon Condensate on the Lattice, Nucl. Phys. B332 (1990) 261–284. doi:10.1016/0550-3213(90)90039-G.

[211] R. K. Ellis, G. Martinelli, Two Loop Corrections to the Λ Parameters of One-Plaquette Actions, Nucl. Phys. B235 (1984) 93–114, [Erratum: Nucl. Phys.B249,750(1985)]. doi:10.1016/0550-3213(85)90034-3,10.1016/0550-3213(84)90150-0.

[212] M. Luscher, R. Sommer, P. Weisz, U. Wolff, A Precise determination of the running coupling in the SU(3) Yang-Mills theory, Nucl. Phys. B413 (1994) 481–502. arXiv:hep-lat/9309005, doi:10.1016/0550-3213(94)90629-7.

[213] M. Della Morte, R. Frezzotti, J. Heitger, J. Rolf, R. Sommer, U. Wolff, Computation of the strong coupling in QCD with two dynamical flavors, Nucl. Phys. B713 (2005) 378–406. arXiv:hep-lat/0411025, doi:10.1016/j.nuclphysb.2005.02.013.

[214] M. Dalla Brida, P. Fritzsch, T. Korzec, A. Ramos, S. Sint, R. Sommer, Determination of the QCD Λ-parameter and the accuracy of perturbation theory at high energies, Phys. Rev. Lett. 117 (18) (2016) 182001. arXiv:1604.06193, doi:10.1103/PhysRevLett.117.182001.

[215] M. Dalla Brida, P. Fritzsch, T. Korzec, A. Ramos, S. Sint, R. Sommer, A non-perturbative exploration of the high energy regime in $N_{\rm f} = 3$ QCD, Eur. Phys. J. C78 (5) (2018) 372. arXiv:1803.10230, doi:10.1140/epjc/s10052-018-5838-5.

[216] M. Lüscher, Properties and uses of the Wilson flow in lattice QCD, JHEP 08 (2010) 071, [Erratum: JHEP03,092(2014)]. arXiv:1006.4518, doi:10.1007/JHEP08(2010)071,10.1007/JHEP03(2014)092.

[217] R. V. Harlander, T. Neumann, The perturbative QCD gradient flow to three loops, JHEP 06 (2016) 161. arXiv:1606.03756, doi:10.1007/JHEP06(2016)161.

[218] J. Artz, R. V. Harlander, F. Lange, T. Neumann, M. Prausa, Results and techniques for higher order calculations within the gradient flow formalism. arXiv:1905.00882.

[219] O. V. Tarasov, A. A. Vladimirov, A. Yu. Zharkov, The Gell-Mann-Low Function of QCD in the Three Loop Approximation, Phys. Lett. 93B (1980) 429–432. doi:10.1016/0370-2693(80)90358-5.

[220] M. Luscher, R. Narayanan, P. Weisz, U. Wolff, The Schrodinger functional: A Renormalizable probe for nonAbelian gauge theories, Nucl. Phys. B384 (1992) 168–228. arXiv:hep-lat/9207009, doi:10.1016/0550-3213(92)90466-O.

[221] G. M. de Divitiis, R. Frezzotti, M. Guagnelli, R. Petronzio, Nonperturbative determination of the running coupling constant in quenched SU(2), Nucl. Phys. B433 (1995) 390–402. arXiv:hep-lat/9407028, doi:10.1016/0550-3213(94)00478-W.

[222] B. Alles, D. Henty, H. Panagopoulos, C. Parrinello, C. Pittori, D. G. Richards, α_s from the nonperturbatively renormalised lattice three gluon vertex, Nucl. Phys. B502 (1997) 325–342. arXiv:hep-lat/9605033, doi:10.1016/S0550-3213(97)00483-5.

[223] S. Booth, et al., The Strong coupling constant from lattice QCD with N(f)=2 dynamical quarks, Nucl. Phys. Proc. Suppl. 106 (2002) 308–310. arXiv:hep-lat/0111006, doi:10.1016/S0920-5632(01)01697-8.

[224] S. Aoki, et al., Precise determination of the strong coupling constant in $N_f = 2+1$ lattice QCD with the Schrodinger functional scheme, JHEP 10 (2009) 053. arXiv:0906.3906, doi:10.1088/1126-6708/2009/10/053.

[225] P. Fritzsch, M. Dalla Brida, T. Korzec, A. Ramos, S. Sint, R. Sommer, Towards a new determination of the QCD Lambda parameter from running couplings in the three-flavour theory, PoS LATTICE2014 (2014) 291. arXiv:1411.7648, doi:10.22323/1.214.0291.

[226] M. Bruno, M. Dalla Brida, P. Fritzsch, T. Korzec, A. Ramos, S. Schaefer, H. Simma, S. Sint, R. Sommer, QCD Coupling from a Nonperturbative Determination of the Three-Flavor Λ Parameter, Phys. Rev. Lett. 119 (10) (2017) 102001. arXiv:1706.03821, doi:10.1103/PhysRevLett.119.102001.

[227] B. S. DeWitt, Quantum Theory of Gravity. 2. The Manifestly Covariant Theory, Phys. Rev. 162 (1967) 1195–1239, [,298(1967)]. doi:10.1103/PhysRev.162.1195.

[228] J. Honerkamp, Chiral multiloops, Nucl. Phys. B36 (1972) 130–140. doi:10.1016/0550-3213(72)90299-4.

[229] G. 't Hooft, An algorithm for the poles at dimension four in the dimensional regularization procedure, Nucl. Phys. B62 (1973) 444–460. doi:10.1016/0550-3213(73)90263-0.

[230] H. Kluberg-Stern, J. B. Zuber, Renormalization of Nonabelian Gauge Theories in a Background Field Gauge. 1. Green Functions, Phys. Rev. D12 (1975) 482–488. doi:10.1103/PhysRevD.12.482.

[231] M. Lüscher, P. Weisz, Background field technique and renormalization in lattice gauge theory, Nucl. Phys. B452 (1995) 213–233. arXiv:hep-lat/9504006, doi:10.1016/0550-3213(95)00346-T.

[232] T. Reisz, Lattice Gauge Theory: Renormalization to All Orders in the Loop Expansion, Nucl. Phys. B318 (1989) 417–463. doi:10.1016/0550-3213(89)90613-5.

[233] L. F. Abbott, The Background Field Method Beyond One Loop, Nucl. Phys. B185 (1981) 189–203. doi:10.1016/0550-3213(81)90371-0.

[234] V. Leino, J. Rantaharju, T. Rantalaiho, K. Rummukainen, J. M. Suorsa, K. Tuominen, The gradient flow running coupling in SU(2) gauge theory with $N_f = 8$ fundamental flavors, Phys. Rev. D95 (11) (2017) 114516. arXiv:1701.04666, doi:10.1103/PhysRevD.95.114516.

[235] M. Bruno, M. Dalla Brida, P. Fritzsch, T. Korzec, A. Ramos, S. Schaefer, H. Simma, S. Sint, R. Sommer, The determination of α_s by the ALPHA collaboration, Nucl. Part. Phys. Proc. 285-286 (2017) 132–138. arXiv:1611.05750, doi:10.1016/j.nuclphysbps.2017.03.024.

[236] A. Hasenfratz, D. Schaich, Nonperturbative β function of twelve-flavor SU(3) gauge theory, JHEP 02 (2018) 132. arXiv:1610.10004, doi:10.1007/JHEP02(2018)132.

[237] C. J. D. Lin, K. Ogawa, A. Ramos, The Yang-Mills gradient flow and SU(3) gauge theory with 12 massless fundamental fermions in a colour-twisted box, JHEP 12 (2015) 103. arXiv:1510.05755, doi:10.1007/JHEP12(2015)103.

[238] R. Horsley, H. Perlt, P. E. L. Rakow, G. Schierholz, A. Schiller, The SU(3) Beta Function from Numerical Stochastic Perturbation Theory, Phys. Lett. B728 (2014) 1–4. arXiv:1309.4311, doi:10.1016/j.physletb.2013.11.012.

[239] M. Luscher, P. Weisz, Two loop relation between the bare lattice coupling and the MS coupling in pure SU(N) gauge theories, Phys. Lett. B349 (1995) 165–169. arXiv:hep-lat/9502001, doi:10.1016/0370-2693(95)00250-O.

[240] K.-I. Ishikawa, I. Kanamori, Y. Murakami, A. Nakamura, M. Okawa, R. Ueno, Non-perturbative determination of the Λ-parameter in the pure SU(3) gauge theory from the twisted gradient flow coupling, JHEP 12 (2017) 067. arXiv:1702.06289, doi:10.1007/JHEP12(2017)067.

[241] F. Herzog, B. Ruijl, T. Ueda, J. A. M. Vermaseren, A. Vogt, The five-loop beta function of Yang-Mills theory with fermions, JHEP 02 (2017) 090. arXiv:1701.01404, doi:10.1007/JHEP02(2017)090.

[242] B. Alles, A. Feo, H. Panagopoulos, The Three loop Beta function in SU(N) lattice gauge theories, Nucl. Phys. B491 (1997) 498–512. arXiv:hep-lat/9609025, doi:10.1016/S0550-3213(97)00092-8.

[243] A. Skouroupathis, H. Panagopoulos, Lambda-parameter of lattice QCD with Symanzik improved gluon actions, Phys. Rev. D76 (2007) 114514. arXiv:0709.3239, doi:10.1103/PhysRevD.76.114514.

[244] V. G. Bornyakov, et al., Determining the scale in Lattice QCD, PoS LATTICE2015 (2015) 264. arXiv:1512.05745.

[245] R. K. Ellis, Perturbative Corrections to Universality and Renormalization Group Behaviour, Proceedings: Gauge Theory on a Lattice: 1984 (1984) 191.

[246] C. Alexandrou, K. Cichy, M. Constantinou, K. Hadjiyiannakou, K. Jansen, A. Scapellato, F. Steffens, Systematic uncertainties in parton distribution functions from lattice QCD simulations at the physical point. arXiv:1902.00587.

[247] A. Bazavov, et al., The chiral and deconfinement aspects of the QCD transition, Phys. Rev. D85 (2012) 054503. arXiv:1111.1710, doi:10.1103/PhysRevD.85.054503.

[248] M. Constantinou, et al., Non-perturbative renormalization of quark bilinear operators with $N_f = 2$ (tmQCD) Wilson fermions and the tree-level improved gauge action, JHEP 08 (2010) 068. arXiv:1004.1115, doi:10.1007/JHEP08(2010)068.

[249] M. Constantinou, R. Horsley, H. Panagopoulos, H. Perlt, P. E. L. Rakow, G. Schierholz, A. Schiller, J. M. Zanotti, Renormalization of local quark-bilinear operators for N_f=3 flavors of stout link nonperturbative clover fermions, Phys. Rev. D91 (1) (2015) 014502. arXiv:1408.6047, doi:10.1103/PhysRevD.91.014502.

[250] K. Orginos, D. Toussaint, R. L. Sugar, Variants of fattening and flavor symmetry restoration, Phys. Rev. D60 (1999) 054503. arXiv:hep-lat/9903032, doi:10.1103/PhysRevD.60.054503.

[251] G. 't Hooft, M. J. G. Veltman, Regularization and Renormalization of Gauge Fields, Nucl. Phys. B44 (1972) 189–213. doi:10.1016/0550-3213(72)90279-9.